The influence of Arctic sea-ice loss on mid-latitude weather and climate: exploring sensitivities and mechanisms

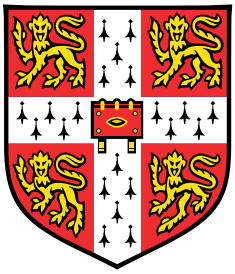

Christine Mary McKenna

British Antarctic Survey

Department of Applied Mathematics and Theoretical Physics
University of Cambridge

This dissertation is submitted for the degree of
Doctor of Philosophy

Christ's College

September 2019

Declaration

This dissertation is the result of my own work and includes nothing which is the outcome of work done in collaboration except as declared in the Acknowledgements and specified in the text. I further state that no substantial part of my dissertation has already been submitted, or, is being concurrently submitted for any such degree, diploma or other qualification at the University of Cambridge or any other University or similar institution except as declared in the Acknowledgements and specified in the text. It does not exceed the prescribed word limit for the relevant Degree Committee.

Abstract for:

The influence of Arctic sea-ice loss on mid-latitude weather and climate: exploring sensitivities and mechanisms

Christine Mary McKenna

Over the past few decades, Arctic sea-ice extent has declined, while there has been an apparent increase in severe winter weather across some mid-latitude regions. This has led to much research into whether these trends are dynamically linked. It has been suggested that the link may involve the Arctic Oscillation (AO), which describes the observed oscillation in geopotential height anomalies between high and middle Northern Hemisphere latitudes. Sea-ice loss has been shown to excite the AO's negative phase, which is linked to colder conditions in key regions of mid-latitudes, through various tropospheric and stratospheric mechanisms.

However, the nature of the response to Arctic sea-ice loss and the mechanisms involved remain uncertain. This is because it is difficult to disentangle the complex web of potential processes involved, the modelled response to sea-ice loss is small relative to internal climate variability, and modelling studies find contrasting climatological mean responses to imposed sea-ice loss. Since all climate models project a continuation of Arctic sea-ice loss during the 21st century in response to anthropogenic greenhouse gas forcing, it is important that the potential influence of this on the highly populated mid-latitudes is better understood.

In this thesis, the issues of complexity and statistical robustness are partly addressed by conducting idealised numerical modelling experiments using an intermediate complexity global circulation model, IGCM4. Such models are useful because they are complex enough to simulate a variety of important processes, but are relatively simple and computationally fast compared to full complexity state-of-the-art climate models. This helps to disentangle different processes from one another and allows for several-century-long simulations, making a statistically robust response more attainable.

To understand the contrasting results of past modelling studies, it is firstly investigated whether the response to sea-ice loss is sensitive to the loss region (the Atlantic or Pacific sector of the Arctic). For different regions of loss, different effects on the

stratospheric circulation are found. While there are negative tropospheric AO responses in both cases, there are contrasting effects on mid-latitude surface temperatures. This is explained in this work using a method of decomposition into an 'indirect' part induced by the large-scale AO response, and a residual 'direct' part that is local to the ice loss region. A low signal-to-noise ratio makes it difficult to robustly determine the linearity of the response to different loss magnitudes.

A stratospheric nudging method is then implemented in IGCM4 to isolate the roles played by tropospheric and stratospheric mechanisms in the remote response to sea-ice loss. For Atlantic sector loss, part of the negative tropospheric AO response is found to likely be caused by tropospheric mechanisms, and the other part likely involves changes in sudden stratospheric warmings (SSWs). For Pacific sector loss, there is likely a non-linear interaction between tropospheric and stratospheric mechanisms, where the stratospheric state alters vertical wave propagation such that the direct stationary Rossby wave response to the ice loss projects onto a negative tropospheric AO.

Finally, motivated by the importance of SSWs in the Atlantic sector sea-ice loss experiment and their potentially large internal variability, this experiment is extended by several centuries to examine the influence of atmospheric internal variability with regard to uncertainty in responses to sea-ice loss produced by model time-slice experiments of different lengths. This leads to a quantification of the minimum experiment length required to separate the signs of forced tropospheric and stratospheric changes due to sea-ice loss from internal variability. This has not been quantified to date for the latter, and is found to be large for both the stratospheric AO and SSW frequency (respectively around 190 and 450 years for the December-March mean). This may explain contrasting stratospheric responses in past studies using an insufficient experiment length, with implications for the robustness (at least quantitatively) of the tropospheric responses in these studies. Here, the responses are qualitatively the same in the shorter and extended experiments, but there are some differences in magnitude and evolution.

In summary, this thesis improves understanding of the influence of Arctic sea-ice loss on mid-latitude weather and climate, and the mechanisms involved. This is done by systematically examining various aspects that may explain contrasting model results – including different regions and magnitudes of loss, as well as atmospheric internal variability – and, hence, current uncertainty regarding the nature of a link. A better understanding of the mechanisms involved is obtained by decomposing the responses into parts due to tropospheric and stratospheric mechanisms.

Acknowledgements

I would like to give a special thanks to my supervisors, Tom Bracegirdle, Peter Haynes, and Emily Shuckburgh, for being a constant source of support and guidance over the duration of my PhD. Their insight, extensive knowledge, and encouragement has been invaluable, and this thesis would not have been possible without them.

A thanks must go to Manoj Joshi for setting up IGCM4 on the local HPC at the British Antarctic Survey (BAS), and for providing IGCM4-related advice throughout the project. To Andy England in the IT team at BAS, thanks for assisting me with setting up IGCM4 for a second time on the local HPC replacement at BAS. Thanks also to Peter Hitchcock, who kindly provided me with a stratospheric nudging code for IGCM1 and with further advice regarding its implementation in IGCM4.

Thanks also to all the members of the Atmosphere-Ocean group in DAMTP, and the Polar Climate and Prediction group in BAS, for all their help, guidance, and companionship during my PhD. A special mention should be given to Alison Ming for all of our insightful discussions over the years, especially regarding statistics, and for being a continual source of enthusiasm. Thanks also to Tony Phillips for helping me to manage the large amount of model data that I produced during my PhD.

BAS has been a wonderful place to work. Thanks to all the students for the many tea-breaks, delicious cakes, pub-trips, and interesting conversations, all of which kept me going. A special thanks to my office-mates, Amy, Ella, Emily, and Mike, for being such good company and providing much needed moral support. In particular, thanks to Emily for putting up with all of my questions, for being an excellent conference-buddy, and for providing much laughter. To Tracey and Rachael, thanks for never failing to lighten my mood, and for always turning up to the pub and for tea-breaks.

To my parents, the rest of my family, and friends, thanks for always being supportive and understanding. Finally, a massive thanks must go to Ryan, whose endless patience helped me through the last year in particular.

Table of contents

List of figures

List of tables

Nomenclature

Roman Symbols

T_s	Surface temperature
U	Zonal wind
Z	Geopotential height

Model experiments

CTL	Control model experiment with climatological ocean surface temperatures (300 years-long)
ATL	Atlantic sector sea-ice loss model experiment, with climatological ocean surface temperatures plus anomalies added in the Barents-Kara Seas to represent future sea-ice retreat (200 years-long)
PAC	Pacific sector sea-ice loss model experiment, with climatological ocean surface temperatures plus anomalies added in the Chukchi-Bering Seas to represent future sea-ice retreat (200 years-long)
0.5ATL	Same as ATL, but with half the magnitude of ocean surface temperature anomalies added (300 years-long)
0.5PAC	Same as PAC, but with half the magnitude of ocean surface temperature anomalies added (300 years-long)
ATL&PAC	Combined Atlantic and Pacific sector sea-ice loss model experiment, with climatological ocean surface temperatures plus anomalies added in the Barents-Kara and Chukchi-Bering Seas (200 years-long)

CTL_{ndgCS}	Same as CTL, but with nudging applied toward the zonal mean climatological mean annual cycle of stratospheric fields in CTL (200 years-long)
ATL_{ndgCS}	Same as ATL, but with nudging applied toward the zonal mean climatological mean annual cycle of stratospheric fields in CTL (200 years-long)
PAC_{ndgCS}	Same as PAC, but with nudging applied toward the zonal mean climatological mean annual cycle of stratospheric fields in CTL (200 years-long)
CTL_{ndgAS}	Same as CTL, but with nudging applied toward the zonal mean climatological mean annual cycle of stratospheric fields in ATL (200 years-long)
CTL_{ndgPS}	Same as CTL, but with nudging applied toward the zonal mean climatological mean annual cycle of stratospheric fields in PAC (200 years-long)
CTL_{ndgSSW}	Same as CTL, but with nudging of the zonal mean stratospheric state toward a specific reference SSW from December in ATL (200 years-long)
CTL_{600}	Extended version of CTL, from 300 years-long to 600 years-long
ATL_{600}	Extended version of ATL, from 200 years-long to 600 years-long

Acronyms / Abbreviations

AA	Arctic Amplification
AGCM	Atmospheric General Circulation Model
AO	Arctic Oscillation
AOGCM	Coupled Atmosphere-Ocean General Circulation Model
BKS	Barents-Kara Seas
CMIP5	Coupled Model Intercomparison Project Phase 5
DJF	December, January, and February (winter)
EOF	Empirical Orthogonal Function
EP-flux	Eliassen-Palm flux
ERA	ECMWF (European Centre for Medium-Range Weather Forecasts) Re-Analysis

GCM	General Circulation Model
GHG	Greenhouse gas
IGCM4	Intermediate Global Circulation Model, version 4
IPCC	Intergovernmental Panel on Climate Change
JJA	June, July, and August (summer)
MAM	March, April, and May (spring)
NAM	Northern Annular Mode
NAO	North Atlantic Oscillation
NSIDC	National Snow and Ice Data Center
PC	Principal Component
RCP8.5	Representative Concentration Pathway 8.5
SIC	Sea-ice concentration
SIE	Sea-ice extent
SON	September, October, and November (autumn)
SST	Sea surface temperature
SSW	Sudden stratospheric warming
Z10	Geopotential height at 10 hPa
Z500	Geopotential height at 500 hPa

Chapter 1

Introduction

Since 1979, Arctic sea-ice extent has declined in all months and, in particular, by more than 13% per decade in September (National Snow and Ice Data Center/NSIDC, 2016a). This has contributed to enhanced near-surface warming in the Arctic, which has occurred at double the rate of lower latitudes in recent decades and is termed 'Arctic Amplification' (Serreze et al., 2009; Screen and Simmonds, 2010). These trends have coincided with an apparent increase in severe winter weather across some mid-latitude regions (Cohen et al., 2014), including central Eurasia where average winter surface air temperatures have reduced by 1.25°C over the past 25 years (McCusker et al., 2016). There have also been recent unusually cold and snowy winters observed in 2006 (year is for January), 2010, 2011, 2017, and 2018 across parts of Eurasia (Petoukhov and Semenov, 2010; Guirguis et al., 2011; Osborn, 2011; Chen et al., 2018; Met Office, 2018; Greening and Hodgson, 2019), and in 2010, 2011, 2014, and 2019 across parts of North America (Guirguis et al., 2011; Van Oldenborgh et al., 2015; Climate Central, 2019).

The simultaneous occurrence of recent Arctic sea-ice loss and apparent increases in severe mid-latitude winters has led to much research into whether they are dynamically linked. For example, it has been suggested that a link might involve the Arctic Oscillation or AO. This describes the observed oscillation in geopotential height anomalies between high and middle Northern Hemisphere latitudes, where anomalous positive and negative heights respectively define the AO's negative phase. Sea-ice loss has been shown to result in a negative AO-like response in climate models – which is linked to colder conditions in key regions of mid-latitudes – through tropospheric eddy feedbacks (Deser et al., 2004; Ruggieri et al., 2019), or a weakening of the stratospheric

polar vortex and the resulting effect on the troposphere (Kim et al., 2014; Peings and Magnusdottir, 2014; Nakamura et al., 2016b; Zhang et al., 2018a,b), or a combination of both (Nakamura et al., 2016a; Wu and Smith, 2016). It has also been suggested that sea-ice loss modifies tropospheric stationary Rossby wave propagation, which leads to a stronger Siberian High and therefore stronger cold air advection over Eurasia (Honda et al., 2009; Petoukhov and Semenov, 2010; Mori et al., 2014).

However, the nature of the response to Arctic sea-ice loss and the mechanisms involved remains uncertain. This is because it is difficult to disentangle the complex web of potential processes involved (Overland et al., 2016), the modelled response to sea-ice loss is small relative to internal climate variability (Screen et al., 2014; McCusker et al., 2016), and modelling studies find contrasting climatological mean responses to imposed sea-ice loss – for example, some studies find a positive AO-like response (Orsolini et al., 2012; Screen et al., 2014), no significant AO-like response (Singarayer et al., 2006; Screen et al., 2013; Boland et al., 2016), or a stronger polar vortex (Scinocca et al., 2009; Cai et al., 2012; Screen et al., 2013; Sun et al., 2014).

Since all climate models project a continuation of Arctic sea-ice loss and associated warming during the 21st century in response to anthropogenic greenhouse gas (GHG) forcing (Collins et al., 2013), it is important that the potential influence of this on the highly populated mid-latitudes is better understood. Furthermore, improving understanding of this influence may help us to better understand projections of future circulation change, not just in response to projected sea-ice loss. Indeed, part of the intermodel spread in the circulation response to the radiative effects of future GHG forcing – which include tropical upper tropospheric warming, as well as Arctic sea-ice loss and associated warming – has been shown to arise from intermodel spread in the circulation response to Arctic sea-ice loss (Cattiaux and Cassou, 2013; Harvey et al., 2014, 2015; Barnes and Polvani, 2015).

In this thesis, the overall aim is to improve understanding of the influence of Arctic sea-ice loss on mid-latitude weather and climate, and the mechanisms involved. The issues of complexity and statistical robustness are partly addressed by conducting idealised several-century-long numerical modelling experiments using an intermediate complexity global circulation model, IGCM4. To understand the contrasting model responses to sea-ice loss in past studies, a series of experiments is conducted to systematically examine various aspects that may explain these contrasting results, including different regions and magnitudes of loss as well as atmospheric internal variability.

A better understanding of the mechanisms involved is obtained by decomposing the response into parts due to tropospheric and stratospheric mechanisms.

The remainder of this chapter will give a thorough background to the topic of this thesis, including: more details on Arctic sea-ice loss, Arctic Amplification, and recent trends in mid-latitude weather and climate; the potential mechanisms involved in the influence of Arctic sea-ice loss on mid-latitudes, as well as current evidence for this influence and reasons for uncertainty in the nature of this influence; further explanation of the wider relevance of understanding the response to Arctic sea-ice loss; and, finally, a note on the benefits of using an intermediate complexity global circulation model. The chapter will finish by re-iterating the overall thesis aim, and by stating the research questions posed to address this aim. A more thorough outline of the original work carried out in the thesis to address these research questions will also be given.

1.1 Literature Review

1.1.1 Changes in the Arctic

1.1.1.1 Arctic sea-ice loss

Since the beginning of the satellite era in 1979, sea-ice cover across the whole Arctic has been continuously monitored with an approximately daily temporal resolution (Vaughan et al., 2013). Sea-ice cover is measured in terms of various different quantities, such as the sea-ice concentration (SIC) – which describes the percentage of an ocean grid cell covered by sea-ice – and the sea-ice extent (SIE) – which describes the area of all ocean grid cells that are defined as 'ice-covered' based on a threshold of at least 15% SIC for each cell.

Climatologically, Arctic sea-ice cover reaches its maximum in February or March with an SIE of $\sim 15 \times 10^6$ km^2, and its minimum in September with an SIE of $\sim 6 \times 10^6$ km^2 (Comiso and Nishio, 2008; Cavalieri and Parkinson, 2012). Since 1979, however, Arctic SIE has declined in all months by varying amounts and, in particular, by more than 13% per decade in September (NSIDC, 2016a). Indeed, very low minimum SIEs have been observed in many years of the past decade or so (NSIDC, 2019), where a record low was reached in 2012 ($\sim 3.4 \times 10^6$ km^2), followed by second lowest minimums in 2007 and 2016 ($\sim 4.2 \times 10^6$ km^2) (Vaughan et al., 2013; NSIDC, 2016b).

As well as there being seasonal differences in the magnitude of sea-ice loss trends, there are also seasonal differences in the spatial pattern of these trends: specifically, these trends are more focused around the southern sea-ice edge in winter and spring (particularly the Barents Sea, Sea of Okhotsk, Greenland Sea, and Baffin Bay), and more focused in the central Arctic in summer and autumn (particularly the Beaufort, Chukchi, East Siberian, Laptev, and Kara Seas) (Vaughan et al., 2013; Onarheim et al., 2018). Differences in the spatial pattern of sea-ice loss also occur from year-to-year, partly due to natural variability of the atmospheric circulation (Deser et al., 2000; Ukita et al., 2007; Chen et al., 2016; Close et al., 2017).

Regarding the cause of the observed decline in Arctic SIE, the Intergovernmental Panel on Climate Change (IPCC) conclude that the primary cause is global warming due to greenhouse gas (GHG) and other anthropogenic forcings (Bindoff et al., 2013). This is based on a large set of climate model results showing that observed sea-ice loss is only simulated when these forcings are included. There is also observational evidence of this, where there is a clear linear relationship between sea-ice loss and cumulative anthropogenic CO_2 emissions in all months (Notz and Stroeve, 2016; Stroeve and Notz, 2018). Other climate modelling studies estimate that a large proportion of observed September sea-ice trends are due to internal climate variability (e.g. 33% in Ding et al. 2019, 33%-48% in Stroeve et al. 2012, and around 50% in England et al. 2019).

Looking to future projections for the late 21st century, the IPCC conclude – based on the results of the Coupled Model Intercomparison Project Phase 5 (CMIP5) – that it is 'very likely' that Arctic SIE will continue to reduce in all months in response to GHG and other anthropogenic forcings (Collins et al., 2013). For a high-end anthropogenic emissions scenario (Representative Concentration Pathway 8.5, RCP8.5), the multi-model ensemble mean projects reductions in Arctic SIE of 34% in February and 94% in September, for 2081-2100 compared to 1986-2005. However, there is large disagreement in both the spatial pattern and magnitude of this projected future sea-ice loss between different climate models (Holland and Bitz, 2003; Stroeve et al., 2012; Screen, 2017b).

1.1.1.2 Arctic Amplification

Arctic sea-ice loss is just one manifestation of changes occurring in the Arctic. In particular, while global mean surface temperatures have risen in response to anthropogenic increases in GHG concentrations, there has been an observed enhancement of this

warming in the Arctic relative to that of lower latitudes (Bindoff et al., 2013). This enhanced warming is commonly referred to as 'Arctic Amplification' or AA (Serreze et al., 2009; Screen and Simmonds, 2010; Cohen et al., 2014).

Both Screen and Simmonds (2010) and Cohen et al. (2014) find evidence of AA in ERA-interim reanalysis data (Dee et al., 2011) for all seasons in recent decades, but particularly in autumn and winter. This AA is a near-surface phenomenon, which mostly occurs below around 850 hPa and strongly decreases with height in all seasons except summer. At its strongest in autumn and winter, AA is associated with lower-tropospheric and polar-cap average temperature trends of around 1°C per decade for 1979-2014 (Cohen et al., 2014) and 1.6°C per decade for 1989-2008 (Screen and Simmonds, 2010), which is around double the rate of warming at lower latitudes. Serreze et al. (2009) find similar evidence of recent AA in NCEP/NCAR and JRA-25 reanalysis data.

The AA observed over recent decades is likely to be a response to increased anthropogenic GHG's rather than being a manifestation of internal variability, since Bindoff et al. (2013) highlight – based on multi-model evidence from the Coupled Model Intercomparison Project Phase 3 (CMIP3) – that AA consistent with observations is found in climate models only when the effects of increased GHG's are included. This also suggests that the observed AA in reanalysis data is not a spurious trend resulting from, for example, the known issue of sparse on-the-ground surface temperature measurements over the Arctic Ocean and reliance, therefore, on satellite data in this region (Screen and Simmonds, 2010).

Looking to future projections of AA, Holland and Bitz (2003) find a range of Arctic warming from 1.5 to 4.5 times that of global mean warming in their 2xCO_2 experiments with various coupled climate models. Furthermore, Barnes and Polvani (2015) find evidence of AA by 2100 in every model and season, for 27 state-of-the-art climate models from CMIP5 forced by RCP8.5 anthropogenic GHG forcing. In the IPCC's Fifth Assessment Report (AR5), it is further concluded based on CMIP5 model simulations for all RCP anthropogenic GHG forcing scenarios that – out of all regions globally – the Arctic region will warm the most by the end of the 21st century (with very high confidence) (Collins et al., 2013).

However, while projections robustly suggest that AA will occur in the future under warming scenarios, there is large disagreement between different climate models in terms of both the spatial pattern and magnitude of this warming (Holland and Bitz,

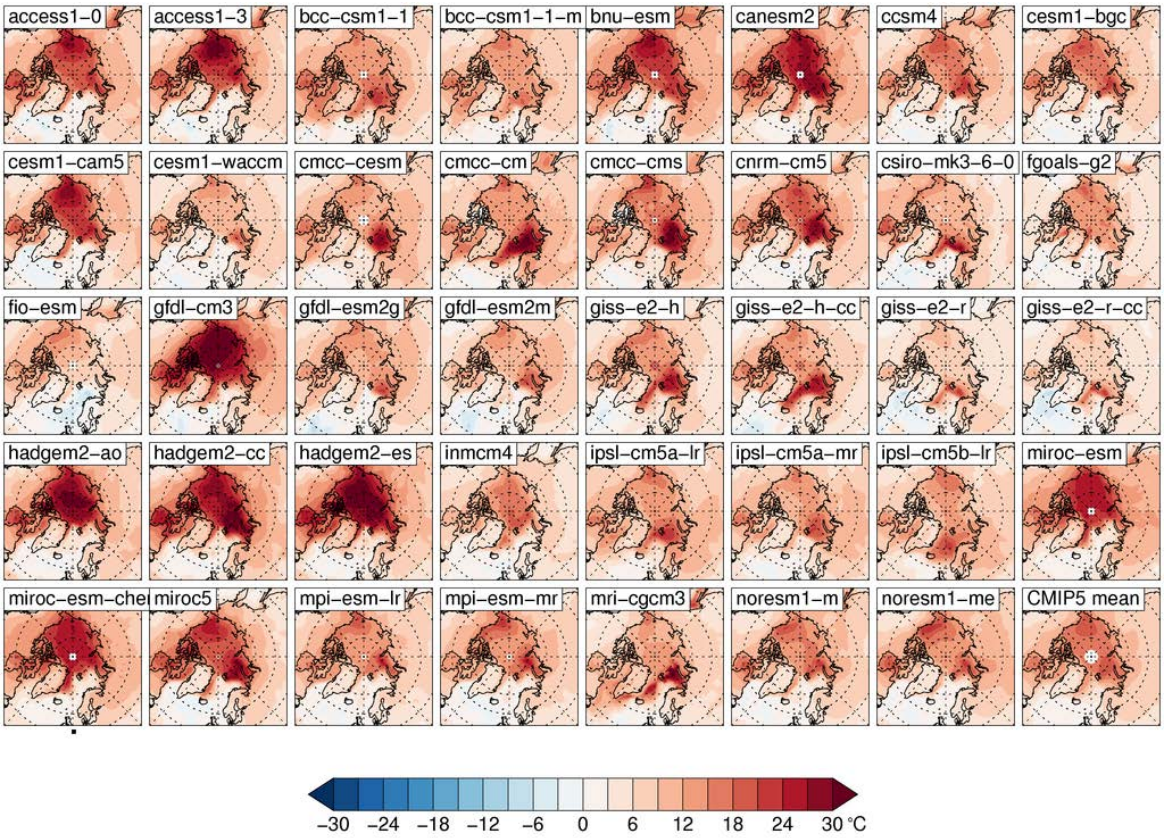

Fig. 1.1 Projected late 21st century change in winter (DJF) surface temperature from different CMIP5 models. Changes are calculated from differences between time-slice means over the period 2070-2099 of the RCP8.5 scenario simulations and 1970-1999 of the historical forcing simulations. The panel in the bottom right-hand corner shows the mean projected change for the CMIP5 models shown. See Appendix A for further details.

2003; Pithan and Mauritsen, 2014; Boeke and Taylor, 2016, 2018). Figure 1.1 shows this model diversity for projections of late 21st century winter surface temperature for CMIP5 models under an RCP8.5 forcing scenario (see Appendix A for a model list).

Mechanisms

There are various mechanisms that have been proposed to explain AA, as detailed in the review papers of Serreze and Barry (2011) and Goosse et al. (2018). These include Arctic sea-ice loss, land snow retreat, temperature feedbacks (including the Planck and lapse rate feedbacks), cloud and water vapour feedbacks, and increased poleward

energy transport by the atmosphere and oceans. Each of these mechanisms will now be explained, and evidence of their importance for AA reviewed.

Arctic sea-ice loss leads to AA by modifying the surface energy budget through a combination of two feedbacks (Serreze et al., 2009; Screen and Simmonds, 2010; Screen et al., 2012; Dai et al., 2019; Duan et al., 2019). In the surface albedo feedback, sea-ice retreat exposes the darker ocean surface below, which has a lower surface albedo and thus absorbs more solar radiation. In the insulation feedback, the removal of sea-ice allows for greater energy exchange between the ocean surface and the atmosphere. Therefore, reductions in Arctic sea-ice cover due to GHG forcing enhance ocean heat uptake in summer – which is when the atmosphere is climatologically warmest relative to the ocean surface and, hence, the air-sea heat flux is downwards. This extra heat is then subsequently released into the atmosphere in autumn and winter – which is when the ocean is climatologically warmest relative to the atmosphere and, hence, the air-sea heat flux is upwards. This extra heat release is also aided by a warmer ocean surface further reducing sea-ice, as well as delaying the annual refreeze in autumn and winter.

One of the central arguments suggesting Arctic sea-ice loss is a key cause of AA is their correspondence in seasonality and spatial pattern. Indeed, Serreze et al. (2009) highlight that AA is confined to the near-surface in NCEP/NCAR and JRA-25 reanalysis data, consistent with an anomalous surface heat source such as sea-ice loss. Furthermore, they also highlight that both AA and atmospheric warming due to Arctic sea-ice loss are largest in autumn and winter. More quantitatively, Screen and Simmonds (2010) linearly regress ERA-interim reanalysis zonal mean temperature data onto SIC averaged north of 70°N for the period 1989-2008, and find that sea-ice trends explain much of the magnitude and pattern of temperature trends in all seasons. Screen et al. (2012) also show – using atmospheric general circulation model (AGCM) simulations – that Arctic SIC and associated local sea surface temperature (SST) changes explain a large portion of observed near-surface Arctic warming.

More recently, Duan et al. (2019) used the NCAR Community Earth System Model (CESM) to show that polar warming in response to increases in CO_2 is doubled in simulations with the existence of sea-ice and land snow. Furthermore, Dai et al. (2019) conducted a comprehensive study using a combination of ERA-interim reanalysis data, CMIP5 model simulations under RCP8.5 anthropogenic forcings up to 2300, and two CESM1 simulations forced by increases in CO_2 with and without fixed SIC. It was

found that sea-ice loss is necessary for large AA, with large AA only occurring when there is large sea-ice loss, and in areas of large sea-ice loss.

The above evidence implies a link between the aforementioned spread in model projections of future Arctic sea-ice loss, and spread in projections of future AA, in terms of both the spatial pattern and magnitude. Indeed, such a link has also been suggested in the IPCC's AR5 report (although intermodel differences in the simulation of other mechanisms playing a role in AA may also contribute in part to this spread in AA projections; Collins et al., 2013). Both Holland and Bitz (2003) and Dai et al. (2019) find that larger future AA is simulated in climate models with larger sea-ice loss, which also tend to be those models with a more extensive historical climatological mean Arctic sea-ice cover. Pithan and Mauritsen (2014) also show that the largest spread in CMIP5 climate model projections of Arctic warming under $4xCO_2$ forcing comes from spread in the surface albedo feedback associated with Arctic sea-ice and land snow retreat. Furthermore, the spatial pattern of simulated Arctic warming in climate models has been found to be related to the initial spatial distribution of Arctic sea-ice, since this determines the subsequent location of sea-ice loss (Holland and Bitz, 2003; Räisänen, 2007; Bracegirdle and Stephenson, 2012).

With regards to mechanisms proposed to explain AA besides sea-ice loss, Pithan and Mauritsen (2014) analyse CMIP5 $4xCO_2$ simulations and find that the largest contribution to AA – in terms of the multi-model mean – is from temperature feedbacks (the Planck and lapse-rate feedbacks), and the second largest is from the surface albedo feedback associated with Arctic sea-ice and land snow retreat. The Planck feedback can be explained by the Stefan-Boltzmann Law, $B \propto T^4$, which describes the longwave radiation B emitted by a body with temperature T. The non-linearity of this relationship means that, since the Arctic is colder than lower latitudes, a larger temperature increase is required in the Arctic to balance a given radiative forcing.

The lapse-rate feedback is explained by the fact that (limited) radiosonde observations indicate that the Arctic boundary layer is characterised by strong temperature inversions, or an increase in temperature with height (Serreze et al., 1992; Liu et al., 2006; Zhang et al., 2011). These inversions result in high levels of vertical stability, thus inhibiting vertical mixing and confining any surface based warming to a limited vertical extent. In the highly convective environment of the tropics, however, a warming climate results in enhanced convection, resulting in greater latent heat release in upper tropospheric levels and enhanced upper tropospheric warming compared to

the surface. This further enhances near-surface warming in the Arctic relative to the tropics. Evidence of the importance of the lapse-rate feedback for AA is also found in the earlier CO_2 doubling experiments of Manabe and Wetherald (1975) using a simplified three-dimensional general circulation model (GCM), and in the idealised climate change experiments of Bintanja et al. (2012) using a coupled climate model.

The water vapour feedback may also play a role in Arctic warming, as shown in various studies using observational data (Dessler et al., 2008; Gordon et al., 2013), individual climate model simulations with increases in GHG's (Graversen and Wang, 2009; Gordon et al., 2013; Taylor et al., 2013), and CMIP5 4xCO_2 simulations (Pithan and Mauritsen, 2014; Goosse et al., 2018). This feedback involves an increase in the amount of water vapour in the atmosphere in response to a warming climate, which amplifies the greenhouse effect and enhances warming. However, due to the Clausius-Clapeyron relationship – in which the saturation water vapour pressure is exponentially related to the temperature, therefore implying that increases in water vapour are larger at higher temperatures – the water vapour feedback is stronger in the tropics than in the Arctic. Therefore, while the water vapour feedback does contribute to Arctic warming, it may not contribute to enhanced warming in the Arctic compared to lower latitudes, i.e. AA (Graversen and Wang, 2009; Taylor et al., 2013; Pithan and Mauritsen, 2014; Goosse et al., 2018).

It has also been found that sea-ice loss leads to an increase in cloud cover and, therefore, increased downwelling longwave radiation and Arctic warming (Vavrus, 2004; Taylor et al., 2013; Kay et al., 2016). However, clouds have also been found to act as a negative feedback: indeed, a warming climate increases the liquid water content in mixed-phase clouds and, therefore, causes a higher cloud reflectivity, greater reflection of incoming shortwave radiation, and reduced Arctic warming (Mitchell et al., 1989; Zelinka et al., 2012; Goosse et al., 2018). Differences in the magnitudes of these feedbacks between different CMIP5 climate models can explain why clouds either have an overall Arctic warming or cooling effect in response to 4xCO_2 forcing in different models (Pithan and Mauritsen, 2014).

Finally, more remote processes such as increased poleward energy transport may contribute to AA. In terms of atmospheric transport, Lee et al. (2011) show using ERA-40 reanalysis data that observed winter surface warming over Arctic sea-ice is explained by increased convection in the tropical Indo-western Pacific region, resulting anomalous Rossby wave propagation, and associated poleward stationary eddy heat

fluxes. Ding et al. (2014) similarly show in reanalysis data and a climate model forced by observed tropical SST's, that recent observed surface and tropospheric warming in Northeastern Canada and Greenland is due to a negative trend in the North Atlantic Oscillation (NAO), which has been caused by anomalous Rossby waves forced by tropical Pacific SST anomalies. Finally, Gong et al. (2017) show using ERA-interim reanalysis data that Arctic winter warming can be partly explained by changes in poleward-propagating Rossby waves enhancing poleward fluxes of moisture.

In terms of oceanic transport, coupled climate model simulations forced by idealised increases in CO_2 show increased heat advection into the Arctic due to increased Atlantic Sector overturning (Graham and Vellinga, 2013), and a 2000 year-long record of past ocean temperatures suggests that recent Arctic warming is linked to the unprecedented warmth of Atlantic Water entering the Arctic Ocean (Spielhagen et al., 2011).

However, in Pithan and Mauritsen (2014)'s comparison of the various feedbacks that contribute to the multi-model mean of AA in CMIP5 4xCO_2 experiments, changes in atmospheric and oceanic poleward energy transport are not as large as, for example, the surface albedo and temperature feedbacks. Furthermore, it is found in the AGCM simulations of Screen et al. (2012) that changes in remote SST's, and associated changes in poleward atmospheric energy transport, do not explain enhanced near-surface Arctic warming; instead these explain most of the observed Arctic tropospheric warming above 700 hPa. Note that they additionally find this upper level warming is enhanced in summer – as mentioned in the previous section – by other radiative forcings, such as changes in GHG's, ozone, and aerosols.

In summary, while various mechanisms have been shown to contribute to AA besides Arctic sea-ice loss – including land snow retreat, temperature feedbacks, cloud feedbacks, and increases in poleward energy transport – sea-ice loss is likely to be one of the major contributors.

1.1.2 Changes in mid-latitude weather and climate

While there has been an observed decline in sea-ice and amplified warming in the Arctic in recent decades, there has been an apparent increase in severe winter weather across some mid-latitude regions. These coincident trends have been commonly referred to as the 'Warm Arctic – Cold Continents' (WACC) pattern (Petoukhov and Semenov, 2010; Overland et al., 2011; Cohen et al., 2014, 2018; Chen et al., 2018).

For example, GISTEMP (GISS Surface Temperature Analysis) data shows that in central Eurasia average winter surface air temperatures have reduced by 1.25°C over the past 25 years (McCusker et al., 2016). Similar trends have been found in the same dataset by Cohen et al. (2014) and Shepherd (2016) for slightly different time-periods, but with an additional small cooling trend found in the eastern United States.

In terms of winter weather extremes, Cohen et al. (2014) show that for time series averaged for the land area between 20°N and 50°N, the annual coldest daily minimum temperature has decreased since 1990, and the frequency of unusually cold winter months – defined as more than two standard deviations below the 1951-1980 mean – reversed its long-term downward trend by the end of the 1990's. Indeed, there have also been recent unusually cold and snowy winters observed in 2006 (year is for January), 2010, 2011, 2017, and 2018 across parts of Eurasia (Petoukhov and Semenov, 2010; Guirguis et al., 2011; Osborn, 2011; Chen et al., 2018; Met Office, 2018; Greening and Hodgson, 2019), and in 2010, 2011, 2014, and 2019 across parts of North America (Guirguis et al., 2011; Van Oldenborgh et al., 2015; Climate Central, 2019).

As a specific example, in December 2016 and January 2017 parts of Siberia were around 20°C colder than the 1979-2000 climatological mean, while parts of the central Arctic were around 20°C warmer (Chen et al., 2018). Similarly, in March 2018 there were two periods of significant snowfall in the UK, temperatures were 2°C below the 1981-2010 mean in most areas, and – very unusually – air temperatures remained below freezing for over 48 hours across large areas at the start of the month (Met Office, 2018). This extreme winter weather – commonly referred to as the 'Beast from the East' in the media – coincided with anomalous warmth in the Arctic, where this warmth was linked to satellite era record-breaking Arctic SIE lows in January and February 2018 (NSIDC, 2018c,b), and an almost record-breaking SIE low in March 2018 (NSIDC, 2018a).

1.1.3 Evidence for an Arctic influence on mid-latitudes

The simultaneous occurrence of recent Arctic sea-ice loss and apparent increases in severe mid-latitude winters has led to much research into whether they are dynamically linked. Since all climate models project a continuation of Arctic sea-ice loss during the 21st century in response to anthropogenic GHG forcing, it is important that the potential influence of this on the highly populated mid-latitudes is better understood.

In this section, various types of evidence will be considered for an influence of Arctic sea-ice loss on mid-latitude weather and climate, following the 'Can it, has it, will it?' framework of Barnes and Screen (2015). Firstly, the mechanisms that can in theory support an Arctic influence on mid-latitudes will be reviewed ('Can it?'). Following this, a review will be given of evidence for an observed Arctic influence ('Has it?'), and of evidence for a potential future Arctic influence ('Will it?'). This framework is useful because it provides some clarity to the problem; indeed, the conclusions of past studies have appeared contradictory, and it can be argued that this has partly been due to confusion over the exact question being posed (Barnes and Screen, 2015).

1.1.3.1 Mechanisms for an Arctic influence: 'Can it?'

Various pathways have been proposed to connect Arctic sea-ice loss with changes in mid-latitude weather and climate, which involve either tropospheric or stratospheric mechanisms. Before explaining these, however, it will be helpful to firstly cover some key equations and approximations, as well as some theory on wave-mean flow diagnostics, where this information will largely be based on Hoskins and James (2014). Key features of the large-scale atmospheric circulation involved in these mechanisms will also be described and explained.

Key equations and approximations

A simplified set of equations, that are important in helping to diagnose mechanisms, comprises the horizontal and vertical momentum equations, the mass continuity or incompressibility equation, and the thermodynamic equation (listed by order of appearance):

$$\frac{D\mathbf{v}}{Dt} + f\,\hat{\mathbf{k}} \times \mathbf{v} = -\nabla_H \left(\frac{p'}{\rho_r}\right) \,, \tag{1.1}$$

$$\frac{Dw}{Dt} + \frac{\partial}{\partial z}\left(\frac{p'}{\rho_r}\right) = b' \,, \tag{1.2}$$

$$\nabla \cdot \mathbf{u} = 0 \,, \tag{1.3}$$

$$\frac{Db'}{Dt} + N^2 w = 0 \,, \tag{1.4}$$

where $\mathbf{v} = (u, v)$ and $\mathbf{u} = (u, v, w)$ (the zonal, meridional, and vertical wind components); $b' = g\theta'/\theta_r$ is the buoyancy (where dashes indicate perturbations, g is the gravitational acceleration, and θ_r is a constant reference potential temperature); f is

the Coriolis parameter; p' is the perturbation pressure; ρ_r is a reference atmospheric density (assumed constant); N^2 is the squared Brunt-Väisälä buoyancy frequency (a measure of the static stability); and $\nabla_H = \partial/\partial x + \partial/\partial y$. These equations neglect dissipation, and have been simplified under the anelastic approximation (an assumption that variations in density and pressure are dominated by their exponential decrease with height) and Boussinesq approximation (an assumption that the density is constant except in the buoyancy term, such that it is only considered when density variations are responsible for vertical motion).

An important consequence of the momentum equations can been seen by applying the hydrostatic and geostrophic balance approximations. Hydrostatic balance assumes that vertical length scales in the atmosphere are much smaller than horizontal length scales; the acceleration term can then be neglected in the vertical momentum equation, meaning that gravity is in balance with the vertical pressure gradient. Geostrophic balance assumes large horizontal length scales, L, or a very small Rossby number ($Ro = U/fL \ll 1$, where U is a typical horizontal wind speed); the acceleration term can then be neglected in the horizontal momentum equation, meaning that the pressure gradient force is in balance with the Coriolis force. Combining these balances gives the thermal-wind relation:

$$f\frac{\partial u}{\partial z} = -\frac{\partial b'}{\partial y} \; ; \; f\frac{\partial v}{\partial z} = \frac{\partial b'}{\partial x} \; . \tag{1.5}$$

Importantly, this shows that the vertical shear in the geostrophic zonal wind is proportional to the meridional temperature gradient.

Wave-mean flow diagnostics

It is also useful to derive wave-mean flow diagnostics to understand the effect of Rossby wave propagation on the mean flow, and conversely the effect of the mean flow on Rossby wave propagation. These effects are respectively diagnosed using Eliassen-Palm flux (EP-flux) vectors and their divergence, and the refractive index.

Firstly, EP-flux vectors, $\mathbf{F} = (F_\phi, F_z)$, and their divergence, $\nabla \cdot \mathbf{F}$, are given by:

$$F_\phi \propto -[u^* v^*] \; , \tag{1.6}$$

$$F_z \propto [v^* b^*] \; , \tag{1.7}$$

$$\frac{\partial [u]}{\partial t} = f[v]_{res} + \frac{1}{\rho_r}\nabla \cdot \mathbf{F} + \text{other terms} \; , \tag{1.8}$$

where ϕ is the latitude, square brackets denote zonal means, asterisks denote deviations from the zonal mean (due to waves), and $[v]_{res}$ is a residual meridional circulation. These are derived by using incompressibility to write the zonal momentum and thermodynamic equations in flux form. Terms are then separated into zonal mean and deviation parts, the zonal mean of each resulting equation is taken, and the quasi-geostrophic approximation is applied (which assumes the system is close to geostrophic balance such that terms of order Ro^2 or greater are neglected).

The EP-flux vectors and their divergence respectively show the direction of energy propagation by quasi-geostrophic Rossby waves, and the forcing on the zonal mean zonal wind due to these waves. Physically, this can be understood as follows. In terms of the meridional component, F_ϕ, this depends on the zonal mean eddy momentum flux, $[u^*v^*]$; as such, this is related to the forcing of waves on the zonal mean zonal wind due to their associated meridional fluxes of zonal momentum (and divergence thereof). As for the vertical component, F_z, this depends on the zonal mean eddy heat flux, $[v^*b^*]$. This describes the meridional flux of heat due to waves, which alters the meridional temperature gradient and results in an adjustment of the vertical shear in the zonal wind to maintain thermal-wind balance. Therefore, the effect of the zonal mean eddy heat flux is to redistribute momentum in the vertical, and it is as if there is a vertical eddy flux of zonal momentum that is proportional to the horizontal eddy flux of heat.

Secondly, Holton and Hakim (2013) define a refractive index, n_k, from the conservation of quasi-geostrophic potential vorticity, $Dq/Dt = 0$. This conservation equation is derived from the quasi-geostrophic thermodynamic and vorticity equations, where the latter is obtained from incompressibility combined with the curl of the horizontal momentum equation. To calculate n_k, the conservation equation is divided into zonal mean and deviation parts, and then linearised (such that products of perturbations are neglected, since perturbations are assumed to be small). The zonal mean zonal wind is then assumed to depend on both latitude and height, $[u] = [u(y, z)]$, and wave-like solutions of the form $\psi^* = e^{z/2H}\mathrm{Re}\left\{\Psi(y, z)e^{ik(x-c_x t)}\right\}$ are sought yielding:

$$\frac{\partial^2\Psi}{\partial y^2} + \frac{f^2}{N^2}\frac{\partial^2\Psi}{\partial z^2} + n_k^2\Psi = 0 \ , \tag{1.9}$$

where:

$$n_k^2(y, z) = \frac{1}{[u] - c_x}\frac{\partial[q]}{\partial y} - k^2 - \frac{f^2}{4H^2N^2} \ . \tag{1.10}$$

H is a scale height, ψ is the streamfunction, Ψ is the wave amplitude, k is the zonal wavenumber, and c_x is the zonal phase speed. Note that equations 1.9 and 1.10 neglect dissipation.

According to equations 1.9 and 1.10, real solutions for Ψ only exist – or Rossby waves can only propagate – for positive n_k^2. As such, large-scale (low wavenumber) stationary waves ($c_x = 0$) will only propagate in a westerly mean flow that is not too strong. Furthermore, they will also not propagate in an easterly flow, since when $[u] = 0$ (known as the 'critical line') n_k^2 becomes singular. This leads to a violation of the linearity assumption or the neglect of dissipation, and subsequent wavebreaking, where this is defined as the rapid and irreversible overturning of waves (Hoskins and Karoly, 1981; McIntyre and Palmer, 1983, 1984, 1985; Barnes and Hartmann, 2012).

The large-scale atmospheric circulation

The mechanisms proposed to explain an influence of Arctic sea-ice loss on mid-latitude weather and climate involve key features of the large-scale atmospheric circulation, including the tropospheric subtropical (or thermally-driven) and eddy-driven jets, the Arctic Oscillation, and the stratospheric polar vortex. These mechanisms and circulation features are depicted in the schematic from Cohen et al. (2014) in Figure 1.2.

The subtropical jet is a strong westerly jet with strong vertical shear that exists in the subtropical upper troposphere at the poleward flank of the Hadley cell. The Hadley cell is a large-scale meridional overturning circulation in the tropics, which describes the rising of air near the equator and the sinking of air in the subtropics, where this is driven by tropical radiative heating and thermal convection (e.g. Holton and Hakim, 2013). The subtropical jet is, to first order, generated by angular momentum transport by the Hadley cell (Held and Hou, 1980). Energy transport by the Hadley cell also respectively weakens and enhances the tropical and subtropical climatological meridional temperature gradients (Lindzen and Hou, 1988), where the latter balances the subtropical jet's strong vertical shear through the thermal-wind relation.

The eddy-driven jet, on the other hand, is a westerly jet that is deeper in structure and defined by a lower tropospheric maximum in zonal winds. This jet is maintained by the eddy momentum flux convergence of baroclinic eddies generated by baroclinic instability in regions of enhanced baroclinicity (regions of strong horizontal and/or vertical temperature gradients) (Held, 1975; Rhines, 1975; Panetta, 1993; Li and Wettstein, 2012). While the subtropics are one such region as outlined above, baroclinic

waves are also prevalent in the strong baroclinic regions of mid-latitudes (e.g. around warm ocean boundary currents such as the North Atlantic Gulf Stream) (Lee and Kim, 2003; Eichelberger and Hartmann, 2007; Shaw et al., 2016). In the North Atlantic sector, mid-latitudes are the region of strongest baroclinicity and, thus, the eddy-driven jet is typically found in mid-latitudes in this sector (distinct from the subtropical jet); in the North Pacific sector, on the other hand, the region of strongest baroclinicity is in the subtropics and, thus, the eddy-driven and subtropical jets are more co-located (Lee and Kim, 2003). Surface orography can also generate stationary waves that converge momentum onto the eddy-driven jet, therefore contributing to its maintenance (Held et al., 2002; Shaw et al., 2016).

The subtropical jet acts as a waveguide for the eddy-driven jet (Lee and Kim, 2003; Brayshaw et al., 2008; Barnes and Hartmann, 2011), and the maintenance of the eddy-driven jet also affects the subtropical jet. This latter effect involves vertical wave propagation in a baroclinic region converging westerly momentum at lower tropospheric levels, which can reduce the vertical shear of the subtropical jet, and meridional wave propagation converging westerly momentum at upper tropospheric levels, which can strengthen the subtropical jet (see the EP-flux equations 1.6-1.8; Gerber and Vallis, 2007; Thompson and Birner, 2012). As such, these jets are highly interconnected (see E in Figure 1.2a) and will sometimes be referred to together as the 'tropospheric jet'.

Variability of the subtropical and eddy-driven jets is associated with the Arctic Oscillation or AO. The AO describes the observed oscillation in geopotential height anomalies between high and middle Northern Hemisphere latitudes, where anomalous positive (negative) and negative (positive) heights respectively define its negative (positive) phase (see Figure 1.2b). The negative and positive AO phases are respectively associated with a strengthening and weakening of the zonal mean subtropical jet as well as Pacific sector eddy-driven jet, and an equatorward and poleward shift of the Atlantic sector eddy-driven jet (Thompson and Wallace, 2000; Ambaum et al., 2001). This respectively results in colder and warmer conditions in key regions of mid-latitudes (Lorenz, 1951; Kutzbach, 1970; Thompson and Wallace, 1998, 2000).

Moving upwards into the stratosphere, the stratospheric polar vortex (or 'polar vortex' for short) will now be described and the dynamics of this vortex explained, where this explanation will be largely based on Holton and Hakim (2013). The polar vortex describes the strong band of westerly winds that circle the Arctic stratosphere in autumn and winter, centred around 60°N. These winds form due to an absence of

incoming solar radiation during the polar night, which leads to stratospheric cooling over the Arctic and, thus, an increase in the zonal wind with height to maintain thermal-wind balance. Over spring and summer, this vortex breaks down due to increases in solar radiation warming the Arctic stratosphere.

The polar vortex exhibits considerable intraseasonal and interannual variability, which includes sudden stratospheric warming (SSW) events. These SSWs occur around every two years during winter (November to March), and are characterised by a sudden breakdown of the polar vortex within a few days. This causes large-scale warming of the Arctic stratosphere, which reverses the meridional temperature gradient and, thus, is associated with a reversal in zonal winds from westerly to easterly. SSWs have been shown in both observational and modelling studies to have a strong downward influence on the troposphere, and are associated with the development of a negative AO pattern in the troposphere within around 10 days of the SSW occurring, which can last for many weeks (Baldwin and Dunkerton, 1999, 2001; Charlton et al., 2004; Simpson et al., 2011; Hitchcock and Simpson, 2014; Hitchcock and Haynes, 2016).

The mechanisms causing an SSW were first shown in numerical integrations of the adiabatic-geostrophic potential vorticity equation by Matsuno (1971), and have also been shown in reanalysis data as well as in full complexity AGCM's (e.g. Garfinkel et al., 2010). In particular, SSWs are caused by the enhanced upward propagation of stationary Rossby waves into the stratosphere, which are generated in the troposphere by orography and land-sea thermal contrasts (Held et al., 2002). Both theoretical arguments and observations show that this only involves large-scale (zonal wavenumber-1/2/3 or wave-1/2/3) waves (Charney and Drazin, 1961; Matsuno, 1970; Hoskins and James, 2014). Indeed, this can be seen from the refractive index equation (1.9 and 1.10), which shows that for a strong westerly flow – such as that associated with the polar vortex – propagation is favoured for a low wavenumber.

As can be seen from the vertical EP-flux (equation 1.7), this anomalous upward wave propagation transports easterly angular momentum upwards which weakens the stratospheric flow (Baldwin and Dunkerton, 2001). This weakening of the flow then increases the refractive index, encouraging more anomalous upward wave propagation into the stratosphere and further deceleration of the zonal winds. Once the wind becomes easterly, a critical line is then formed, above which linear waves can no longer propagate. This leads to wavebreaking and strong EP-flux convergence below the critical line, encouraging stronger deceleration of the zonal winds at this lower level. As

such, the process then repeats itself over and over, resulting in a subsequent downward propagation of the critical line and associated easterly wind anomalies. In this way, SSWs have a downward influence on the tropospheric circulation or AO.

Alternative theories of how SSWs can influence the troposphere have also been reviewed by Song and Robinson (2004). For example, various studies suggest that while anomalous wave driving in the stratosphere and associated EP-flux convergence leads to a weakening of the zonal wind, this is partially offset by an anomalous poleward flow (as can be seen from the $f[v]_{res}$ term in the EP-flux divergence equation, 1.8). This generates anomalous secondary meridional circulations, which can extend downward into the troposphere (e.g. Haynes et al., 1991). It has also been suggested that SSWs are associated with a redistribution of mass in the stratosphere toward the North Pole, which may itself directly influence surface pressure (e.g. Baldwin and Dunkerton, 1999). Furthermore, when nudging an AGCM toward a specific reference SSW, Hitchcock and Simpson (2016) find that the anomalous tropospheric winds caused by the downward influence of the SSW can only explain part of the total tropospheric negative AO response; the remainder is caused by tropospheric eddy feedbacks.

Tropospheric mechanisms for an Arctic influence

Various tropospheric mechanisms have been proposed to potentially explain an influence of Arctic sea-ice loss on mid-latitude weather and climate (see Figure 1.2).

For instance, it has been found using both observations and models that Arctic sea-ice loss can modify tropospheric stationary Rossby wave propagation, which leads to a local anticyclonic response and stronger cold air advection over adjacent continents (Honda et al., 2009; Petoukhov and Semenov, 2010; Mori et al., 2014, 2019). Indeed, theoretical arguments show that the steady linear response to a shallow thermal anomaly in the extratropics – similar to the AA associated with sea-ice loss – is a local anticyclone in the mid-troposphere (Hoskins and Karoly, 1981). This can be seen from the thermal-wind relation written in terms of the vertical component of relative vorticity, $\xi = \partial v/\partial x - \partial u/\partial y$:

$$f\frac{\partial \xi}{\partial z} = \nabla_H^2 b' \ . \tag{1.11}$$

Assuming a wave-like thermal anomaly in the x direction of wavenumber k, $b' \propto \sin(kx)$, it is found that:

$$f\frac{\partial \xi}{\partial z} \propto -k^2 b' \ , \tag{1.12}$$

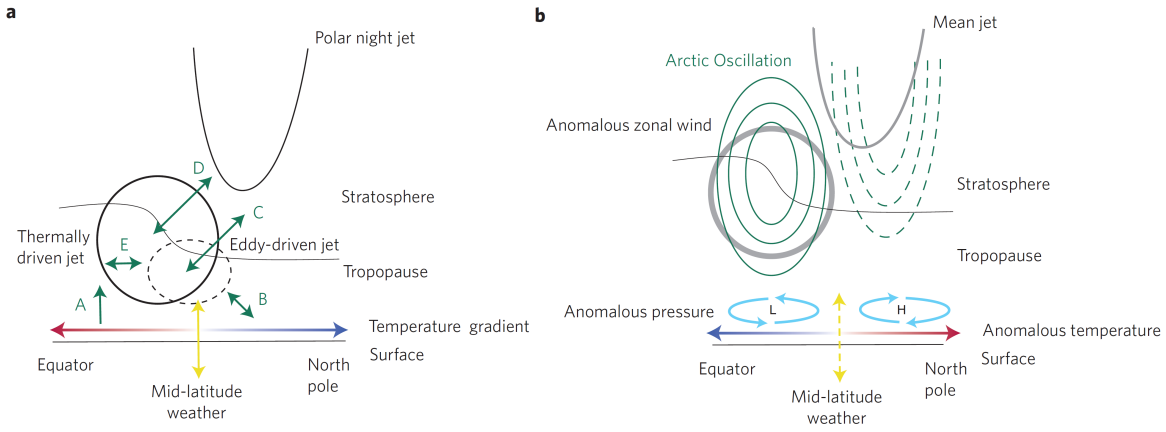

Fig. 1.2 Schematic from Cohen et al. (2014) summarising key mechanisms for the influence of Arctic sea-ice loss and associated warming on mid-latitude weather and climate. (a) Mechanisms involving the tropospheric thermally-driven (subtropical) and eddy-driven jets, and the stratospheric polar vortex (night jet). Green arrows indicate feedbacks. (b) Changes in the large-scale atmospheric circulation and surface temperature associated with a negative Arctic Oscillation (AO). The green solid (dashed) lines indicate positive (negative) zonal wind anomalies, and the grey lines indicate the climatological tropospheric jet and stratospheric polar vortex. [Reprinted by permission from Springer Nature Customer Service Centre GmbH: Nature Geoscience, 'Recent Arctic amplification and extreme mid-latitude weather', Cohen et al. (2014).]

and, therefore, for a shallow positive buoyancy anomaly, the vorticity must decrease with height from the surface (i.e. must become more anticyclonic).

It has also been shown in the observational studies of Francis and Vavrus (2012, 2015) that Arctic sea-ice loss and associated AA weakens the climatological meridional temperature gradient, thereby potentially resulting in a weakening of the subtropical jet to maintain thermal-wind balance (see A in Figure 1.2a). These studies, and Capua and Coumou (2016), further show that this is associated with a more meandering flow and, therefore, slower and more persistent eastward moving weather systems (or an increase in atmospheric 'blocking'). However, while Screen and Simmonds (2014) show that significantly larger amplitude Rossby waves are indeed associated with extreme mid-latitude weather in particular regions, other observational studies using different methodologies find no evidence of a link between AA and the Rossby wave amplitude or blocking frequency (Barnes, 2013; Screen and Simmonds, 2013; Barnes et al., 2014). Furthermore, Ronalds et al. (2018) find little mechanistic evidence of this in barotropic model simulations run with a polar forcing designed to represent AA, which instead show a decrease in tropospheric jet latitude variability.

Arctic sea-ice loss and associated warming may also result in a negative AO-like response – and therefore lower temperatures in Europe and the eastern United States – through various mechanisms, including tropospheric eddy feedbacks. In particular, this involves the modification of tropospheric eddy heat and momentum fluxes, and the associated effect of this on the eddy-driven jet and, thus, the AO (see B in Figure 1.2a). For example, it has been shown in modelling studies that the warming associated with Arctic sea-ice loss results in a direct stationary Rossby wave response, which itself can result in anomalous stationary eddy momentum and heat fluxes (Nakamura et al., 2016a), or in the subsequent modification of non-linear transient eddy momentum and heat fluxes (Magnusdottir et al., 2004; Deser et al., 2004, 2007; Ruggieri et al., 2019), both of which can project onto a negative AO-like response. Sellevold et al. (2016) do find limited evidence of the former mechanism, however, in baroclinic stationary wave model experiments with anomalous thermal forcing imposed in the Arctic.

The mechanisms proposed immediately above assume that the circulation (or vorticity) response to the anomalous diabatic heating associated with Arctic sea-ice loss is important for the initiation of tropospheric eddy feedbacks. Some studies have found though that the anomalous diabatic heating itself is more directly important. For example, in the observational study of Jaiser et al. (2012) they find that Arctic sea-ice loss and associated warming results in a reduction in vertical static stability and, therefore, an increase in baroclinic instability over the heating region. This results in the growth of baroclinic waves that, through transient eddy feedbacks, affect the eddy-driven jet and project onto a negative AO. Alternatively, Yang et al. (2016) find in observations that sea-ice loss in the Barents-Kara Seas results in a reduction of the meridional temperature gradient south of the heating region. This reduces the zonal wind in this region (to maintain thermal-wind balance), which sharpens the meridional wind shear on the poleward side of the tropospheric jet. Subsequent barotropic instability then results in eddy growth, facilitating stationary and transient eddy feedbacks which project onto a negative AO.

Stratospheric mechanisms for an Arctic influence

Sea-ice loss has also been shown to result in a negative AO through stratospheric mechanisms (see C and D in Figure 1.2a). Specifically, the anomalous thermal forcing associated with sea-ice loss has been shown to enhance upward wave propagation, due to the constructive interference (Nishii et al., 2009; Smith et al., 2010) of anomalous forced and climatological large-scale stationary Rossby waves. This weakens the stratospheric

polar vortex, which subsequently results in a negative tropospheric AO response (Kim et al., 2014; Peings and Magnusdottir, 2014; García-Serrano et al., 2015; Nakamura et al., 2015; King et al., 2016; Nakamura et al., 2016a,b; Wu and Smith, 2016; Zhang et al., 2018a). It has also been specifically found that an increased frequency of stratospheric weak polar vortex events is important for the stratospheric response to recent sea-ice loss (Kim et al., 2014; Peings and Magnusdottir, 2014; Jaiser et al., 2016) and future loss in autumn (Sun et al., 2015), and that stronger stratosphere-troposphere coupling occurs during these events in response to recent ice loss (Hoshi et al., 2019).

Climate modelling experiments using a stratospheric nudging method to constrain the stratospheric evolution have provided objective evidence that stratospheric mechanisms may play a dominant role in the tropospheric AO response to past sea-ice loss (Nakamura et al., 2016b; Zhang et al., 2018a,b). However, Wu and Smith (2016) also use this technique and find equal roles played by stratospheric and tropospheric mechanisms for various amplitudes of imposed AA-like thermal forcings (ranging from smaller AA to late 21st century AA).

Summary: 'Can it?'

In summary, a multitude of tropospheric and stratospheric mechanisms – most likely tropospheric stationary Rossby wave propagation, tropospheric eddy feedbacks, and changes in the stratospheric polar vortex – can potentially explain an influence of Arctic sea-ice loss on mid-latitude weather and climate. While this multitude does highlight a lack of agreement between studies regarding the dominant mechanisms involved (Barnes and Screen, 2015), the evidence presented in this section supports the plausibility of a causal link.

1.1.3.2 Evidence for an observed Arctic influence: 'Has it?'

It will now be examined whether there is evidence that Arctic sea-ice loss has had an influence on mid-latitude weather and climate in the recent past, by reviewing both observational and modelling studies.

Observational studies

There is a large amount of observational evidence suggesting that recent Arctic sea-ice loss – through changes in tropospheric stationary Rossby wave propagation – may be

responsible for recent wintertime cooling trends in parts of Eurasia. Indeed, statistical analysis performed for a variety of different sea-ice and reanalysis datasets has suggested that, in recent decades, sea-ice loss in the Barents-Kara Seas (BKS) in autumn and winter has led to a local strengthening of the Siberian High, resulting in stronger northerly advection of cold Arctic air towards central Eurasia in winter (Honda et al., 2009; Inoue et al., 2012; Mori et al., 2014; Yao et al., 2017). For example, Luo et al. (2016) find evidence of this link by linearly regressing winter mean mid-tropospheric geopotential height and surface air temperature anomalies onto BKS sea-ice extent over the period 1979-2013 (with and without long-term trends removed). Furthermore, Kretschmer et al. (2016) show evidence of this link using a 'Causal Effect Networks' method, which – for a set of chosen 'actors' or variables – tests for all possible relationships between different actors (e.g. for all leads and lags, for whether actors are indirectly related through another actor, and so on). Kug et al. (2015) additionally show using lead-lag regression that recent severe winters in parts of North America may be explained by anomalous warming in the East Siberian-Chukchi Seas leading to a local anticyclonic response, the downstream development of a trough over North America, and increased northerly cold air advection.

Observational studies also suggest that recent sea-ice loss may have influenced mid-latitude weather and climate through stratospheric mechanisms. For instance, Zhang et al. (2016) and Seviour (2017) show that over the last three decades, there has been a statistically significant shift of the stratospheric polar vortex toward the Eurasian continent in winter. Zhang et al. (2016) show that this shift may have been caused by the enhanced upward propagation of wave-1 stationary Rossby waves due to BKS sea-ice loss, and that it may explain recent wintertime cooling trends in parts of Eurasia and North America. Similarly, many studies have shown that recent autumn and early winter sea-ice loss – particularly in the BKS region – may have enhanced the upward propagation of wave-1/2 stationary Rossby waves, leading to a weakening of the stratospheric polar vortex and a negative tropospheric AO-like response in the following winter (Jaiser et al., 2013; Kim et al., 2014; García-Serrano et al., 2015; King et al., 2016; Ruggieri et al., 2016; Kretschmer et al., 2016, 2018).

However, in terms of weather extremes, Screen (2014) show that there has in fact been a significant decrease in autumn (and to a lesser extent winter) intraseasonal temperature variability over mid- to high-latitudes in recent decades (using ERA-interim reanalysis and HadGHCND daily near-surface temperature data). They find

that this is a thermodynamic rather than dynamic effect, involving a warming of cold days (due to AA) associated with northerly advection, and a less rapid warming of warm days associated with southerly advection. Other observational analysis using NCEP/NCAR reanalysis data and a different methodology does, however, suggest an increase (decrease) in winter intraseasonal lower tropospheric temperature variability over mid-latitudes (high-latitudes) during the period of AA (Cohen, 2016).

In short, there is largely a consensus among observational studies that a correlation exists between recent Arctic sea-ice loss and trends in severe mid-latitude winters. However, a limitation of such observation-based analysis is that correlation does not imply causation. Instead, causation is better tested by running numerical model simulations with and without recent sea-ice loss imposed, which can then be used to objectively determine the response to sea-ice loss.

Modelling studies

There are many climate modelling studies that support observational evidence of an Arctic influence on mid-latitude winters through tropospheric stationary Rossby wave propagation. For example, studies imposing recent sea-ice loss in ensemble simulations with different climate models have found a local anticyclonic response aloft and, therefore, increased cold air advection over central Eurasia and/or North America (Honda et al., 2009; Mori et al., 2014; Kug et al., 2015; Mori et al., 2019). Similar evidence is also found in transient CMIP5 multi-model experiments with historical anthropogenic and natural forcings (Kug et al., 2015). Evidence of an initial local anticyclonic response to sea-ice loss is also found in the climate model experiments of Magnusdottir et al. (2004) and Deser et al. (2004, 2007), but subsequent non-linear transient tropospheric eddy feedbacks additionally transform the response into a large-scale negative AO response.

A large number of climate modelling studies also show that recent mid-latitude late-winter trends can be explained, at least in part, by autumn and early winter sea-ice loss resulting in a weaker stratospheric polar vortex, which leads to a late-winter negative tropospheric AO response (Kim et al., 2014; Peings and Magnusdottir, 2014; Nakamura et al., 2015, 2016a; Jaiser et al., 2016). This is also in agreement with observational studies.

There are however also many modelling studies that are not supportive of a dominant influence of Arctic sea-ice loss on mid-latitude winters. For example, several modelling

studies find no robust evidence that recent BKS sea-ice loss has forced the observed strengthening of the Siberian High and colder central Eurasian winters (McCusker et al., 2016; Sun et al., 2016; Ogawa et al., 2018). Indeed, McCusker et al. (2016) found for very large ensembles of AGCM and coupled atmosphere-ocean GCM (AOGCM) simulations, that none of the AGCM ensemble members and only one of the fifty AOGCM ensemble members reproduced a strengthening of the Siberian High and central Eurasian winter cooling of the observed magnitude. It is therefore concluded that the observed cooling trend could be largely explained by a strengthening of the Siberian High associated with internal climate variability. Furthermore, Blackport et al. (2019) recently applied two independent causal inference methods – including a physics-based approach and lead-lag analysis – to interannual variability within large ensembles of present-day climate simulations using two coupled AOGCM's (and also within ERA-interim reanalysis data). This showed that atmospheric circulation anomalies simultaneously drive cold mid-latitude winters and warm Arctic conditions, where these anomalies precede – but importantly do not follow – regional sea-ice loss.

Contrasting stratospheric responses have also been found in climate models with imposed recent sea-ice retreat, where Screen et al. (2013) find a significant strengthening of the polar vortex in late-winter in CAM3, and Seviour (2017) find no robust evidence of a weakening or shift in the polar vortex in recent decades in the CESM1 Large Ensemble. This latter result is in contrast to the modelling results of Zhang et al. (2016), but likely reflects the use of a much larger ensemble in Seviour (2017); indeed, Seviour (2017) shows that a small number of individual ensemble members do simulate vortex trends similar to those in observations, leading to the conclusion that these observed trends may be largely associated with internal climate variability.

Similarly contradictory results are found for the tropospheric AO and North Atlantic Oscillation or NAO (similar to the AO but more confined to the North Atlantic). For instance, Orsolini et al. (2012) find a positive NAO in response to the large sea-ice loss in the Pacific and Siberian sectors of the Arctic in 2007, Screen et al. (2014) respectively find a positive AO response and no AO-like response for recent observed sea-ice loss imposed in the climate models CAM3 and UM7.3, and Smith et al. (2017) find oppositely signed NAO responses to recent sea-ice loss imposed in two simulations using the same climate model but with different background SST states. Furthermore, Screen (2017a) conduct two large (502 member) ensemble AGCM simulations with either high-ice or low-ice conditions, and show that although recent sea-ice loss does

lead to a negative NAO, the dynamical cooling this causes in Northern Europe is counteracted by the advection of warmed air from the Arctic.

Summary: 'Has it?'

To summarise, while there is largely a consensus among observational studies that a correlation exists between recent Arctic sea-ice loss and trends in mid-latitude winters, there is little consensus among modelling studies that sea-ice loss is the dominant cause of these mid-latitude trends. It has been suggested that this disparity between observations and models could be because observed winter trends are largely associated with internal climate variability, which dominates over any forced response to observed sea-ice loss. This will be discussed in more detail shortly.

1.1.3.3 Evidence for a potential future Arctic influence: 'Will it?'

It will now be examined whether there is evidence that projected Arctic sea-ice loss will potentially have an influence on future mid-latitude weather and climate.

As for recent sea-ice loss, model studies have shown that late 21st century sea-ice loss in the BKS region leads to a simulated local strengthening of the Siberian High and increased northerly advection over parts of Eurasia (Deser et al., 2010; Sun et al., 2015; Blackport and Kushner, 2017; McCusker et al., 2017; Oudar et al., 2017). It has also been shown that future sea-ice loss results in a simulated equatorward shift of the tropospheric jet in winter, or a negative tropospheric AO-like response, in a large number of different AGCM's and coupled AOGCM's (Scinocca et al., 2009; Seierstad and Bader, 2009; Deser et al., 2010; Peings and Magnusdottir, 2014; Sun et al., 2014, 2015; Nakamura et al., 2016a; Wu and Smith, 2016; Blackport and Kushner, 2017; McCusker et al., 2017; Oudar et al., 2017; England et al., 2018).

Some studies have found that a weakening of the stratospheric polar vortex is important for this negative AO response (Wu and Smith, 2016; Blackport and Kushner, 2017; McCusker et al., 2017), while others suggest that tropospheric mechanisms are more important. Indeed, it has been suggested that for the large Arctic warming associated with future sea-ice loss, a negative AO-like response is predominantly caused by a reduction in the climatological meridional temperature gradient and associated weakening of the poleward flank of the tropospheric jet to maintain thermal-wind balance (Peings and Magnusdottir, 2014; Nakamura et al., 2016a; Oudar et al., 2017).

However, there are also some studies that find either a positive AO-like tropospheric response in February (Petoukhov and Semenov, 2010), or no evidence of an AO-like response (Singarayer et al., 2006; Cai et al., 2012; Boland et al., 2016). Similarly, some studies have found contrasting responses in the stratospheric polar vortex, including a strengthening (Scinocca et al., 2009; Cai et al., 2012; Sun et al., 2014, 2015; Nakamura et al., 2016a; England et al., 2018), or no response (Peings and Magnusdottir, 2014).

Furthermore, while some studies do find that the circulation response to future sea-ice loss results in colder winters in parts of mid-latitudes (Sun et al., 2015; Nakamura et al., 2016a; England et al., 2018), some – similarly to studies of recent sea-ice loss – instead find a surface warming response in mid- to high-latitudes due to the counteraction of dynamical cooling by sea-ice loss induced thermodynamic warming (Peings and Magnusdottir, 2014; McCusker et al., 2017). Furthermore, Ayarzagüena and Screen (2016) find that mid-latitude 'Cold Air Outbreaks' become less severe in response to future sea-ice loss due to the advection of warmed Arctic air, and many studies find a reduction in surface temperature variability within winter (Screen, 2014; Sun et al., 2015; Blackport and Kushner, 2017).

Summary: 'Will it?'

To summarise, there is some consensus among modelling studies that future Arctic sea-ice loss could potentially result in a negative tropospheric AO response, and an anticyclonic response aloft of the ice loss. There is more consensus than modelling studies simulating the influence of recent Arctic sea-ice loss, likely because future sea-ice loss represents a much larger perturbation than recent sea-ice loss and, therefore, the response may be more robust. However, there is little consensus regarding whether dynamical cooling will be offset by thermodynamic warming. Other aspects of disagreement are that a few studies do find different tropospheric AO responses, and contrasting responses in the stratospheric polar vortex have been found.

1.1.4 Sources of uncertainty in an Arctic influence on mid-latitudes

It is clear that in both observational and modelling studies, there is disagreement regarding the mechanisms that can explain an influence of Arctic sea-ice loss on mid-latitude weather and climate. Secondly, while observational studies find a correlation

between recent observed Arctic sea-ice loss and mid-latitude winter trends, there is little consensus among modelling studies that sea-ice loss is the dominant cause of these mid-latitude trends. Finally, there is also a lack of agreement between modelling studies regarding the potential influence of future sea-ice loss. In short, there is large uncertainty within the scientific community regarding the nature of the mid-latitude atmospheric response to sea-ice loss (if a significant response even exists), and the dominant mechanisms involved.

In this section, various sources of this uncertainty will be discussed, some of which will form the basis for the subsequent investigations in this thesis. Many of these sources of uncertainty have been highlighted in the recent review papers of Overland et al. (2016), Shepherd (2016), Francis (2017), and Screen et al. (2018b).

1.1.4.1 Internal climate variability

The fact that a correlation exists between observed recent Arctic sea-ice loss and mid-latitude winter trends, but that modelling studies do not support sea-ice loss as a dominant cause of these winter trends, suggests that these trends could be largely associated with internal climate variability. Internal climate variability is defined as variability of the climate system that is internally generated by the system itself – i.e. without any external forcing – and is partly caused by atmospheric internal variability (see Deser et al. 2012 and references therein). While the autocorrelation (or memory) of atmospheric processes is low beyond a few weeks, the intrinsic non-linearity of these processes results in the chaotic generation of long timescales of variability. Low frequency variability of the ocean – such as that associated with the Atlantic Multidecadal Oscillation (AMO) or Pacific Decadal Oscillation (PDO), for example – can also contribute to internal climate variability through ocean-atmosphere coupling.

It has been suggested that the magnitude of the large-scale atmospheric circulation response to sea-ice loss may be small compared to internal climate variability (or that there is a low 'signal-to-noise' ratio), since modelling studies typically require very long simulations – from decades to hundreds of years long – to detect a statistically significant response (Screen et al., 2018b). Indeed, Screen et al. (2014) quantify the signal-to-noise ratio for observed sea-ice loss imposed in the CAM3 and UM7.3 climate models, and find that an approximately 70 year-long simulation is required to detect a response in the mid and upper level tropospheric circulation. Thus, it is possible

that trends found in the 40 year-long observational record are largely associated with internal climate variability, and that modelling studies finding no robust evidence of an influence of past sea-ice loss on mid-latitudes (e.g. McCusker et al., 2016; Seviour, 2017) are correct. Contrasting results between modelling studies, both for past and future sea-ice loss, may also be explained by an insufficient simulation length: for example, Orsolini et al. (2012) and Kim et al. (2014) run 30 and 40 year-long simulations respectively, and find opposite tropospheric AO-like responses for past sea-ice loss.

Screen et al. (2018b) do highlight, however, that climate models may underestimate the signal-to-noise ratio of the 'real-world', as shown for predictions of the NAO; this has been referred to as the 'signal-to-noise paradox' (Eade et al., 2014; Scaife et al., 2014; Dunstone et al., 2016). Recently it has been suggested that this underestimation may be because climate models do not have a sufficiently fine resolution to accurately simulate the magnitude of the eddy feedbacks involved in generating anomalous NAO phases (Scaife et al., 2019).

In response to McCusker et al. (2017) and others, Mori et al. (2019) show using 7 different AGCM's that each model does produce an ensemble mean strengthening of the Siberian High and central Eurasian winter cooling in response to observed BKS sea-ice loss, but that the mean underestimates the observed magnitude of these trends. Correcting for a potential underestimation of the signal-to-noise ratio suggests that 44% of observed recent central Eurasian cooling is due to BKS sea-ice loss. However, the signal-to-noise paradox is an ongoing topic of research, and coordinated experiments using a large number of different climate models will be required to determine whether models do in general (i.e. not just for the NAO and a small number of models) have a signal-to-noise ratio that is systematically too low (Screen et al., 2018b).

1.1.4.2 Sensitivity to the region and magnitude of sea-ice loss

Disparity among studies may also arise from differences in the sea-ice loss anomaly considered. Indeed, the spatial pattern of observed sea-ice loss varies between different seasons and years (see Section 1.1.1.1), the magnitude of projected sea-ice loss will depend on the considered time period (e.g. mid versus late 21st century) and anthropogenic emissions scenario (e.g. RCP4.5 versus RCP8.5), and the spatial pattern and magnitude of projected Arctic warming for the late 21st century – which is related to sea-ice loss – is diverse across different climate models (Figure 1.1).

Various studies have shown that different regions or spatial patterns of sea-ice loss or Arctic warming can result in contrasting atmospheric responses (Alexander et al., 2004; Koenigk et al., 2016; Pedersen et al., 2016; Screen, 2017b; Ruggieri et al., 2019). In particular, the modelling study of Sun et al. (2015) shows that when future sea-ice loss is mainly confined to the Atlantic sector of the Arctic (in their case the Barents-Kara, Greenland, and Labrador Seas), the polar vortex weakens in winter; if it is mainly confined to the Pacific sector (in their case the Bering and Okhotsk Seas), the vortex strengthens. Their explanation is that the anomalous stationary Rossby waves generated in the Atlantic (Pacific) case constructively (destructively) interfere with climatological stationary Rossby waves, which enhances (suppresses) upward wave propagation into the stratosphere and decelerates (accelerates) the stratospheric flow. This contrast in interference occurs because the climatological waves are fixed in phase – since they are generated by fixed orography and land-sea thermal contrasts – but the phase of the anomalous waves depends on the longitude of the sea-ice loss. Smith et al. (2010) previously argued for similar effects of varying longitudinal positions of snow cover anomalies.

Similarly, some studies have examined the response to different magnitudes of sea-ice loss (Petoukhov and Semenov, 2010; Peings and Magnusdottir, 2014; Nakamura et al., 2016a; Wu and Smith, 2016), where the first three find it to be non-linear. For example, Petoukhov and Semenov (2010) show that for increasing magnitudes of wintertime sea-ice loss in the BKS region, between low loss and 100% loss, the response transitions from negative AO-like to positive AO-like and then back again.

1.1.4.3 Sensitivity to the background state

It has also been shown that the background atmospheric and oceanic state – which varies for different climate models, experimental setups, and over time due to internal climate variability – can alter the response to sea-ice loss. For example, Smith et al. (2017) show that the tropospheric NAO response to sea-ice loss is opposite in two AGCM experiments, where one experiment is forced with observed SST's and the other with SST's from a coupled atmosphere-ocean version of the model. They find that this is because the different SST states lead to different climatological eddy-driven jet strengths and latitudinal positions, which alters the refractive index and therefore the nature of Rossby wave propagation. This in turn alters the nature of feedbacks of Rossby waves on the mean flow, which are important for determining the development

of latitudinal jet shifts or NAO-like responses (Limpasuvan and Hartmann, 2000; Barnes et al., 2010; Barnes and Hartmann, 2011).

Osborne et al. (2017) similarly find that the atmospheric response over North America is different in two AGCM experiments forced with sea-ice loss and climatological SST's resembling opposite phases of the AMO. Furthermore, Labe et al. (2019) show that the phase of the Quasi-Biennial Oscillation (QBO) can modulate the atmospheric response to sea-ice loss, using simulations from an atmospheric GCM with a QBO prescribed from observations. The QBO is an observed oscillation in equatorial stratospheric winds between easterlies (QBO-E) and westerlies (QBO-W) with an approximately two-year period. It is found that only under QBO-E is there a robust weakening of the stratospheric polar vortex; this results in a stronger reinforcement of the Siberian High than for QBO-W, and therefore an intensification of cold extremes over Eurasia which is only statistically significant for QBO-E. This stratospheric response is driven by anomalous wave propagation into the stratosphere due to QBO-E, which constructively interferes with the climatological zonal wavenumber-1 pattern.

1.1.4.4 Model representation

Disparity among modelling studies in terms of the response to sea-ice loss may also reflect differences in the representation of key processes between different models. For example, as previously mentioned, studies using a stratospheric nudging method to objectively quantify the role played by stratospheric mechanisms in the tropospheric response to sea-ice loss have found that they are important (Wu and Smith, 2016; Nakamura et al., 2016b; Zhang et al., 2018a,b). Similarly, Sun et al. (2015) show that the tropospheric response is weaker in a low-top version of the climate model WACCM than in a high-top version, which indicates a key role played by the stratosphere. As such, climate models with an inadequate representation of the stratosphere may not realistically simulate the response to sea-ice loss (Zhang et al., 2018a).

There is also a large amount of evidence to suggest that atmosphere-ocean coupling, particularly through dynamical ocean feedbacks, strongly amplifies the magnitude and spatial extent of the response to sea-ice loss (Deser et al., 2015, 2016a; Blackport and Kushner, 2018). As such, the response in AGCM's may be underestimated in comparison to that in coupled AOGCM's and in observations. Since this then implies a lower signal-to-noise ratio in AGCM's, this may explain why the response to sea-ice loss

is less consistent in studies that use AGCM's compared to those that use AOGCM's (Blackport and Kushner, 2018; Screen et al., 2018b). Indeed, Screen et al. (2018b) show that the large-scale atmospheric circulation response to sea-ice loss is consistent for six coupled AOGCM's, including a strengthening of the Siberian High, and a weakening and equatorward shift of the tropospheric jet in winter.

1.1.4.5 Complexity of mechanisms

Disagreement among both observational and modelling studies regarding the dominant mechanisms involved in the response to sea-ice loss is most likely due to the inherent complexity and non-linearity of atmospheric dynamics (Overland et al., 2016). Indeed, Overland et al. (2016) highlight that there may not be a simple linear cause-and-effect pathway connecting sea-ice loss to a subsequent response, which has made it difficult for studies to disentangle the complex web of potential processes involved. This difficulty may have also been exacerbated by a low signal-to-noise ratio, which may have made it difficult to detect mechanisms robustly in both the short observational record and model simulations of insufficient length or ensemble size.

Futhermore, Overland et al. (2016) additionally suggest that the notion of there being 'dominant' mechanisms involved in the response is unhelpful, since it is possible that the mechanisms found to be important will be sensitive to various factors. This links to the above discussed sources of uncertainty regarding the nature of the response to sea-ice loss. Indeed, mechanisms may also be sensitive to the region and magnitude of sea-ice loss, the background atmospheric and oceanic state, or to the different representation of key processes in different models. For example, Nakamura et al. (2016a) and Peings and Magnusdottir (2014) show that both current and future sea-ice losses – which are of a different spatial pattern and magnitude – lead to a tropospheric negative AO response, but attribute this to a weakening of the stratospheric polar vortex for current loss, and to a reduction in the meridional temperature gradient for future loss.

1.1.5 Wider relevance

Improving our understanding of the response to Arctic sea-ice loss, and specifically of the sources of uncertainty that may contribute to spread in the response across models, has a wider relevance. In particular, this may help us to better understand intermodel

spread in projections of future circulation change in response to the radiative effects of anthropogenic GHG forcing.

Besides Arctic sea-ice loss and associated warming, the other main radiative effect of GHG forcing is tropical upper tropospheric warming, which can be understood from the lapse-rate feedback mechanism discussed in Section 1.1.1.2. While Arctic warming has been found to reduce the equator-to-pole temperature gradient resulting in a negative AO-like response, tropical upper tropospheric warming has been found to enhance this temperature gradient resulting in a positive AO-like response (e.g. Butler et al., 2010; McCusker et al., 2017; Oudar et al., 2017). As such, many studies have suggested that the circulation response to future GHG forcing will involve a 'tug-of-war' between the tropics and the poles (Barnes and Screen, 2015; Screen et al., 2018a).

Indeed, in studies using single AGCM's or coupled AOGCM's, Arctic sea-ice loss or warming is found to either reduce or entirely cancel the wintertime zonal mean poleward shift in the tropospheric jet or storm tracks found in response to tropical upper tropospheric warming (Butler et al., 2010; Deser et al., 2015; Blackport and Kushner, 2017). In other similar studies, on the other hand, this cancellation is only found for the North Atlantic tropospheric jet, while both Arctic and tropical warming are found to result in an equatorward shift of the North Pacific tropospheric jet (McCusker et al., 2017; Oudar et al., 2017).

However, for larger multi-model datasets the circulation response to future GHG forcing is still uncertain. While the state-of-the-art CMIP5 models do simulate a positive AO response to future GHG forcing in terms of the multi-model mean, there is a large intermodel spread in this response (Cattiaux and Cassou, 2013; Yim et al., 2016), particularly in the North Atlantic sector (Harvey et al., 2014; Barnes and Polvani, 2015; Zappa et al., 2018). Many studies have found that, in winter at least, this spread in the AO response can be largely attributed to intermodel spread in the simulated magnitude of AA or sea-ice loss (Cattiaux and Cassou, 2013; Harvey et al., 2014, 2015; Barnes and Polvani, 2015; Yim et al., 2016).

As highlighted in the previous section, there are various other sources of uncertainty in the circulation response to future sea-ice loss and, therefore, spread in the simulated magnitude of sea-ice loss may not be the only significant source of intermodel spread in projections of future circulation change in response to future GHG forcing. As such, a better understanding of projections of future circulation change may require a better

understanding of all the sources of uncertainty that contribute to intermodel spread in the response to sea-ice loss.

1.2 Thesis aim and research questions

This chapter has clearly demonstrated that uncertainty still exists within the scientific community regarding the nature of the response to Arctic sea-ice loss and the mechanisms involved. It has also been shown that various sources could contribute to this uncertainty, including: the influence of internal climate variability; a sensitivity of the response to the region and magnitude of sea-ice loss, as well as the background state; intermodel differences in the representation of key processes such as stratospheric dynamics; and the fact that the response involves a complex web of potential processes, which are difficult to disentangle. Since all climate models project a continuation of Arctic sea-ice loss in response to future increases in anthropogenic radiative forcing, it is important that the influence of this on future circulation changes in the highly populated mid-latitudes is better understood.

In this thesis, the issues of complexity and statistical robustness in the response to Arctic sea-ice loss are partly addressed by conducting idealised numerical modelling experiments using an intermediate complexity global circulation model, IGCM4. Such models are useful because they are complex enough to simulate a variety of important processes, but are relatively simple and computationally fast compared to full complexity state-of-the-art climate models. This helps to disentangle different processes from one another and allows for several-century-long simulations, making a statistically robust response more attainable. Furthermore, the computational speed of IGCM4, as well as the ease with which the model code can be edited, allows for many different experiments to be run, which can be designed to systematically target and isolate different parts of the response.

The majority of previous modelling studies investigating the atmospheric response to sea-ice loss, including those finding contrasting responses, have used full complexity state-of-the-art climate models (e.g. Blackport and Kushner, 2017; Deser et al., 2016a; England et al., 2018; Kim et al., 2014; McCusker et al., 2017; Mori et al., 2014, 2019; Peings and Magnusdottir, 2014; Petoukhov and Semenov, 2010; Screen et al., 2013, 2014; Screen, 2017a; Screen and Blackport, 2019; Seviour, 2017; Smith et al., 2017; Sun et al., 2015; Zhang et al., 2018a). These models include, for example: AM3, CAM3, CAM4,

CAM5, CanESM2, CCSM4, CESM1, CESM-CAM5, ECHAM5, GEOS-5, GFSv2, HadGEM3, HadGEM2-ES, MIROC4, WACCM4, SC-WACCM4, and UM7.3. A more limited set of studies have used less complex models to understand the circulation response to idealised AA-like thermal or polar forcings: for example, Butler et al. (2010) and Wu and Smith (2016) use simplified dry atmospheric GCMs, Ronalds et al. (2018) use a barotropic model, Sellevold et al. (2016) use a baroclinic linear stationary wave model, and (Ruggieri et al., 2019) use a simple storm-track model. The work detailed in this thesis using IGCM4 will add to this more limited set of idealised studies, which are important for obtaining a better understanding of physical mechanisms and their robustness.

The overall aim of the thesis will be to improve understanding of the influence of Arctic sea-ice loss on mid-latitude weather and climate, and the mechanisms involved. This will be done by conducting a series of experiments with IGCM4, which will systematically examine various aspects that may explain contrasting results and, hence, current uncertainty regarding the nature of a link. A better understanding of the mechanisms involved will be obtained by decomposing the responses into parts due to tropospheric and stratospheric mechanisms. In particular, experiments will be designed to address the following research questions:

1. What is the nature of the response to Arctic sea-ice loss within IGCM4, in terms of the impact on the large-scale atmospheric circulation and on mid-latitude surface temperatures? To what extent is the response sensitive to the region or magnitude of sea-ice loss?

2. What is the relative importance of tropospheric and stratospheric mechanisms in producing remote responses to sea-ice loss?

3. How large is the influence of atmospheric internal variability with regard to uncertainty in responses to sea-ice loss produced by model time-slice experiments of different lengths?

While questions are not directly asked regarding the sensitivity of the response to the model representation of stratospheric dynamics, or to the background atmospheric state, the experiments designed in relation to question 2 will provide a test of these two aspects.

1.3 Thesis outline

This section gives a thorough outline of the original work carried out in this thesis to address the above overall aim and associated research questions. It should be noted that this work will be presented chronologically, where any model experimental design was based on the knowledge at the time, and this knowledge subsequently evolved throughout the thesis. The final chapter will reflect on the evolution of this knowledge.

Following this first chapter, Chapter 2 describes IGCM4 in detail, and evaluates its representation of key features of the large-scale atmospheric circulation that may be important in the response to sea-ice loss. Details will also be given of any datasets and data analysis methods used, including various diagnostics and statistical tests.

Chapter 3 investigates the extent to which the atmospheric response to sea-ice loss is sensitive to the loss region – the Atlantic or Pacific sector of the Arctic – and, secondly, to the loss magnitude – large-magnitude, i.e. late 21st century, or moderate-magnitude (research question 1). This work is based on the Geophysical Research Letters paper, McKenna et al. (2018). It is found that for different regions of large-magnitude sea-ice loss, there are different effects on the stratospheric polar vortex. While there are negative tropospheric Arctic Oscillation (AO) responses in both cases, there are contrasting effects on mid-latitude surface temperatures. This is explained in this work using a method of decomposition into an 'indirect' part induced by the large-scale tropospheric AO response, and a residual 'direct' part that is local to the region of ice loss. Since the spatial pattern of future Arctic surface warming – which is related to sea-ice loss – is uncertain across the CMIP5 (Coupled Model Intercomparison Project Phase 5) climate models, these results may indicate the range of potential atmospheric responses for studies using these models. A low signal-to-noise ratio makes it difficult to robustly determine the linearity of the response to different loss magnitudes.

In Chapter 4, a stratospheric nudging method is implemented in IGCM4 to isolate the roles played by tropospheric and stratospheric mechanisms in the remote response to sea-ice loss (research question 2). For large-magnitude Atlantic sector loss, part of the negative tropospheric AO response is found to likely be caused by tropospheric mechanisms, and another part likely involves changes in sudden stratospheric warmings (SSWs). For large-magnitude Pacific sector loss, there is likely a non-linear interaction between tropospheric and stratospheric mechanisms, where the stratospheric state

alters vertical wave propagation in such a way that the direct stationary Rossby wave response to the sea-ice loss projects onto a negative tropospheric AO. It is found that this approach of isolating the responses for different regions of sea-ice loss, and further isolating the different mechanisms involved in these responses, makes understanding the response to sea-ice loss more tractable. In particular, it is shown that past studies may find contradictory responses and different dominant mechanisms due to different model representations of stratospheric dynamics, and a sensitivity of the response to the stratospheric state (when ice loss including the Pacific sector is considered).

Finally, motivated by the importance of SSWs in the large-magnitude Atlantic sector sea-ice loss experiment and their potentially large internal variability, Chapter 5 extends this experiment by several centuries to examine the influence of atmospheric internal variability with regard to uncertainty in responses to sea-ice loss produced by model time-slice experiments of different lengths (research question 3). This leads to a quantification of the minimum experiment length required to separate the signs of forced tropospheric and stratospheric changes due to sea-ice loss from internal variability. This has not been quantified to date for the latter, and is found to be large for both the stratospheric AO and SSW frequency (around 190 and 450 years respectively for the December-March mean). This may explain contrasting stratospheric responses in past studies using an insufficient experiment length, with implications for the robustness (at least quantitatively) of the tropospheric responses in these studies. Here, the responses are qualitatively the same in the shorter and extended experiments, but there are some differences in magnitude and evolution.

In Chapter 6, the results from Chapters 3 to 5 are drawn together, summarised, and discussed in terms of their wider implications. Based on these results, possible areas of further research are also suggested.

Chapter 2

Methods

This chapter describes and explains the methods used throughout this thesis. In particular, a description is given of the numerical model used to conduct the model experiments, and an evaluation is made of the model's representation of key features of the large-scale atmospheric circulation that could be important in the response to sea-ice loss. A description is also given of the reanalysis data used to evaluate the model and to prescribe the model's lower boundary conditions. Specific details of the experiments conducted will be given later in each results chapter (Chapters 3 to 5).

The data analysis methods used in the results chapters are also detailed, including: various wave diagnostics, Empirical Orthogonal Function (EOF) analysis, a sudden stratospheric warming (SSW) detection method, and various statistical methods including tests for statistical significance.

2.1 Reanalysis data

Throughout this thesis, reanalysis data will be used to prescribe climatological ocean surface temperatures in the numerical modelling experiments conducted, and will be used in this chapter to evaluate the model's climatology. Hence, this short section aims to explain what a reanalysis dataset is and how it is produced.

A reanalysis dataset is essentially created by using numerical weather prediction (NWP) simulations to interpolate in space and time between observational data, with the aim of producing an optimal gridded historical dataset of the full three-dimensional

structure of the real atmosphere. Many observational sources across the globe are used including aircraft, satellites, radiosondes (weather balloons; these record vertical atmospheric profiles of variables such as temperature and winds), buoys, and ship reports. One of the most common datasets used is ERA-interim (Dee et al., 2011), which is produced by the ECMWF (European Centre for Medium-range Weather Forecasting) using the IFS (Integrated Forecasting System) model. The dataset extends from January 1979 to August 2019 at a minimum of 6-hourly time intervals, has a horizontal grid spacing of 80 km, and 60 vertical levels from the surface up to 0.1 hPa. A key feature of this dataset is the use of the 4D-Var data assimilation system, which assimilates all available observations into the model over a 12 hour analysis period and optimises them in both space and time. The ECMWF also produced the ERA-40 reanalysis dataset (Uppala et al., 2005) for the period 1957-2002. This data is also at a minimum of 6-hourly time intervals and has 60 levels from the surface up to 0.1 hPa, but has a larger horizontal grid spacing of 125 km. The main difference from ERA-interim is the use of 3D-Var, which does optimise the observations in both space and time, but does not properly account for the exact time at which an observation is taken (it rounds the time by up to 3 hours).

2.2 Numerical model

2.2.1 Description

The model used in this thesis is the spectral primitive equation atmospheric model, IGCM4 (Intermediate Global Circulation Model, version 4; Joshi et al., 2015). It originated as the baroclinic model of Hoskins and Simmons (1975), which – along with subsequent model versions – has been used in many studies of atmospheric dynamics (e.g. Thorncroft et al., 1993; Winter and Bourqui, 2011; O'Callaghan et al., 2014; Hitchcock and Haynes, 2016). It has a horizontal resolution of T42 ($\sim 2.8°$ latitude and longitude) and 35 vertical model levels, which are written in terms of sigma coordinates rather than pressure coordinates. These follow the model's orography and, therefore, simplify the lower boundary conditions. The levels extend from the surface up to approximately 0.1 hPa ($\sim$ 65 km), where 19 levels are in the troposphere and 13 levels are in the stratosphere. IGCM4 is therefore a 'high-top' model, making it suitable for studying the stratospheric processes that may be important in the response to sea-ice

loss. The model's ability to simulate stratospheric processes has also been substantially improved by a new gravity wave drag scheme in this model version (Joshi et al., 2015). It should be noted, however, that IGCM4 does not produce an internally generated Quasi-Biennial Oscillation (QBO), as is the case for most climate models (Schenzinger et al., 2017). As explained in Section 1.1.4.3 of Chapter 1, the response to sea-ice loss is sensitive to the phase of the QBO and, therefore, it is acknowledged that this is a limitation; this will be discussed further in Chapter 6.

In terms of chemistry, the model includes all of the main greenhouse gases (CO_2, CH_4, N_2O, CFC's, ozone, and water vapour). CO_2, CH_4, N_2O, and CFC's are prescribed at climatological concentrations and assumed to be well-mixed throughout the atmosphere, while ozone is prescribed as a zonally averaged monthly mean climatology. Water vapour is prescribed at climatological values above the tropopause, but is advected by the model in the troposphere. Moist processes, such as cloud formation and evaporation, are also parameterised by the model albeit in a simplified manner. Further details can be found within Joshi et al. (2015).

Since the model is atmosphere-only, climatological monthly mean surface temperatures (T_s) are prescribed over the ocean using ERA-interim reanalysis data. There is no explicit sea-ice field, but its effects on key surface properties – including the albedo, heat capacity, and roughness – are parameterised through the ocean T_s. Specifically, a linear change in these properties is assumed between the temperatures of 0°C and −2°C, where the former is assumed to be fully sea-water covered and the latter fully sea-ice covered. This takes into account that sea-water freezes at −2°C, while sea-ice (which is mostly fresh-water due to brine rejection) melts at 0°C; thus, there should be a mixture of both sea-water and sea-ice between these temperatures. The T_s over land is not prescribed, but computed from the surface heat fluxes at each time-step.

2.2.2 Model evaluation

Before running the numerical modelling sea-ice loss experiments, an evaluation was made of the model's ability to adequately represent key features of the large-scale atmospheric circulation that could be important in the response to sea-ice loss.

For example, the model's zonal mean zonal wind, [U], climatology was evaluated for its representation of the Northern Hemisphere tropospheric jet stream. It is important that this representation is realistic, because – as discussed in Chapter 1

– the tropospheric circulation response to sea-ice loss can be opposite for different climatological eddy-driven jet strengths and latitudinal positions (Smith et al., 2017). Figure 2.1 shows the [U] climatology in summer and winter for ERA-interim reanalysis data averaged over 1979-2016, compared to a 200 year-long IGCM4 control run, CTL (this will be introduced in more detail in Chapter 3). This shows that the Northern Hemisphere tropospheric jet stream in IGCM4 has a similar latitudinal position to that in reanalysis data, and is only slightly weaker. Therefore, the jet stream is adequately represented for the purposes of this thesis.

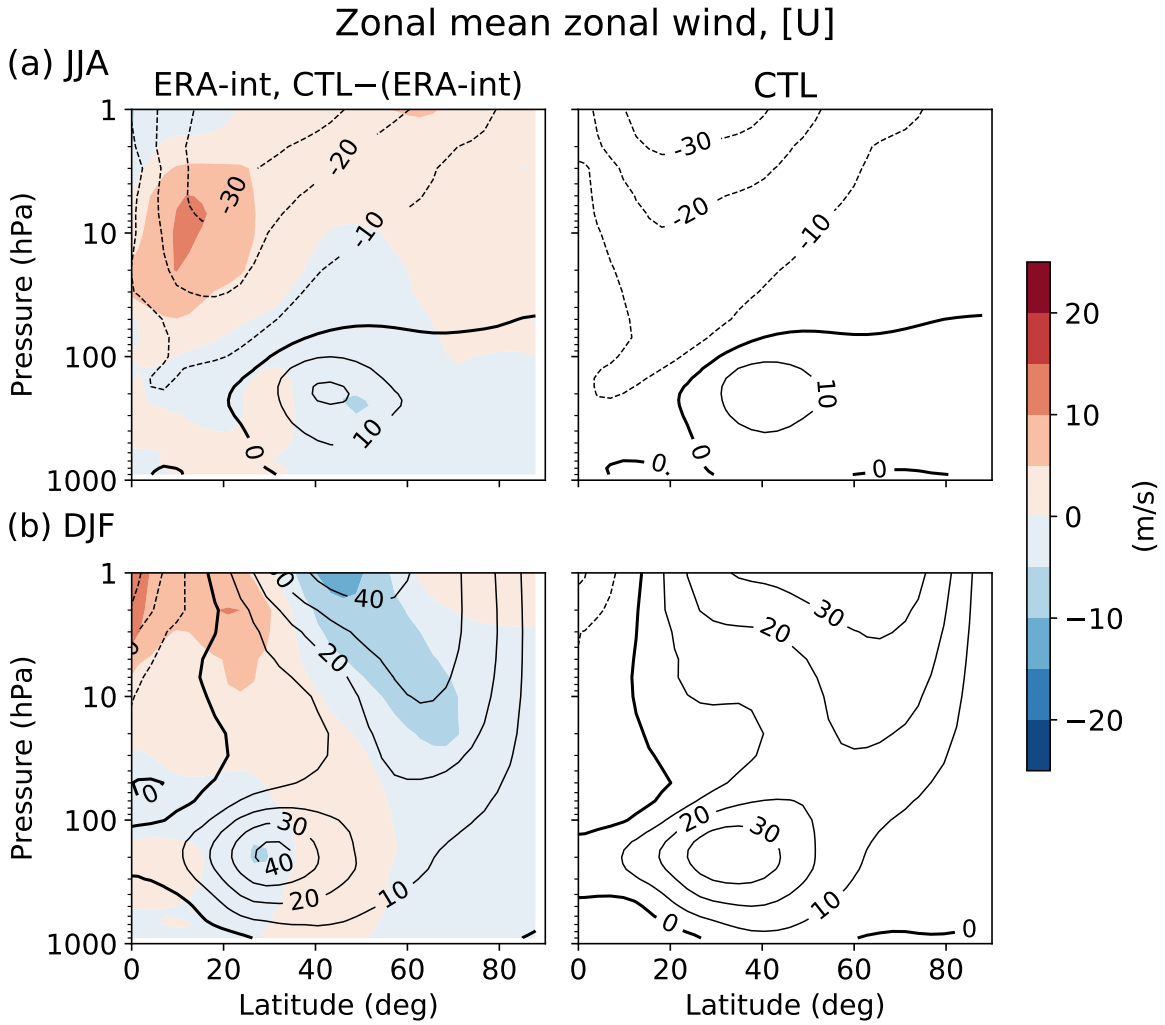

Fig. 2.1 Zonal mean zonal wind in (a) June-August, and (b) December-February, for [Left] ERA-interim reanalysis data averaged over 1979-2016 (year is for December; contours), and [Right] the IGCM4 control run (CTL – see Chapter 3; contours). The shading on the [Left] shows CTL minus ERA-interim.

The decorrelation timescale of the tropospheric (500 hPa) Arctic Oscillation (AO) was also checked against reanalysis data, since the magnitude of this timescale is thought to scale with the magnitude of the AO response to an external forcing (this will be explained in Section 2.3.2.2 shortly). In the IGCM4 CTL run, the AO decorrelation timescale was found to have an approximate maximum of 14 days in winter, which compares well with NCEP reanalysis data from 1958 to 2002 (an approximate maximum of 15 days in winter; Baldwin et al., 2003). This implies that the response of the AO to sea-ice loss in IGCM4 will likely be of a representative magnitude.

It was also important to evaluate the model's ability to simulate stratospheric processes, considering the key role the stratosphere may play in the response to sea-ice loss. Firstly, the [U] climatology was used to evaluate the model's representation of the climatological mean stratospheric polar vortex. Figure 2.1b shows that the polar vortex in IGCM4 is only slightly weaker than in ERA-interim, and has a similar position.

Secondly, it was checked that IGCM4 can adequately simulate variability of the stratospheric polar vortex in terms of sudden stratospheric warmings or SSWs (see Chapter 1 for a detailed explanation of stratospheric dynamics). This was to investigate whether the model can adequately represent the influence of a wave disturbance on the vortex, and the process by which the stratospheric wind anomalies subsequently descend into the troposphere. This allows us to have more confidence that the imposed sea-ice anomalies, and resulting Rossby wave anomalies, will have a realistic effect on the vortex, and that the vortex will subsequently have a realistic effect on the surface.

In terms of the climatological mean SSW frequency per year, this was calculated for November-March according to the method of Charlton and Polvani (2007), but with an additional requirement to adhere to the World Meteorological Organisation's SSW definition (see Section 2.3.3 for more details). For the CTL run, this was found to be 0.71 ± 0.05 ($\pm$ standard error) per year, which compares well with the SSW frequency in 40 years of ERA-40 reanalysis data (0.6 ± 0.1 per year; Charlton and Polvani, 2007). O'Callaghan et al. (2014) also show that for their 200 year-long IGCM4 control run, the frequencies of different types of SSWs – including 'displacement' or 'split' events (in which the vortex either becomes strongly displaced from the pole or splits in two) – agree well with reanalysis data (Charlton and Polvani, 2007). While O'Callaghan et al. (2014) do find that the stratospheric anomalies associated with SSWs are too weak, they do result in tropospheric anomalies of a realistic strength, indicating that the descent of stratospheric anomalies into the troposphere – in other words, the strength

of stratosphere-troposphere coupling – is adequately represented by the model. In the CTL run here, SSWs are of an adequate strength at all heights from the stratosphere to the near-surface, as can be seen when comparing height-time plots of the AO index for a composite SSW in CTL versus a composite SSW in ERA-interim data (Figure 2.2). Coupling between the stratosphere and troposphere appears to weaken slightly earlier for SSW events in IGCM4 than in ERA-interim, but note this difference may be at

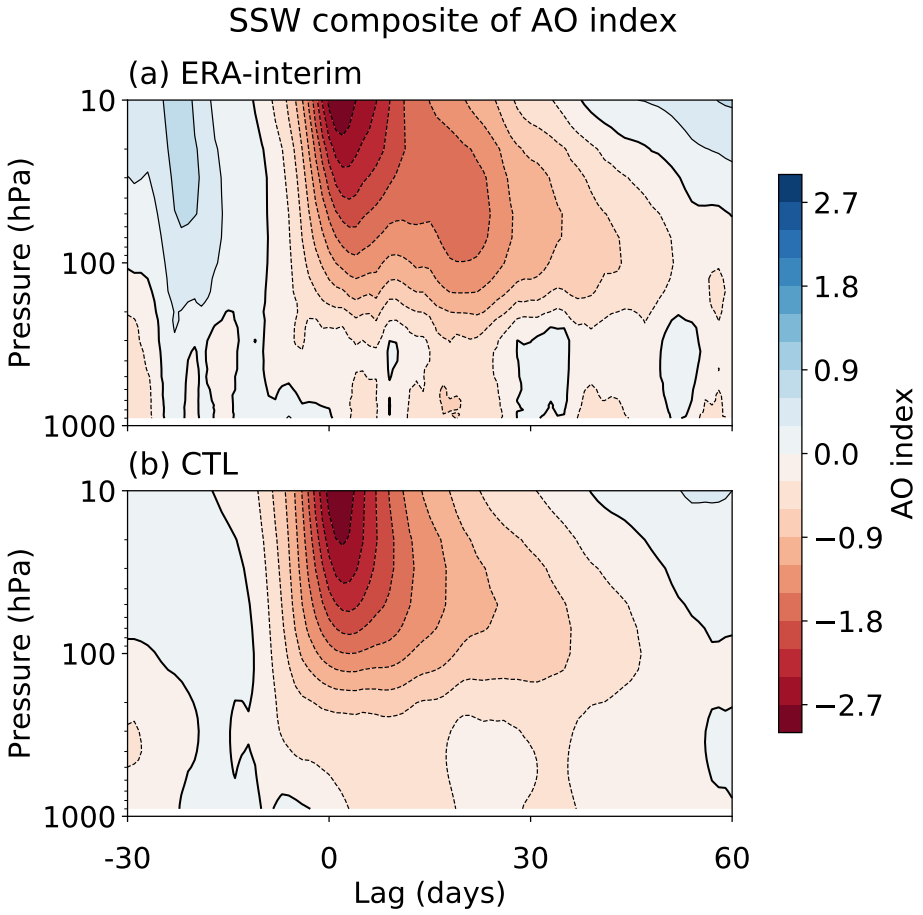

Fig. 2.2 Time-height evolution of the daily AO index for a composite SSW in (a) ERA-interim reanalysis data over 1979-2014, and (b) in the IGCM4 control run (CTL). The composites are calculated by centering all the SSWs (N = 26 in ERA-interim and N = 142 in CTL) about their central date, which is indicated by a lag of 0, and then calculating an average. Note that blue is positive and red is negative (to depict the polar cap warming, or increase in polar cap geopotential height, associated with the SSW). AO index data were obtained from the 'Sudden Stratospheric Warming Compendium' dataset (Butler et al., 2017) for ERA-interim, and were calculated according to the method of Baldwin and Thompson (2009)

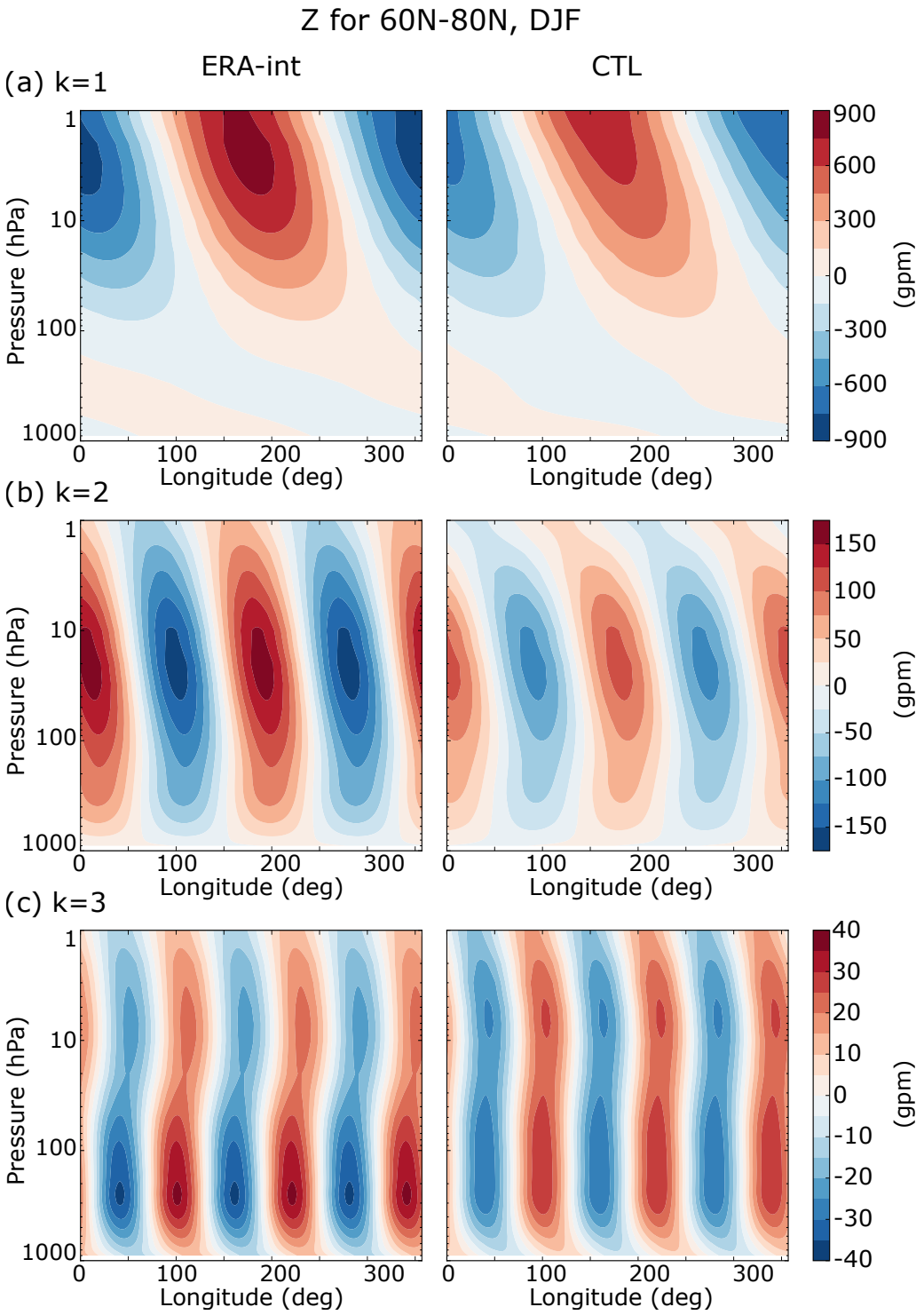

Fig. 2.3 Geopotential height averaged over 60°N-80°N in December-February for zonal wave- (a) 1, (b) 2, and (c) 3. [Left] ERA-interim reanalysis data averaged over 1979-2016 (year is for December), and [Right] the IGCM4 control run (CTL – see Chapter 3).

least in part due to sampling error (the ERA-interim dataset is much shorter than CTL and, as such, there are only 26 events in the former compared to 142 in the latter).

A final important feature of the model is its climatological stationary waves, since – as described in Chapter 1 – the response of the stratospheric polar vortex to sea-ice loss involves the interference of these waves with anomalous forced waves. As such, the climatological wave phase needs to be represented correctly. To evaluate the climatological stationary waves in IGCM4, plots are shown of the zonal wavenumber-1/2/3 (wave-1/2/3) components of the climatological winter mean geopotential height at all pressure levels for CTL and ERA-interim reanalysis data (Figure 2.3). The contributions of each wavenumber are calculated using an inbuilt Fast Fourier Transform function in Python. While the wave-1/2/3 amplitudes in CTL are smaller than in ERA-interim, their phases compare very well.

In summary, IGCM4 does an adequate job of representing tropospheric and stratospheric processes and, therefore, is appropriate for the purposes of this thesis.

2.3 Data analysis

2.3.1 Wave diagnostics

2.3.1.1 The EP-flux

In Chapters 3 to 5, the effect of sea-ice loss on Rossby wave propagation with latitude and height (i.e. in a zonal mean sense) and the subsequent effect of this on the zonal mean flow will be examined. To do this, Eliassen-Palm flux (EP-flux) vectors and their divergence will be calculated, the physical relevance of which was explained in detail in Chapter 1. The EP-flux, $\mathbf{F} = (F_\phi, F_z)$, is calculated in log pressure co-ordinates as:

$$F_\phi = -\rho_0 a \cos\phi [u^* v^*] \ , \tag{2.1}$$

$$F_z = \rho_0 a f \cos\phi \frac{[v^* \theta^*]}{\partial [\theta]/\partial z} \ , \tag{2.2}$$

where $\rho_0 = \rho_r \exp(-z/H)$, a is the Earth's radius, ϕ is the latitude, u and v are the zonal and meridional wind components, f is the Coriolis parameter, θ is the potential temperature, $z = -H \ln(p/p_r)$ is the pressure height, H is the scale height (a value of 7 km is used here), ρ_r is the reference atmospheric density (1.2 kg/m^3), p is the

atmospheric pressure, and p_r is the reference pressure (10^5 Pa). The square brackets denote zonal means and the asterisks denote deviations from the zonal means.

The EP-flux vectors are calculated using daily data and then averaged for the desired time-period. Following Baldwin et al. (1985), the EP-flux vectors are plotted as $\mathbf{F}/\rho_0$ to account for them becoming very small as density decreases with height. F_ϕ is multiplied by α (the vertical distance spanned by the plot divided by the horizontal distance) to account for the exaggerated vertical scale of the plots (Palmer, 1981).

2.3.1.2 The Plumb flux

The EP-flux describes the zonal mean propagation of quasi-geostrophic Rossby waves, and is therefore two-dimensional. However, in Chapter 4 the response in Rossby wave propagation will also be examined in three-dimensions, in terms of latitude and longitude, as well as longitude and height. To do this, Plumb wave activity flux (or Plumb flux) vectors will be calculated, which describe the full three-dimensional direction of energy propagation by stationary quasi-geostrophic Rossby waves (Plumb, 1985). The Plumb flux, $\mathbf{F} = (p/p_r)\cos\phi\,(F_\lambda, F_\phi, F_z)$, is expressed as:

$$F_\lambda = \frac{1}{2a^2\cos^2\phi}\left[\left(\frac{\partial\psi^*}{\partial\lambda}\right)^2 - \psi^*\frac{\partial^2\psi^*}{\partial\lambda^2}\right] , \tag{2.3}$$

$$F_\phi = \frac{1}{2a^2\cos\phi}\left[\frac{\partial\psi^*}{\partial\lambda}\frac{\partial\psi^*}{\partial\phi} - \psi^*\frac{\partial^2\psi^*}{\partial\lambda\partial\phi}\right] , \tag{2.4}$$

$$F_z = \frac{2\Omega^2\sin^2\phi}{N^2 a\cos\phi}\left[\frac{\partial\psi^*}{\partial\lambda}\frac{\partial\psi^*}{\partial z} - \psi^*\frac{\partial^2\psi^*}{\partial\lambda\partial z}\right] , \tag{2.5}$$

where λ is the longitude, ψ is the geostrophic streamfunction (calculated from $\psi = Zg/f$, where Z is the geopotential height), Ω is the Earth's rotation rate, N^2 is the squared Brunt-Väisälä buoyancy frequency, and all other symbols are as defined in the previous section for the EP-flux.

Since the Plumb flux is only applicable for stationary waves, it is calculated using monthly mean fields. Similarly to the EP-flux, in longitude-height plots the Plumb flux vectors are plotted as $\mathbf{F}/(p/p_r)$ to account for them becoming very small with height, and F_λ is multiplied by α to account for the exaggerated vertical scale of the plots.

2.3.1.3 Linear versus non-linear interference

The vertical wave propagation response to sea-ice loss can be decomposed into different parts to examine the contribution of linear and non-linear processes. This will be relevant to the interference mechanism described in Chapter 1, which will be a particular focus of Chapter 3.

As shown in Smith et al. (2010), the total anomalous vertical wave propagation – which is proportional to the zonal mean eddy heat flux response (see Section 2.3.1.1) – is composed of a time-mean linear component ($\mathrm{TM_{LIN}}$), a time-mean non-linear component ($\mathrm{TM_{NLIN}}$), and a high-frequency wave fluctuation (FL) component:

$$\Delta\overline{[v^*T^*]} = \mathrm{TM_{LIN}} + \mathrm{TM_{NLIN}} + \mathrm{FL}\ , \tag{2.6}$$

where

$$\begin{aligned} \mathrm{TM_{LIN}} &= [(\Delta\overline{v^*})\ \overline{T_c^*}\,] + [(\Delta\overline{T^*})\ \overline{v_c^*}\,]\ , \\ \mathrm{TM_{NLIN}} &= [\Delta\overline{T^*}\Delta\overline{v^*}\,]\ , \\ \mathrm{FL} &= \Delta\overline{[v^{*\prime}T^{*\prime}]}\ , \end{aligned}$$

and v is the meridional wind component, T is the temperature, v and T are daily variables, Δ is the difference between a perturbation (sea-ice loss) run and a control run, square brackets denote a zonal mean, asterisks denote deviations from the zonal mean, bars denote a time mean, primes denote deviations from the time mean, and the c subscript denotes the control run.

$\mathrm{TM_{LIN}}$ represents the component of the eddy heat flux response due to interference (or correlations) between the time-mean wave response and the control run climatological waves (the component described in Chapter 1). $\mathrm{TM_{NLIN}}$ represents the component that is due to interference between the time-mean wave responses in v and T. FL is the component due to interference between high-frequency wave fluctuations about the time-mean. See Smith et al. (2010) for more details on this decomposition.

2.3.2 Empirical Orthogonal Function (EOF) analysis

Throughout this thesis, Empirical Orthogonal Function (EOF) analysis will be used extensively. For a time-series of spatial data, EOF analysis aims to extract the spatial

modes or patterns of variability in the data – known as the EOF's – and the time-series that describe the amplitude of each mode – known as the Principal Components (PCs). The method is purely mathematical and involves decomposing the data into mathematically orthogonal (independent) modes. As such, the method does not have any physical basis, but many studies have found that it can effectively identify physically relevant modes in the atmosphere such as the AO, North Atlantic Oscillation, and Pacific-North American pattern (Lorenz, 1951; Kutzbach, 1970; Wallace and Gutzler, 1981; Thompson and Wallace, 1998; Ambaum et al., 2001).

Technically, the method involves firstly putting the data into a two-dimensional matrix, A, such that the first dimension is time and the second dimension is space. A singular value decomposition function in Python is then used to decompose A into three matrices:

$$A = U\,D\,V^T\ , \tag{2.7}$$

where V^T and U are orthogonal, and D is diagonal. The rows of V^T contain the eigenvectors of A^TA, the columns of U contain the eigenvectors of AA^T, and in both cases the corresponding eigenvalues are given by D^2. Each EOF is contained in each row of V^T, while the PC's for each EOF are contained in each column of UD. The eigenvalues in D^2 can be used to calculate the percentage of variance explained by each EOF. The first EOF will explain the highest variance, the second EOF the second highest variance, and so on.

2.3.2.1 AO loading pattern and index

To find the climatological winter (November-February) mean AO loading pattern with latitude and longitude for a given pressure level, and its associated AO index for each winter month in each year, the method of the NOAA (National Oceanic and Atmospheric Administration) Climate Prediction Center is used.

This method involves calculating the first EOF of time-series of monthly mean geopotential height (Z) anomalies north of 20°N, and its associated monthly PC time-series. The anomalies are defined as deviations from the seasonal cycle, where this cycle is defined by climatological monthly means. Before calculating the first EOF, the Z anomalies – which are in latitude and longitude – are weighted by the square-root of the cosine of latitude to account for the decrease in area towards the pole.

The resulting monthly PC time-series is normalised by the standard deviation of the time-series so that it has unit variance; this gives the AO index for each winter month in each year. The associated climatological winter mean AO loading pattern is found by calculating, for each latitude and longitude, the gradient of a temporal regression between the time-series of the monthly AO index and the time-series of the monthly mean Z anomalies (see Section 2.3.4.4). As such, this loading pattern shows the Z anomalies associated with an AO index of 1.

The daily AO index is calculated according to the method of Baldwin et al. (2003), unless indicated otherwise. This involves projecting time-series of daily Z anomalies onto the AO loading pattern calculated as above, where both the anomalies and pattern are area-weighted by the square-root of the cosine of latitude. The daily Z anomalies are defined as deviations from the seasonal cycle, where this cycle is defined by climatological daily means smoothed with a 90-day low-pass filter.

2.3.2.2 AO decorrelation timescale

Important checks on the model dynamics are made in Section 2.2.2 of this chapter, and in Chapter 4, by calculating the AO decorrelation timescale. This timescale is found by first calculating the autocorrelation function, ACF, of the daily AO index, I, as a function of the day of the year, d, and lag, l (Simpson et al., 2011):

$$ACF(d,l) = \frac{\sum_{y=1}^{N_y-1} I(d,y)I(d+l,y)}{\sqrt{\sum_{y=1}^{N_y-1} I(d,y)^2 \sum_{y=1}^{N_y-1} I(d+l,y)^2}} \ , \tag{2.8}$$

where y is the year and N_y is the total number of years. The AO decorrelation timescale for each day of the year is then calculated as the e-folding timescale of the ACF, using a least squares fit to an exponential.

In terms of its physical relevance, the AO decorrelation timescale essentially characterises the typical timescale of AO variability, which itself is partly determined by the strength of internally generated feedbacks (as discussed by Barnes et al. 2010, Shepherd 2014, Hitchcock and Simpson 2016, and references therein). For example, in the case of the tropospheric AO (or jet stream), natural shifts in the jet stream are known to result in a response in tropospheric synoptic eddies; this results in a response in eddy momentum fluxes, which enhance the persistence of the original jet

shift. In addition, natural variability external to the tropospheric jet can also have an influence on jet shifts. For instance, through stratosphere-troposphere coupling, a natural fluctuation in the stratospheric polar vortex (e.g. due to an SSW) will also act to shift the tropospheric jet for an extended time-period. Together, the strength of internal feedbacks and the influence of external variability determine the persistence of a tropospheric jet (AO) shift and, therefore, the timescale of tropospheric jet (AO) variability (and, as such, the AO decorrelation timescale).

The AO decorrelation timescale is particularly important as a consequence of the fluctuation-dissipation theorem (Kubo, 1966; Leith, 1975). This is because the theorem suggests that the response of the tropospheric AO to an external forcing – such as sea-ice loss – should scale with this decorrelation timescale; indeed, this has been found to be the case in many studies (Gerber et al., 2008; Simpson et al., 2010; Garfinkel et al., 2013). The idea behind this is that when the AO is disturbed by an external forcing, this induces the same feedbacks that occur as a part of natural tropospheric AO variability, and the strength of these feedbacks – which determines the magnitude of the AO decorrelation timescale – may influence the magnitude of the response. There are studies that have, however, found limited applicability of the fluctuation-dissipation theorem in some cases (e.g. McGraw and Barnes, 2016; Simpson and Polvani, 2016).

2.3.2.3 Spatial projections

In many parts of thesis, spatial patterns will be 'projected' onto other spatial patterns to determine the degree of their resemblance. The most frequent example of this will involve projecting the 500 hPa geopotential height (Z) response for an IGCM4 perturbation run onto the 500 hPa AO loading pattern for the IGCM4 control run CTL, in order to calculate the response in the AO index.

To do this, a spatial least squares linear regression method is used, in which the spatial data are fitted to the following model (Faraway, 2016):

$$y = \beta X + E \ , \tag{2.9}$$

where – in the example here – y is the 500 hPa Z response (known), X is the AO loading pattern – essentially the first EOF – at 500 hPa (known), β is the regression coefficient (the unknown AO index response), and E is the residual (unknown). The method aims to find the value of β such that E is minimised.

For other examples, X could be a different spatial pattern, and y could be fit to multiple spatial patterns X_i simultaneously giving multiple regression coefficients β_i (where i is the number of patterns). Indeed, this will be done at various points in this thesis and will be described then.

2.3.3 Detection of sudden stratospheric warmings

The method used in this thesis – particularly in Chapters 4 and 5 – to detect sudden stratospheric warmings (SSWs) is based on the method of Charlton and Polvani (2007). In this method, a major SSW event is identified by a reversal from westerly to easterly in the zonal mean zonal wind at 60°N and 10 hPa, over the months of November to March. The first day on which this reversal occurs is referred to as the SSW central date, which is used to identify the SSW. To ensure there are no duplicate SSWs identified, an interval of 20 consecutive days with westerly winds must occur after the SSW before another SSW can be detected. Final warmings – which refer to the annual breakdown of the polar vortex in spring – are removed by ensuring that the wind after an SSW returns to westerly for at least 10 consecutive days before April 30.

As in O'Callaghan et al. (2014), one final criterion is included in the SSW detection method used here, which is in addition to Charlton and Polvani (2007)'s criteria. This requires that there is warming poleward of 50°N on an SSW central date, which adheres more closely to the World Meteorological Organisation's (WMO's) definition of SSWs. To do this, spatial averages over 50°N-70°N and 70°N-90°N are calculated at 10 hPa. If the poleward region is warmer than the equatorward region then the SSW central date is kept, but if it is not then the SSW central date is discarded.

2.3.4 Statistical methods

2.3.4.1 Response

In this thesis, the climatological mean difference in a variable between a model perturbation (e.g. sea-ice loss) experiment and a model control experiment is henceforth defined as the 'response' in that variable to the imposed perturbation. Since experiments are necessarily finite in length, this difference in the means will contain the model's forced change due to the specified perturbation plus the influence of atmospheric internal variability. Therefore, the response as defined above only provides an estimate of the

model's forced change. The longer the experiments are, the smaller the influence of internal variability on the difference in the experiment means, and the more accurately the response will estimate the model's forced change.

2.3.4.2 T-test for the difference between two means

The statistical significance of the response in a variable is evaluated – unless otherwise stated – using a standard two-sample two-sided t-test, for the null hypothesis that the two experiments have identical climatological means in that variable. The test is two-sided because the sign of the response is unknown. This was calculated using a t-test function in the 'scipy.stats' Python module.

A response will be defined as statistically significant for a p-value of $p \leq 0.05$, meaning that the probability of the difference occurring by chance is 5% or less (i.e. we can be at least 95% confident that the difference was forced by the imposed perturbation).

2.3.4.3 Bootstrap test for the difference between two means

When testing whether the difference in the climatological means of two experiments (i.e. the response) is statistically significant, and the data is non-normally distributed, the t-test is inappropriate because it assumes the data is normally distributed. In this case a bootstrapping method will be used, since bootstrapping makes no assumptions about the data distribution.

The bootstrapping method involves the following steps, which were coded in Python by the author. Firstly, each of the two N year-long experiments are randomly resampled with replacement (i.e. N randomly picked years are chosen from each), and the difference in the means of these two resampled datasets is calculated. This is then done 10000 times, to give 10000 differences in the mean. These 10000 differences in the mean are then plotted on a histogram to give the 'bootstrap distribution'. This bootstrap distribution is used to calculate a bootstrapped 2-sided p-value for the null hypothesis that the difference in the climatological means of the two experiments is equal to zero. If the difference in the climatological means (i.e. the mean of the bootstrap distribution) is positive, then the following is calculated:

$$p = [\ (\text{no. resampled differences} \leq 0)\ \times\ 2\ ]\ /\ 10000\ , \tag{2.10}$$

whereas if the difference is negative, then the following is instead calculated:

$$p = [\ (\text{no. resampled differences} \geq 0)\ \times\ 2\ ]\ /\ 10000\ . \tag{2.11}$$

The idea behind this method arises from the issue that when sampling a normally distributed population, the resulting dataset's distribution – the sample distribution – may not provide the best estimate of the population distribution. In particular, the sample may be skewed by a few extreme values (i.e. it may be non-normally distributed), which can skew the sample mean. Since the bootstrap distribution is calculated by resampling the dataset many thousands of times, where the few extreme values will only be resampled very occasionally, this bootstrap distribution should give a better estimate of the population distribution. In short, the bootstrapping method tests whether there is a statistically significant difference in the means of two datasets, even when the dataset means are not skewed by a few extreme values.

2.3.4.4 Temporal least squares linear regression

To find the linear relationship between an independent variable X and dependent variable Y, where there are n pairs of observations of X and Y in time $\{(\mathbf{x}, \mathbf{y}) = (x_i, y_i) : i = 1, .., n\}$, a least squares linear regression function in the Python 'scipy.stats' module is used. This regression model can be used to predict the mean value of Y, $\hat{\mu}$, for a given value of X, x. Use of this method will be made in Section 3.4.3 of Chapter 3, and also for calculating the AO loading pattern throughout this thesis (see Section 2.3.2.1).

2.3.4.5 Confidence intervals

A two-sided $p \times 100\%$ confidence interval for the mean μ of a variable is calculated according to the method of von Storch and Zwiers (1999):

$$\left(\mu - t\frac{S}{\sqrt{n}}, \mu + t\frac{S}{\sqrt{n}}\right)\ , \tag{2.12}$$

where t is the $0.5 + p/2$ quantile of the t-distribution with $(n-1)$ degrees of freedom, S is the standard deviation, and n is the number of independent samples.

To calculate a two-sided $p \times 100\%$ confidence interval for $\hat{\mu}$, as defined in Section 2.3.4.4 and found in Section 3.4.3 of Chapter 3, the method of von Storch and Zwiers (1999) is used:

$$\hat{\mu} \pm t\hat{\sigma}_E \sqrt{\frac{1}{n} + \frac{(x - \bar{\mathbf{x}})^2}{S_{XX}}} \ , \tag{2.13}$$

where t is as defined above, and the overbar denotes a mean. $\hat{\sigma}_E$ is the standard error of the estimate (a measure of the accuracy of the predictions of Y, $\hat{y}_i$, for each value of x_i):

$$\hat{\sigma}_E = \sqrt{\frac{\sum_{i=1}^{n}(y_i - \hat{y}_i)^2}{n-2}} \ , \tag{2.14}$$

and S_{XX} is defined as:

$$S_{XX} = \sum_{i=1}^{n}(x_i - \bar{\mathbf{x}})^2 \ . \tag{2.15}$$

Chapter 3

Sensitivity to the region and magnitude of sea-ice loss

3.1 Introduction

This chapter's contents have been published as a paper in Geophysical Research Letters (McKenna et al., 2018). This paper appears here with some edits. For example, more detailed explanations have been provided where helpful or interesting, and material has been moved from the Supplementary Items to the main text. The paper has also been edited to avoid overlap with other chapters – specifically, parts of the introduction and method sections instead appear in Chapters 1 and 2 – and to be consistent with the results of other chapters – for example, small parts of the method and discussion/conclusions sections have been added to or edited for consistency with Chapters 4 and 5.

The aim of this chapter is to understand the extent to which the atmospheric response to sea-ice loss is sensitive to first and foremost the region of loss, and secondly to the magnitude of this loss. This is with the wider aim of understanding whether the different spatial patterns and magnitudes of loss assumed by different studies can explain why they find contrasting results, as detailed in Chapter 1. For example, this may be relevant for understanding contrasting results for studies using different CMIP5 (Coupled Model Intercomparison Project Phase 5) climate models, since the spatial pattern and magnitude of future Arctic surface warming – which is related to sea-ice loss – is uncertain across these models (see Figure 1.1 in Chapter 1).

The focus is first on whether the contrasting stratospheric responses of past studies can be explained by the different spatial patterns of sea-ice loss assumed. This was examined previously by Sun et al. (2015), who found that Atlantic and Pacific sector sea-ice losses respectively lead to a weakening and strengthening of the stratospheric polar vortex due to differences in linear wave interference (see Chapter 1).

Two further questions that are addressed are whether different spatial patterns of sea-ice loss can also explain the contrasting tropospheric responses in previous studies, and what effects different loss regions have on mid-latitude surface temperatures. Since Baldwin and Dunkerton (2001) and many subsequent studies find that a weaker (stronger) polar vortex is often followed by a negative (positive) tropospheric AO/NAO (Arctic Oscillation/North Atlantic Oscillation), in studies with more Atlantic (Pacific) sector sea-ice loss we might expect a negative (positive) AO/NAO – indeed, this is the case in Kim et al. (2014) (Cai et al., 2012) – and colder (warmer) regions in mid-latitudes. However, while Sun et al. (2015) find that the zonal mean tropospheric eddy-driven jet shifts south (a negative AO) for their Atlantic experiment, they find no shift for their Pacific experiment. They also do not examine the surface temperature response in the separate Atlantic and Pacific cases. Therefore, this chapter looks in detail at stratosphere-troposphere interactions and the surface temperature response in each case. Other studies examine the tropospheric and surface temperature responses to regional sea-ice anomalies, but do not focus on the role of the stratosphere (Alexander et al., 2004; Koenigk et al., 2016; Pedersen et al., 2016; Screen, 2017b).

The second focus of this chapter is on whether different magnitudes of sea-ice loss can help to explain the contrasting results of previous studies. As discussed in Chapter 1, previous studies have compared the responses to different loss magnitudes and find the response to be non-linear, and sometimes even opposite. Here, the linearity of the response is examined for different regions of sea-ice loss; previously only Atlantic sector (Petoukhov and Semenov, 2010; Nakamura et al., 2016a) and whole-Arctic (Peings and Magnusdottir, 2014; Nakamura et al., 2016a; Wu and Smith, 2016) sea-ice losses have been considered.

3.2 Aim and research questions

In summary, this chapter aims to understand whether the contrasting results of previous studies can be explained by the different spatial patterns and magnitudes of sea-ice loss

that were assumed. To do this, idealised modelling experiments are conducted using an intermediate global circulation model, IGCM4, to address the following research questions:

1. Do sea-ice losses confined to the Atlantic or Pacific sector of the Arctic have opposite effects on the stratospheric polar vortex?
2. Are there correspondingly opposite effects on the tropospheric AO?
3. What are the effects on mid-latitude surface temperatures?

Questions 1 and 2 have been examined previously by Sun et al. (2015) using the full complexity atmosphere-only model WACCM4. It will be shown in this chapter, and in subsequent chapters, that the more idealised approach taken here using IGCM4 is particularly useful for obtaining a better understanding of the responses and mechanisms involved.

3.3 Method

3.3.1 Numerical modelling experiments

Three main experiments – one control run and two perturbation runs – were conducted, each of which consists of a 1 year spin-up (discarded in the results) followed by another 200 years. This run length is longer than used in many similar modelling studies investigating the stratospheric and tropospheric responses to sea-ice loss, in which run lengths have typically been between 20 years and 161 years (Cai et al., 2012; Kim et al., 2014; Peings and Magnusdottir, 2014; Sun et al., 2015; Nakamura et al., 2015, 2016a,b; Zhang et al., 2018a,b). The 200 year run length also satisfies the Polar Amplification Model Intercomparison Project (PAMIP) requirement that runs should be at least 100 years-long (or consist of 100 ensemble members), and longer if possible, in order to obtain statistically robust results (Smith et al., 2019).

In the control run (CTL), an annually repeating cycle of historical monthly mean surface temperatures (T_s) is prescribed over the ocean using ERA-interim reanalysis data averaged over 1979-2014. In the Atlantic/Pacific sector perturbation run (ATL/PAC), the same boundary conditions are used as in CTL, but with an annually

repeating cycle of monthly mean T_s anomalies added in the Barents-Kara/Chukchi-Bering Seas representing late 21st century sea-ice retreat. As in Koenigk et al. (2016), the Barents-Kara Seas are defined as the region between 70°N-82°N and 15°E-100°E, and the Chukchi-Bering Seas are defined as the region between 50°N-82°N and 170°E-200°E. The anomalies here are more regionally confined than in Sun et al. (2015) to allow a 'clean' comparison of the effects of sea-ice loss in the Atlantic versus Pacific sectors and the mechanisms involved. The Barents-Kara and Chukchi-Bering Seas were chosen because it is in these regions that late 21st century projections of surface temperature appear most diverse across the CMIP5 models (Figure 1.1).

The T_s anomalies are derived using projections of sea-ice concentration (SIC) for 2070-2099 by the CMIP5 coupled atmosphere-ocean model HadGEM2-ES under a high anthropogenic emissions scenario (RCP8.5). HadGEM2-ES was chosen because it projects warming of a similar magnitude in the Atlantic and Pacific sectors of the Arctic, while other CMIP5 models project warming that is more weighted to one sector (Figure 1.1). Note that HadGEM2-ES also projects warming that is in the upper range of the CMIP5 model projections, so the T_s anomalies in ATL and PAC will be referred to as 'large-magnitude' anomalies.

The following method was used in the derivation (see Section 2.2.1 of Chapter 2 for some useful background). For example, at grid-points where there is full sea-ice cover in CTL (where the ocean T_s < -2°C, since sea-ice forms at this temperature) but 0% SIC in projections, the T_s is set to 0°C in ATL/PAC (representing full melting of the sea-ice). The T_s anomaly is then defined by: [T_s anomaly] = [T_s in ATL/PAC] - [T_s in CTL]. Similarly, where there is full sea-ice cover in CTL but 50% SIC in projections, the T_s is increased from its CTL value halfway to 0°C in ATL/PAC (representing half of the sea-ice melting). This is repeated similarly for other projected values of SIC. The anomalies are also smoothed linearly in space and between months. Anomalies are only prescribed where there is sea-ice loss to directly isolate the atmospheric response to sea-ice changes alone. Deser et al. (2016a) found that taking broader changes in sea surface temperature into account through ocean-atmosphere coupling does not change the overall pattern of the extratropical atmospheric response to Arctic sea-ice loss, but does amplify it by approximately 50%.

Figures 3.1a and 3.2a show the seasonal evolution of ocean T_s in each run, and T_s anomalies for ATL and PAC. The anomalies emerge in autumn (SON), peak in winter (DJF), then reduce going into spring (MAM). The resulting anomalous upward surface

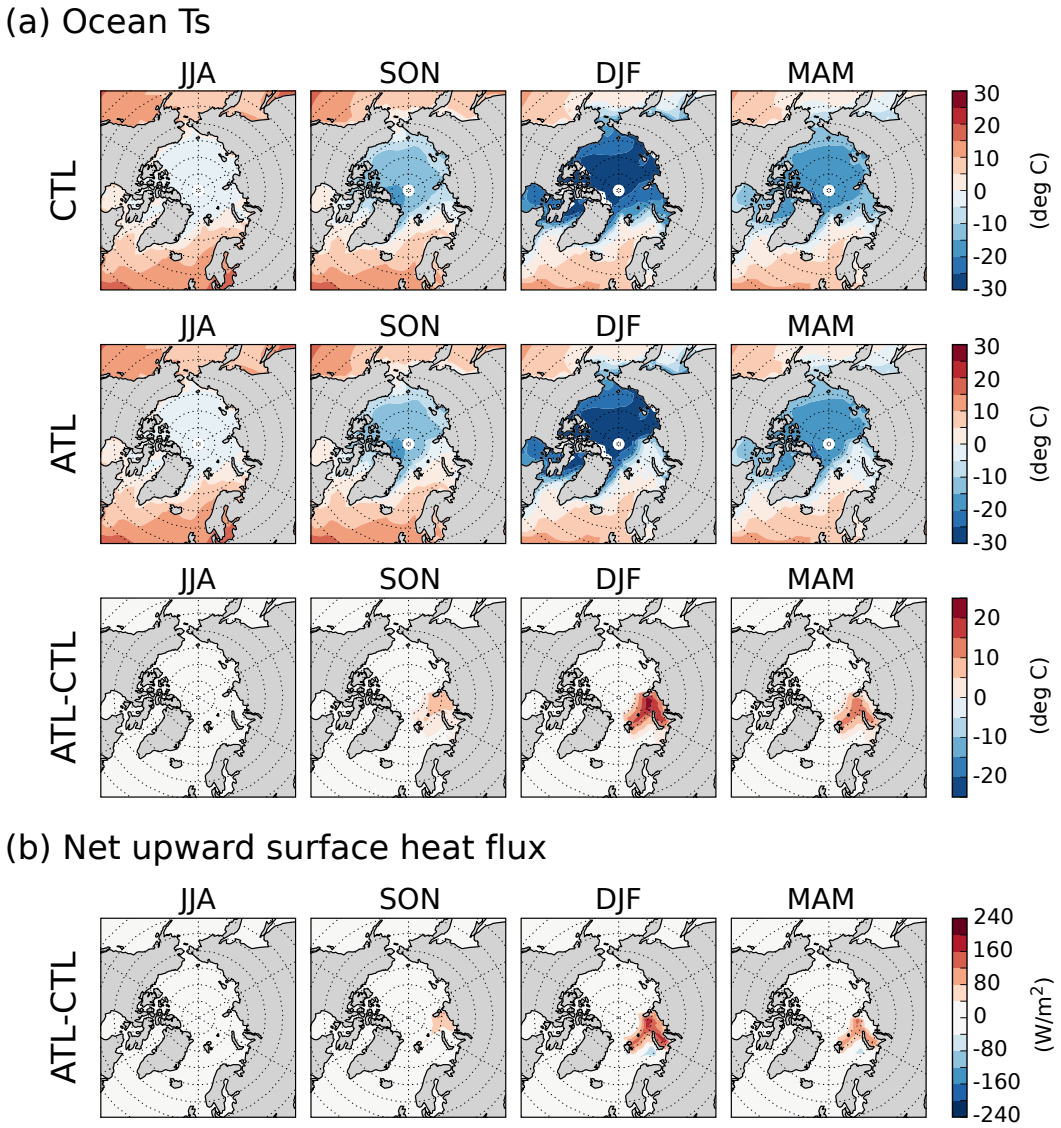

Fig. 3.1 (a) Annually repeating cycle of seasonal mean surface temperature (T_s) imposed over the ocean in the [Top] control run (CTL), [Middle] large-magnitude Atlantic sector sea-ice loss run (ATL), and [Bottom] ATL-CTL. Note that the ocean T_s is actually imposed in monthly means, but is shown here in seasonal means. (b) Response of the net surface heat flux (positive upwards) in ATL, based on the sum of turbulent (sensible plus latent) and longwave radiative heat fluxes. The longwave radiative flux is driven by the temperature of the surface and the amount of downwelling longwave radiation (e.g. due to clouds). The sensible and latent heat fluxes are driven by the gradients in temperature and water vapour pressure respectively between the sea surface and air above, which themselves are also influenced by the surface wind speed (since winds replenish air at the sea-air interface and enhance these gradients). The turbulent fluxes dominate here, as in other studies looking at the response to sea-ice loss (e.g. Kim et al., 2014; Peings and Magnusdottir, 2014; Sun et al., 2015).

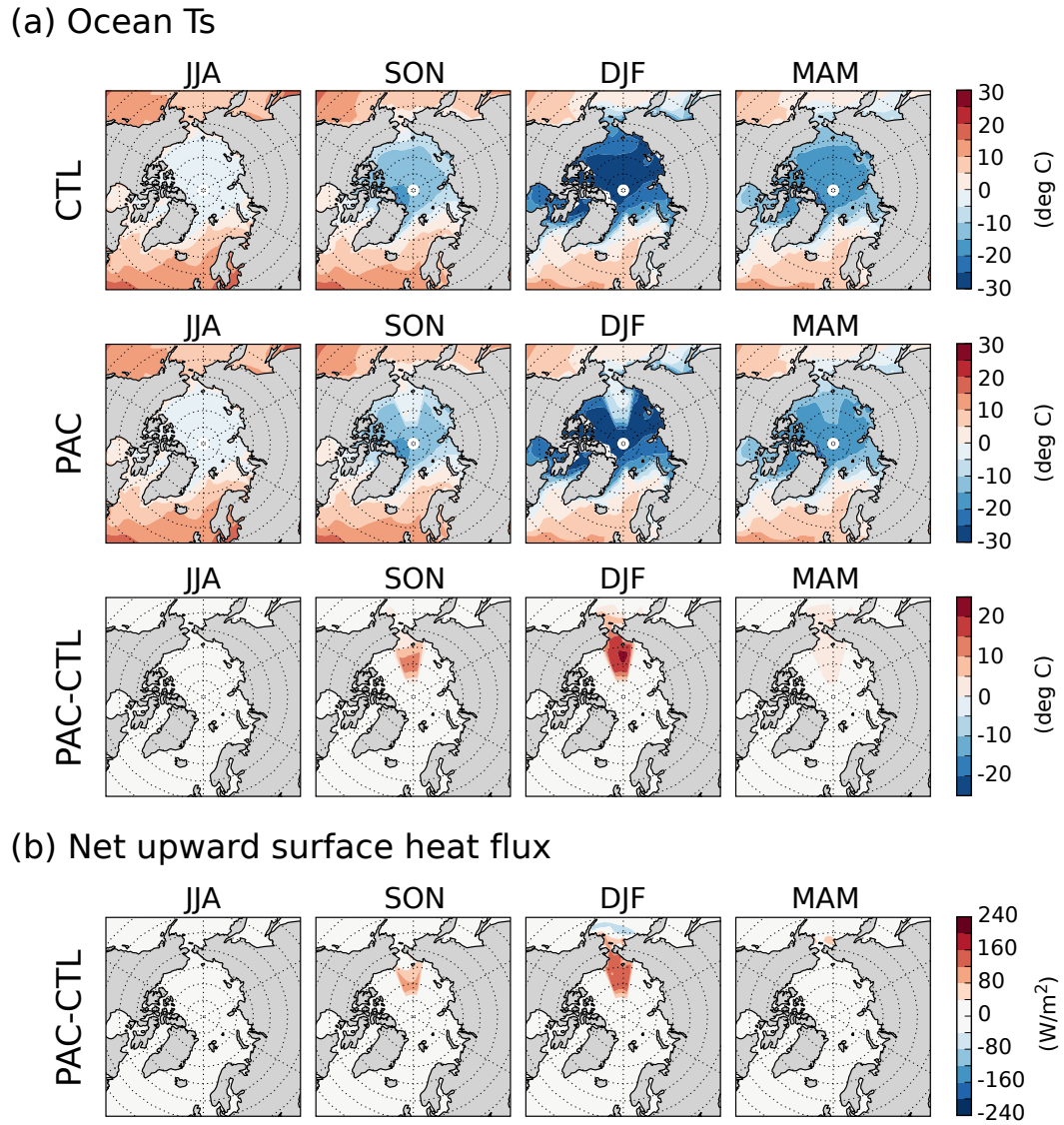

Fig. 3.2 As in Figure 3.1, but for the large-magnitude Pacific sector sea-ice loss run (PAC).

heat fluxes follow a similar seasonal evolution (Figures 3.1b and 3.2b), reflecting that the T_s anomalies are largest in winter when the overlying air is also coldest relative to the surface climatologically. These fluxes peak at $\sim$ 240 W/m^2 in winter, while Sun et al. (2015)'s peak at $\sim$ 250 W/m^2, showing that the anomalous forcing here is comparable in magnitude.

The linearity of the key results in ATL and PAC is examined by conducting two further perturbation runs (0.5ATL and 0.5PAC) with half the magnitude of imposed T_s anomalies (Figures 3.3a and 3.4a). These anomalies represent warming that is in

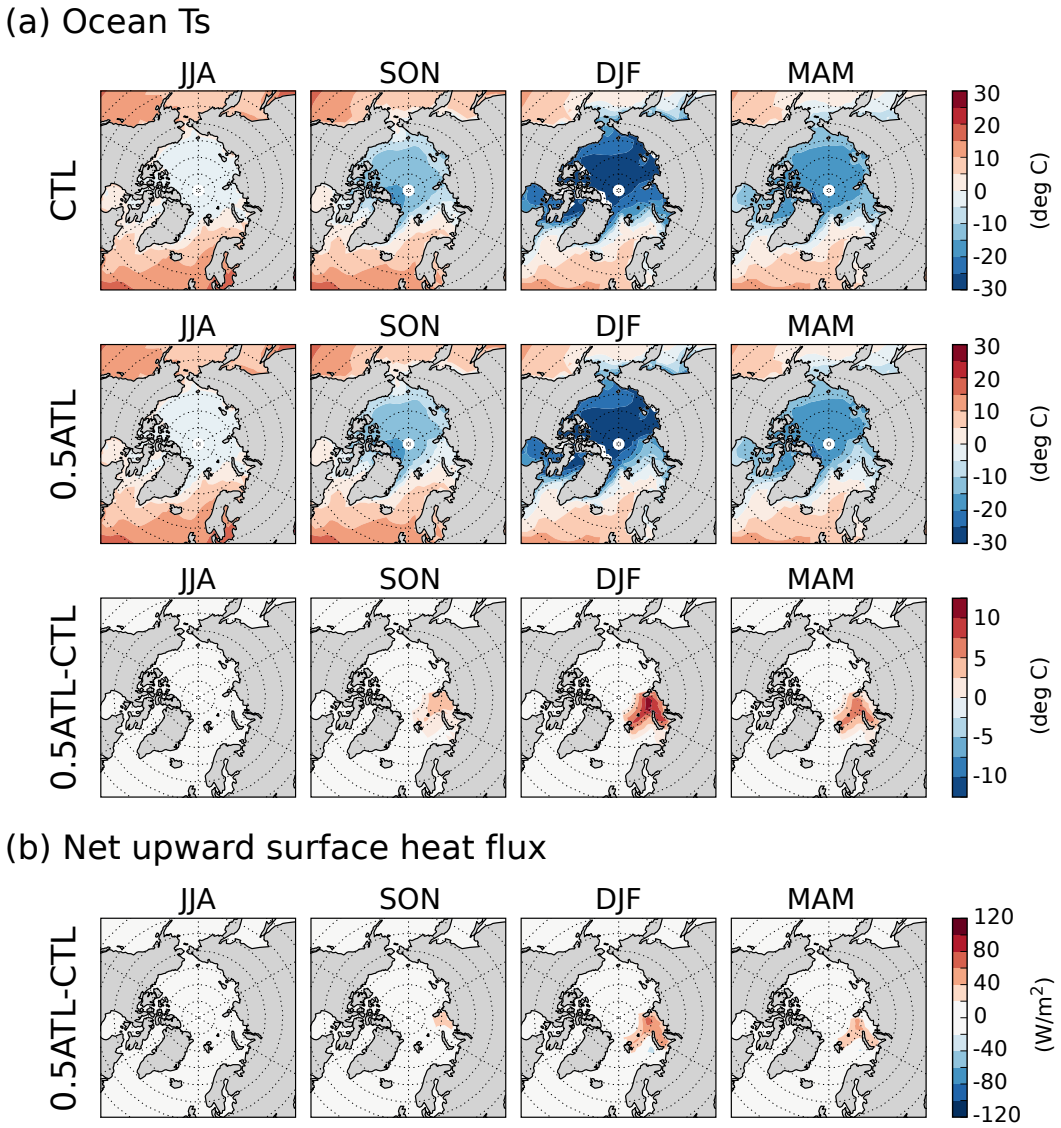

Fig. 3.3 As in Figure 3.1, but for the moderate-magnitude Atlantic sector sea-ice loss run (0.5ATL). For ease of comparison, the colourbar intervals in the 0.5ATL-CTL plots are half the magnitude of those in the ATL-CTL plots in Figure 3.1.

the lower range of late 21st century CMIP5 model projections (Figure 1.1), and could also represent a mid 21st century warming for those models in the upper range of late 21st century projections. As such, the T_s anomalies in 0.5ATL and 0.5PAC will be referred to as 'moderate-magnitude' anomalies. The 0.5ATL and 0.5PAC runs were conducted for 300 years, since for a smaller forcing a longer run is required to achieve statistical significance. When analysing these runs an extended 300 year-long version of CTL is used.

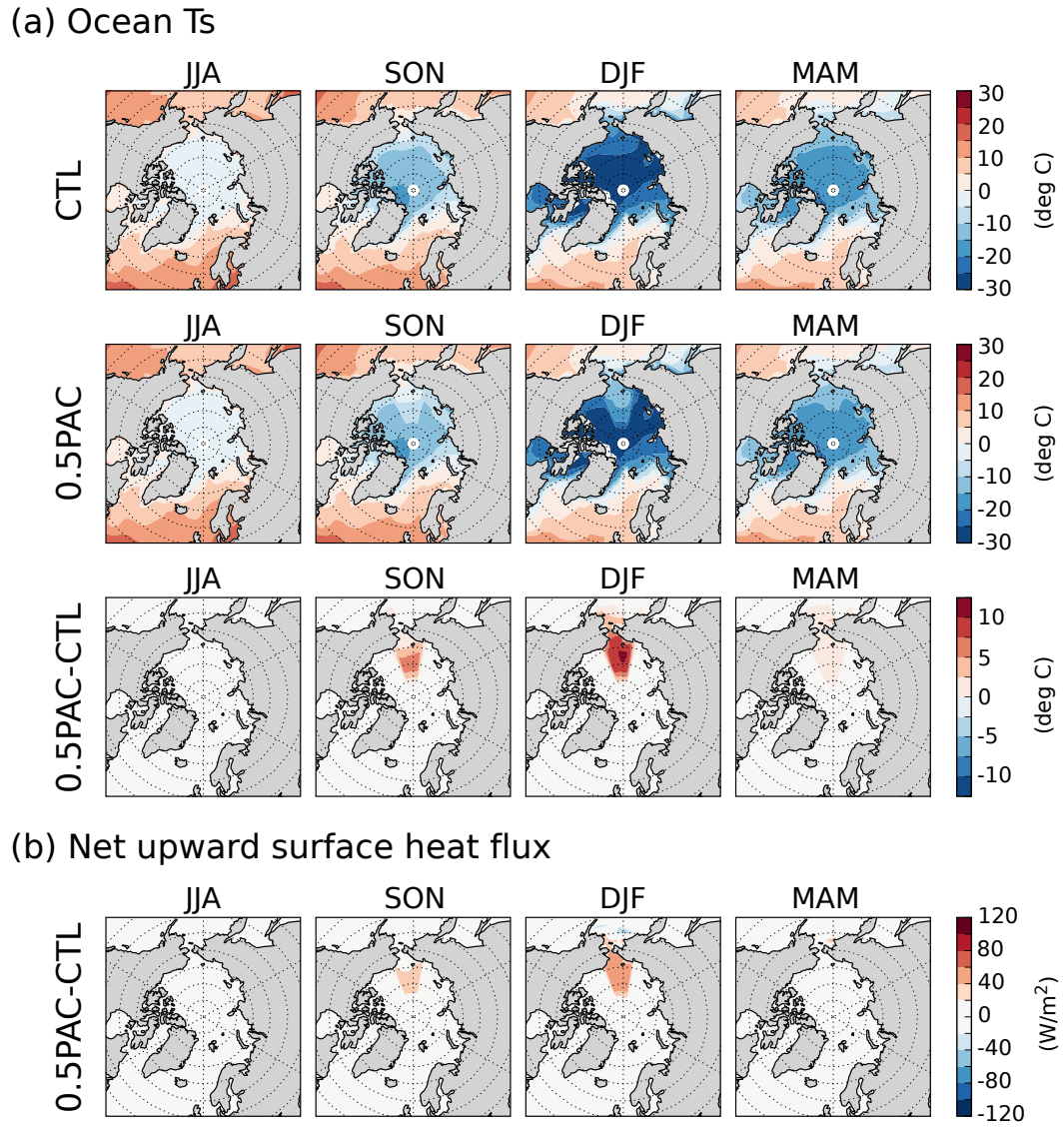

Fig. 3.4 As in Figure 3.2, but for the moderate-magnitude Pacific sector sea-ice loss run (0.5PAC). For ease of comparison, the colourbar intervals in the 0.5PAC-CTL plots are half the magnitude of those in the PAC-CTL plots in Figure 3.2.

Finally, while many CMIP5 models project late 21st century warming that is weighted toward either the Atlantic or Pacific sectors of the Arctic, many also project warming that is of equal magnitude in these regions (recall HadGEM2-ES for example in Figure 1.1). Therefore, an additional 200 year-long experiment is conducted with large-magnitude T_s anomalies imposed in the Atlantic and Pacific sectors simultaneously (ATL&PAC run). The results of this experiment will be discussed near the end of this chapter.

3.3.2 Response and statistical significance

The response of any variable is defined by its climatological mean difference between a perturbation (sea-ice loss) run and the control run (e.g. ATL-CTL). November to January is chosen as a common period for comparing the response in key meteorological fields in ATL and PAC, since this is when the imposed ocean T_s anomalies are strongest and most comparable in magnitude in both runs. Indeed, Figure 3.5 shows that while the anomalous forcing increases steeply into November and peaks in December or January in both runs, in PAC the forcing steeply drops off in magnitude in February, whereas in ATL strong forcing is sustained until April. These different monthly evolutions likely explain why a strong robust response in the large-scale atmospheric circulation is found in ATL from November to March only, while in PAC from November to January only (not shown). The response is similar in each month of November to March in ATL, and in each month of November to January in PAC.

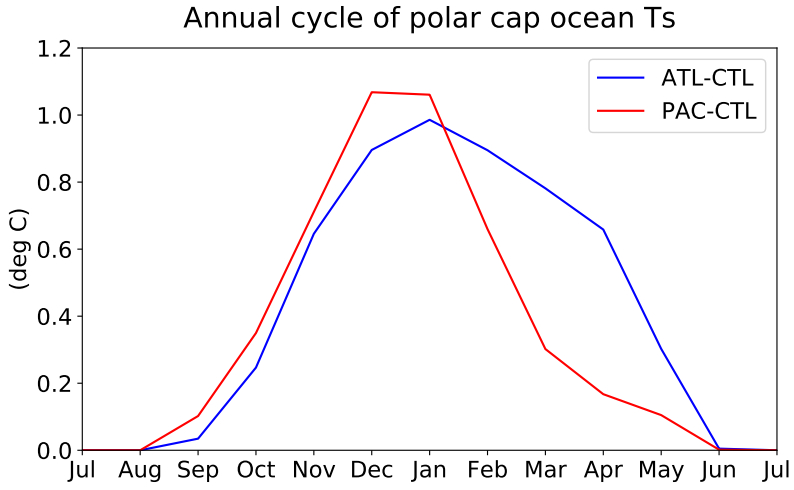

Fig. 3.5 Annual cycle of polar cap (60°N-90°N) averaged, monthly mean ocean surface temperature anomalies imposed in the ATL (blue line) and PAC (red line) experiments. A polar cap average was calculated in order to compare the anomalous forcing in each run over the same area, ensuring a like-for-like comparison of the forcing magnitude.

The statistical significance (hereafter 'significance') of the response is evaluated – unless otherwise stated – using a t-test as detailed in Section 2.3.4.2 of Chapter 2. The t-test is conducted with 200 (300) degrees of freedom for the ATL/PAC (0.5ATL/0.5PAC) runs, since there are 200 (300) years of data and in each run there is negligible auto-correlation in the winter mean large-scale atmospheric circulation for

any yearly lag (based on the 500 hPa and 10 hPa AO indices, and SSW frequency). This is also justified because no significant changes in the raw meteorological fields (including T_s) remain throughout the summer months in the perturbation runs. In all figures, stippling indicates significance at a 95% confidence level. The significance was also tested using the bootstrapping method described in Section 2.3.4.3 of Chapter 2, which shows very similar results to the t-test (not shown). However, this additionally suggests that the significance of the response is not dependent on only a few extreme years and, therefore, that the response is qualitatively consistent over the length of the runs.

3.4 Results

3.4.1 Stratospheric response

In the ATL/PAC runs the stratospheric polar vortex is significantly weaker/non-significantly stronger in November-January than in CTL (Figure 3.6a; note that while the response in PAC was initially thought to be significant in November-December – see McKenna et al. (2018) – Chapter 5's findings suggest this is non-robust). Plots of the Eliassen-Palm (EP-flux) and its divergence (Figure 3.7a) show that this is consistent with an enhancement/suppression of upward Rossby wave propagation in November-December around the latitudinal range of the imposed T_s anomalies ($\sim$ 60°N-80°N). Decomposing the EP-flux into its zonal wavenumber-1/2/3 (wave-1/2/3) components shows that wave-1 waves explain most of these changes (not shown). Indeed, if we examine the wave-1 component of geopotential height (Z) averaged over 60°N-80°N and November-December, this enhancement/suppression appears to be due to constructive/destructive linear interference between anomalous and climatological wave-1 stationary waves (Figure 3.7b). The amplitude of the waves naturally increases with height because of decreasing density, and the westward tilt of the waves with height indicates they are upward propagating (since it can be shown that the vertical EP-flux component, $F_z = \frac{\rho_0 a \cos\phi}{N^2}\left[\frac{\partial\Phi^*}{\partial x}\frac{\partial\Phi^*}{\partial z}\right]$ (where Φ is the geopotential), for which the expression in the square brackets is positive for a westward tilt). Figure 3.7c demonstrates this interference mechanism geographically, where the 500 hPa Z response in ATL/PAC constructively/destructively interferes with the climatological wave-1 500 hPa Z at high latitudes.

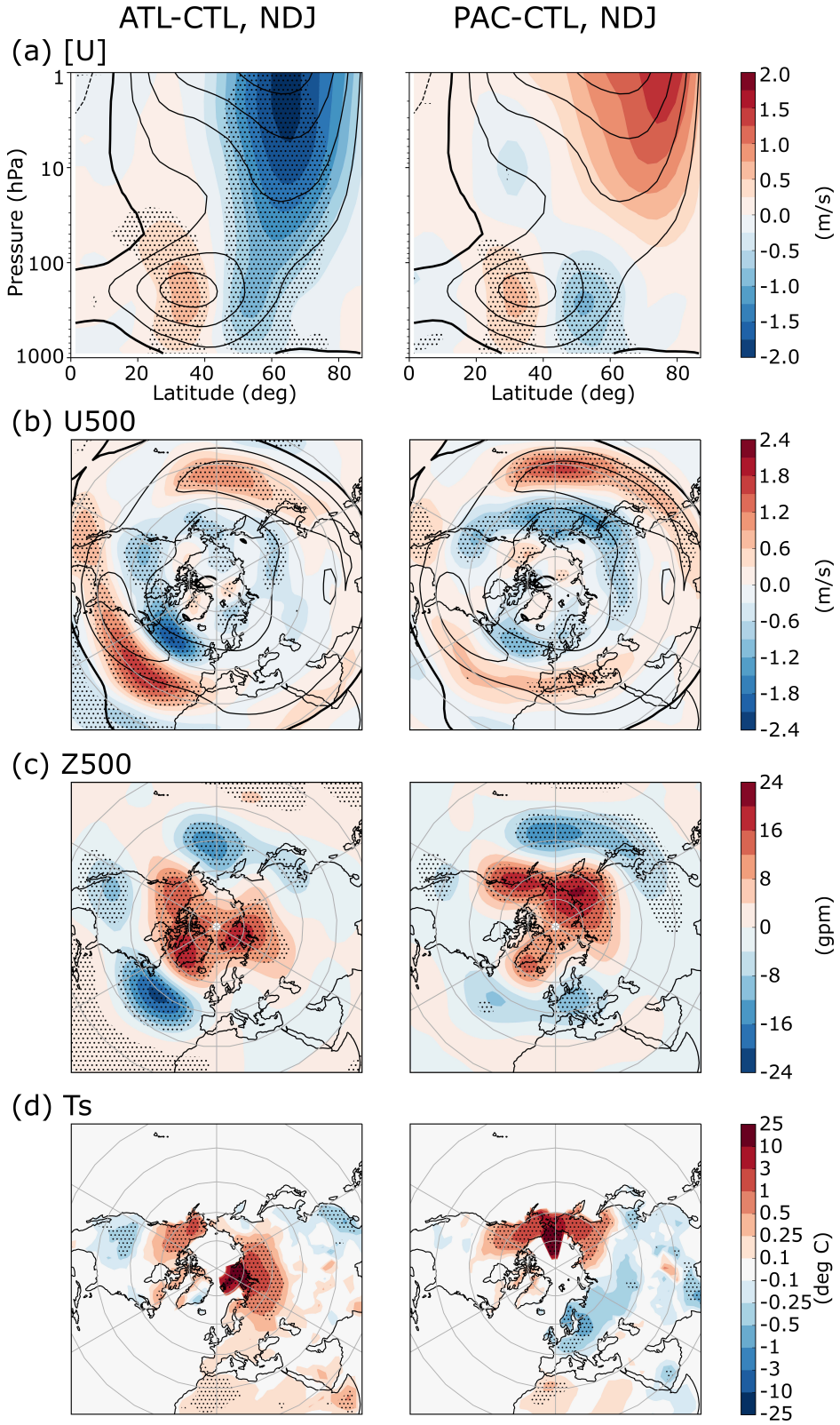

Fig. 3.6 NDJ response (shading) of (a) zonal mean zonal wind, (b) 500 hPa zonal wind, (c) 500 hPa geopotential height, and (d) surface temperature, in [Left] ATL and [Right] PAC. Contours show climatological values from the control run CTL (interval: 10 m/s) and stippling indicates a significant response at a 95% confidence level.

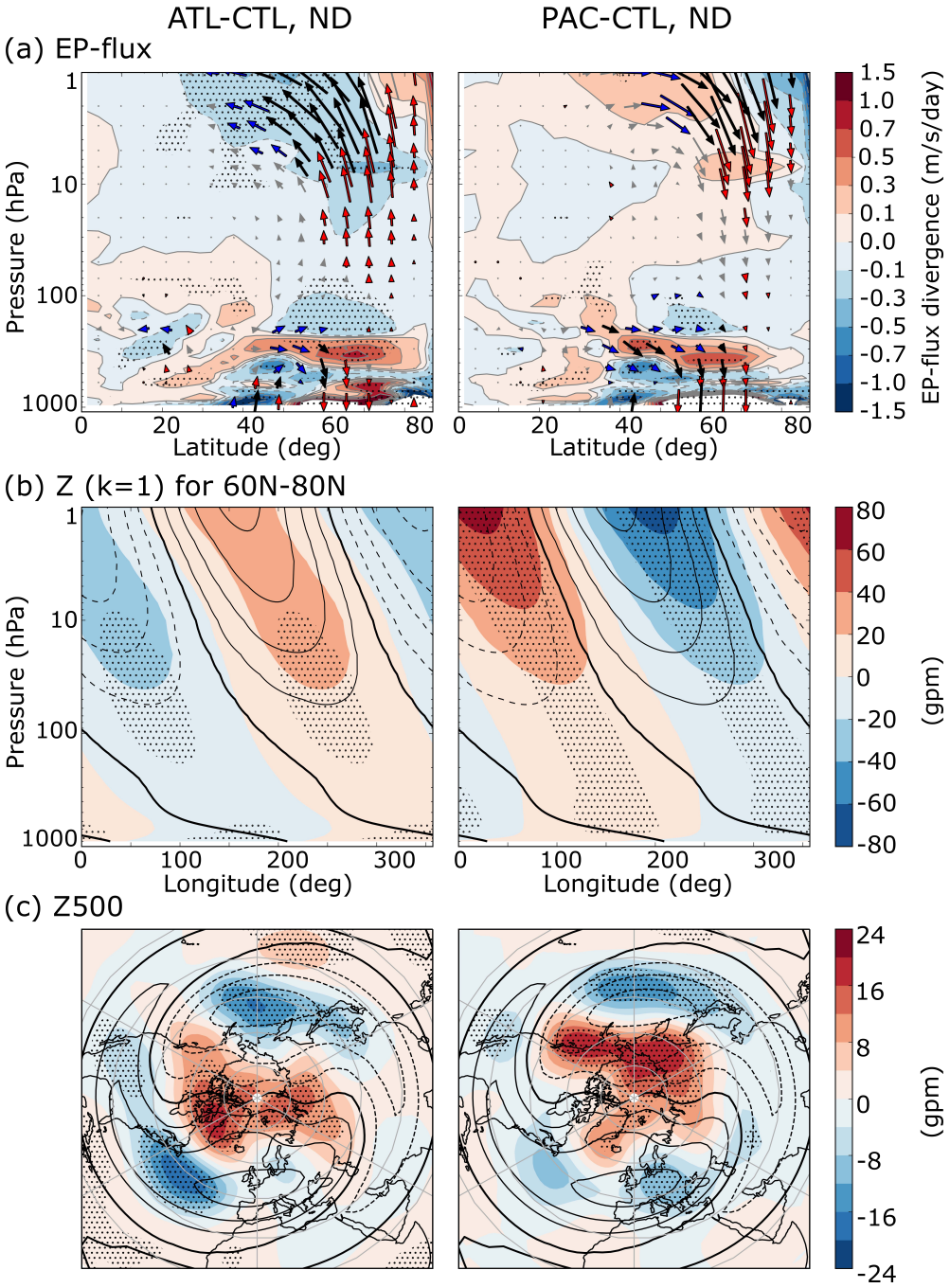

Fig. 3.7 ND response of (a) EP-flux (arrows) and EP-flux divergence (shading), (b) zonal wave-1 geopotential height averaged over 60°N-80°N (shading), and (c) 500 hPa geopotential height (shading). [Left] ATL and [Right] PAC. EP-flux vectors are coloured blue/red if the meridional/vertical component is significant, and black if both are. Stippling indicates a significant response for shaded fields at a 95% confidence level. Contours in (b) and (c) show climatological wave-1 values from the control run CTL (interval in (b)/(c): 150 gpm/15 gpm). See Section 2.3.1.1 in Chapter 2 for further details on how the EP-flux and its divergence are calculated.

Note that the total anomalous vertical wave propagation is in fact composed of the previously described time-mean linear (TM_{LIN}) component as well as a time-mean non-linear (TM_{NLIN}) component, and a high-frequency wave fluctuation (FL) component (Smith et al., 2010; see Section 2.3.1.3 in Chapter 2 for further details on this decomposition). However, it is found that the TM_{LIN} component does indeed dominate in both ATL and PAC (Figure 3.8). Sun et al. (2015) use a different decomposition method (Nishii et al., 2009), but the results of this method are more difficult to interpret since it mixes the FL component in with the other terms. As such, this method is more suitable for observational data records, which are often limited in time. Smith et al. (2010)'s method is more suitable for long model experiments, since they allow fluctuations about the time-mean to be more easily extracted. Regardless, it is also found that the linear component dominated using the Nishii et al. (2009) decomposition, in agreement with Sun et al. (2015).

Focusing now on 0.5ATL/0.5PAC, the polar vortex is weaker/stronger in November-January than in CTL (Figure 3.9a) consistent with ATL/PAC. The responses are not significant, but the vortex is significantly stronger in 0.5PAC than in 0.5ATL (Figure 3.10a). Further plots (not shown) are mostly consistent with ATL and PAC, but in both 0.5ATL and 0.5PAC there are limited regions of significance in the stratospheric EP-flux divergence and 60°N-80°N wave-1 Z. As in ATL and PAC, the time-mean linear component of the zonal mean eddy heat flux response explains a large part of the anomalous vertical wave propagation in 0.5ATL and 0.5PAC.

3.4.2 Tropospheric response

While there are opposite stratospheric responses in the ATL and PAC runs, the tropospheric responses both resemble a negative AO. This is shown in Figure 3.6a - 3.6c by the response in zonal mean zonal wind (an equatorward shift of the zonal mean eddy-driven jet), the 500 hPa zonal wind (an equatorward shift of the Atlantic eddy-driven jet and strengthening of the Pacific eddy-driven jet as in Ambaum et al. 2001), and the 500 hPa geopotential height, Z500 (positive/negative heights at higher/lower latitudes). Indeed, projecting the November-January Z500 response in ATL/PAC onto the winter mean 500 hPa AO loading pattern from CTL gives an AO index of -0.25/-0.26, and shows that the AO explains 61%/75% of the response's spatial variance (see Sections 2.3.2.1 and 2.3.2.3 in Chapter 2 for details on calculating the AO loading pattern and this projection method).

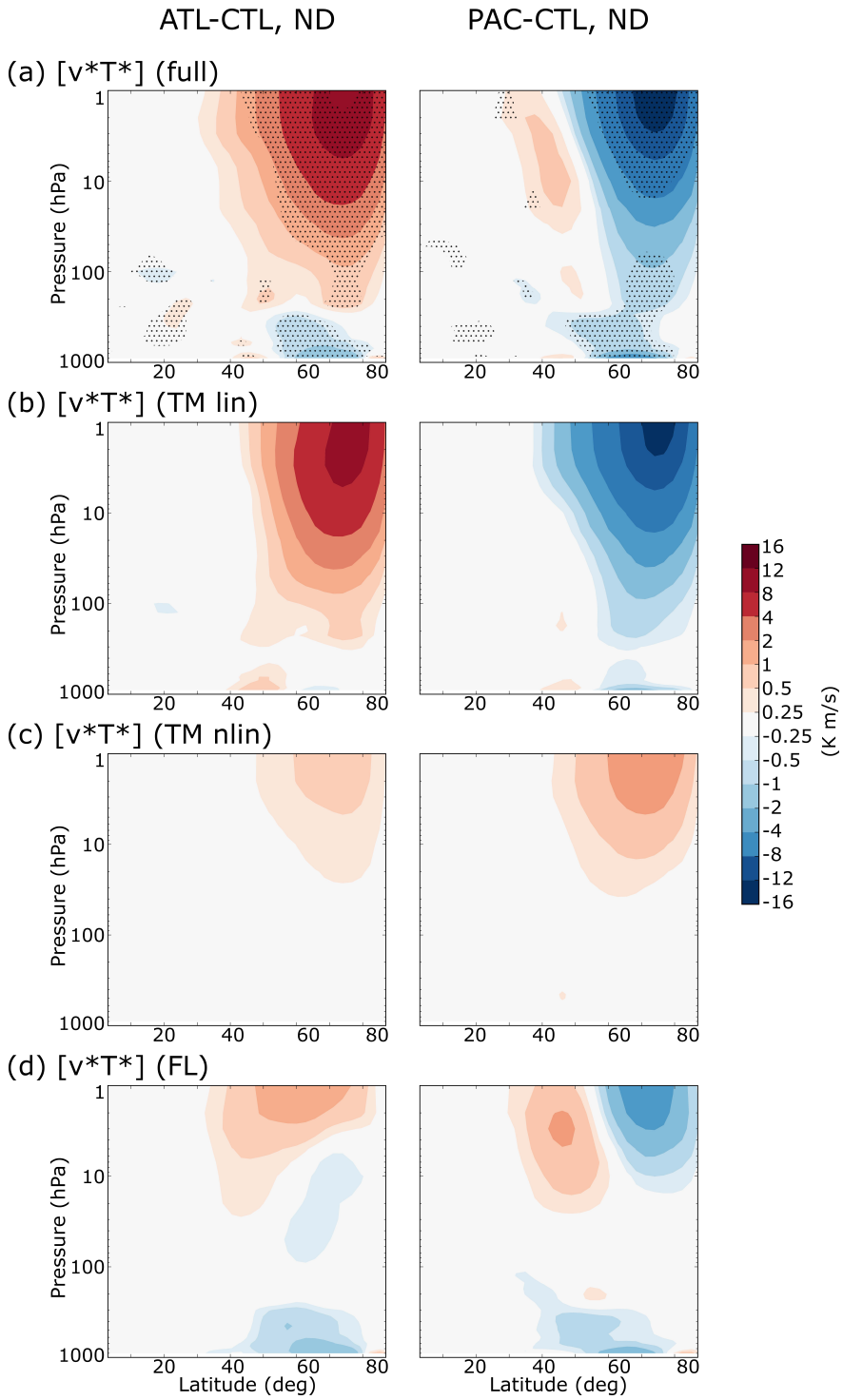

Fig. 3.8 ND response of the (a) zonal mean eddy heat flux, and its decomposition into a (b) time-mean linear component (TM_{LIN}), (c) time-mean non-linear component (TM_{NLIN}), and (d) high-frequency wave fluctuation component (FL). [Left] ATL response and [Right] PAC response. Stippling in (a) indicates a significant response at a 95% confidence level. See Section 2.3.1.3 in Chapter 2 for details of this decomposition.

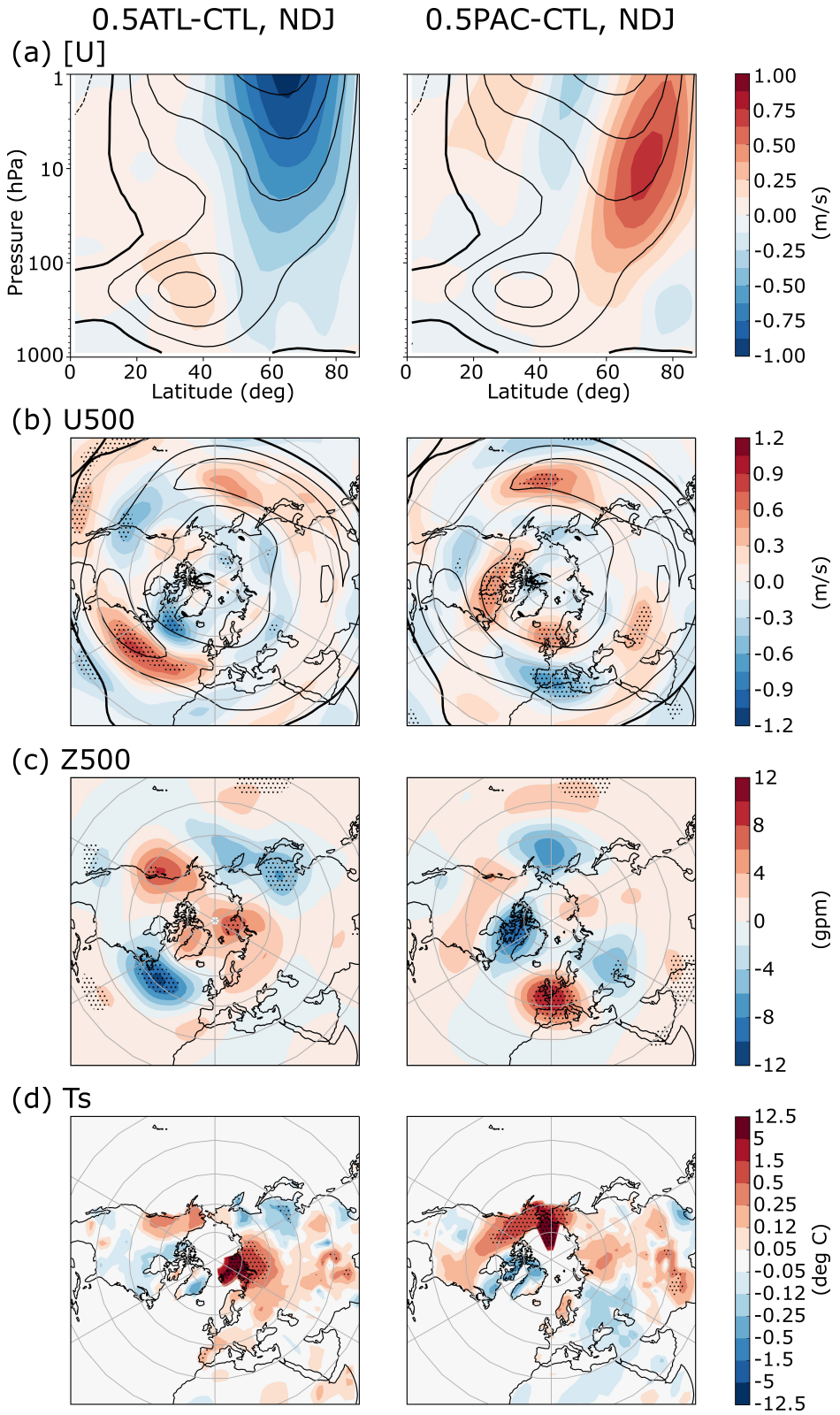

Fig. 3.9 As in Figure 3.6, but for 0.5ATL and 0.5PAC. For ease of comparison, the colourbar intervals are half the magnitude of those in Figure 3.6.

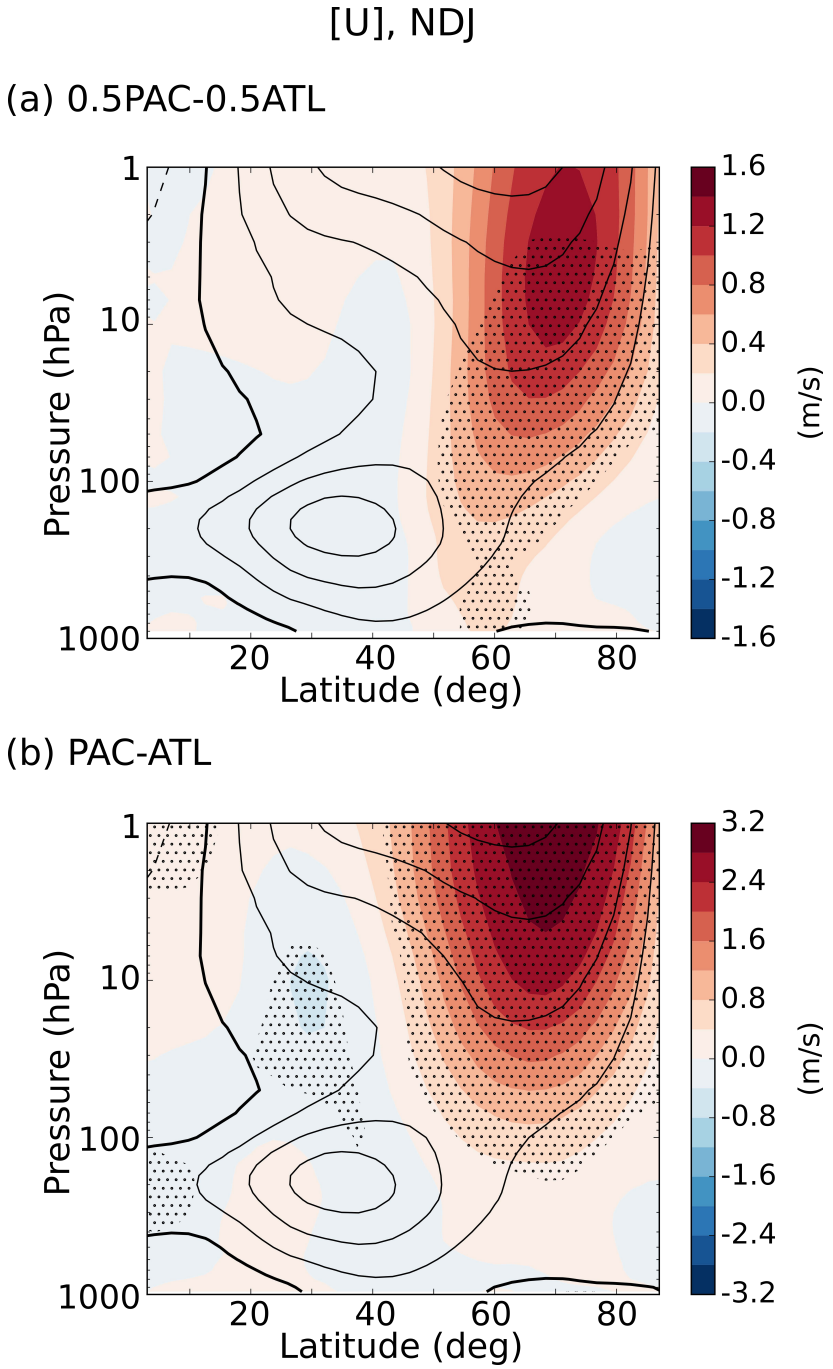

Fig. 3.10 Zonal mean zonal wind in NDJ for (a) 0.5PAC-0.5ATL and (b) PAC-ATL (shading). Contours show climatological values from (a) 0.5ATL and (b) ATL (interval: 10 m/s), and stippling indicates a significant response at a 95% confidence level. For ease of comparison, the colourbar intervals in (a) are half the magnitude of those in (b).

In 0.5ATL/0.5PAC, the tropospheric responses resemble a negative/positive AO (Figure 3.9a - 3.9c), which is consistent with the weaker/stronger polar vortex and agrees/disagrees with ATL/PAC. However, the response in zonal mean zonal wind is non-significant, and the responses in 500 hPa zonal wind and geopotential height are only significant over a small area. Figure 3.10 highlights that there are significant stratospheric differences between ATL and PAC, and 0.5ATL and 0.5PAC, but only in the latter there are corresponding significant differences in the tropospheric AO.

3.4.3 Surface response

While the tropospheric circulation response resembles a negative AO in both the ATL and PAC runs, there are contrasts between ATL and PAC in the T_s response (Figure 3.6d). Specifically, whilst a negative AO is associated with Northern European cooling, this only occurs in PAC, and in ATL there is no evidence of this. Additionally, a negative AO is associated with cooling in eastern North America, but this does not occur in PAC, and in ATL cooling only occurs in western North America.

To understand this, the T_s response is decomposed into an 'indirect' part and a 'direct' part. This is done by extending the approach of Deser et al. (2004), who decompose the circulation response into an 'indirect' part and a 'direct' part, where the former is defined as the part that projects onto the model's leading mode of internal variability (i.e. the large-scale AO-like part hypothesised to be generated indirectly through tropospheric non-linear eddy feedbacks), and the latter is defined as the residual (the full minus indirect circulation response).

Specifically, the indirect T_s response is defined as the part induced by the indirect circulation response (although further leading modes of variability are used here, as explained shortly). To compute this part, the indirect circulation response is firstly found by projecting the Z500 response onto the leading empirical orthogonal functions (EOF's) from CTL (see Section 2.3.2 in Chapter 2 for details on this projection method and calculating the EOF's). The EOF's are defined at 500 hPa as in Deser et al. (2004), since Z may be influenced by boundary layer and orographic effects near the surface, and the interest here is in large-scale changes. Deser et al. (2004)'s approach is then extended, by temporally regressing the normalised principal components (PC's) associated with each EOF onto the T_s in CTL (see Section 2.3.4.4 in Chapter 2). This gives a map of the indirect T_s response for each EOF for a PC value of 1. The maps are

then scaled by the regression coefficients obtained for each EOF in the Z500 projections. To calculate the significance of the indirect T_s response, a two-sided 95% confidence interval obtained from the PC-T_s regressions is used (see Section 2.3.4.5 of Chapter 2); if 0 lies outwith this interval, the response is defined as statistically significant.

In terms of the direct T_s response, this is defined as the residual (the full minus indirect T_s response), similar to Deser et al. (2004)'s definition of the direct circulation response. While the direct T_s response is related to the direct circulation response, the former is also influenced by other factors (e.g. the interaction of climatological winds with the imposed T_s anomalies). They should be similar, however, in terms of being local to the sea-ice loss region. Hence for the Z500 projections the first three EOF's are used, since only projecting onto EOF1 (the AO) gave a Z500 residual containing EOF2 (the Pacific-North American pattern) in ATL and PAC, and EOF3 (a dipole between the North Atlantic and North Pacific) in ATL. The significance of the direct T_s response is calculated by finding the residual response in each year, and applying a one-sample two-sided t-test for the mean of this dataset (with a null hypothesis expected mean of zero).

Figure 3.11 shows the indirect and direct parts of the T_s and Z500 responses in ATL and PAC. Only the EOF1-induced indirect T_s response is shown, since the EOF2-induced and EOF3-induced responses are small. Focusing first on the indirect T_s response, notice it is large-scale in both ATL and PAC, as expected from the large-scale nature of the AO. The most notable features are a cooling in eastern North America and Northern Europe, the latter of which explains a large part of the Northern European cooling in the full PAC response. Moving onto the direct T_s response, notice that it and the related direct Z500 response are indeed relatively local to the loss region in both ATL and PAC. Furthermore, it is encouraging that the direct Z500 response becomes more anticyclonic with height above the forcing (cyclonic near the surface – not shown – to anticyclonic (less cyclonic) at 500 hPa in ATL (PAC)) as predicted by linear theory (Hoskins and Karoly, 1981; also see equation 1.12 in Chapter 1). In ATL, the anticyclone above the forcing is consistent with advection of anomalously warm air from the Barents-Kara Seas to Northern Europe and the counteraction of AO-induced cooling there. Additionally, the direct Z500 anomalies downstream of the forcing may induce the dipole in direct T_s anomalies over North America, which counteract AO-induced eastern North American cooling and explain the western North American cooling in the full response. In PAC, the high over western North America

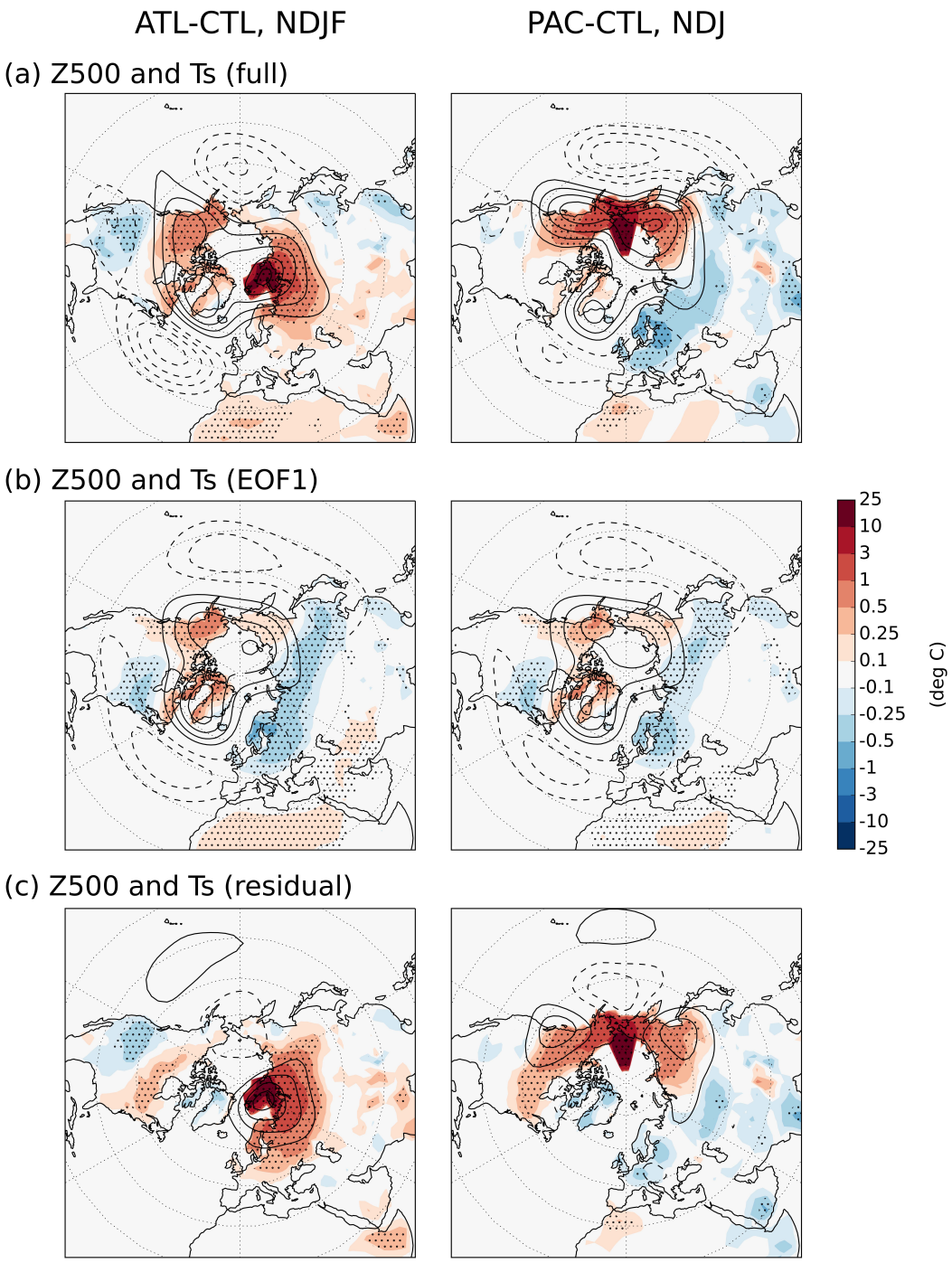

Fig. 3.11 Response of surface temperature (shading) and 500 hPa geopotential height (contours; interval: 4 gpm) in [Left] ATL NDJF and [Right] PAC NDJ. (a) Full response, (b) indirect part due to EOF1 (the AO), and (c) direct part (residual). Stippling indicates a significant surface temperature response at a 95% confidence level. Note that (a), (b), and (c) are almost unchanged when ATL is replotted for NDJ.

and low north of Hudson Bay in the direct Z500 response are consistent with advection of anomalously warm air from the Chukchi-Bering Seas to eastern North America and the counteraction of AO-induced cooling there. However, note that there is residual cooling in Northern Europe. This may be associated with the residual low; indeed, the NAO low center appears eastward shifted in the full Z500 response (similar to the findings of Pedersen et al. 2016) – a pattern not captured by the EOF's used in the projections.

The T_s responses are not decomposed for 0.5ATL and 0.5PAC since they have limited significance. However, in November-January in 0.5ATL/0.5PAC there is cooling/warming in eastern North America and warming in Northern Europe, consistent with the negative/positive AO and a direct warming effect local to the loss region (Figure 3.9d).

3.5 Discussion and conclusions

The research questions from the introduction will now be addressed, which – by considering different spatial patterns and magnitudes of sea-ice loss – broadly aim to improve mechanistic understanding of the link between Arctic sea-ice loss and changes in mid-latitude surface temperatures. A schematic summarising the proposed key mechanisms is shown in Figure 3.12. It will be shown that this improved understanding helps to explain contrasting results found by previous studies.

With respect to the first research question (Do sea-ice losses confined to the Atlantic or Pacific sector of the Arctic have opposite effects on the stratospheric polar vortex?), the model experiments presented here show that Atlantic sector (Barents-Kara Seas) and Pacific sector (Chukchi-Bering Seas) sea-ice loss have different effects on the stratospheric polar vortex. Specifically, in the moderate- and large-magnitude Atlantic/Pacific sea-ice loss cases, the vortex weakens/strengthens in November-January due to enhanced/suppressed upward Rossby wave propagation (indicated respectively in Figure 3.12 by the grey arrows and vortex thickness, and black wavy arrows). This enhancement/suppression is due to constructive/destructive linear interference (indicated in Figure 3.12 by the relative phase of the grey and red wavy arrows). Only the large-magnitude Atlantic case is found to have a statistically significant vortex response in November-January (with respect to its climatological state), but a statistically significant difference in the vortex state is found between the Atlantic and

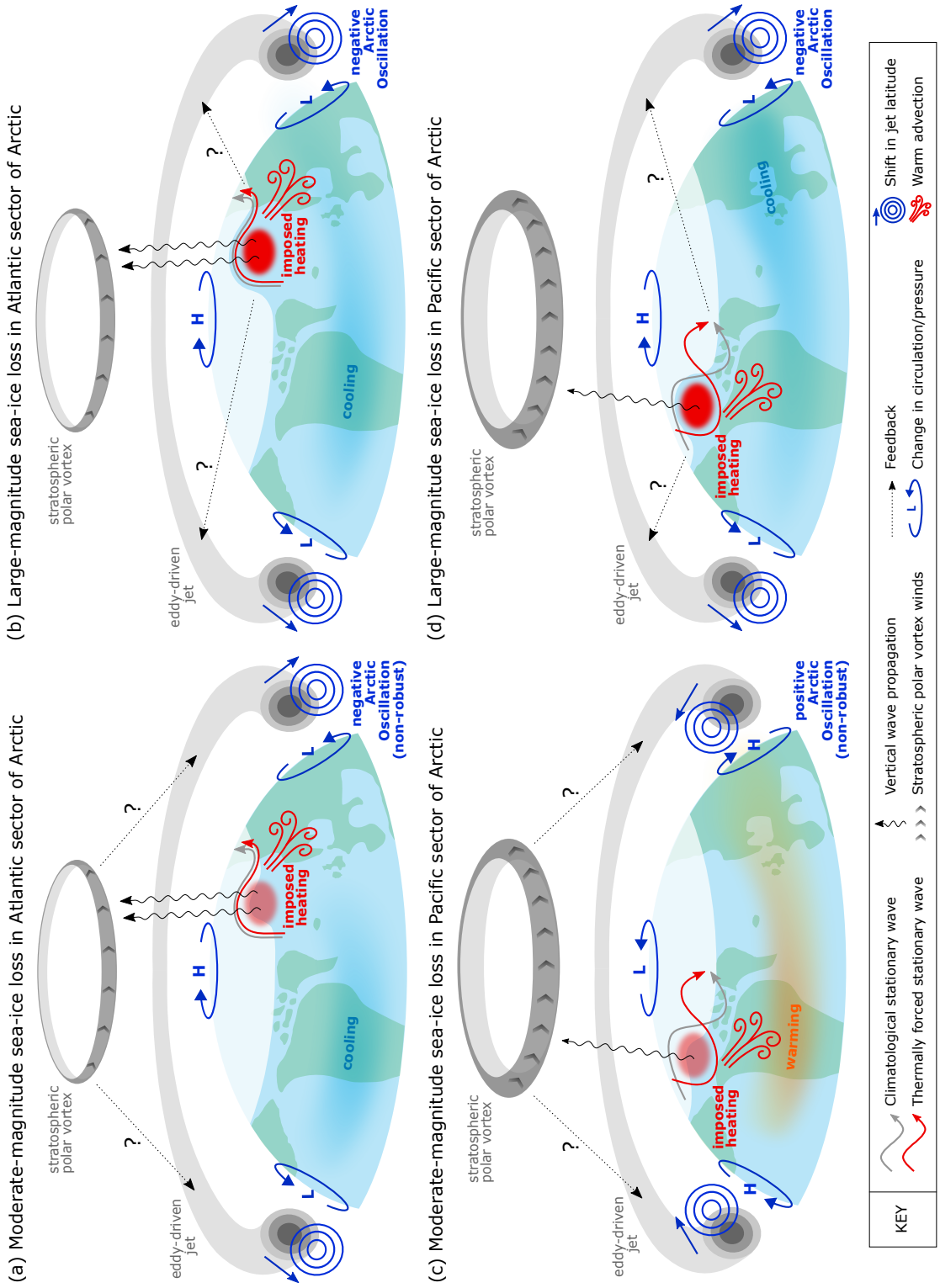

Fig. 3.12 Schematic summarising the key mechanisms that may link Arctic sea-ice loss with changes in mid-latitude surface temperatures, for different sectors and magnitudes of loss. (a)/(c) Moderate-magnitude sea-ice loss and (b)/(d) large-magnitude (late 21st century) sea-ice loss in the Atlantic/Pacific sector. Features of the direct/indirect response are shaded in red/dark blue.

Pacific cases for both magnitudes of sea-ice loss. Therefore, different spatial patterns of moderate- and large-magnitude sea-ice loss can explain the different (but not necessarily opposite) stratospheric responses in previous studies. These results provide insight that is additional to Sun et al. (2015)'s finding that different spatial patterns of (large-magnitude) sea-ice loss can explain the opposite stratospheric responses in previous studies. Note that it was initially thought that there is a statistically significant strengthening of the polar vortex in PAC in November-December (McKenna et al., 2018); however, Chapter 5 will show that the 200 year-long simulations used here are not sufficiently long to determine the robustness of the stratospheric response for short sub-seasonal time-periods.

Now the second research question is addressed (Are there correspondingly opposite effects on the tropospheric AO?). It is found that Atlantic or Pacific sector sea-ice losses of moderate-magnitude lead respectively to a statistically insignificant negative or positive AO response in the large-scale tropospheric circulation (indicated in Figures 3.12a and 3.12c by the dark blue features), consistent with the stratospheric responses. Therefore, for moderate-magnitude sea-ice loss, it cannot be robustly concluded whether different spatial patterns of sea-ice loss can explain the contrasting tropospheric responses in previous studies. However, for large-magnitude sea-ice loss, a statistically significant negative AO response is found in both cases (Figure 3.12b and 3.12d). This suggests that for large-magnitude sea-ice loss, different spatial patterns of sea-ice loss cannot explain the contrasting tropospheric responses in previous studies.

Furthermore, it implies that for large-magnitudes of sea-ice loss, tropospheric mechanisms (which may tend to lead to a negative AO for both Atlantic and Pacific sea-ice loss through, for example, reductions in meridional temperature gradient) are relatively more important than stratospheric mechanisms (which lead to oppositely signed AO responses) – see the dotted arrows in Figures 3.12b and 3.12d. As discussed in Chapter 1, different studies find tropospheric and stratospheric mechanisms to have different levels of importance (e.g. Nakamura et al., 2016b, find stratospheric mechanisms are crucial in the response to recent sea-ice loss, while Wu and Smith, 2016, find that tropospheric and stratospheric mechanisms are equally important for late 21st century sea-ice loss). Sun et al. (2015)'s Pacific experiment also suggests that tropospheric mechanisms are more important for large-magnitude sea-ice loss, since they find a stronger polar vortex but no northward shift of the zonal mean tropospheric eddy-driven jet. The same can also be said for the future pan-Arctic sea-ice loss

experiments of Peings and Magnusdottir (2014), Sun et al. (2015) and Nakamura et al. (2016a), since these studies find very different responses in the stratospheric polar vortex – respectively no change, a non-significant weakening in winter and significant strengthening in spring, and a strengthening – but in all cases a negative tropospheric AO-like response is found.

However, within the current experimental setup the roles that stratospheric and tropospheric mechanisms played in the tropospheric AO responses cannot be definitively quantified. In the following chapter this is addressed by conducting additional experiments designed to decompose the responses into parts due to tropospheric and stratospheric mechanisms (e.g. Hitchcock and Simpson, 2014). This will also allow a 'cleaner' look to be taken at the specific mechanisms involved.

In answer to the third research question (What are the effects on mid-latitude surface temperatures?), it is found that while there is a negative tropospheric AO in response to large magnitudes of both Atlantic and Pacific sector sea-ice loss, there are still contrasting effects on mid-latitude surface temperatures (compare Figures 3.12b and 3.12d). Specifically, in the Atlantic (Pacific) case AO-induced cooling is absent in Northern Europe (North America), and any cooling only occurs in North America (Northern Europe). It is shown that this can be understood by decomposing the temperature response into an indirect part induced by the large-scale indirect circulation (AO) response, and a residual direct part, which is demonstrated to be local to the loss region, and is partly explained by the direct circulation response. In the Atlantic (Pacific) case, the direct circulation response is consistent with warm advection over Northern Europe (North America), and the counteraction of AO-induced cooling there (indicated in Figures 3.12b and 3.12d by the warm advection symbol). Thus, in the Atlantic (Pacific) case any cooling only occurs in North America (Northern Europe).

This decomposition of the temperature response into direct and indirect parts is a new approach, but is similar in concept to the 'thermodynamic' versus 'dynamic' decomposition described by Screen et al. (2015) and others. However, the direct versus indirect terminology is used here, since the direct temperature response involves both thermodynamic and dynamic processes. It is also similar in concept to Deser et al.'s (2016b) decomposition of air temperature trends into dynamical internal and forced components, and thermodynamic internal and forced components. Due to a lack of robustness, a decomposition of the temperature response was not performed here for the moderate-magnitude sea-ice loss experiments. However, the temperature changes

for moderate-magnitude Atlantic or Pacific sea-ice loss are consistent with the AO responses and a direct warming effect local to the loss region (Figures 3.12a and 3.12c).

The temperature responses in the large-magnitude sea-ice loss cases contrast with the study of Kug et al. (2015), who find that warming in the Barents-Kara (East Siberian-Chukchi) Seas is connected to wintertime cooling in Eurasia (North America). However, their results are for past warming, which is much smaller in magnitude to the anomalies here. Therefore, the direct warming effect is likely not large enough to counteract the indirect cooling effect. Recent papers (e.g. McCusker et al., 2016) also show that recent wintertime Eurasian cooling may be dominantly associated with internal climate variability.

The wider relevance of the large-magnitude sea-ice loss results will now be considered. Since the spatial pattern of future Arctic surface warming – which is related to sea-ice loss – is uncertain across the CMIP5 climate models (Figure 1.1), they may indicate the range of potential atmospheric responses for studies using these models.

For instance, for climate models with sea-ice loss weighted toward the Atlantic sector (e.g. GISS), there could be a negative tropospheric AO and a cooler North America. However, for models with more Pacific sector sea-ice loss (e.g. ACCESS), there could be a negative AO and a cooler Northern Europe. These scenarios put into context, for example, Screen (2017a)'s finding that Northern European cooling is absent in the response to Arctic sea-ice loss; this was for large-magnitude sea-ice loss that is equally weighted towards the Atlantic and Pacific sectors.

Regarding models with large-magnitude ice loss equally weighted towards both sectors (e.g. HadGEM2), an additional 200 year-long experiment with large-magnitude T_s anomalies imposed in the Atlantic and Pacific sectors simultaneously (ATL&PAC run) suggests that the circulation response in the combined case is consistent with a linear addition of the responses in the separate cases (Figure 3.13). The combined case response appears weaker than this addition suggests, as found by Screen (2017b) but for a greater number of sea-ice loss regions. However, the right-hand column of Figure 3.13 suggests that the difference can largely be explained by sampling error. Chapter 5 will explore the influence of sampling error on the circulation response to sea-ice loss in more detail.

Regarding the surface temperature response, the ATL&PAC run suggests that rather than cooling occurring in North America and Northern Europe, as suggested

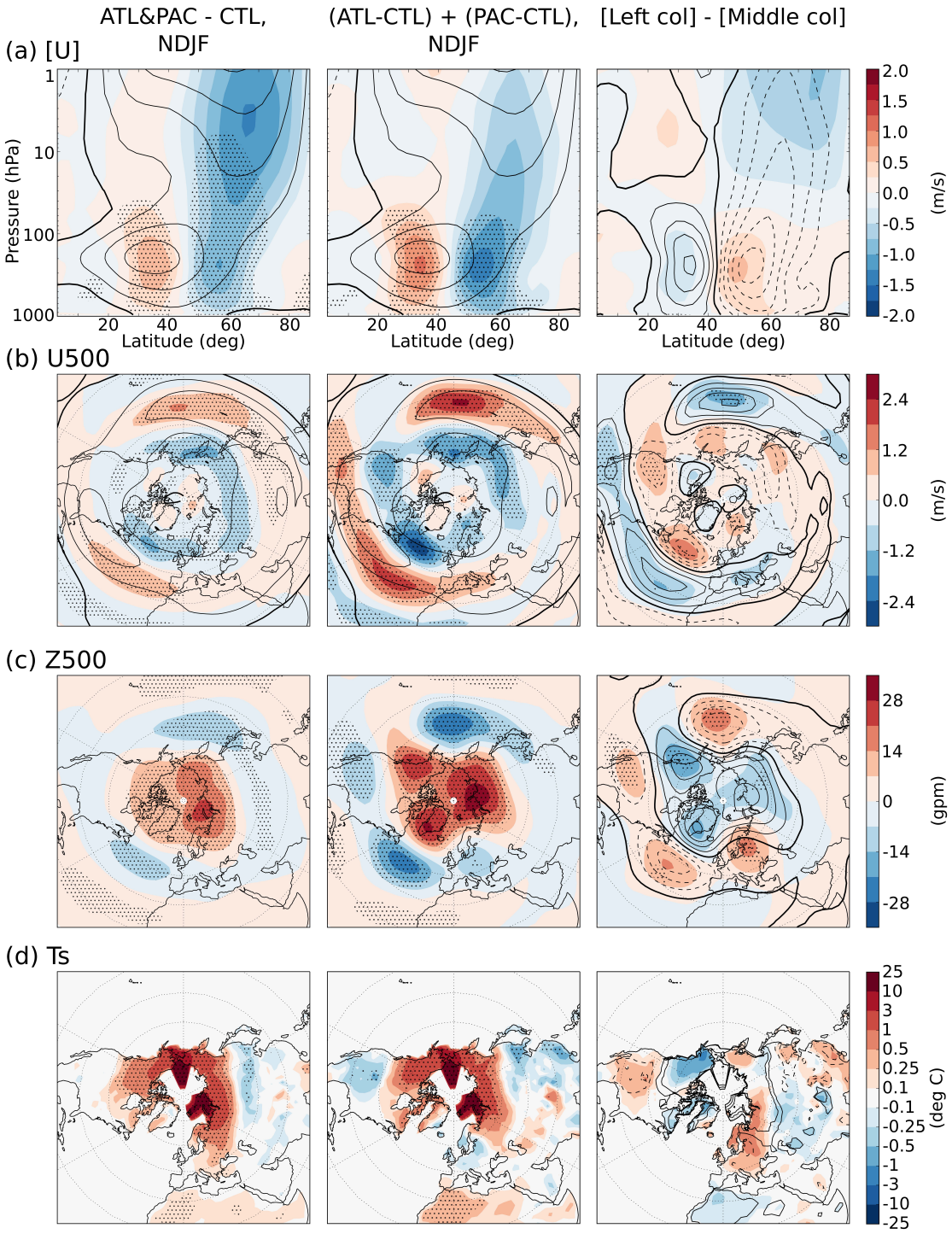

Fig. 3.13 [Left] NDJF response (shading) of (a) zonal mean zonal wind, (b) 500 hPa zonal wind, (c) 500 hPa geopotential height, and (d) surface temperature, in ATL&PAC. [Middle] A linear addition of the separate ATL and PAC responses (shading), and [Right] the left minus middle columns (shading). Contours in [Left] and [Middle] show climatological values from control run CTL (interval: 10 m/s), and in [Right] show shading in the middle column (surface temperature contour levels are $[\pm 0.25, \pm 0.5, \pm 5, \pm 10, \pm 25]$ deg C). Stippling indicates a significant response at a 95% confidence level.

by linearity, there would be no cooling in North America, and warming in Northern Europe. Screen (2017b) find a similar result, and suggest that the thermodynamic (direct) warming effect outweighs the dynamic (indirect) cooling effect for pan-Arctic sea-ice loss, while the balance is more in favour of dynamic cooling for individual regions of loss. However, as for the circulation response, the right-hand column of Figure 3.13 suggests the difference is largely due to sampling error here. It is also found here that there is cooling in central Eurasia in ATL&PAC, as suggested by linearity and found by many previous studies simulating the response to sea-ice loss (see Sections 1.1.3.2 - 1.1.3.3 in Chapter 1).

With regards to the wider relevance of the moderate-magnitude sea-ice loss results, it was found that even a long simulation of length 300 years is insufficient to obtain a statistically robust response. As such, this makes it difficult to assess the linearity of the response to different magnitudes of sea-ice loss. Previous studies have compared the responses to different loss magnitudes and have found the response to be non-linear, using simulation lengths of between 50 years and 150 years. (Petoukhov and Semenov, 2010; Peings and Magnusdottir, 2014; Nakamura et al., 2016a). Chapter 5 will further investigate the influence of internal variability on the response to sea-ice loss, and will further discuss whether such simulation lengths are sufficient to make robust statements about linearity.

Chapter 4

Isolating the roles of tropospheric and stratospheric mechanisms

4.1 Introduction

As discussed in Chapter 1, various pathways have been proposed to connect Arctic sea-ice loss to a subsequent tropospheric response, which involve either tropospheric or stratospheric mechanisms. These pathways will hereafter be referred to as the 'tropospheric pathway' and 'stratospheric pathway' respectively, as in Wu and Smith (2016), Nakamura et al. (2016a,b), and Zhang et al. (2018a,b). A third distinct pathway will also be considered shortly, but for now the focus will be on these first two pathways.

The 'stratospheric pathway' is defined here as a pathway in which sea-ice loss alters the stratospheric state through changes in vertical wave propagation, and this altered stratospheric state – through subsequent downward propagation of the stratospheric anomalies and their effect on the tropospheric circulation – is a key mechanism in generating a tropospheric response. On the other hand, the 'tropospheric pathway' is here defined as a pathway in which tropospheric mechanisms alone generate a tropospheric response, independent of any changes in the stratospheric state. For example, this could be a pathway in which sea-ice loss and the associated warm anomaly results in a reduction in the meridional temperature gradient and subsequent adjustment of the large-scale tropospheric winds to maintain thermal-wind balance, or in horizontal stationary Rossby wave propagation that excites a large-scale atmospheric mode of variability.

Understanding the relative importance of these pathways is important for obtaining a better understanding of the response to sea-ice loss, including whether it is sensitive to different model representations of stratospheric dynamics. However, there is little consensus between past studies regarding the relative importance of these pathways (see Chapter 1), an issue which is very much reflected by the results of Chapter 3. Indeed, recall that for the Atlantic and Pacific sector sea-ice loss experiments in this chapter, it was not possible to conclude whether a tropospheric or stratospheric pathway generated the tropospheric Arctic Oscillation (AO) responses. It was hypothesised that a tropospheric pathway was key in the large-magnitude (late 21st century) ice loss cases (ATL and PAC runs), since there were different responses in the stratospheric polar vortex, but in both cases there was a negative tropospheric AO response. However, it is possible that a stratospheric pathway played some role: for example, in ATL the negative tropospheric AO response may have been at least partly caused by the weakened stratospheric polar vortex.

In this chapter, the responses in ATL and PAC are decomposed into parts due to the tropospheric and stratospheric pathways, which allows their roles to be quantitatively evaluated. This is done by conducting experiments in which the evolution of the stratosphere is constrained using a stratospheric nudging method (Simpson et al., 2011). In particular, for the ATL or PAC case, the tropospheric pathway is quantified by imposing ATL or PAC sea-ice loss, and nudging the stratospheric state toward that of the original control run CTL (in other words, the stratosphere is prevented from responding to the sea-ice loss, thereby 'shutting-down' the stratospheric pathway). On the other hand, the stratospheric pathway is quantified by nudging the stratospheric state toward that of the ATL or PAC runs, and imposing no sea-ice loss (thereby shutting-down the tropospheric pathway). Nudging experiments are not conducted for the moderate-magnitude sea-ice loss runs from Chapter 3 (0.5ATL and 0.5PAC) since the responses in these runs were less statistically robust.

Further details regarding the specific mechanisms involved in the stratospheric pathway will be determined by conducting two types of stratospheric pathway nudging experiment, in which the stratospheric state is perturbed in two different ways. In the first experiment type, the stratospheric state will be nudged toward the climatological mean annual cycle of ATL or PAC, such that interannual and intraseasonal stratospheric variability – including that associated with sudden stratospheric warming (SSW) events – is not included. This experiment type will therefore test for the effect of a small mean

change in the stratospheric polar vortex that occurs over every winter, rather than for the effect of a change in – for example – the frequency or structure of SSW events, which are observed to occur approximately every second winter season, and are associated with much larger perturbations. In the second experiment type, the stratosphere will instead be nudged toward a specific reference SSW that is representative of the changes in SSWs in ATL or PAC. The exact design of this latter experiment type will be informed by firstly conducting some statistical analysis within ATL and PAC, which will examine changes in SSWs and the impact of these changes. Taken together, this statistical analysis and the two types of stratospheric pathway nudging experiment will determine the extent to which stratospheric pathways involving a winter mean change in the stratospheric polar vortex, and/or a change in SSW events, are important for the tropospheric AO responses in ATL and PAC. These pathways will hereafter be referred to as the 'winter mean stratospheric pathway' and 'SSW stratospheric pathway' respectively.

To the best of the author's knowledge, the work presented here will be the first quantitative comparison of the roles of both winter mean and SSW stratospheric pathways in the response to sea-ice loss. Indeed, in other studies using a nudging method to isolate the stratosphere's role in the tropospheric response to Arctic sea-ice loss or warming, the stratosphere has either been nudged toward the same perturbed winter mean state in every year (Wu and Smith, 2016) or toward a perturbed state including interannual and intraseasonal variability (Zhang et al., 2018a) – where the effects of each are separately found to be important – but in neither study is the choice of state discussed in detail. As mentioned in Chapter 1, it has been suggested in both modelling and observational studies that changes in stratospheric extreme events can be important for some cases of ice loss (Kim et al., 2014; Peings and Magnusdottir, 2014; Sun et al., 2015; Jaiser et al., 2016; Hoshi et al., 2019); however, these findings are not tested quantitatively using a stratospheric nudging method. This would be useful in order to determine specific aspects of model representation of the stratosphere that the response to sea-ice loss may be sensitive to.

A third distinct pathway is also considered in this chapter, since established literature suggests that is may be relevant to the Pacific sea-ice loss case. This literature will now be briefly reviewed to give some context before defining this pathway.

Castanheira and Graf (2003) find in reanalysis data that an anti-correlation between pressure in the North Pacific (the Aleutian Low) and northern North Atlantic (the

Icelandic Low) only exists when the stratospheric polar vortex is strong. They suggest that this is because the strength of the stratospheric zonal mean winds controls the ability of Rossby waves to propagate in the stratosphere (Charney and Drazin, 1961; see the refractive index equation, 1.10, in Chapter 1). When the stratospheric winds are westerly but not too strong, vertically propagating waves generated in the North Pacific propagate upwards into the stratosphere; however, if the winds are strong, the waves become tropospherically trapped due to reflection by these winds, causing them to amplify and affect the tropospheric circulation in the North Atlantic, and subsequently generate a large-scale tropospheric AO-like response (similar to the findings of Perlwitz and Graf, 2001). Sun and Tan (2013) also find a similar connection between the Aleutian and Icelandic Lows in reanalysis data, but additionally use a stationary wave activity flux to demonstrate the reflection of the waves. In particular, they show that under strong polar vortex conditions, a disturbance to the Aleutian Low generates a wave that propagates upward and then eastward across North America in the upper troposphere and lower stratosphere; upon reaching eastern North America and Greenland, the wave is then reflected strongly downward by the strong stratospheric winds, causing it to disturb the Icelandic Low and generate a large-scale tropospheric AO-like response. For weak polar vortex conditions, this reflection does not occur and a large-scale tropospheric response does not develop.

Castanheira and Graf (2003) also highlight that further evidence of this connection is apparent when comparing models with observations. When observations are considered as a whole (i.e. not split into strong and weak vortex periods), no relationship is found between pressure in the North Pacific and northern North Atlantic. However, in some models a significant relationship does exist, which may be attributed to the fact that some models have too strong a stratospheric polar vortex compared to observations (e.g. HadCM2 and ECHAM3; Osborn et al. 1999, and May and Bengtsson 1998).

This literature suggests that, in PAC at least, the stratospheric state could alter vertical wave propagation in such a way that the direct stationary Rossby wave response to the sea-ice loss projects onto the tropospheric AO's negative phase. If this is true, then the responses in the tropospheric and stratospheric pathway nudging experiments – which occur in isolation and, therefore, cannot interact – will not add up to the total response in ATL or PAC. Therefore, a third distinct pathway is proposed here, which will be referred to as the 'combined non-linear tropospheric and stratospheric pathway' (or the 'combined non-linear pathway' for short). Specifically, this refers to a pathway

in which tropospheric and stratospheric mechanisms in isolation do not generate a large tropospheric response, but when operating together their interaction results in a combined effect that is significantly greater than the linear addition of their individual effects. This combined non-linear effect is similar to the 'combined synergistic effect' of Li et al. (2019), which is defined to describe a pathway of influence of the Northern Hemisphere mid-high latitudes on East Asian climate.

Evidence of such a pathway will be examined in both ATL and PAC, and also in the tropospheric and stratospheric pathway nudging experiments presented in this chapter. This examination would be difficult to do using the ATL and PAC experiments alone, since it is difficult to disentangle multiple mechanisms that are occurring simultaneously. By decomposing the response into different parts, the tropospheric and stratospheric pathway nudging experiments – which will have different nudged stratospheric states – will allow for a clearer investigation of the causal mechanisms involved in the potential effect of the stratospheric state on vertical wave propagation.

4.2 Aim and research questions

To summarise, this chapter aims to investigate key gaps in our understanding that remain from Chapter 3, including the roles played by tropospheric and stratospheric mechanisms in the responses to large-magnitude (late 21st century) Atlantic and Pacific sector sea-ice loss (ATL and PAC runs). To do this, stratospheric nudging experiments are conducted using IGCM4 and statistical analysis is performed within ATL and PAC, with the aim of addressing the following research questions:

1. Does a tropospheric pathway play a role in the negative tropospheric AO responses in the ATL and PAC runs?

2. Do stratospheric pathways associated with (a) a winter mean change in the stratospheric polar vortex, and/or (b) a change in SSW events, play a role in the negative tropospheric AO responses in the ATL and PAC runs?

3. Does a combined non-linear tropospheric and stratospheric pathway play a role in the negative tropospheric AO responses in the ATL and PAC runs?

The answers to these questions may, for example, help to improve understanding of how model stratospheric representation can affect the simulated response to sea-ice

loss. They will also help to explain why the tropospheric AO responses were negative in both ATL and PAC, despite the different stratospheric responses. As discussed at the end of Chapter 3, this is not just relevant to understanding the experiments in this thesis, since Sun et al. (2015) similarly found opposite stratospheric responses to future Atlantic and Pacific sea-ice loss, and did not find opposite tropospheric AO responses. Furthermore, in the future pan-Arctic sea-ice loss experiments of Peings and Magnusdottir (2014), Sun et al. (2015), and Nakamura et al. (2016a), many different responses in the stratospheric polar vortex are found – from a weakening to a strengthening – but in all cases there is a negative tropospheric AO-like response.

In terms of the novelty of the experiments conducted here – besides that already discussed in this chapter's introduction – it is highlighted that few previous studies have used a stratospheric nudging method to quantitatively evaluate the roles played by stratospheric and tropospheric mechanisms in the response to sea-ice loss (Nakamura et al., 2016b; Wu and Smith, 2016; Zhang et al., 2018a,b). In particular, only one of these studies (Zhang et al., 2018b) has done a comparison of this for different regions of sea-ice loss and, even so, only calculated the stratospheric pathway contribution implicitly (by subtracting the tropospheric pathway's contribution from the total response). Here, the experiments conducted will add to and advance this previous work, by comparing the pathways involved in the responses to different regions of sea-ice loss, and by explicitly isolating both the tropospheric and stratospheric pathways, as well as considering the possibility of a combined non-linear pathway.

4.3 Method

4.3.1 Stratospheric nudging method

In this chapter the stratospheric nudging method of Simpson et al. (2011) is used, which has been used in many other studies investigating the influence of the stratosphere on the troposphere (Hitchcock and Simpson, 2014, 2016; Hitchcock and Haynes, 2016; Nakamura et al., 2016b; Wu and Smith, 2016; Zhang et al., 2018a,b). This was implemented in IGCM4 by adapting a nudging code for IGCM1, which was used by Hitchcock and Haynes (2016), and was kindly provided by Peter Hitchcock. In terms of structure and equations used, the code edits for IGCM4 were the same as for IGCM1, but had to be adapted to work in parallel by the author (see Appendix B).

The method constrains the stratospheric evolution in a model experiment, by nudging the zonal mean (wavenumber-0) spectral co-efficients of the temperature, vorticity and divergence fields toward a chosen reference state above a certain height. This nudging takes the form:

$$- K(\sigma)(X - X_{ref})/\tau_N \ , \tag{4.1}$$

where X is the instantaneous zonal mean value of the field, X_{ref} is a zonal mean reference state (with daily time-resolution in this thesis), τ_N is the nudging timescale (essentially the nudging strength), σ is the model hybrid sigma-pressure level, and K is a height-dependent co-efficient valued from 0 to 1 that allows for vertical variation in the nudging strength. The nudging is applied at every model time-step, of which there are 96 time-steps per day. Cubic spline interpolation is used to calculate the reference state for the model time-steps between each new model day, in order to avoid a sudden change in the reference state at midnight.

The nudging timescale is set to $\tau_N = 6$ hours, and the nudging co-efficient K is linearly increased from 0 to 1 over sigma levels 0.07 to 0.03 (around 70 hPa to 30 hPa). These are similar values to those used in other stratospheric nudging studies (Simpson et al., 2011; Hitchcock and Simpson, 2014, 2016; Wu and Smith, 2016). The vertical increase in K is done gradually over a few levels rather than suddenly setting it to 1, since this could have undesirable effects. Note that while this chosen parameter combination was shown to be effective and produce useful results in the above studies, other parameter combinations were tested here before confirming that this choice was most effective for IGCM4. Section 4.3.3.1 will present plots demonstrating the effectiveness of this chosen parameter combination.

By only nudging toward the zonal mean, this method is advantageous in that it effectively prevents the zonally asymmetric spectral co-efficients (i.e. waves) from influencing the zonal mean flow, but still allows them to evolve freely. This means that for a given zonal mean stratospheric state, wave propagation should in theory be relatively unaffected by whether this state is associated with a freely evolving or nudged stratosphere. This is important given the key role played by wave propagation in Chapter 3's experiments.

Other methods to isolate the stratosphere's role were also considered, such as using a low-top version of IGCM4 (which has 20 model levels up to 50 hPa, compared to 35 model levels up to 0.1 hPa in the high-top version used here; Joshi et al., 2015). Indeed,

Sun et al. (2015) use a low-top version of their model for this purpose. However, the lower model lid could introduce spurious wave reflection effects and, therefore, the nudging method proposed is likely to be preferable in this respect.

4.3.2 Increased hyper-diffusion in uppermost model levels

During the process of implementing the stratospheric nudging method in IGCM4, it was found that a small number of test nudging runs crashed. These crashes occurred at very different points in the runs – sometimes within 10 years of model time, and in many cases not until over 50 years of model time – and did so for a wide range of nudging parameter combinations. Before the crashes occurred, snapshots of the divergence field revealed the development of high frequency gravity waves in the uppermost model levels, which blew-up in amplitude within only a few model time-steps.

Since the zonal mean stratospheric state is constrained by the nudging to remain unchanged, it was thought that the crashes were likely related to a change in the asymmetric stratospheric state. Indeed, the nudging is associated with a stronger planetary wave field, and an associated enhancement of upward wave propagation into and in the stratosphere (as will be shown in Section 4.3.3.1). This may increase the likelihood of periods with very high static stability in the uppermost model levels, which provide ideal conditions for the presence of high frequency gravity waves. Further evidence that this explains the crashes is the fact that the crashes were more likely to occur when ATL rather than CTL ocean surface temperatures were imposed; this is because there is a stronger planetary wave field in the ATL run (see Figure 3.7 in Chapter 3), which will further enhance the aforementioned conditions. Moreover, very similar model crashes have occurred in IGCM1, which have also been linked to high frequency gravity waves blowing-up due to the static stability becoming too strong in some part of the stratosphere (personal communication with Peter Hitchcock).

With the help of Manoj Joshi – one of the developers of IGCM4 (Joshi et al., 2015) – various attempts were made to fix the direct cause of this issue, including modifications to the gravity wave drag scheme in the uppermost model levels. However, these did not prevent the runs from crashing. Instead, the model code was edited to increase the strength of the hyper-diffusion already present in the uppermost model levels (by a factor of 1.25 to 7, respectively between around 5 hPa and the model top at around 0.1 hPa); these edits are shown in Appendix B. This was the minimum increase

in hyper-diffusion required to prevent high frequency waves from blowing-up in the uppermost model levels. Importantly, a 200 year-long control run with this increased hyper-diffusion implemented was not found to be significantly different from the CTL run climatologically (which is also the case when stratospheric nudging is additionally implemented – see the plots for the control nudging run, $\text{CTL}_{\text{ndgCS}}$, in Section 4.3.3.1). This solution was therefore used in all the nudging experiments conducted here.

4.3.3 Tropospheric and winter mean stratospheric pathway nudging experiments

This section describes the experiments designed to isolate the tropospheric pathway, and the winter mean stratospheric pathway. All experiments are run for 200 years following 1 year of spin-up time, as was the case for the ATL and PAC experiments, and the 200 year-long version of the CTL experiment in Chapter 3. A summary of the nudging experiments can be found in Table 4.1.

In the experiments isolating the tropospheric pathway, anomalous ocean surface temperatures from either the ATL or PAC runs are imposed (see Figures 3.1 and 3.2 in Chapter 3), while the stratosphere is prevented from responding by nudging the stratospheric state toward the zonal mean climatological mean annual cycle of CTL. These experiments will be named $\text{ATL}_{\text{ndgCS}}$ and $\text{PAC}_{\text{ndgCS}}$, where the full-size capitals denote the ocean surface temperatures used, and the subscript denotes the stratospheric state nudged toward (here 'CS' denotes 'control run stratosphere').

In the experiments isolating the winter mean stratospheric pathway, ocean surface temperatures from the CTL run are imposed, and the stratospheric state is nudged toward the zonal mean climatological mean annual cycle of ATL or PAC. These experiments will be named $\text{CTL}_{\text{ndgAS}}$ and $\text{CTL}_{\text{ndgPS}}$, where the subscripts 'AS' and 'PS' denote 'Atlantic run stratosphere' and 'Pacific run stratosphere'.

One final nudging experiment is run as a control experiment. In this experiment, CTL ocean surface temperatures are imposed, and the stratosphere is nudged toward the zonal mean climatological mean annual cycle of CTL. As such, this experiment is named $\text{CTL}_{\text{ndgCS}}$.

Figure 4.1 shows the reference states of wind and temperature used for nudging toward in the —_{ndgCS}, —_{ndgAS}, and —_{ndgPS} runs. Note that while the nudging is

Table 4.1 Descriptions of 200 year-long stratospheric nudging experiments conducted using IGCM4 in Chapter 4

Experiment	Description
CTL_{ndgCS}	Control run (CTL) ocean surface temperatures and nudging of the stratospheric state toward the zonal mean climatological mean annual cycle of CTL
ATL_{ndgCS}	Atlantic sector sea-ice loss run (ATL) ocean surface temperatures and nudging of the stratospheric state toward the zonal mean climatological mean annual cycle of CTL
PAC_{ndgCS}	Pacific sector sea-ice loss run (PAC) ocean surface temperatures and nudging of the stratospheric state toward the zonal mean climatological mean annual cycle of CTL
CTL_{ndgAS}	CTL ocean surface temperatures and nudging of the stratospheric state toward the zonal mean climatological mean annual cycle of ATL
CTL_{ndgPS}	CTL ocean surface temperatures and nudging of the stratospheric state toward the zonal mean climatological mean annual cycle of PAC
CTL_{ndgSSW}	CTL ocean surface temperatures and nudging of the zonal mean stratospheric state toward a specific reference SSW from December in ATL

performed at every latitude, the zonal mean zonal wind at 60°N and the polar cap average temperature are shown in the figure for ease of presentation. Similarly to Simpson et al. (2011), the climatologies have been low-pass filtered (with a cut-off frequency of 90 days) to extract the seasonally varying part; otherwise the climatology is rather noisy, which could cause issues with the nudging. These climatologies are then converted into zonal mean (wavenumber-0) spectral coefficients of temperature, vorticity, and divergence.

To quantify the tropospheric and winter mean stratospheric pathways, the responses in the relevant perturbation nudging runs are compared to the responses in ATL or PAC. CTL_{ndgCS} will be used to calculate the responses in each of the perturbation nudging runs. Defining the response with respect to CTL_{ndgCS} is comparable to defining the response with respect to CTL, since the climatology of CTL_{ndgCS} is very similar

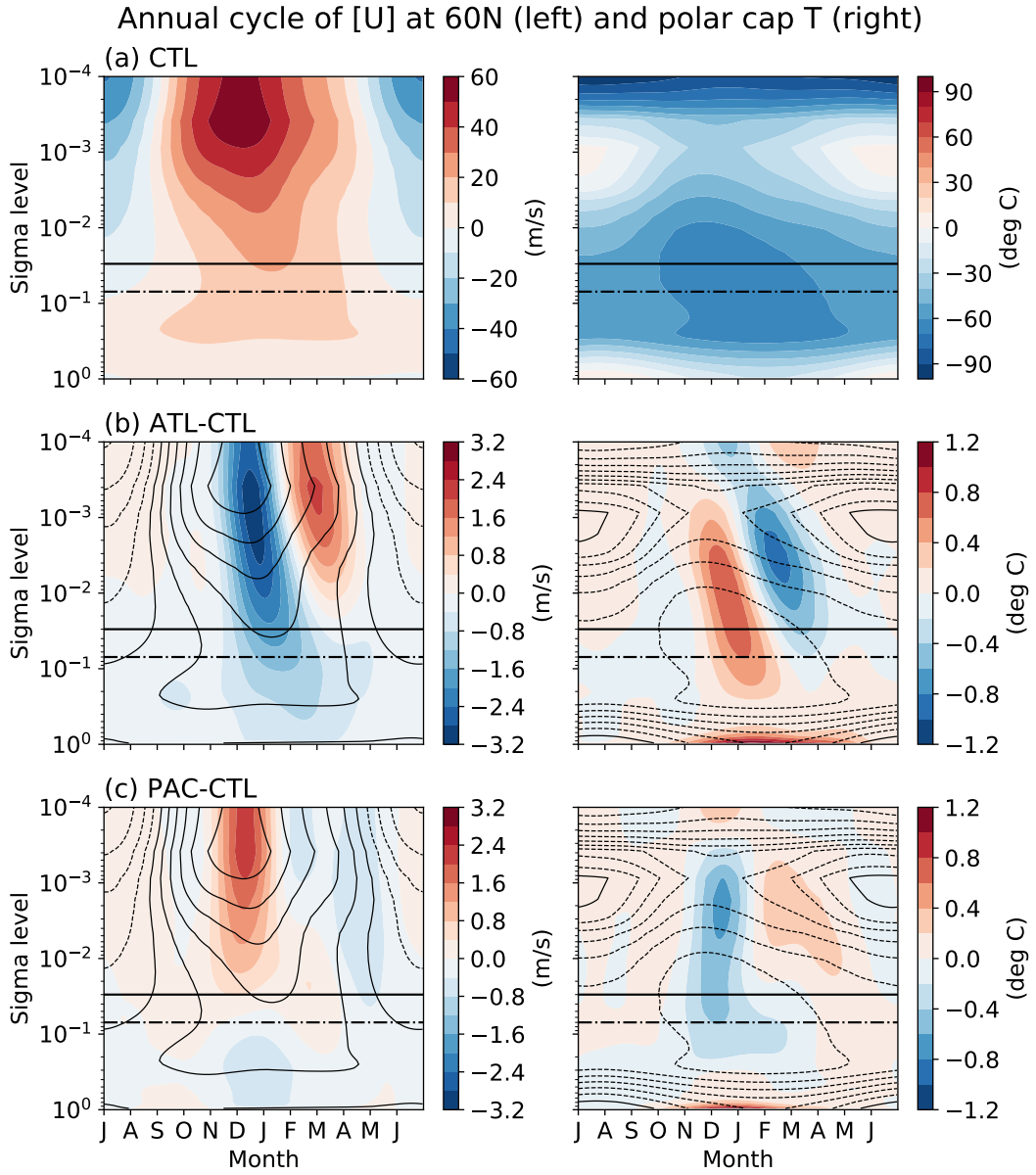

Fig. 4.1 Smoothed climatologies of [left] zonal mean zonal wind at 60°N and [right] polar cap (poleward of 60°N) temperature for (a) CTL, (b) ATL-CTL, and (c) PAC-CTL (all in shading). These are used as reference states for nudging toward in the —$_{\text{ndgCS}}$, —$_{\text{ndgAS}}$, and —$_{\text{ndgPS}}$ experiments respectively (note that the absolute climatologies for ATL and PAC are used in reality, but are shown here as a response to highlight the difference between the climatologies). The thin contours in (b) and (c) are the CTL climatology (interval: 10 m/s and 10°C). The nudging strength is increased linearly from 0 to 1, between sigma levels 0.07 (the horizontal thick dashed-dotted line) and 0.03 (the horizontal thick solid line). Note that the amplitude of the fields naturally increases with height because of decreasing density. x-axis ticks fall on the start of the month (as in all similar plots in this thesis).

to CTL (as will be shown in Section 4.3.3.1). Using the Atlantic case as an example, if the tropospheric response in ATL_{ndgCS} is equal to that in ATL (i.e. [ATL_{ndgCS} - CTL_{ndgCS}] = [ATL - CTL]), then a tropospheric pathway can explain the full response. Alternatively, if the tropospheric response in CTL_{ndgAS} is equal to that in ATL (i.e. [CTL_{ndgAS} - CTL_{ndgCS}] = [ATL - CTL]), then a winter mean stratospheric pathway can explain the full response. It could also be the case that both pathways play a partial role in the full response.

4.3.3.1 Initial experiment checks

This section checks that the nudging works effectively in the aforementioned experiments. Specifically, it is checked that the nudging is strong enough to damp out much of the zonal mean stratospheric variability (so that the zonal mean stratospheric state is kept very close to the nudged-toward reference state, with little variability about this state). This is important, because to properly isolate the tropospheric pathway any response in the stratosphere needs to be entirely prevented, and to properly isolate the winter mean stratospheric pathway the stratospheric responses from ATL and PAC need to be reproduced exactly. However, at the same time, the effect of the nudging on the stratospheric variability cannot be so strong that it has a strong effect on the climatology of the troposphere. This is key because, as discussed in Chapter 1, the tropospheric circulation response to sea-ice loss can be opposite for different climatological tropospheric eddy-driven jet strengths and latitudes (Smith et al., 2017).

Control nudging experiment

Various plots of different fields from CTL_{ndgCS} highlight that the nudging is indeed working effectively, and that the differences between CTL_{ndgCS} and CTL in the troposphere are reasonably small compared to the absolute climatological values in CTL.

Firstly, Figure 4.2 shows the November-February EP-flux and its divergence for CTL_{ndgCS} compared to CTL. This highlights that the nudging has little effect on tropospheric wave propagation, and only results in a relatively small increase in vertical wave propagation in the upper stratosphere compared to the CTL climatology. The resulting change in EP-flux divergence in the stratosphere is also relatively small.

Figure 4.3 shows the November-February zonal mean zonal wind, also for CTL_{ndgCS} compared to CTL. This shows that the changes in EP-flux divergence in the stratosphere

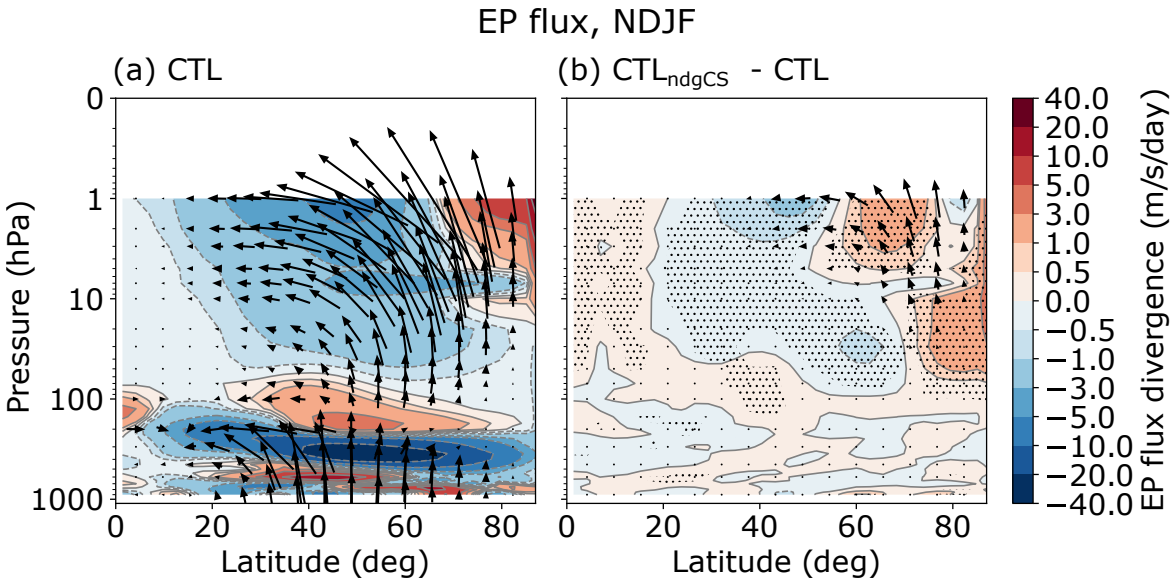

Fig. 4.2 Climatologies of EP-flux (arrows) and EP-flux divergence (shading) in NDJF for (a) CTL, and (b) CTL$_{ndgCS}$-CTL. Note that the scale of arrows in (a) and (b) is the same. Stippling indicates a significant difference for shaded fields at a 95% confidence level. All arrows shown in (b) are significant at a 95% confidence level in one direction, but most are significant in both the meridional and vertical directions (not shown).

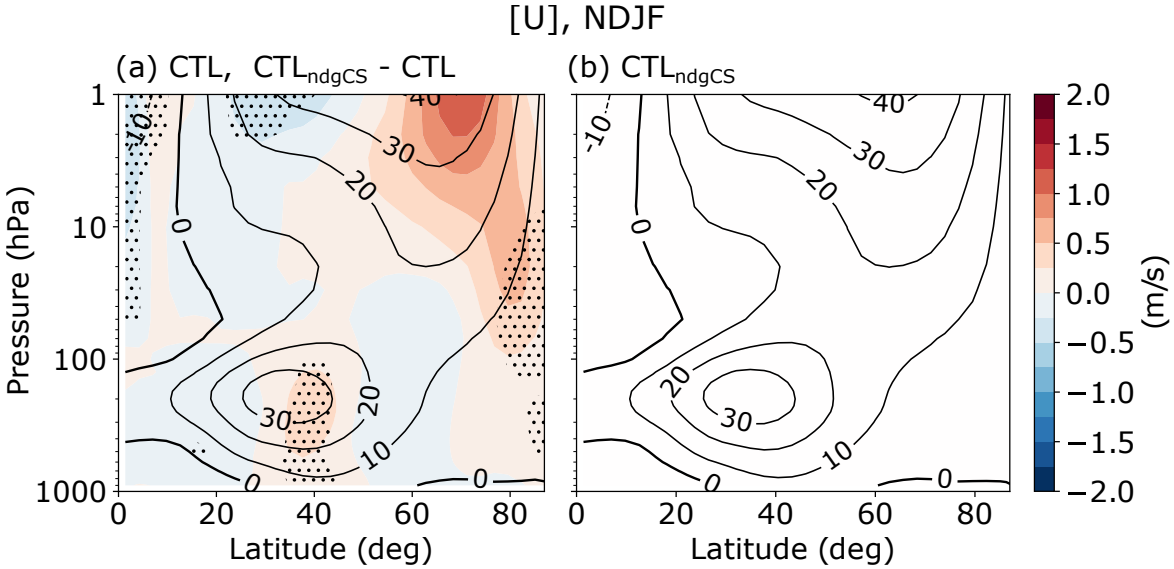

Fig. 4.3 Climatologies of zonal mean zonal wind in NDJF for (a) CTL$_{ndgCS}$-CTL (shading), CTL (contours), and (b) CTL$_{ndgCS}$ (contours). Stippling indicates a significant difference for shaded fields at a 95% confidence level.

have only a small – and mostly statistically insignificant – effect on the stratospheric zonal mean winds, as would be expected since the stratosphere is being nudged toward a CTL-like state. The effect on the tropospheric jet stream is also relatively small.

Focusing now on the AO, Figure 4.4 shows a plot of the zonal mean AO loading pattern with height for CTL and CTL_{ndgCS}, calculated according to the method used by Simpson et al. (2011). This shows that the nudging is effectively damping out most of the structures of stratospheric (above 100 hPa) AO variability, but has relatively little effect on the structures of tropospheric AO variability, as was aimed for.

It can also be seen in Figure 4.5 that the latitude-longitude structure of the November-February AO loading pattern at 500 hPa in CTL_{ndgCS} is similar to that in CTL (where these patterns are calculated as detailed in Section 2.3.2.1 of Chapter 2). There is a notably large reduction in the magnitude of the North Atlantic centre of action – likely due to the removal of the stratospheric influence on the tropospheric AO, an influence which tends to be focused on the North Atlantic (Baldwin and Dunkerton, 2001) – but the overall AO pattern is comparable. This is reassuring, because the AO loading pattern from CTL – not CTL_{ndgCS} – will be used to calculate the AO responses in the nudging runs, so that they are directly comparable to the AO responses in the original ATL and PAC experiments from Chapter 3. To justify this, the AO loading patterns in CTL and CTL_{ndgCS} need to therefore represent the same mode of variability.

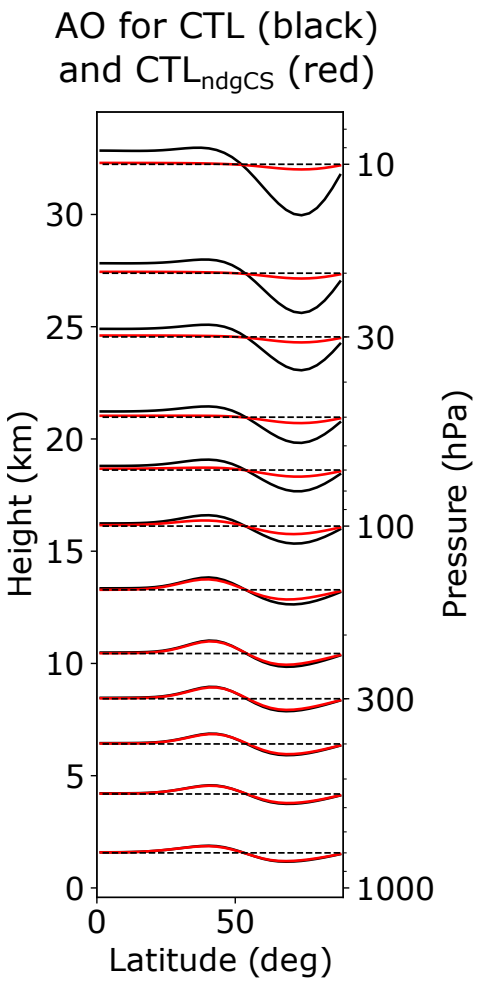

Fig. 4.4 The zonal-mean AO loading pattern with height for CTL (black) and CTL_{ndgCS} (red). This was calculated by projecting zonal-mean geopotential height anomalies (in km), weighted by the cosine of latitude, onto the AO index. The pattern for each level is displaced by its level height and multiplied by 30 to increase visibility.

As a final check on the properties of the AO, a look is taken at the AO decorrelation timescale (calculated for the zonal mean version of the AO as in Figure 4.4; see Section 2.3.2.2 in Chapter 2 for a detailed explanation of this timescale). Figure 4.6 shows the climatological mean annual cycle of the AO decorrelation timescale with height for CTL and CTL_{ndgCS}. This shows that in CTL, the timescales of AO variability are greatly enhanced in winter throughout the depth of the atmosphere, but particularly in the stratosphere. In CTL_{ndgCS}, however, the long timescales of winter stratospheric AO variability are almost entirely removed, and there is a small reduction in tropospheric AO timescales (by around 3 days on average at 500 hPa in November-February).

This is promising, because it shows that the nudging is effectively shutting down the contribution of eddies to the long timescales of variability in the stratospheric zonal mean flow or AO, and implies the removal of the effect that the long timescales of stratospheric AO variability have on the troposphere. This means that in the tropospheric pathway nudging experiments, only the strength of internal feedbacks generated by the troposphere will govern the timescale of tropospheric AO variability and, by the fluctuation-dissipation theorem, the magnitude of the tropospheric AO response to the imposed sea-ice loss. In other words, we can be sure that the AO response will be due to a tropospheric pathway alone, distinct from the effects of the stratosphere.

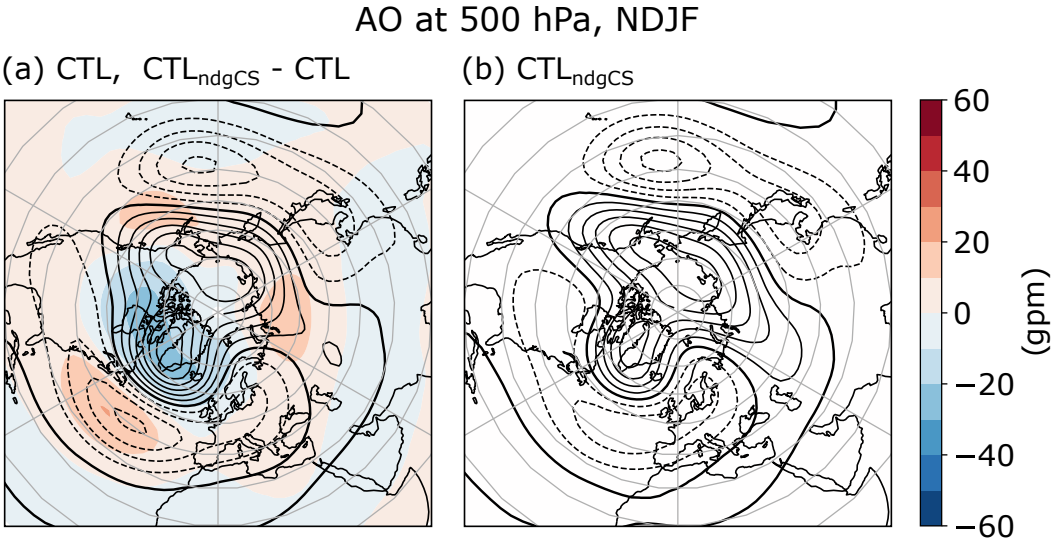

Fig. 4.5 The AO loading pattern at 500 hPa in NDJF for (a) CTL_{ndgCS}-CTL (shading), CTL (contours), and (b) CTL_{ndgCS} (contours). Contours are in intervals of 10 gpm.

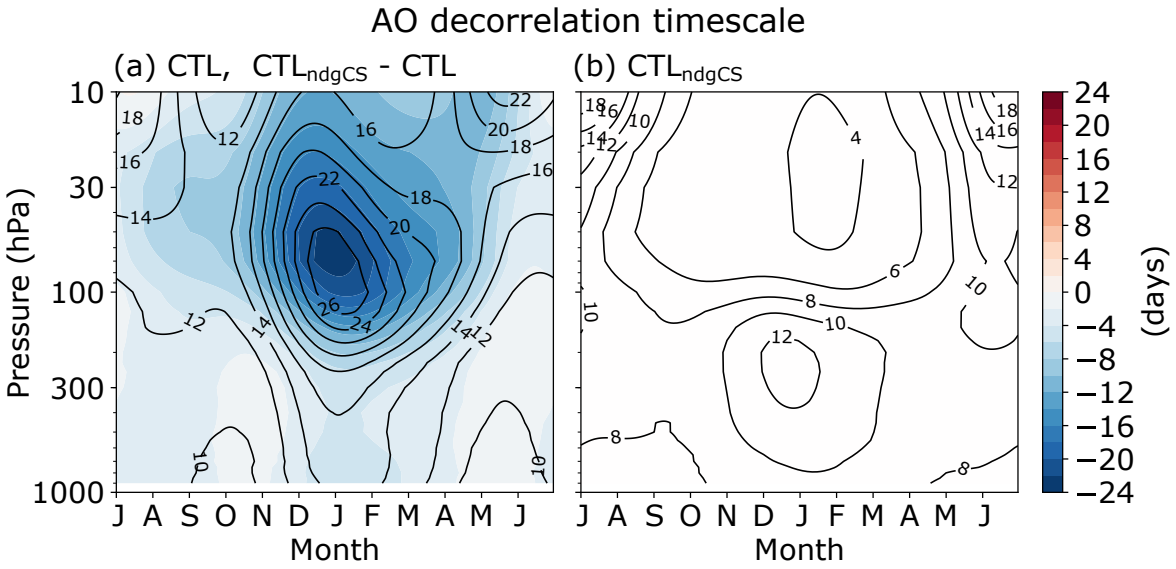

Fig. 4.6 The climatological mean annual cycle of the AO decorrelation timescale for (a) CTL_{ndgCS}-CTL (shading), CTL (contours), and (b) CTL_{ndgCS} (contours).

Perturbation nudging experiments

Figure 4.7 shows that the annual cycle of wind and temperature in the stratosphere in each of the ATL_{ndgCS}, PAC_{ndgCS}, CTL_{ndgAS}, and CTL_{ndgPS} runs follows the relevant climatological reference state well (compare with Figure 4.1). This means that the stratosphere is effectively prevented from responding in the tropospheric pathway nudging runs (ATL_{ndgCS} and PAC_{ndgCS}), and the stratospheric responses from ATL and PAC are effectively reproduced in the winter mean stratospheric pathway nudging runs (CTL_{ndgAS} and CTL_{ndgPS}).

4.3.4 SSW stratospheric pathway nudging experiment

This section describes the experiment designed to isolate the SSW stratospheric pathway. As before, this experiment is run for 200 years following 1 year of spin-up time, and is also summarised in Table 4.1.

The exact design of this experiment has been informed by a statistical analysis within ATL and PAC of the changes in SSWs, and the impact of these changes. These statistical results will be presented later in this chapter in Section 4.4.3, but for now it is simply stated that they reveal a prominent increase in the frequency of SSWs in December in ATL, and that changes in SSWs in PAC are less clear.

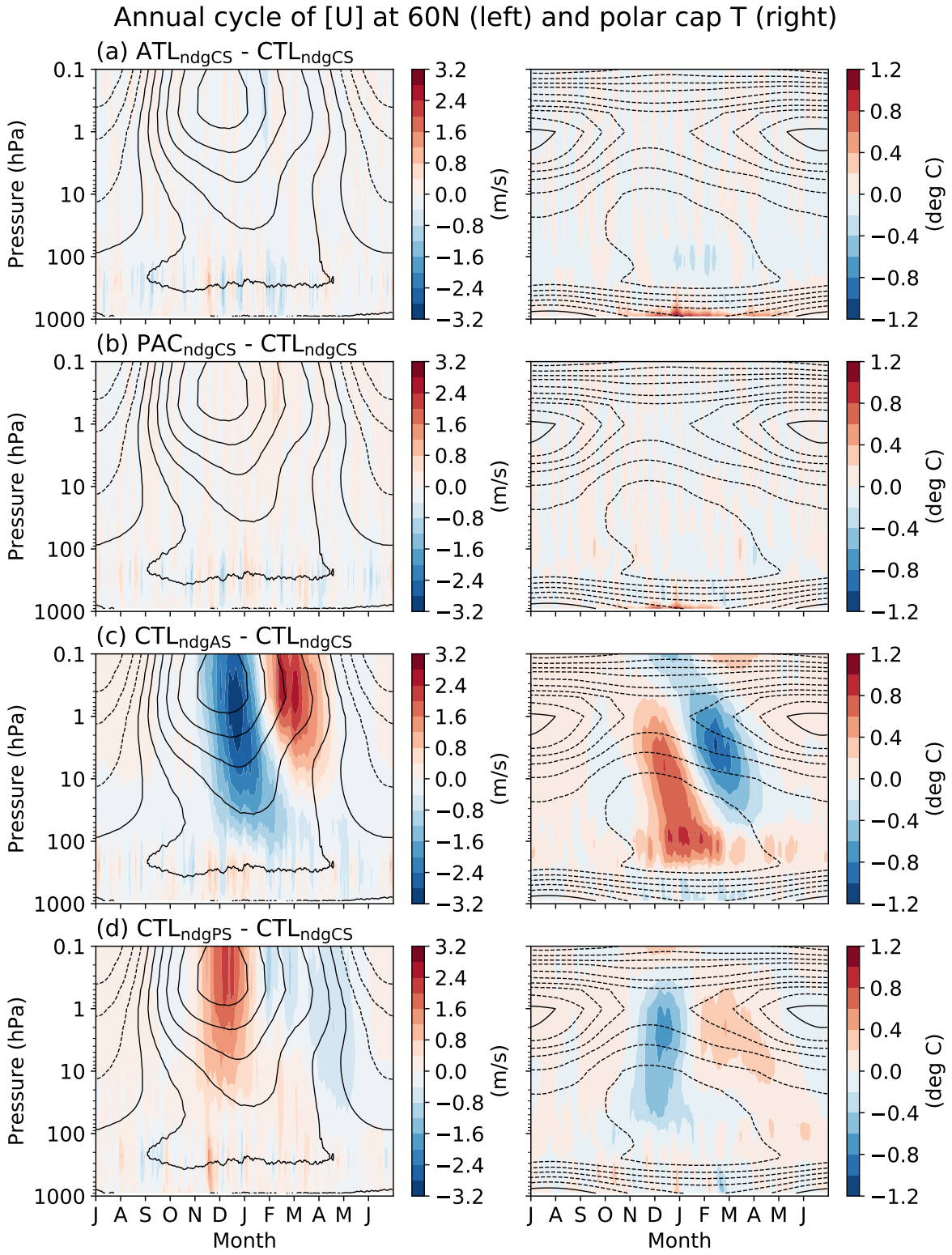

Fig. 4.7 Climatologies of [left] zonal mean zonal wind at 60°N and [right] polar cap (poleward of 60°N) temperature for the (a)/(b) tropospheric pathway and (c)/(d) winter mean stratospheric pathway nudging experiments, minus CTL$_{ndgCS}$ (shading). The black contours are the CTL$_{ndgCS}$ climatology (interval: 10 m/s and 10°C).

The experiment is designed to objectively determine the influence of a change in December SSW frequency on the troposphere. Specifically, CTL ocean surface temperatures are imposed, and the zonal mean stratospheric state is nudged in every year toward a specific reference SSW from December in ATL. This experiment will be referred to as $\mathrm{CTL_{ndgSSW}}$, and is similar to the experiments of Hitchcock and Simpson (2014, 2016). The relatively simple design is advantageous since it makes the problem more tractable. Specifically, since the same SSW is nudged toward in every year, it will be relatively easy to obtain a robust tropospheric response, and to understand the effect of a change in December SSW frequency on the troposphere. To estimate the climatological mean impact of a change in December SSW frequency over a given number of years, the AO response in $\mathrm{CTL_{ndgSSW}}$ (with respect to $\mathrm{CTL_{ndgCS}}$) can be multiplied by the change in SSW frequency for those years.

The reference SSW that was chosen occurred on December 10 in year 14 of ATL. This SSW was chosen because it was thought to be the most representative of the 22 SSWs that occurred in December in this run. Specifically, it is associated with a 10 hPa AO index evolution that is similar in shape (but not magnitude) to the evolution of the daily 10 hPa AO response in ATL. This suggests that the AO evolution associated with the reference SSW is representative of the AO evolution associated with the amalgamated effect of December SSWs in ATL (again in terms of shape, not magnitude). Secondly, the chosen SSW has a representative magnitude – in other words, it is not too weak or too strong – and therefore is likely to have a representative effect on the troposphere.

Figure 4.8a shows the evolution of the wind and temperature for the chosen reference SSW minus the CTL climatology. In $\mathrm{CTL_{ndgSSW}}$, the nudging is performed towards the smoothed control state used in $\mathrm{CTL_{ndgCS}}$ between May 1 and November 24 (Figure 4.1a), and toward the instantaneous reference SSW state between November 24 and May 1. The choice of November 24 as a start date for nudging toward the SSW was based on the method of Hitchcock and Simpson (2014). Specifically, the date was chosen to balance two requirements: firstly, it had to be close enough to the SSW central date to isolate the influence of the SSW as opposed to the influence of any preconditioning, and secondly, it had to be early enough to minimise any discontinuity in the nudging reference state. November 24 is ideal, because it excludes the effect of the warming and weakening of winds in the stratosphere from early November and, also, the wind anomalies on November 24 are similar in magnitude (5-10 m/s) to the anomalies on

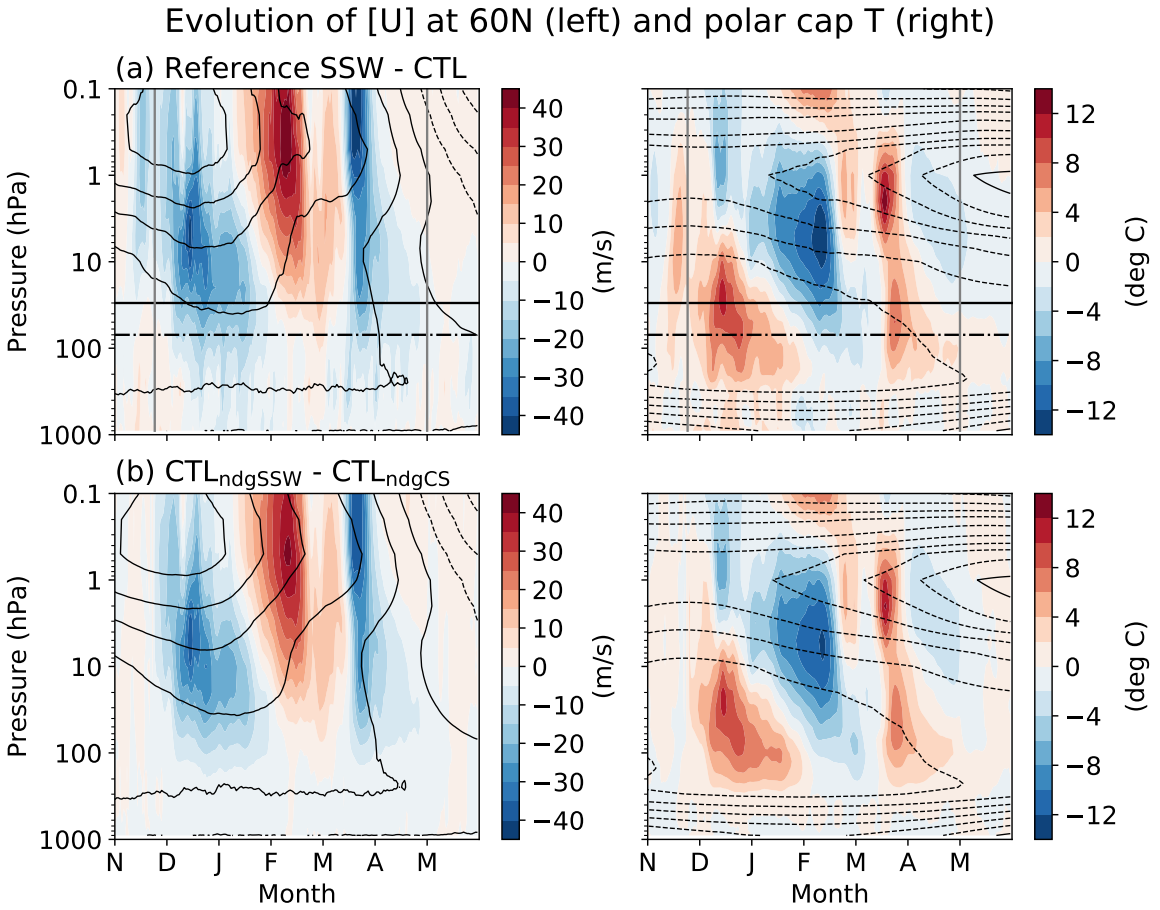

Fig. 4.8 Evolution of [left] zonal mean zonal wind at 60°N and [right] polar cap (poleward of 60°N) temperature, for (a) a specific reference SSW minus the CTL climatology (shading), and (b) the SSW stratospheric pathway nudging experiment response (CTL$_{ndgSSW}$-CTL$_{ndgCS}$; shading). Thin black contours in (a) and (b) are the CTL and CTL$_{ndgCS}$ climatologies respectively (interval: 10 m/s and 10°C). The reference state nudged toward in CTL$_{ndgSSW}$ consists of the reference SSW in (a) from November 24 until May 1 (dates indicated by vertical thick gray lines), and the smoothed control state used in CTL$_{ndgCS}$ otherwise (Figure 4.1a). The nudging strength is increased linearly from 0 to 1, between around 70 hPa and 30 hPa (the horizontal thick dashed-dotted and solid lines respectively in (a)). Only November-May is shown in this figure because this is when anomalies occur in CTL$_{ndgSSW}$ (as expected from the experiment design).

the start date used by Hitchcock and Simpson (2014). The end date of May 1 was also chosen to minimise any discontinuity in the nudging reference state.

Figure 4.8b shows that the evolution of the stratospheric zonal mean wind and polar cap temperature in CTL$_{ndgSSW}$ follows the reference SSW state well, and that

there appear to be no issues associated with the discontinuities in the nudging reference state.

To check that the chosen reference SSW has an effect on the troposphere, and is therefore suitable for the purposes of this chapter, the daily evolution of the AO index response at 10 hPa and 500 hPa is examined for CTL_{ndgSSW}-CTL_{ndgCS} (see Figure 4.9). This shows that the SSW does indeed have an effect on the troposphere, with a maximum tropospheric AO response of around -1 for a stratospheric AO response of around -3.

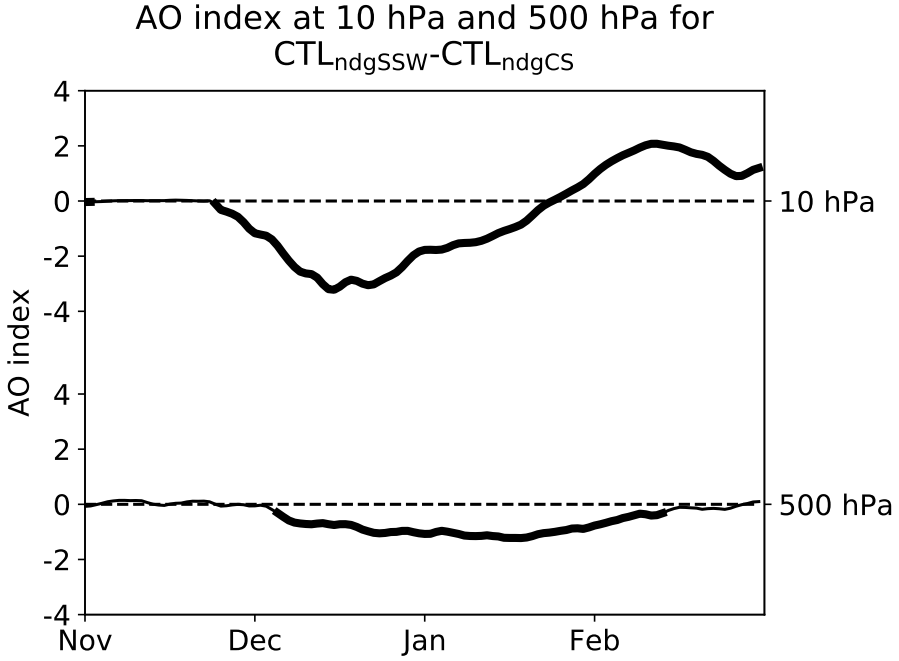

Fig. 4.9 Daily evolution of the AO index response at 10 hPa and 500 hPa over winter for CTL_{ndgSSW}-CTL_{ndgCS} (thin line). Thick lines indicate statistical significance at a 95% confidence level for the daily response, calculated using a t-test.

4.4 Results

4.4.1 Tropospheric pathway

This section uses the tropospheric pathway nudging experiments, ATL_{ndgCS} and PAC_{ndgCS}, to investigate research question 1: 'Does a tropospheric pathway play a role in the negative tropospheric AO responses in the ATL and PAC runs?'.

To do this, the 500 hPa geopotential height (Z500) responses in $\text{ATL}_{\text{ndgCS}}$ and $\text{PAC}_{\text{ndgCS}}$ are decomposed into 'direct' and 'indirect' or AO-like parts (hereafter referred to as just 'indirect' when used in this context). Recall that this was done for the ATL and PAC experiments in Chapter 3, where the indirect part of the response was defined as the part that projects onto the AO loading pattern – or first EOF – from CTL (i.e. the large-scale part hypothesised to be generated indirectly by non-linear tropospheric eddy feedbacks), and the direct part was defined as the residual (the full minus indirect response). This direct part was found to be local to the sea-ice loss region and resembled a stationary Rossby wave as predicted by linear theory (Hoskins and Karoly, 1981).

Here, the direct and indirect responses for $\text{ATL}_{\text{ndgCS}}$ and $\text{PAC}_{\text{ndgCS}}$ are calculated by projecting each Z500 response onto the relevant direct response calculated for ATL or PAC (contours in Figure 3.11c), and onto the 500 hPa AO loading pattern from CTL (contours in Figure 4.5a). The direct responses are calculated in this way so that they can be directly compared to the direct responses in ATL and PAC. Note that the second and third EOF's (the Pacific-North American pattern, and a dipole between the North Pacific and North Atlantic) from CTL are also included in the projections to be consistent with the projections in Chapter 3; the projections onto these EOF's are, however, small.

The projections result in a regression coefficient, β_i, for each part of the response, X_i, which describes the magnitude of that part (see Section 2.3.2.3 of Chapter 2). Specifically, the coefficient for the direct response describes its similarity to the direct response in ATL or PAC (1.0 meaning exactly the same), and the coefficient for the indirect response is the AO index.

4.4.1.1 The direct response

A look is firstly taken at the winter evolution of the direct responses in $\text{ATL}_{\text{ndgCS}}$ and $\text{PAC}_{\text{ndgCS}}$, compared to ATL and PAC – see the black lines in Figure 4.10.

For the Atlantic case, the direct response in $\text{ATL}_{\text{ndgCS}}$ reaches a similar peak magnitude to the direct response in ATL, but appears generally weaker across all months. This is confirmed by the winter (November-February) mean, for which the direct response has a magnitude of 0.6 in $\text{ATL}_{\text{ndgCS}}$ compared to 1.0 in ATL. For the Pacific case, the direct response in $\text{PAC}_{\text{ndgCS}}$ only becomes established in late

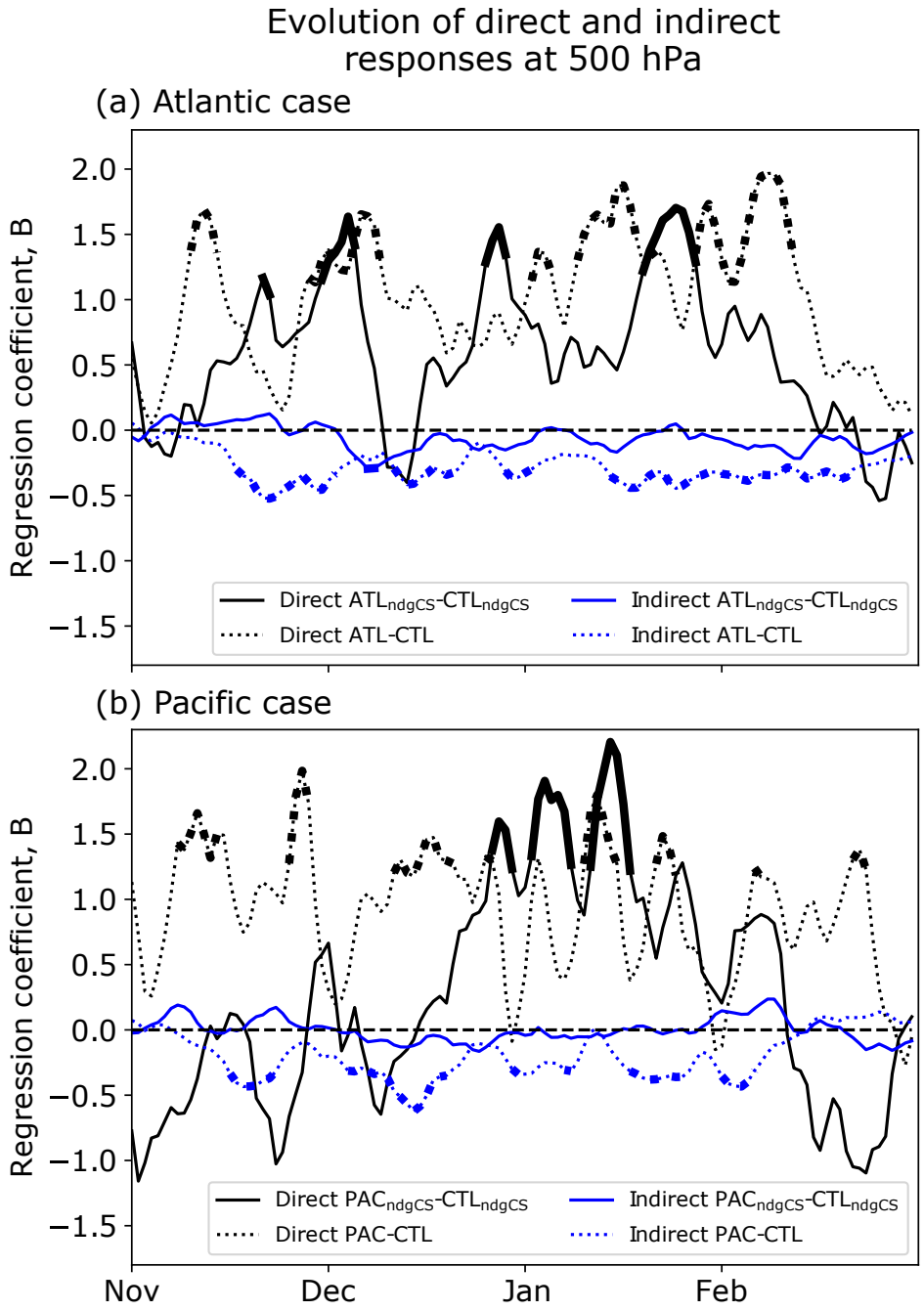

Fig. 4.10 Daily evolution of the direct (black) and indirect (blue) responses at 500 hPa over winter for (a) ATL_{ndgCS}-CTL_{ndgCS} (thin solid lines) and ATL-CTL (thin dotted lines), and (b) PAC_{ndgCS}-CTL_{ndgCS} and PAC-CTL. Thick solid and dotted lines indicate statistical significance at a 95% confidence level for the daily response, calculated using a t-test.

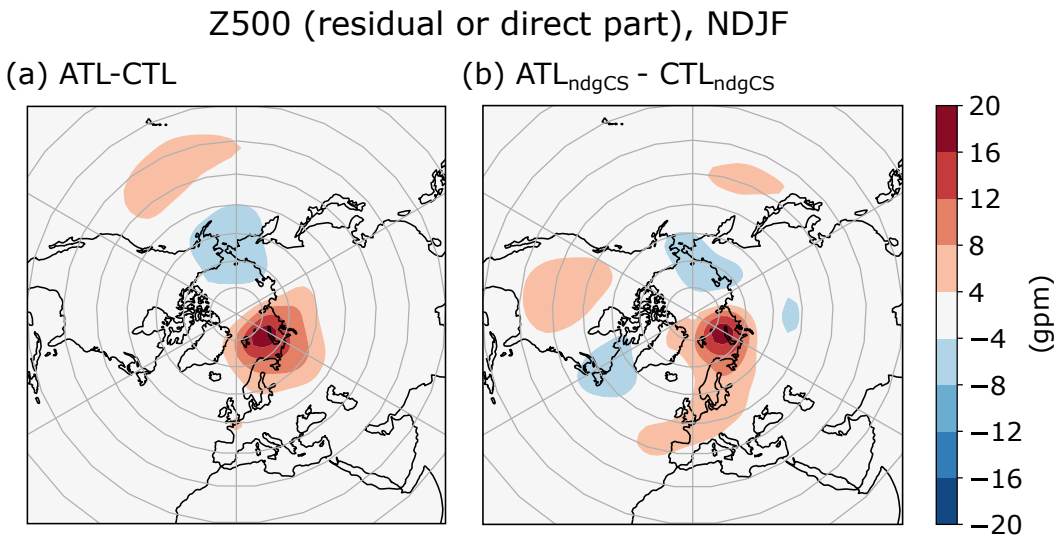

Fig. 4.11 Residual from a projection of the November-February mean 500 hPa geopotential height (Z500) response in (a) ATL$_{ndgCS}$, and (b) ATL, onto the first three EOF's from CTL. This residual can be interpreted as the direct part of the response, as in Figure 3.11c in Chapter 3.

December, reaches an average magnitude of around 1.0 for the month of January, and then disappears in February. The winter (November-January; as for PAC in Chapter 3) mean is therefore much weaker in PAC$_{ndgCS}$ (0.4) than in PAC (1.0).

To double-check that the direct response in ATL$_{ndgCS}$ is weaker than in ATL, it is alternatively calculated as the residual from a projection of the winter (November-February) mean Z500 response onto the first three EOF's from CTL (Figure 4.11b). This shows that when the direct response in ATL$_{ndgCS}$ is calculated independently of the direct response in ATL, it is still very similar in pattern to the direct response in ATL (Figure 4.11a) – i.e. it resembles a stationary Rossby wave local to the Barents-Kara Seas – but indeed appears visually weaker (or at least is more horizontally confined in the Barents-Kara Seas region). For PAC$_{ndgCS}$, the same method gives a residual that is very similar to the full Z500 response, since there is little projection onto the EOF's from CTL; therefore, a visual check is simply made of the full Z500 response. This indeed shows no robust stationary Rossby wave response local to the Chukchi-Bering Seas in November or February, but does indicate the appearance of such a response in December, which is similar to that in January but weaker (not shown). In January, the local geopotential height response in PAC$_{ndgCS}$ is very similar in pattern and magnitude to that in PAC in November (this is the most suitable month for comparison because

it is when the PAC response is dominated by its direct part) – compare regions A and B in Figures 4.20 and 4.22 in Section 4.4.4.2.

The direct responses in ATL_{ndgCS} and PAC_{ndgCS} could be weaker than those in ATL and PAC for the following reason. Firstly, recall that the direct response in ATL or PAC was simply calculated as a residual and, therefore, assumptions were made about the physical basis of this residual. If these assumptions were correct – that the residual is indeed a linear stationary Rossby wave generated locally and directly by the sea-ice loss, without the involvement of any indirect non-linear feedbacks – then the direct responses calculated for ATL and ATL_{ndgCS}, and PAC and PAC_{ndgCS}, should be the same. The fact that they are not suggests that the assumptions made were not fully successful and, therefore, that the 'direct' responses calculated for ATL and PAC are not entirely direct. Indeed, it could be that the stratosphere has some control over the development of the local response to sea-ice loss, and that this process is restricted when the stratosphere is constrained using a nudging method as in ATL_{ndgCS} and PAC_{ndgCS}.

4.4.1.2 The indirect response

The indirect responses are also much weaker in ATL_{ndgCS} and PAC_{ndgCS}, than in ATL and PAC (see the blue lines in Figure 4.10). In ATL_{ndgCS} the winter (November-February) mean response is -0.06 compared to -0.25 in ATL, and in PAC_{ndgCS} the winter (November-January) mean response is -0.01 compared to -0.26 in PAC. The indirect response in ATL_{ndgCS} does remain mostly below zero following the first large peak in the direct response at the end of November, but in PAC_{ndgCS} there is no indication of a negative indirect response – even in January when the direct response averages a magnitude of around 1.0. Note that it was considered that the indirect responses in the nudged runs are calculated using the AO loading pattern from CTL, rather than CTL_{ndgCS}, and that differences between these patterns – particularly in the North Atlantic sector (Figure 4.5) – could explain a lack of projection onto the former. However, projections calculated using the AO loading pattern from CTL_{ndgCS} actually resulted in slightly weaker indirect responses.

The weaker indirect response in ATL_{ndgCS} compared to ATL could be partly explained by the weaker direct response, if a linear relationship between the indirect and direct responses is assumed. Specifically, since the direct response in ATL_{ndgCS}

is 40% weaker than in ATL (0.6 compared to 1.0), linearity implies that the indirect response in ATL_{ndgCS} is 40% weaker than it would be for a direct response of magnitude 1.0 (-0.06 compared to -0.1). However, a similar argument does not help to explain the absent indirect response in PAC_{ndgCS}. Even when the direct response is of the correct magnitude in January, there is still no indirect response, and therefore the most likely explanation is that an indirect response simply cannot be generated by a tropospheric pathway alone. It could be that the direct response occurs for too short a time in PAC_{ndgCS} to generate the indirect response, but this seems unlikely since the indirect response in PAC appears around 1 week after the direct response first peaks in November.

To conclude, in relation to research question 1, these results imply that a solely tropospheric pathway can only explain a small portion (-0.06) of the negative tropospheric AO response in ATL (a total of -0.25), and essentially no portion (-0.01) of the negative tropospheric AO response in PAC (a total of -0.26). Therefore, stratospheric mechanisms must have been involved in someway. In the Atlantic case, an 'active' stratosphere may enhance the magnitude of the direct response by 0.4, which implies an additional AO response of -0.04 if linearity is assumed. This brings the total explained response in ATL to -0.1, leaving -0.15 of the AO response to be accounted for.

4.4.2 Winter mean stratospheric pathway

This section uses the winter mean stratospheric pathway nudging experiments, CTL_{ndgAS} and CTL_{ndgPS}, to investigate research question 2 (a): 'Does a stratospheric pathway involving a winter mean change in the stratospheric polar vortex play a role in the negative tropospheric AO responses in the ATL and PAC runs?'.

Figure 4.12 shows the winter evolution of the AO index response at 10 hPa and 500 hPa for (a) CTL_{ndgAS} compared to ATL, and (b) CTL_{ndgPS} compared to PAC (calculated as detailed in Section 2.3.2.1 of Chapter 2). Baldwin and Dunkerton (2001) show that weak and strong stratospheric polar vortex events are respectively associated with a negative and positive stratospheric AO index, and the subsequent development of a negative and positive tropospheric AO index. However, while CTL_{ndgAS} (CTL_{ndgPS}) does reproduce the negative (positive) stratospheric AO response associated with the weaker (stronger) polar vortex in ATL (PAC) correctly, this results in no tropospheric AO response. Therefore, the small change in the strength of the polar vortex associated

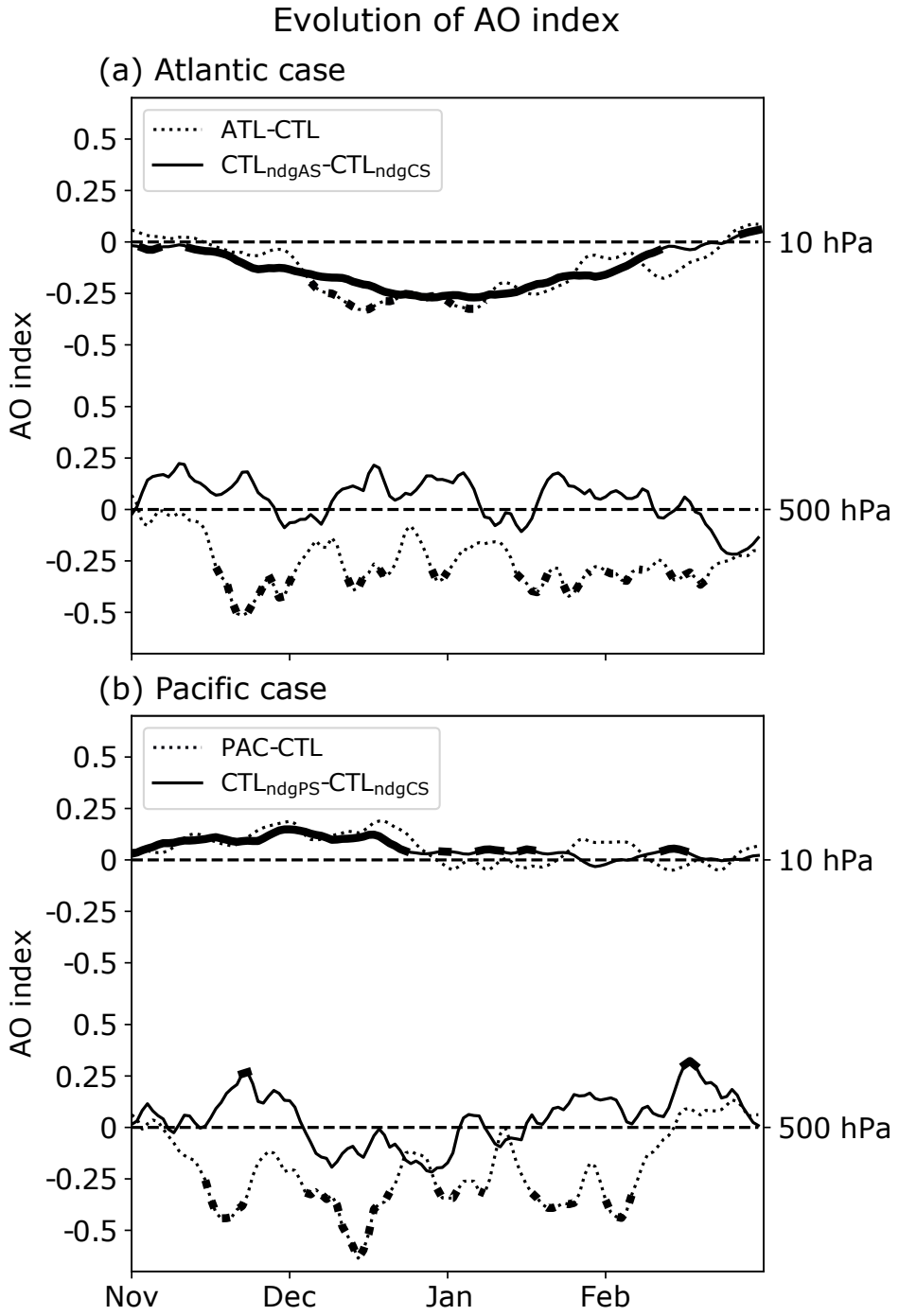

Fig. 4.12 Daily evolution of the AO index response at 10 hPa and 500 hPa over winter for (a) CTL_{ndgAS}-CTL_{ndgCS} (thin solid line) and ATL-CTL (thin dotted line), and (b) CTL_{ndgPS}-CTL_{ndgCS} and PAC-CTL. Thick solid and dotted lines indicate statistical significance at a 95% confidence level for the daily response, calculated using a t-test.

with the winter mean stratospheric pathway must be too small to have a downward effect on the troposphere (unlike for the large stratospheric perturbations associated with the weak and strong polar vortex events in Baldwin and Dunkerton, 2001, and the reference SSW nudged toward in CTL_{ndgSSW}; Figure 4.9).

To conclude, in relation to research question 2 (a), these results imply that a stratospheric pathway involving a winter mean change in the stratospheric polar vortex cannot play a role in the negative tropospheric AO responses in the ATL and PAC runs.

4.4.3 SSW stratospheric pathway

This section uses a combination of statistical analysis within ATL and PAC, and the SSW stratospheric pathway nudging experiment CTL_{ndgSSW}, to investigate research question 2 (b): 'Does a stratospheric pathway involving a change in SSW events play a role in the negative tropospheric AO responses in the ATL and PAC runs?'. The statistical analysis aims to determine whether changes in SSWs contribute to the stratospheric responses in ATL and/or PAC, and to indicate whether these changes could have an impact on the tropospheric AO responses. CTL_{ndgSSW} is used to more objectively determine the impact of these changes on the troposphere.

4.4.3.1 Atlantic case

Figure 4.13a shows the climatological (200 year) mean daily evolution of the AO index at 10 hPa over November-February for ATL-CTL, decomposed into a multi-year mean evolution for years in which at least one SSW occurs (SSW years) and for years in which none occur (non-SSW years). Only SSWs occurring in November-February are considered, since an SSW occurring in March has little relevance for the November-February AO. This shows that a systematic response in the AO index only occurs in SSW years. Furthermore, if a look is taken at the individual SSW and non-SSW years in CTL and ATL rather than their multi-year means, then it appears that the multi-year mean response for SSW years is due to a cluster of very negative AO values in December in ATL, which is not as apparent in CTL (Figures 4.13b and 4.13c). It is suggested that this is because there are more SSWs occurring in December in ATL (22 SSWs) than in CTL (8 SSWs) – see Figure 4.14. This increase in December SSW frequency is significant at a 99% confidence level based on a bootstrap test for the

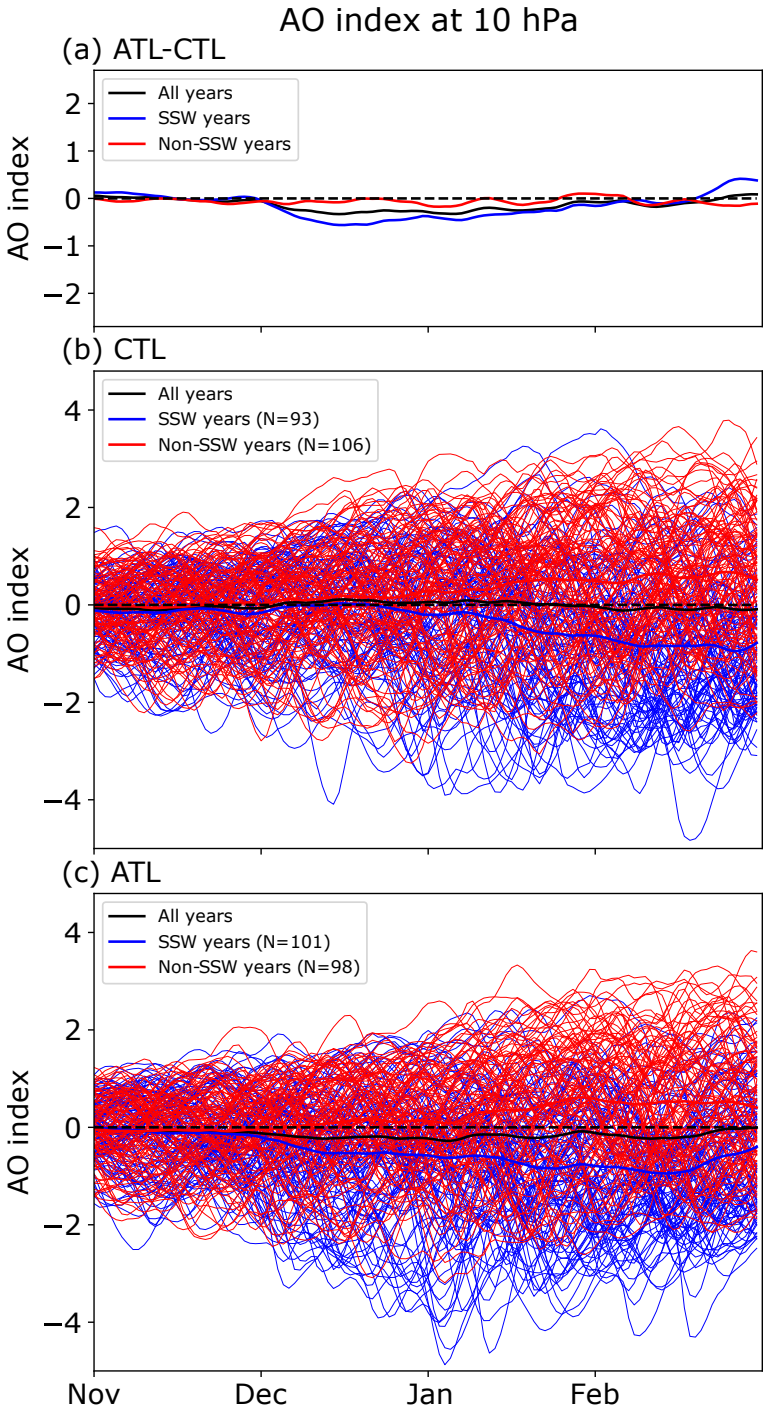

Fig. 4.13 Daily evolution of the AO index at 10 hPa over winter for (a) ATL-CTL, (b) CTL, and (c) ATL. This is shown for all years (black lines), and for subsets of years in which at least one SSW occurs (blue lines) or in which none occur (red lines) over November-February. Thick lines show the climatological (200 year) or multi-year mean, and thin lines show individual years. Note that the thick blue (red) line in (a) is the difference between the thick blue (red) lines in (b) and (c), so that only SSW (non-SSW) years from both CTL and ATL are included in the difference.

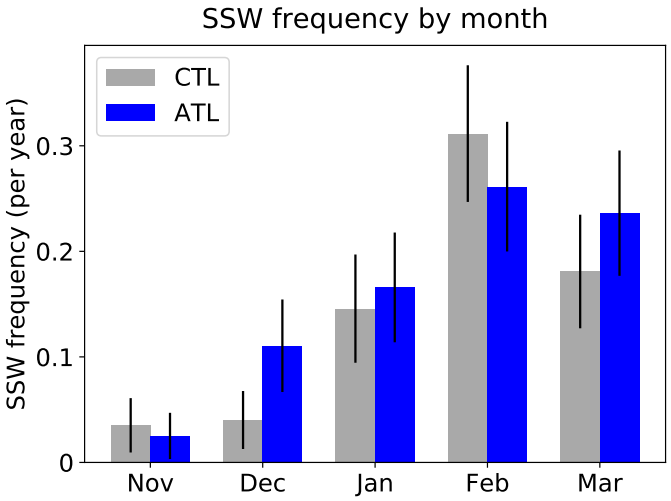

Fig. 4.14 Climatological mean SSW frequency by month in CTL (grey) and ATL (blue). The black bars show the 95% confidence interval for the mean, calculated using a t-distribution (see Section 2.3.4.5 of Chapter 2 for more details).

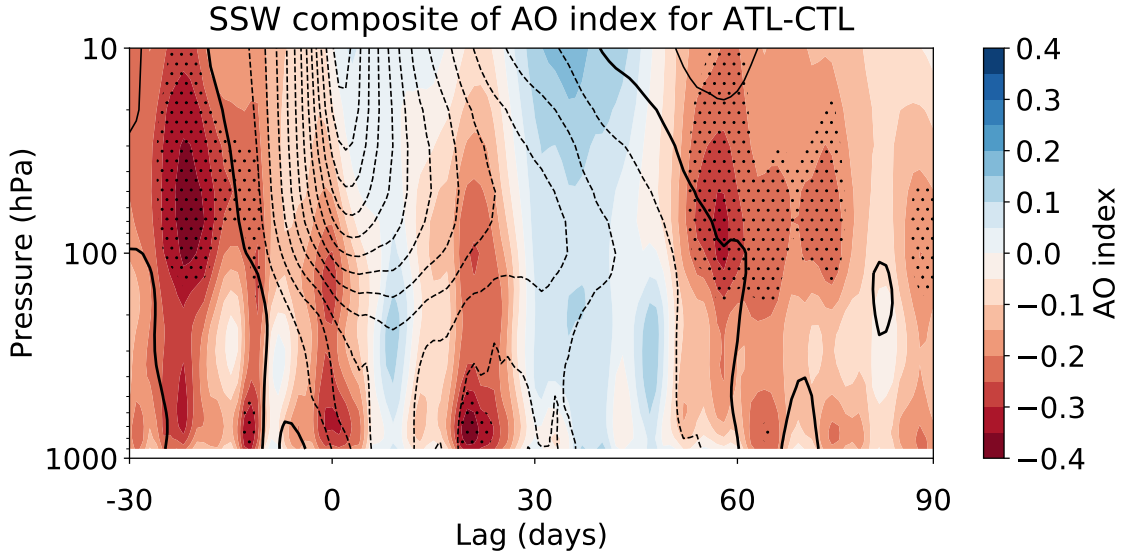

Fig. 4.15 Time-height evolution of the daily AO index for a composite SSW in CTL (contours; interval of 0.2), and for a composite SSW in ATL minus a composite SSW in CTL (shading). The composites are calculated by centering all the SSWs occurring in a run (N = 142 in CTL and N = 159 in ATL) about their central date, which is indicated by a lag of 0, and then calculating an average. Stippling indicates statistical significance at a 95% confidence level for the mean daily difference, calculated using a t-test. Note that blue is positive and red is negative (to depict the polar cap warming, or increase in polar cap geopotential height, associated with the SSW).

difference between two means (see Section 2.3.4.3 of Chapter 2; this method is used rather than a t-test, since the data is non-normally distributed).

It does, however, seem unlikely that these changes in December SSW frequency alone can fully explain the stratospheric AO response in ATL. Indeed, it could be that changes in the SSW strength or duration (hereafter referred to as changes in SSW 'structure') are important as well. Figure 4.15 shows the difference between a composite SSW for ATL and a composite SSW for CTL, in terms of the AO index with time and height. This shows that SSWs in ATL compared to CTL are associated with a slightly earlier weakening in the AO index prior to an SSW central date (see lags -30 to 0), are stronger in the mid to lower stratosphere in the first month following an SSW central date (see lags 0 to 30), and are longer in duration (see lags 50 to 90).

To estimate how much the above differences in SSW frequency and structure contribute to the total AO response at 10 hPa, three different datasets are artificially constructed. As an aid to the following explanation, the construction of these datasets is depicted in schematic form in Figure 4.16. To construct a dataset for CTL, named CTL_{con}, a 120 (day) by 199 (year) array is created to hold the November-February evolution of the AO index at 10 hPa for each year (note the run is 200 years long, but it is started in January and so there are only 199 continuous winters). An SSW composite of the AO index at 10 hPa for CTL is then inserted about each of the SSW central dates for CTL. Similarly, to construct a dataset for ATL that only contains differences in SSW frequency (named $ATL_{conFreq}$), the CTL SSW AO composite is inserted into a second array, but about each of the ATL SSW central dates. Finally, to construct a dataset for ATL that contains differences in both SSW frequency and structure (named $ATL_{conBoth}$), the ATL SSW AO composite is inserted into a third array, again about each of the ATL SSW central dates.

Figure 4.17 shows the winter evolution of the AO index at 10 hPa for ATL-CTL, calculated using the actual run datasets and the artificially constructed datasets. $ATL_{conFreq}$-CTL_{con} estimates the effect of differences in SSW frequency, and $ATL_{conBoth}$-CTL_{con} estimates the effect of differences in both SSW frequency and structure. This highlights that the stratospheric AO response in ATL is largely explained by differences in SSW frequency and structure, with each contributing to around half of the total response.

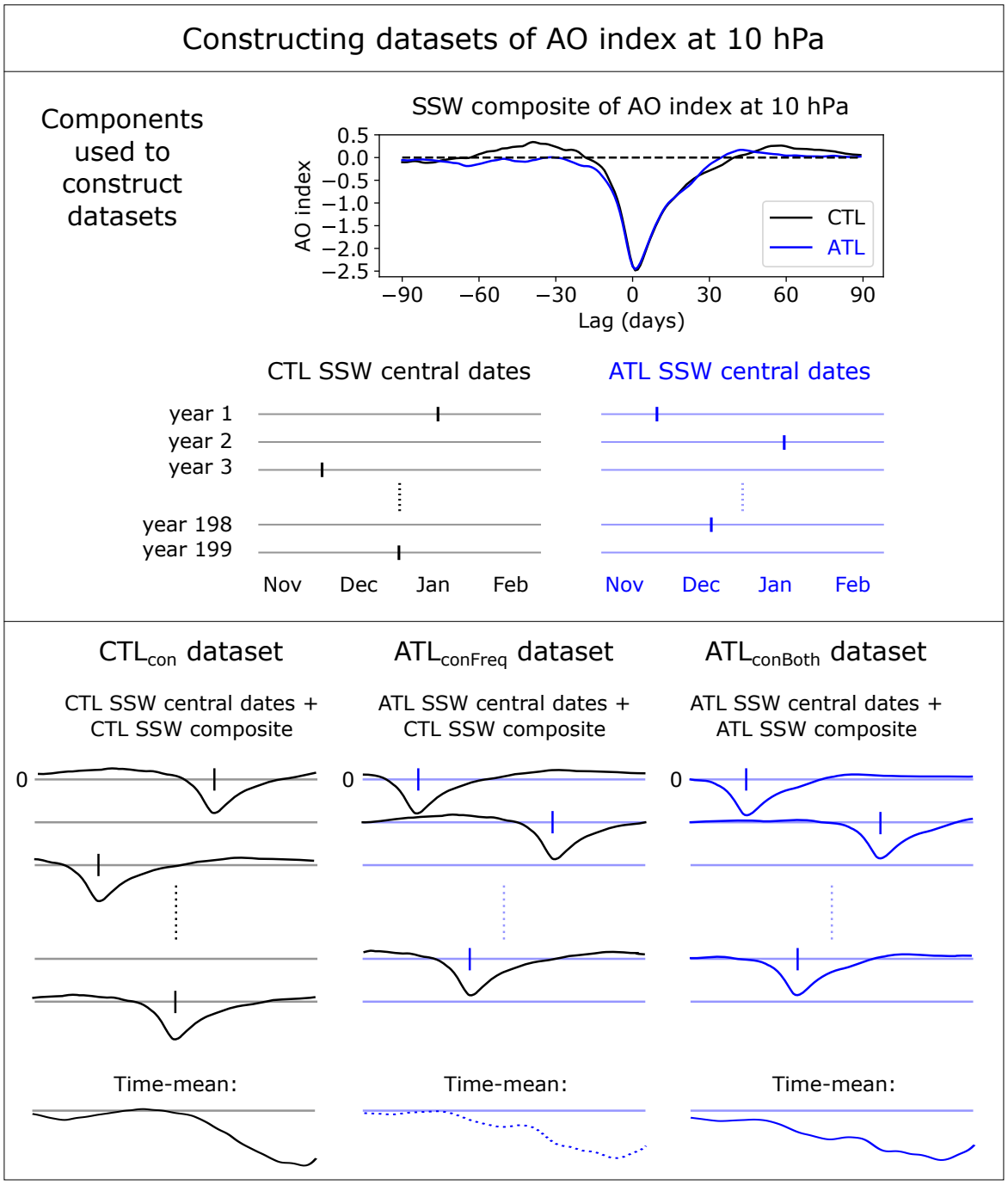

Fig. 4.16 Schematic showing how datasets of the AO index at 10 hPa are artificially constructed for CTL and ATL, to test for the effect of differences in SSW frequency and structure. The former is tested by changing the SSW central dates used (CTL or ATL), and the latter by changing the SSW composite used (CTL or ATL). A lag of 0 in the top plot indicates the SSW central date.

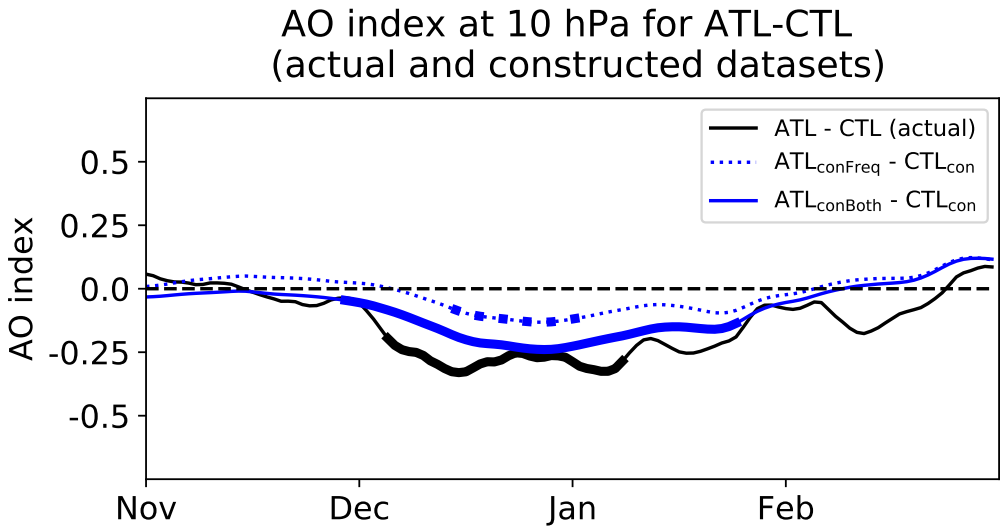

Fig. 4.17 Daily evolution of the AO index response at 10 hPa over winter for ATL-CTL (thin black line), and for datasets constructed to estimate the effect of changes in SSW frequency (ATL$_{conFreq}$-CTL$_{con}$; thin blue dotted line), and the effect of changes in both SSW frequency and structure (ATL$_{conBoth}$-CTL$_{con}$; thin blue solid line). Thick solid and dotted lines indicate statistical significance at a 95% confidence level for the daily response, calculated using a t-test. See Figure 4.16 for a schematic showing how the constructed datasets were created.

It will now be determined whether these changes in SSWs could have an impact on the tropospheric AO response. Similarly to Figure 4.13, Figure 4.18 shows the climatological (200 year) mean daily evolution of the AO at 10 hPa and 500 hPa over November-February for ATL-CTL, which is decomposed into a multi-year mean evolution for SSW years and non-SSW years. While there appears to be a large amount of intraseasonal variability at 500 hPa within the SSW and non-SSW year subsets, there is some indication of a strong negative AO response at 500 hPa in late December and January (i.e. mid-winter) in the SSW year subset, but not in the non-SSW year subset. This occurs after the strongly negative stratospheric AO response in mid-December, suggesting that a stratospheric pathway involving SSWs may be important in the mid-winter tropospheric AO response. However, it is difficult to be sure of cause and effect within this type of analysis: it could be a coincidence that the strong mid-winter tropospheric response in SSW years occurs after the strong stratospheric response. Furthermore, the large intraseasonal variability does make it difficult to be sure that there is a difference in the tropospheric response between SSW years and non-SSW years.

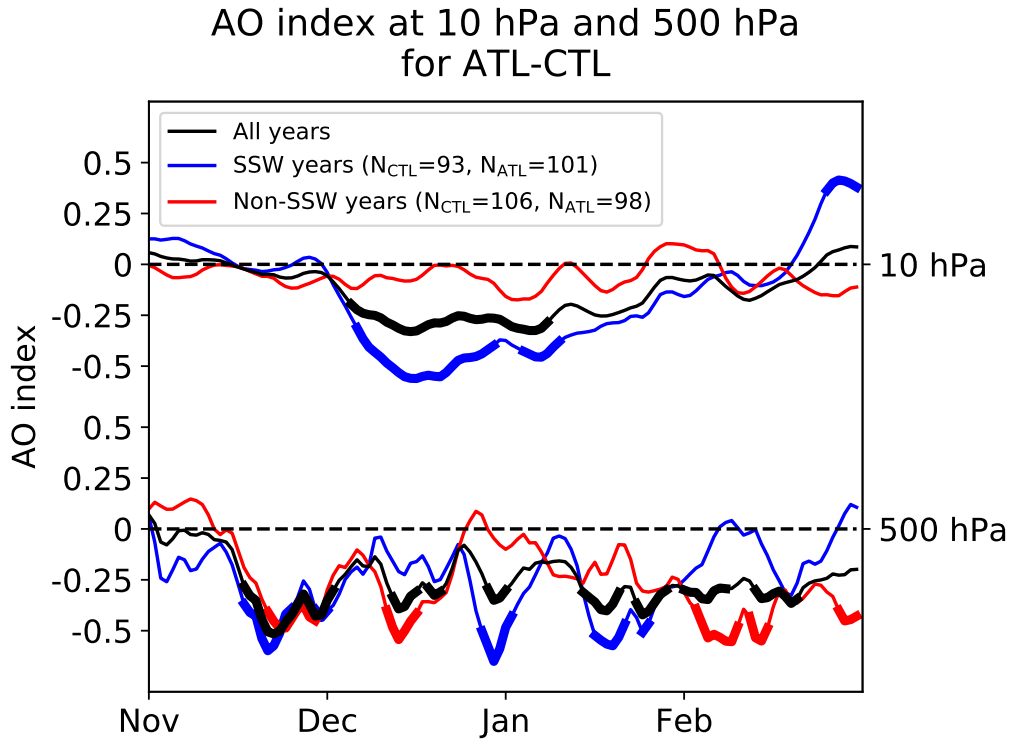

Fig. 4.18 Daily evolution of the AO index response at 10 hPa and 500 hPa over winter for ATL-CTL (thin black lines). This is also shown for subsets of years in which at least one SSW occurs (thin blue lines) or in which none occur (thin red lines) over November-February. Thick lines indicate statistical significance at a 95% confidence level for the daily response, calculated using a t-test.

To determine more objectively whether the increase in December SSW frequency in ATL has an influence on the tropospheric AO response, the CTL_{ndgSSW} experiment is used. Figure 4.19 shows the winter evolution of the AO index at 10 hPa and 500 hPa for ATL-CTL, compared to CTL_{ndgSSW}-CTL_{ndgCS}, where the latter response has been scaled by the December SSW frequency response for ATL-CTL. This shows that the increase in December SSW frequency in ATL does indeed have a large influence on the troposphere in mid-winter. In particular, in terms of the December-January mean this increase in SSW frequency accounts for 36% of the negative tropospheric AO response in ATL (-0.09 out of -0.25).

To conclude, regarding research question 2 (b) for the Atlantic case, these results imply that a stratospheric pathway involving a change in SSW events does play a role in the negative tropospheric AO response in the ATL run. In particular, the stratospheric response in ATL is largely explained by changes in SSW structure and an

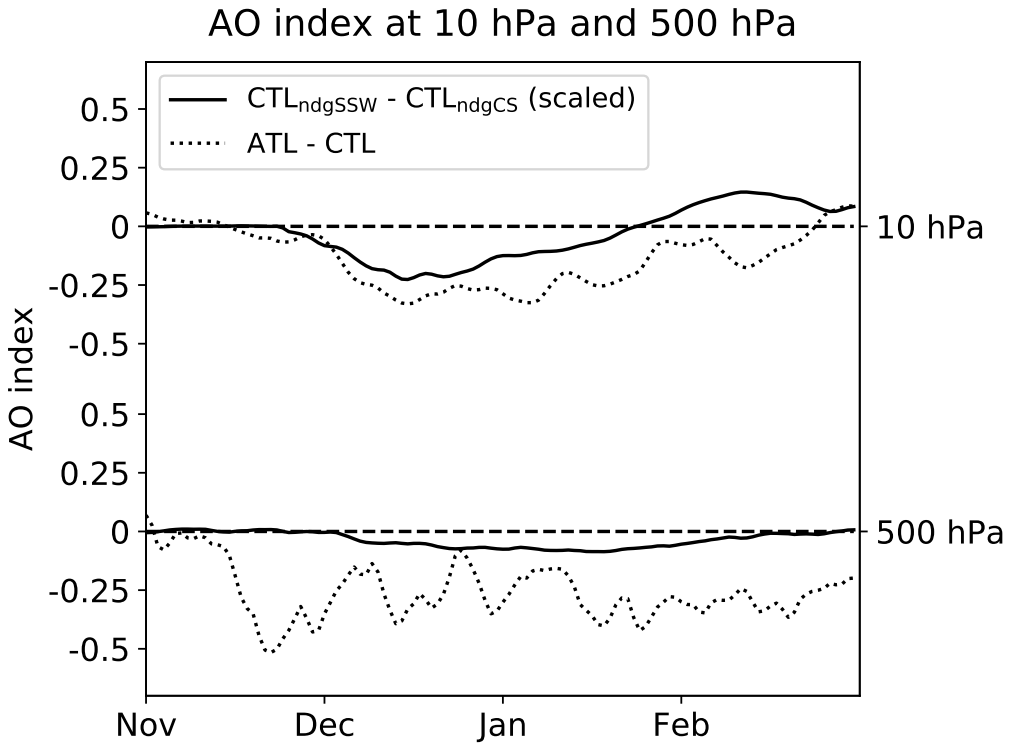

Fig. 4.19 Daily evolution of the AO index response at 10 hPa and 500 hPa over winter for ATL-CTL (dotted lines), compared to CTL$_{ndgSSW}$-CTL$_{CS}$ (scaled; solid lines). The scaling of the latter curves involves multiplying the CTL$_{ndgSSW}$-CTL$_{ndgCS}$ response (Figure 4.9) by the December SSW frequency response for ATL-CTL (Figure 4.14).

increase in December SSW frequency, and this increase in December SSW frequency can explain 36% of the mid-winter negative tropospheric AO response in ATL. While it would be interesting to determine the extent to which the changes in SSW structure have an influence on the troposphere, this is not examined here due to time constraints.

4.4.3.2 Pacific case

In the Pacific case, no statistically significant changes in SSWs were found in PAC for either the winter as a whole, or in any individual month. Since the stratospheric polar vortex is stronger in PAC than in CTL, it was thought that strong stratospheric polar vortex events – as defined in Baldwin and Dunkerton (2001) – could be more relevant, but there were no statistically significant changes found in these events either. As such, in relation to research question 2 (b) for the Pacific case, these results imply that a

stratospheric pathway involving a change in SSW events does not play a role in the negative tropospheric AO response in the PAC run.

4.4.4 Combined non-linear pathway

This section uses ATL and PAC, and the tropospheric and winter mean stratospheric pathway experiments (ATL_{ndgCS}, PAC_{ndgCS}, CTL_{ndgAS}, and CTL_{ndgPS}), to investigate research question 3: 'Does a combined non-linear tropospheric and stratospheric pathway play a role in the negative tropospheric AO responses in the ATL and PAC runs?'.

Recall from this chapter's introduction that the combined non-linear pathway refers to a pathway in which tropospheric and stratospheric mechanisms in isolation do not generate a large tropospheric response, but when operating together their interaction results in a combined effect that is significantly greater than the linear addition of their individual effects. Specifically, this pathway is hypothesised to involve the stratospheric state in PAC (and potentially ATL) altering vertical wave propagation in such a way that the direct stationary Rossby wave response to the sea-ice loss projects onto a negative tropospheric AO. This hypothesised pathway is based on established literature showing that a stationary Rossby wave generated in the North Pacific can only project onto the tropospheric AO when the stratospheric polar vortex is strong (e.g. Castanheira and Graf, 2003; Sun and Tan, 2013).

To explore whether this hypothesised pathway is correct, plots of the geopotential height (Z) and the Plumb flux are examined. The Plumb flux is parallel to the group velocity of stationary Rossby waves, and therefore indicates the direction of wave propagation (Plumb, 1985); more details are given in Section 2.3.1.2 of Chapter 2. The fields are plotted with latitude and longitude at 500 hPa, and with longitude and height (averaged over the latitudes for which the direct response occurs), to examine the full three-dimensional propagation of the waves.

4.4.4.1 Atlantic case

For the Atlantic case, there was no obvious evidence of a combined non-linear pathway in the Z and Plumb flux plots examined (plots not shown). If such a pathway is important, then it appears to not be easily detectable through such an analysis.

4.4.4.2 Pacific case

Figure 4.20 shows the Plumb fluxes and Z for PAC in mid-November before the negative tropospheric AO has developed, and at the beginning of December when the negative AO first appears. These show that the stationary Rossby wave associated with the direct response propagates eastward away from the Chukchi-Bering Seas region (see A), and upward into the stratosphere initially (see B). However, by the beginning of December the strengthened polar vortex response is at its maximum, and the anomalous waves in the stratosphere appear to be refracted back downwards toward the Icelandic Low region, where there is an increase in Z (see C). This is concurrent with the time that the AO-like dipole first appears in the Atlantic sector (see D), and is similar to the mechanism described by Castanheira and Graf (2003), and Sun and Tan (2013) in particular. These results therefore support the pathway hypothesised above: the strengthened polar vortex in PAC alters vertical wave propagation in such a way that the direct stationary Rossby wave response to sea-ice loss projects onto a negative tropospheric AO. It is, however, difficult to be conclusive based on evidence from PAC alone.

More objective evidence supporting the above hypothesised pathway is found by examining how the different stratospheric states in $\mathrm{CTL_{ndgPS}}$ and $\mathrm{PAC_{ndgCS}}$ affect vertical wave propagation.

Figure 4.21 shows the Plumb fluxes and Z for the beginning and middle of December in $\mathrm{CTL_{ndgPS}}$, in which the stratosphere is nudged toward a PAC-like (strengthened polar vortex) zonal mean state. Note that this is a slightly later time-period than was shown for PAC: this is because while the zonal mean stratospheric response appears at the same time in PAC and $\mathrm{CTL_{ndgPS}}$ (Figure 4.12b), the zonally asymmetric part of the response (i.e. the wave response, the part of interest here) takes a couple of weeks longer to become similar in pattern and magnitude. This is perhaps to be expected based on the results of Hitchcock and Simpson (2014), who find that nudging toward a specific SSW does not reproduce the zonally asymmetric part of the stratospheric flow associated with observed SSWs. It is therefore in fact promising that the zonally asymmetric part of the response does become similar in $\mathrm{PAC_{ndgCS}}$ to PAC.

The Plumb flux and Z plots for $\mathrm{CTL_{ndgPS}}$ show that at the beginning of December (when the stratospheric Z anomalies are similar in magnitude and pattern to mid-November in PAC; see left-hand plots in Figure 4.20), there is predominantly anomalous

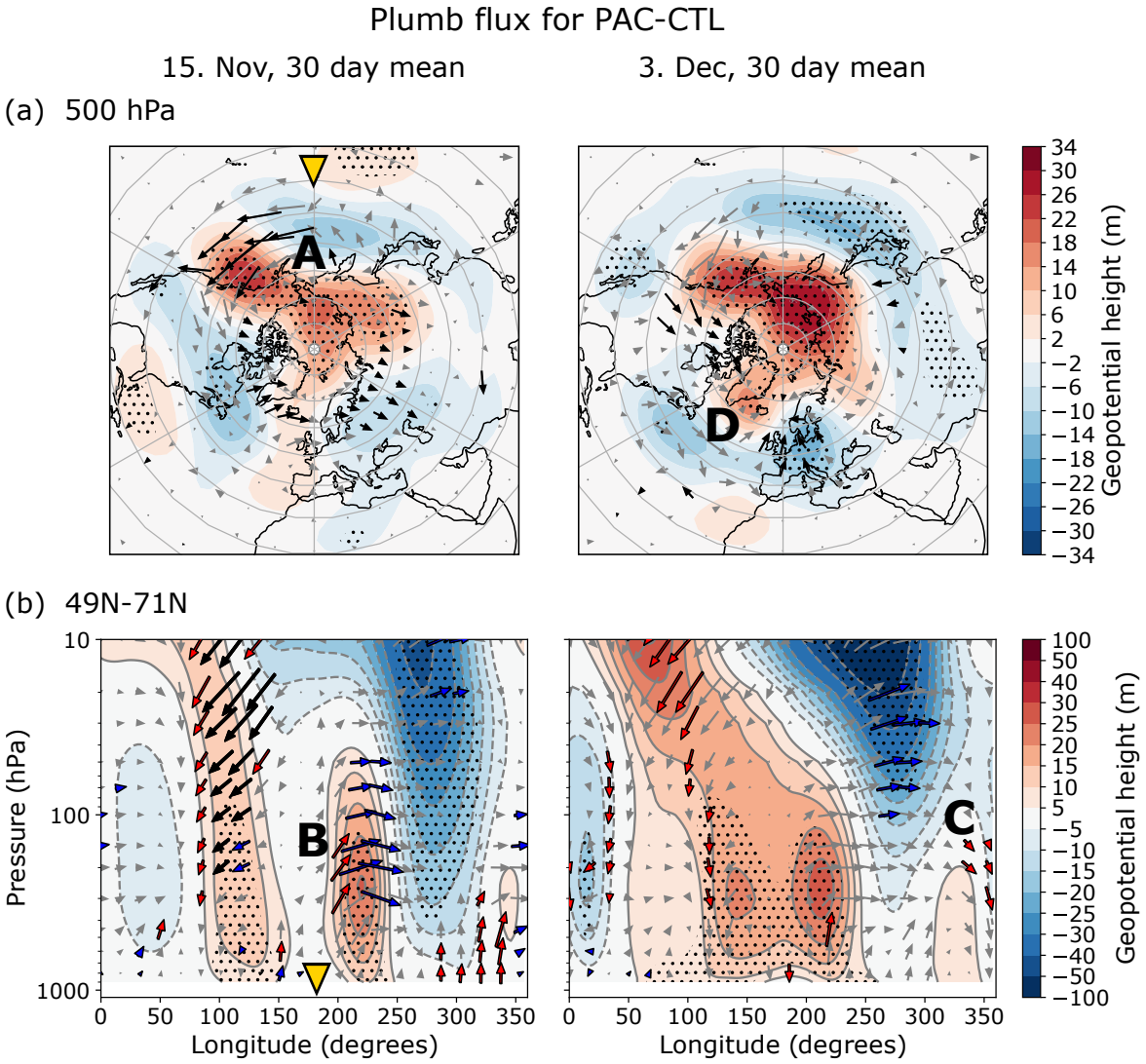

Fig. 4.20 Plumb fluxes (arrows) and geopotential height (shading) for PAC-CTL, calculated for (a) 500 hPa and (b) 49°N-71°N, and averaged for the 30 days about [left] November 15 and [right] December 3. Plumb flux vectors in (a) are coloured black if they are significant in either a meridional or zonal direction, and in (b) are coloured black if they are significant in both meridional and vertical directions, and blue/red if only the meridional/vertical component is significant. Large yellow triangles on left-hand plots indicate the same longitude. Large capital letters on plots indicate features referred to in the text. Stippling indicates significance at a 95% confidence level for shaded fields, calculated using a t-test.

upward wave propagation into the stratosphere (see A). However, by mid-December (when the stratospheric Z anomalies are similar to the beginning of December in PAC; see right-hand plots in Figure 4.20), there is predominantly anomalous downward wave propagation toward the Icelandic Low region (see B). Since only the zonal mean

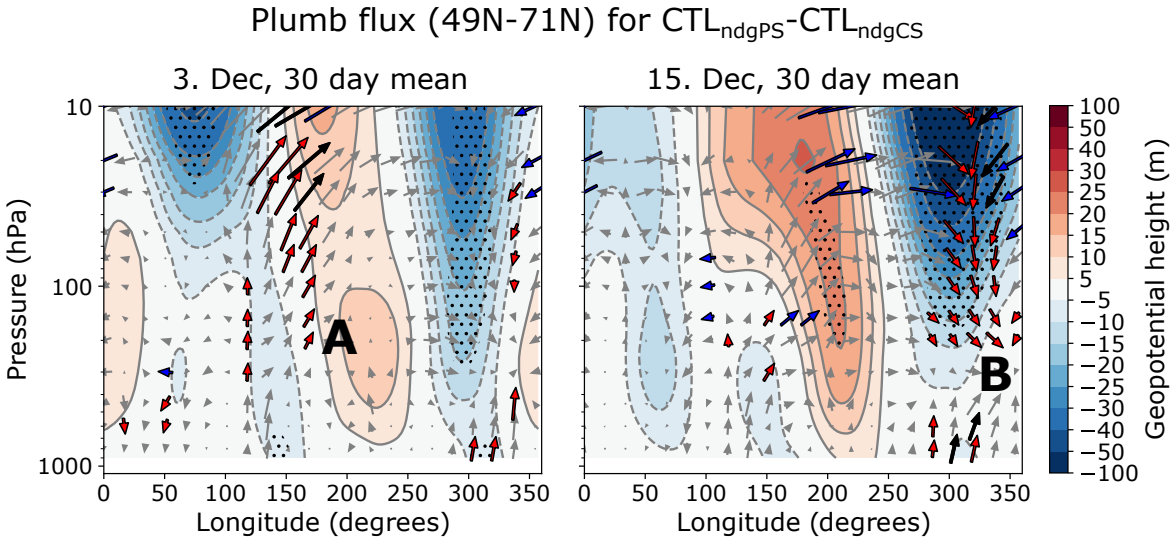

Fig. 4.21 Plumb fluxes (arrows) and geopotential height (shading) for CTL_{ndgPS}-CTL_{ndgCS}, averaged over 49°N-71°N, and for the 30 days about [left] December 3 and [right] December 15. See Figure 4.20 for further plot details.

stratospheric state is perturbed in CTL_{ndgPS}, it can be fairly confidently concluded that the changes in vertical wave propagation described are due to this perturbed state. These results therefore provide further evidence in support of the hypothesised pathway.

A look is also taken at the Plumb fluxes and Z for PAC_{ndgCS} in mid-January (the only month in which the direct response occurred); see Figure 4.22. In this run, the stratosphere is nudged toward a CTL-like state and, therefore, for the proposed hypothesis to be correct, the changes in vertical wave propagation seen in PAC and CTL_{ndgPS} should not occur in PAC_{ndgCS}. Indeed, notice that while the stationary Rossby wave associated with the direct response in PAC_{ndgCS} is very similar to that in PAC (see A), it propagates eastward away from the Chukchi-Bering Seas region along an entirely tropospheric pathway into the Atlantic sector (see B). Furthermore, in the Atlantic sector it appears to project onto the positive phase of the NAO (see C), rather than the negative phase, explaining why no negative AO response develops in this run. These results again provide further evidence in support of the hypothesised pathway.

There is one last piece of evidence to consider. Similarly to Figure 4.18, Figure 4.23 shows the climatological mean daily evolution of the AO at 10 hPa and 500 hPa over November-February for PAC-CTL, which is decomposed for SSW years and non-SSW years. This shows that a more strongly negative tropospheric AO response occurs in

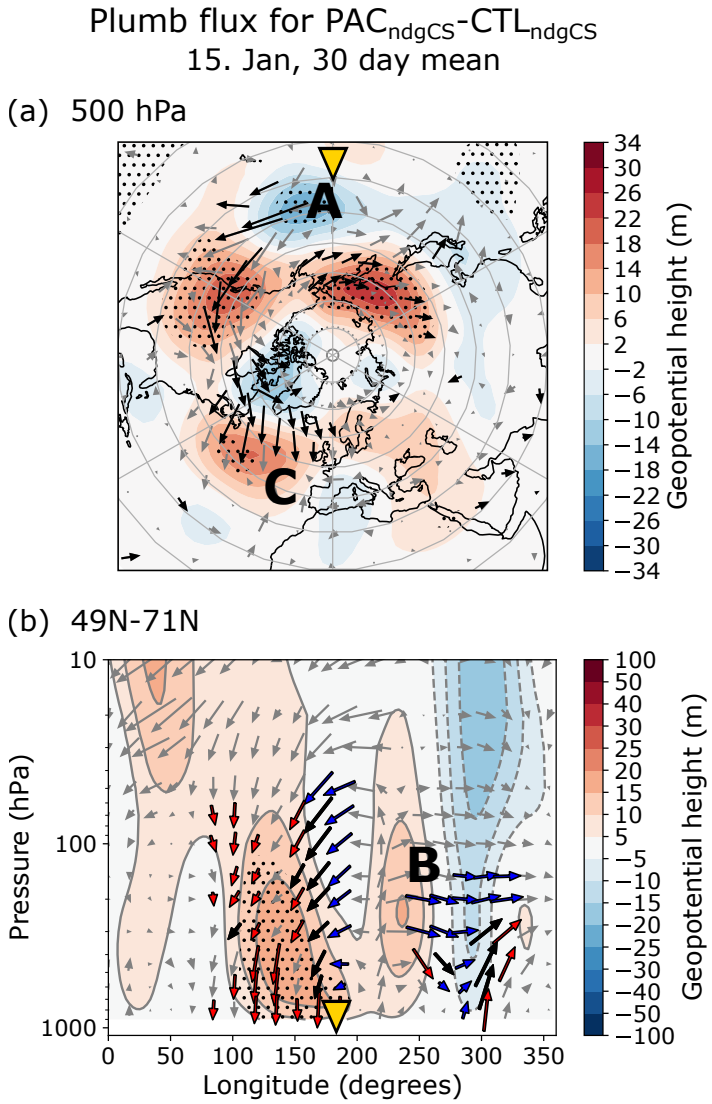

Fig. 4.22 Plumb fluxes (arrows) and geopotential height (shading) for PAC$_{ndgCS}$-CTL$_{ndgCS}$, calculated for (a) 500 hPa and (b) 49°N-71°N, and averaged for the 30 days about January 15. See Figure 4.20 for further plot details.

non-SSW years, which also tend to be years in which the stratospheric polar vortex is stronger on average (in SSW years the 10 hPa AO index is -0.35 in CTL and -0.27 in PAC for November-February, and in non-SSW years it is 0.28 in CTL and 0.31 in PAC). The fact that the tropospheric AO response is more strongly negative in a subset of years when the polar vortex is stronger on average is further evidence that a strengthened polar vortex plays a key role in the negative tropospheric AO response in PAC. In years in this subset, the strengthened polar vortex is further strengthened

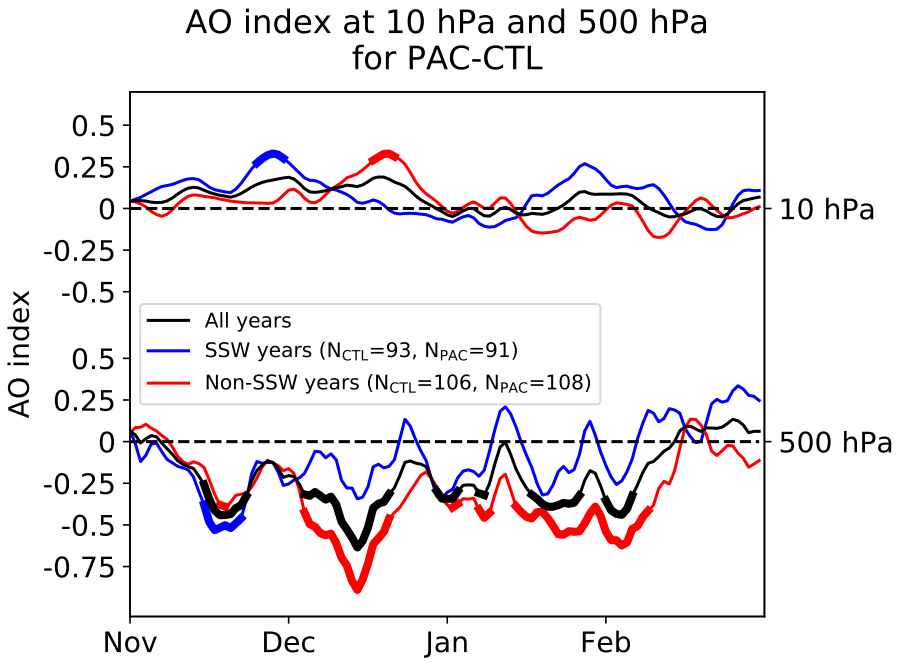

Fig. 4.23 Daily evolution of the AO index response at 10 hPa and 500 hPa over winter for PAC-CTL (thin black lines). This is also shown for subsets of years in which at least one SSW occurs (thin blue lines) or in which none occur (thin red lines) over November-February. Thick lines indicate statistical significance at a 95% confidence level for the daily response, calculated using a t-test.

by the effects of stratospheric interannual variability, likely explaining the enhanced tropospheric negative AO response.

To conclude, regarding research question 3 for the Pacific case, the above results suggest that a combined non-linear tropospheric and stratospheric pathway plays an important role in the negative tropospheric AO response in PAC. In particular, the negative AO response seems to be very much dependent on a strengthened stratospheric polar vortex. This is because a strengthened polar vortex alters vertical wave propagation in such a way that the direct stationary Rossby wave response to the sea-ice loss projects onto a negative tropospheric AO.

4.5 Discussion and conclusions

As a recap, the aim of this chapter was to investigate key gaps in our understanding that remain from Chapter 3, including the roles played by tropospheric and stratospheric

mechanisms in the responses to large-magnitude (late 21st century) Atlantic and Pacific sector sea-ice loss (ATL and PAC runs). To do this, stratospheric nudging experiments were conducted using IGCM4 and statistical analysis was performed within ATL and PAC, with the aim of addressing the following research questions:

1. Does a tropospheric pathway play a role in the negative tropospheric AO responses in the ATL and PAC runs?

2. Do stratospheric pathways associated with (a) a winter mean change in the stratospheric polar vortex, and/or (b) a change in SSW events, play a role in the negative tropospheric AO responses in the ATL and PAC runs?

3. Does a combined non-linear tropospheric and stratospheric pathway play a role in the negative tropospheric AO responses in the ATL and PAC runs?

The results found relating to these research questions are summarised with the aid of a schematic (Figure 4.24), which is a revised version of the schematic shown in Figure 3.12 of Chapter 3. This revised schematic shows a revised view of the key mechanisms proposed to link large-magnitude Arctic sea-ice loss to changes in mid-latitude surface temperatures. It will be subsequently shown that this improved mechanistic understanding enables a better understanding of many aspects of the response to sea-ice loss.

Recall that for the sea-ice loss in the ATL run, the total winter (November-February) mean response in the tropospheric AO index is -0.25. With respect to question 1, the ATL_{ndgCS} nudging experiment implies that 24% (-0.06) of this is due to a tropospheric pathway alone (indicated by the dotted arrows directly connecting the sea-ice loss with the eddy-driven jet in Figure 4.24a). This experiment also shows that an additional 16% (-0.04) can be explained by an active stratosphere enhancing the magnitude of the direct stationary Rossby wave response to sea-ice loss, if a linear relationship between the direct and AO responses is assumed. It is difficult to say anything specific about the mechanisms involved in this enhancement of the direct response, other than that constraining the stratosphere may place some constraint on the free evolution of the troposphere. In relation to question 2 (a), the CTL_{ndgAS} nudging experiment implies that none of the AO response can be explained by a stratospheric pathway involving a winter mean change in the stratospheric polar vortex. Instead, with respect to question 2 (b), it is found using statistical analysis within the ATL experiment that

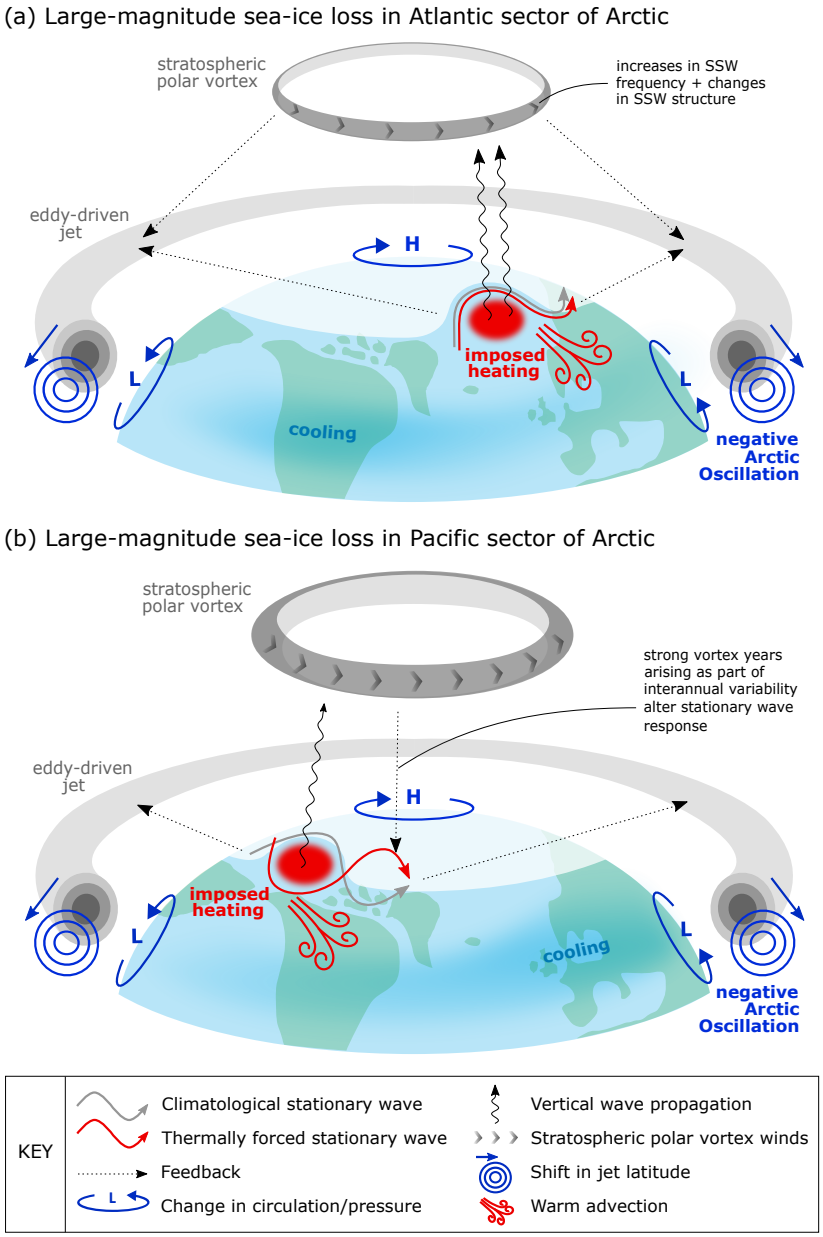

Fig. 4.24 Revised version of the schematic shown in Figure 3.12 of Chapter 3, which incorporates the important advances and new knowledge gained from the results presented in this chapter. This schematic summarises the key mechanisms that may link large-magnitude (late 21st century) Arctic sea-ice loss with changes in mid-latitude surface temperatures, for (a) Atlantic and (b) Pacific sector sea-ice loss. Features of the direct/indirect response are shaded in red/dark blue.

the stratospheric response to ATL sea-ice loss can largely be explained by changes in SSW structure and an increase in December SSW frequency (indicated in Figure 4.24a by the vortex thickness, grey arrows, and related text). The CTL_{ndgSSW} nudging experiment shows that this increase in SSW frequency can explain 36% (-0.09) of the mid-winter (December-January) tropospheric AO response (indicated in Figure 4.24a by the dotted arrows directly connecting the polar vortex with the eddy-driven jet). In relation to question 3, a combined non-linear pathway is not found to be important for ATL sea-ice loss.

As for the sea-ice loss in the PAC run, the total winter (November-January) mean response in the tropospheric AO index is -0.26. Regarding question 1, the PAC_{ndgCS} nudging experiment suggests that a negligible (-0.01) part of this is due solely to a tropospheric pathway. This experiment does show however that – similarly to the Atlantic case – a role is played by an active stratosphere extending the duration of the direct response. Furthermore, with respect to questions 2 (a) and (b), it is suggested by the CTL_{ndgPS} nudging experiment and statistical analysis within the PAC experiment respectively, that none of the AO response can be explained by either a winter mean change in the stratospheric polar vortex or changes in SSW events. However, in relation to question 3, it is shown using the PAC experiment and above nudging experiments that a combined non-linear pathway is important. Specifically, the stratospheric state alters vertical wave propagation in such a way that the direct stationary Rossby wave response projects onto a negative tropospheric AO (indicated in Figure 4.24b by the dotted arrows connecting the polar vortex to the red wavy arrow, and the red wavy arrow to the eddy-driven jet). This effect occurs in strong vortex years arising as part of interannual variability (indicated in Figure 4.24b by the text relating to the dotted arrow). Note that the results presented here suggest that a time-mean strengthening of the stratospheric polar vortex in PAC could also play a role in this pathway. However, while this strengthening appeared to be statistically significant in November-December based on the PAC run alone (see Chapter 3), Chapter 5 will show that a 200 year-long simulation is not sufficiently long to determine the robustness of the stratospheric response for this short sub-seasonal time-period. As such, it cannot be robustly concluded whether a sea-ice loss induced strengthening of the stratospheric polar vortex plays a role in the combined non-linear pathway.

In summary, while the nudging experiments for both ATL and PAC sea-ice loss do not give linearly additive results, they are still very insightful. In particular, it is

clear that constraining the stratosphere has a large effect on the negative tropospheric AO responses found for ATL and PAC and, therefore, that the stratosphere plays an important role in these responses (although a role is also found in the Atlantic case for tropospheric mechanisms alone). In the Atlantic case, this role most likely involves changes in SSW events, and in the Pacific case, this role likely involves a dependency of the negative tropospheric AO response on a strengthened stratospheric polar vortex. These results therefore revise Chapter 3's suggestion that stratospheric mechanisms may not play an important role in the negative tropospheric AO responses for ATL and PAC sea-ice loss, which was based on the fact that there are different stratospheric responses in ATL and PAC.

However, there are remaining gaps in our understanding and the quantitative robustness of the results should be questioned. This will now be discussed, which will provide the motivation for further work in the following chapter.

For example, for the Atlantic case 24% (-0.06) of the total negative tropospheric AO response remains to be explained for mid-winter, and 60% (-0.15) remains to be explained for the rest of winter. This lack of linear additivity could be at least partly explained by internal variability leading to sampling error in the magnitude of each pathway (for instance, the tropospheric pathway may have been underestimated in $\mathrm{ATL}_{\mathrm{ndgCS}}$).

There are also questions that should be asked regarding the changes in SSWs found to contribute to the stratospheric response in ATL. In particular, while a large increase in SSW frequency is found in December (there are almost 3 times more SSWs in ATL than CTL), and the sign of this response is statistically significant with a confidence level of 99%, the 95% confidence intervals for the mean December SSW frequencies in CTL and ATL are similar in size to the difference in the means (Figure 4.14). This suggests that while the sign of the model's forced change in December SSW frequency is separable from internal variability of SSWs within the 200 year-long ATL experiment, this internal variability is still relatively too large to accurately determine the magnitude of the forced change in SSWs. This uncertainty leads to the question of the accuracy of this chapter's estimated contribution of forced changes in December SSW frequency to forced changes in the tropospheric AO due to ATL sea-ice loss within the model.

To obtain a more quantitatively robust estimate of the model's forced changes in SSWs and the influence of these changes on the troposphere, much longer experiments

may be required than previously expected before designing and conducting the analysis in this chapter. Furthermore, in more general terms, by showing that internal variability in SSWs may have a sizeable quantitative impact on the mean tropospheric response in ATL, the results of this chapter potentially suggest that even when model time-slice experiments containing 200 years and longer are used to estimate forced changes due to sea-ice loss, atmospheric internal variability may remain an important consideration. This could have wider implications, since studies using models to estimate forced stratospheric and tropospheric changes due to sea-ice loss typically use experiments that contain less than 200 years (see Section 3.3.1 of Chapter 3), and the Polar Amplification Model Intercomparison Project (PAMIP) recommends that experiments should contain at least 100 years (or ensemble members).

To examine the influence of atmospheric internal variability with regard to uncertainty in responses to sea-ice loss produced by model time-slice experiments of different lengths, the lengths of the CTL and ATL experiments are increased to 600 years in the following chapter. Note that this experiment length was only recently made more feasible in late 2018 by the replacement of the local HPC (High-Performance Computer) at the British Antarctic Survey, which IGCM4 is run on. This reduced the computational time of an IGCM4 run – including the time to output data – fivefold, such that a 600 year-long experiment now only takes 2-3 weeks. Previously, a 600 year-long experiment would have taken around 3 months to conduct and, therefore, run-time was a factor that had to be considered more carefully in this chapter and the previous chapter, particularly because several (11) experiments were conducted.

For the Pacific case, the majority of the total negative tropospheric AO response remains to be explained for the whole of winter. In this chapter, evidence is presented that suggests the combined non-linear pathway could explain this lack of linear additivity. Indeed, the results of PAC and $\text{PAC}_{\text{ndgCS}}$ reveal that the tropospheric response is dependent on the stratospheric state, and the Plumb flux diagnostic is used to suggest a possible mechanism. While the details of the suggested mechanism are arguably subjective, it is still true that the only specified difference between PAC and $\text{PAC}_{\text{ndgCS}}$ is a difference in the stratospheric state (PAC-like with stratospheric interannual variability in the former, and CTL-like with no stratospheric interannual variability in the latter). Combined with the existence of established literature in support of such a mechanism, it seems likely that this difference in state at least partly explains the differences in the tropospheric responses. Sampling error could however

also contribute to the lack of linear additivity, a point which will be explored in detail in Chapter 5.

4.5.1 Wider relevance

The wider relevance of the above results in terms of understanding the response to sea-ice loss will now be discussed.

Firstly, a key result is that constraining the stratosphere has a large effect on the tropospheric responses for both ATL and PAC sea-ice loss. This has a wider relevance because it suggests that climate models with an inadequate representation of the stratosphere may not realistically simulate the response to sea-ice loss. As such, this could explain differences in the responses and dominant mechanisms found in past studies using different models. This finding is in agreement with other studies that quantitatively show the importance of stratospheric mechanisms in the response to sea-ice loss by using either a stratospheric nudging technique (Nakamura et al., 2016b; Wu and Smith, 2016; Zhang et al., 2018a,b), or high versus low top versions of a climate model (Sun et al., 2015). A difference, however, is that the aforementioned studies either examine past regional sea-ice loss (Nakamura et al., 2016b; Zhang et al., 2018a,b) or future pan-Arctic warming (Wu and Smith, 2016), while here the result is found for large-magnitude (late 21st century) regional sea-ice loss (thus suggesting that model stratospheric representation is important regardless of whether future sea-ice retreat is weighted towards either the Atlantic or Pacific sectors).

The results here also enable an understanding of specific aspects of model stratospheric representation that are important for simulating the response to sea-ice loss. Firstly, with regards to ATL sea-ice loss, while the importance of an increase in December SSW frequency – and hence also the influence of this on the troposphere – remains to be re-evaluated in Chapter 5, the stratospheric pathway nudging experiments (CTL_{ndgAS} and CTL_{ndgSSW}) still provide useful results. In particular, these experiments still quantitatively show that a stratospheric pathway involving changes in SSW events can generate a negative tropospheric AO response, but a pathway involving a winter mean change in the stratospheric polar vortex cannot. As such, if a stratospheric pathway is important in the response to Atlantic sector sea-ice loss, realistic simulation of the response will specifically require an adequate model representation of SSWs. This work provides the first quantitative evidence of the potential importance of SSWs

in particular, as opposed to a winter mean change in the polar vortex, in the response to Atlantic sector sea-ice loss (see the introduction for a review of related studies).

It should of course be discussed whether part of this result – that a winter mean change in the stratospheric polar vortex does not play a role in the tropospheric AO response in ATL – is just specific to IGCM4. Indeed, Wu and Smith (2016) conduct nudging experiments with a different model, and find that such a stratospheric pathway can explain half of the equatorward tropospheric jet shift found in response to a late 21st century RCP8.5 'Arctic Amplification' or AA-like forcing (the scenario used for ATL). However, in the experiments conducted here, a regional ocean surface temperature anomaly representing sea-ice retreat is imposed, whilst in the Wu and Smith (2016) experiments the AA-like forcing is zonally symmetric (i.e. pan-Arctic) and extends upwards to 600 hPa. Wu and Smith (2016) therefore consider the response to a more extensive Arctic warming, which includes not just the effects of sea-ice loss, but factors such as the Planck feedback (see Chapter 1 for a discussion of the contributions to AA). It is therefore not surprising that they find a weakening of the stratospheric polar vortex that is around five times the magnitude of the response in ATL and, therefore, a stronger effect on the troposphere when the stratosphere is nudged toward this strongly perturbed state. It is also unlikely that IGCM4 would underestimate the tropospheric response to a stratospheric perturbation, because – as shown in Figure 2.2 of Chapter 2 – the strength of stratosphere-troposphere coupling in IGCM4 is adequately represented when compared with reanalysis data.

The PAC sea-ice loss case highlights a second important aspect of model stratospheric representation that could lead to contrasting results. This relates to the finding that the tropospheric AO response in PAC is sensitive to the strength of the stratospheric polar vortex. Specifically, this suggests that for sea-ice loss including the Pacific sector, the tropospheric response may vary across climate models due to intermodel differences in the climatological mean stratospheric polar vortex strength and/or stratospheric interannual variability (where these differences may be due to different model representations of stratospheric dynamics). For example, regarding Chapter 3's discussion of the range of potential atmospheric responses to future sea-ice loss across the CMIP5 models, it may be the case that a negative AO would not occur for a model with sea-ice loss weighted toward the Pacific sector and a particularly weak climatological polar vortex, and/or with particularly weak interannual stratospheric variability.

Differences in the representation of the stratospheric polar vortex between models may also explain differences in the dominant mechanisms found by past studies. For example, Zhang et al. (2018b) find for East Siberian Seas sea-ice loss – which is similar in longitude and latitude to the sea-ice loss in PAC – that a tropospheric pathway alone contributes to half of the negative tropospheric AO-like response. This is in contrast to the PAC experiment here, where a tropospheric pathway alone explains none of the AO response, and instead a combined non-linear pathway is found to be important. These differences may be because the climate model used by Zhang et al. (2018b) has an approximately 5 m/s stronger climatological mean stratospheric polar vortex than IGCM4 (compare Figure 2.1b in Chapter 2 with Figure 2a in Wu and Smith, 2016), which will be present in their tropospheric pathway experiment.

Furthermore, the fact that a strengthened polar vortex is found to alter the direct stationary Rossby wave response to PAC sea-ice loss in such a way that it projects onto a negative AO may help to explain the apparently contradictory results of previous modelling studies. Specifically, this can help us to understand why a negative tropospheric AO-like response has been found even when there is a strengthening of the polar vortex – e.g. during winter in Sun et al. (2015)'s future Pacific sea-ice loss experiment (although there is only a slight weakening of the wind on the poleward flank of the tropospheric jet), and during spring and November-February respectively in Sun et al. (2015)'s and Nakamura et al. (2016a)'s future pan-Arctic sea-ice loss experiments. However, it is acknowledged that the pan-Arctic sea-ice anomalies used in these studies are extensive (zonally and meridionally), and that for these extensive anomalies a tropospheric pathway involving thermal wind balance may play an important role in generating the negative AO response. Indeed, in Peings and Magnusdottir (2014)'s future pan-Arctic sea-ice loss experiment, they find no response in the stratospheric polar vortex, but a negative tropospheric AO, and attribute this to thermal wind balance.

In summary, the approach taken in this chapter of isolating the responses for different regions of sea-ice loss, and further isolating the different mechanisms involved in these responses, makes understanding the response to sea-ice loss more tractable. In particular, it shows that past studies may find contradictory responses and different dominant mechanisms due to different model representations of stratospheric dynamics (including SSWs potentially), and a sensitivity of the response to the stratospheric state (when ice loss including the Pacific sector is considered).

Chapter 5

The influence of internal variability and sudden stratospheric warmings

5.1 Introduction

In this chapter, it is important to note that the term 'response' is specifically defined in Section 2.3.4.1 of Chapter 2 as the climatological mean difference between a model perturbation (e.g. sea-ice loss) experiment and a model control experiment. Since experiments are necessarily finite in length, this difference in the means will contain the model's forced change due to the specified perturbation plus the influence of atmospheric internal variability. Therefore, the response as defined above only provides an estimate of the model's forced change. The longer the experiments are, the smaller the influence of internal variability on the difference in the experiment means, and the more accurately the response will estimate the model's forced change.

The phrase 'variability in the response' used in this chapter should be taken as meaning variability, spread, or uncertainty in the response for model experiments of a given length due to atmospheric internal variability, where this variability would be apparent if these experiments were repeated many times with unique initial conditions. It should not be taken as meaning variability in the model's forced change due to the specified perturbation, which is a fixed quantity that model experiments aim to estimate.

In Chapter 4, it was shown that the stratospheric response in Chapter 3's large-magnitude (late 21st century) Atlantic sector sea-ice loss experiment (ATL) can largely be explained by changes in sudden stratospheric warmings (SSWs). In particular,

it was found that around half of the response can be explained by changes in SSW frequency – specifically an increase in SSW frequency in December – and that the other half can be explained by changes in SSW structure – specifically an increase in the duration of stratospheric anomalies both before and after an SSW central date, and a strengthening of anomalies in the mid to lower stratosphere during an SSW event. By conducting an experiment in which the zonal mean stratospheric state is nudged toward a specific reference SSW from December in ATL (the $\text{CTL}_{\text{ndgSSW}}$ experiment), it was shown that the increase in December SSW frequency in ATL can explain 36% of the mid-winter negative tropospheric AO response.

However, while Chapter 4's results suggest that the sign of the model's forced change in December SSW frequency is separable from internal variability of SSWs within the 200 year-long ATL experiment, this internal variability is still relatively too large to accurately determine the magnitude of the forced change in December SSWs (i.e. there is a low 'signal-to-noise' ratio – see Chapter 1 for details). This uncertainty leads to the question of the accuracy of Chapter 4's estimated contribution of forced changes in December SSWs to forced changes in the tropospheric AO due to ATL sea-ice loss within the model.

To obtain a more quantitatively robust estimate of the model's forced changes in SSWs and the influence of these changes on the troposphere, much longer experiments may be required than previously expected before the analysis in Chapter 4 was designed and conducted. Furthermore, in more general terms, by showing that internal variability in SSWs may have a sizeable quantitative impact on the mean tropospheric response in ATL, the results of Chapter 4 potentially suggest that even when model time-slice experiments containing 200 years and longer are used to estimate forced changes due to sea-ice loss, atmospheric internal variability may remain an important consideration. This could have wider implications, since studies using models to estimate forced stratospheric and tropospheric changes due to sea-ice loss typically use experiments that contain less than 200 years (see below), and the Polar Amplification Model Intercomparison Project (PAMIP) recommends that experiments should contain at least 100 years (or ensemble members).

In this chapter, the CTL and ATL experiments are extended in length to 600 years to examine the influence of atmospheric internal variability with regard to uncertainty in responses to sea-ice loss produced by model time-slice experiments of different lengths.

In particular, the response for the extended experiments is used as a more accurate estimate of the model's forced changes due to ATL sea-ice loss, and the CTL_{ndgSSW} experiment is used in combination with the extended experiments to specifically provide a more accurate estimate of the contribution of forced changes in December SSWs to forced changes in the tropospheric AO. The difference in the responses between the extended and shorter experiments is used to quantify the influence of internal variability on the response for the shorter experiments, and CTL_{ndgSSW} is used to specifically estimate the influence of internal variability in December SSWs on the stratospheric and tropospheric AO responses for the shorter experiments.

To address the wider motivations for this chapter, the above more specific investigation will be conducted as part of a broader exploration of SSW variability within the 600 year-long experiments, and the influence of this on the stratospheric and tropospheric AO responses. The newly extended 600 year-long experiments provide a unique and ideal opportunity to do this since they are relatively long (indeed much longer than in many modelling studies looking at the response to sea-ice loss – see below).

This broad investigation is conducted using thousands of N year randomly resampled sub-ensembles of the extended experiments, where each ensemble member is one year of an experiment (valid here because in each experiment there is negligible year-to-year autocorrelation in the winter mean tropospheric AO, stratospheric AO, or SSW frequency, as also noted in Section 3.3.2 of Chapter 3 for the shorter experiments). For 200 year sub-ensembles specifically, the variability in SSW responses for different months and the winter mean is examined, as well as the influence of this on the variability of AO responses for these time-periods. Variability in each of the SSW and AO responses is then compared for a wide range of different sub-ensemble sizes. This will be particularly useful, since it will enable a quantification of the minimum ensemble sizes for which the signs of the model's forced changes in SSW frequency and the AO due to sea-ice loss are statistically separable from internal variability, a quantity which can be considered as a measure of the signal-to-noise ratio (where larger and smaller minimum ensemble sizes imply a lower and higher ratio respectively). The minimum ensemble sizes will be quantified both for specific months and across the extended winter season, and it will be examined whether the ensemble sizes for each variable are related.

There are many previous studies that have investigated the influence of stratospheric or tropospheric internal variability on model-produced stratospheric or tropospheric responses for a given external forcing. These will now be discussed for context, and the novelty of the investigations conducted here highlighted. The potential usefulness of the results will also be discussed.

In transient model experiments forced by future changes in greenhouse gases (GHG's), Butchart et al. (2000) find it difficult to detect a robust trend in SSWs – and therefore in the winter mean stratospheric state – over a 60 year time-period due to relatively large decadal variability of SSWs. Similar issues are also highlighted in other modelling studies aiming to estimate forced changes in SSWs due to future GHG forcing (Charlton-Perez et al., 2008; McLandress and Shepherd, 2009; Mitchell et al., 2012; Ayarzagüena et al., 2018), as well as to tropical SST forcing (Polvani et al., 2017), and to observed Arctic sea-ice loss (Jaiser et al., 2016; Seviour, 2017). However, none of these studies quantify the minimum ensemble size required to detect a robust sign of stratospheric response for the given forcing. This has been quantified for the tropospheric response (in various variables) to observed sea-ice loss in the 60 and 100 year-long time-slice simulations of Screen et al. (2014), as well as for the surface Northern Annular Mode (NAM) response to projected changes in many anthropogenic radiative forcings in the transient simulations of Deser et al. (2012). However, in neither case is a quantification determined for aspects of the stratospheric response to the given forcing. The investigations conducted here will fill this gap for a sea-ice forcing, by providing the first guidance on the minimum ensemble size required to obtain a robust sign of stratospheric response to late 21st century sea-ice loss.

This will be very useful because there is currently a large variety of ensemble sizes (or time-slice experiment lengths) used by modelling studies aiming to estimate forced stratospheric and tropospheric changes due to sea-ice loss: for instance, 20 members/years in Cai et al. (2012); 40 years in Kim et al. (2014); 50 years in Peings and Magnusdottir (2014), and Zhang et al. (2018a); 60 years in Nakamura et al. (2015, 2016b); 80 years in Zhang et al. (2018b); 150 years in Nakamura et al. (2016a); and 161 years in Sun et al. (2015). In particular, it is currently unclear which of these studies – if any – use an ensemble size that is sufficient to separate forced changes in SSWs due to sea-ice loss from the internal decadal variability of SSWs that is found by Butchart et al. (2000) and others. As such, it is also unclear whether the different stratospheric responses found by some of these studies is due to internal variability: for example, for

a future sea-ice loss scenario, Peings and Magnusdottir (2014) find no response in the stratospheric polar vortex for their 50 year ensemble, whilst Nakamura et al. (2016a) find a significant strengthening in December-January for their 150 year ensemble.

The planned investigations into the minimum ensemble size required to detect a robust sign of stratospheric response for different time-period lengths will also be very useful. This is because many modelling studies find stratospheric responses to sea-ice loss that are not necessarily for the winter mean, but for shorter (sub-seasonal) time-periods: for example, in response to past sea-ice loss, Peings and Magnusdottir (2014) and Kim et al. (2014) respectively find a significant weakening of the stratospheric polar vortex from early February to early March (over one month), and early January to early March (over two months). Since the signal-to-noise ratio is likely to be lower for shorter sub-seasonal time-periods, due to relatively higher variability, a larger minimum ensemble size may also be expected.

A final novelty is that this chapter investigates whether stratospheric internal variability can have an influence on model-produced tropospheric AO responses to sea-ice loss, while previous studies (listed three paragraphs above) have only investigated the respective influences of stratospheric or tropospheric internal variability on model-produced stratospheric or tropospheric responses for a given forcing. Since SSWs have a downward effect on the troposphere, a relationship is naturally expected, but it is currently unclear whether the amounts of SSW variability present are large enough to have a sizeable effect on tropospheric AO variability and, therefore, on tropospheric AO responses to sea-ice loss. If this influence is sizeable, then it would suggest that the ensemble size required to detect a robust tropospheric AO response – or at least to make confident statements regarding the magnitude of this response, rather than just the sign – should take into account the ensemble size that would be required to detect a robust response in SSW frequency.

5.2 Aim and research questions

To summarise, in this chapter the control (CTL) and large-magnitude Atlantic sector sea-ice loss (ATL) experiments from Chapter 3 are extended in length to 600 years, and the December SSW nudging (CTL_{ndgSSW}) experiment from Chapter 4 is used, to address the following research questions:

1. For 200 year sub-ensembles of the 600 year-long CTL and ATL experiments, how variable are the responses in SSW frequency for different months and the winter mean?

2. For 200 year sub-ensembles of the 600 year-long CTL and ATL experiments, to what extent does variability in the SSW frequency responses result in variability in the stratospheric and tropospheric AO responses?

3. How does variability in the SSW frequency, stratospheric AO, and tropospheric AO responses compare for different sub-ensemble sizes, and what is the minimum ensemble size required to obtain a statistically significant sign of response in each variable?

The answers to these questions will help to address important gaps in literature by, for example, providing a quantification of the minimum ensemble size required to obtain a robust sign of stratospheric response to sea-ice loss. They will also provide insight into the influence of atmospheric internal variability on Chapter 4's results and, in particular, on Chapter 4's estimated contribution of forced changes in SSWs to forced changes in the tropospheric AO due to ATL sea-ice loss within the model.

5.3 Method

5.3.1 Extended experiments

In this chapter, the original CTL and ATL experiments from Chapter 3 are extended in length to 600 years. These new experiments will be referred to as CTL_{600} and ATL_{600}, and the original shorter experiments will still be referred to as CTL and ATL for consistency with the rest of this thesis.

As mentioned in Chapter 4, these experiments were extended by running IGCM4 on the new local HPC at the British Antarctic Survey. For the ATL_{600} experiment, ATL was restarted on the new HPC from its last restart record and run for an extra 400 years. The CTL_{600} experiment was formed by appending together two almost 300 year-long experiments. The first segment is the 300 year-long version of CTL from Chapter 3, and the second segment is a 299 year-long experiment started from unique initial conditions on the new HPC. As noted in the introduction, and also for

the shorter CTL and ATL experiments in Chapter 3, in CTL_{600} and ATL_{600} there is negligible year-to-year autocorrelation in the winter mean large-scale atmospheric circulation and, therefore, each year can be considered independent. As such, CTL_{600} and ATL_{600} can be considered as 600 year-long ensembles, where each year is one ensemble member.

It was considered that running IGCM4 on the new HPC could potentially result in a different control state from running it on the old HPC, due to computational differences. However, there were no statistically significant differences found between the climatologies of the two almost 300 year-long control experiments on the two different computers, for all of the meteorological fields and diagnostics tested (the zonal mean zonal wind and temperature, the zonal wind and geopotential height at 500 hPa and 10 hPa, the AO loading pattern, the SSW frequency for the winter mean and individual months, and the EP-flux).

5.3.2 Statistical methods

To compare the variability in the response for different sub-ensemble sizes, a bootstrapping method similar to that described in Section 2.3.4.3 of Chapter 2 is used. The main difference here is that an N-year ensemble is randomly resampled into smaller sub-ensembles, rather than into resampled ensembles of size N. In particular, for a given sub-ensemble size, the 600 year-long CTL_{600} and ATL_{600} ensembles are randomly resampled with replacement 10000 times into smaller sub-ensembles of that size. The sub-ensemble means of each of the 10000 CTL_{600} sub-ensembles are then subtracted from the sub-ensemble means of each of the 10000 ATL_{600} sub-ensembles, giving 10000 differences in the sub-ensemble means. These differences are plotted on a histogram to give the bootstrap distribution, which provides a measure of the spread in the response due to internal variability for that sub-ensemble size. This is then repeated for different sub-ensemble sizes, and the bootstrap distributions for each sub-ensemble size are compared.

The bootstrap distributions are used to calculate a bootstrapped 2-sided p-value for the sign of the response for each sub-ensemble size, where the method described in Chapter 2 is used but with 'resampled differences' replaced by 'resampled sub-ensemble differences'. The p-values are then plotted against the sub-ensemble size to estimate

the minimum number of ensemble members (or years) required to obtain a statistically significant sign of response (defined here as $p \leq 0.05$).

For larger sub-ensemble or resample sizes, the above bootstrapping method may underestimate the uncertainty in the response since the resamples are not independent. This could lead to an underestimation of the minimum ensemble size required to obtain a robust response. Therefore, an additional estimate of the minimum ensemble size is calculated using standard errors in the sample means, following the method of Screen et al. (2014) and Deser et al. (2012).

This method uses the Student's t-statistic for the difference between two means (von Storch and Zwiers, 1999):

$$t = \frac{\mid \bar{x} - \bar{y} \mid}{s_p \sqrt{\frac{2}{N}}} \ , \tag{5.1}$$

where $\bar{x}$ and $\bar{y}$ are the ensemble means from ATL_{600} and CTL_{600} respectively, N is the ensemble size, and s_p is the pooled standard deviation:

$$s_p = \sqrt{\frac{\sum_{i=1}^{n}[(x_i - \bar{x})^2 + (y_i - \bar{y})^2]}{2N - 2}} \ , \tag{5.2}$$

where x_i and y_i are single ensemble members from ATL_{600} and CTL_{600}. The t-statistic gives a measure of how large the difference in the means is compared to the pooled standard error in the means and, therefore, gives a measure of the signal-to-noise ratio.

The difference in the means is considered statistically significant here when $t \geq t_c$, where t_c is the cut-off value of the Student's t-distribution for a 2-sided p-value of 0.05 and $2N - 2$ degrees of freedom. Hence, the minimum ensemble size required to obtain a statistically significant sign of response, N_{min}, is calculated by re-arranging equation 5.1, and replacing t with t_c and N with N_{min}:

$$N_{min} = 2t_c^2 \left(\frac{s_p}{\bar{x} - \bar{y}} \right)^2 \ . \tag{5.3}$$

It is assumed that s_p does not depend on the ensemble size; instead, it is calculated using all ensemble members in ATL_{600} and CTL_{600}. Screen et al. (2014) highlight that this is not true for small N_{min}, but that in this case $s_p \ll \mid \bar{x} - \bar{y} \mid$ and, as such, N_{min} is relatively unaffected by errors in s_p.

5.4 Results

5.4.1 SSW frequency response for ATL versus ATL_{600}

This section aims to address research question 1 specifically for the 200 year-long CTL and ATL experiments: 'For 200 year sub-ensembles of the 600 year-long CTL and ATL experiments, how variable are the responses in SSW frequency for different months and the winter mean?'. A particular focus will be placed on December given that an increase in December SSW frequency was found to be important in Chapter 4.

Figure 5.1 shows the climatological mean SSW frequency for each winter month in CTL and ATL, compared to CTL_{600} and ATL_{600}. This shows that there is an increase in the mean December SSW frequency in ATL_{600}, but this increase is smaller than in ATL and is not statistically significant. It appears that internal variability in SSWs led to a lower mean frequency in CTL than in CTL_{600}, and a higher mean frequency in ATL than in ATL_{600}, resulting in a larger difference in the means between ATL and CTL. Indeed, this is not just unique to December: larger differences in the means between ATL and CTL than between ATL_{600} and CTL_{600} are also apparent in other months including February and March, and in February the differences are in opposite directions for the 200 and 600 year cases.

In contrast to ATL and CTL, the differences in the means between ATL_{600} and CTL_{600} for each month are all in the same direction and of a similar magnitude, where there is a small increase in mean frequency in all months between December and March in ATL_{600}. These increases are not statistically significant in any individual month, but they are likely to be somewhat robust because the difference in the winter mean is statistically significant unlike for ATL and CTL (there is an increase in frequency of 0.084/year (p=0.03) in ATL_{600}, compared to an increase in frequency of 0.085/year (p=0.19) in ATL, where the p-values are calculated using a bootstrap test for the difference between two means as detailed in Section 2.3.4.3 of Chapter 2).

5.4.2 Variability in the SSW frequency and AO responses

In the previous section, it was shown that internal variability of SSWs led to a December SSW frequency response in ATL that overestimates the model's forced changes in December SSWs due to ATL sea-ice loss. Here, the nature of internal variability in the

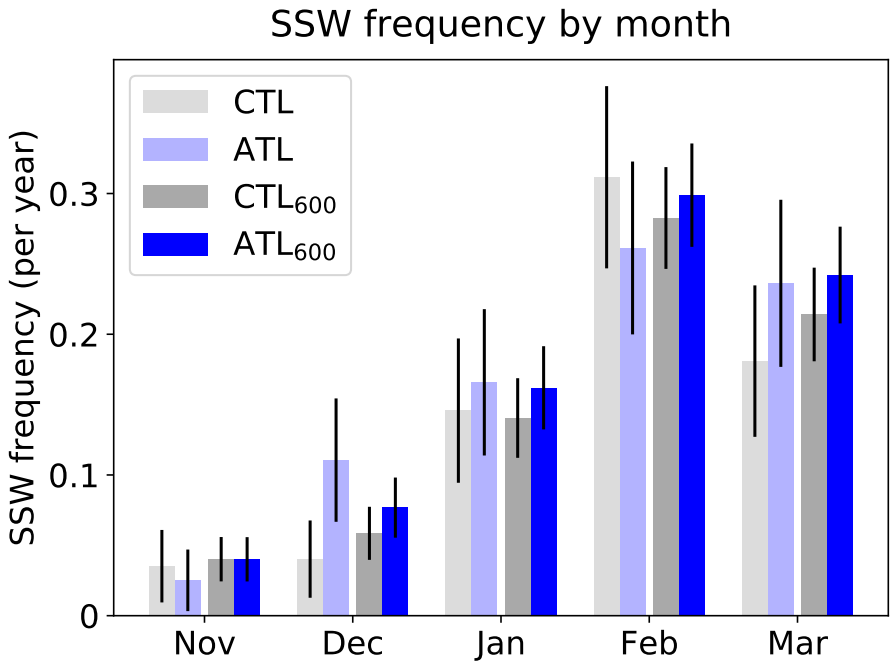

Fig. 5.1 Climatological mean SSW frequency by month in CTL and ATL (respectively light grey and light blue), compared to CTL_{600} and ATL_{600} (respectively dark grey and dark blue). CTL_{600} and ATL_{600} are the extended 600 year-long versions of CTL and ATL, which are 200 years-long. The black bars show the 95% confidence intervals for the mean, calculated using a t-distribution (see Section 2.3.4.5 of Chapter 2).

SSW frequency is broadly investigated by examining further 200 year sub-ensembles of CTL_{600} and ATL_{600} (i.e. not just CTL and ATL). The extent to which internal variability of SSWs has an influence on the stratospheric and tropospheric AO responses for these sub-ensembles is also determined. This investigation will firstly focus on December as a case-study month, but will then be expanded out to other months and the winter mean.

In short, this section aims to broadly address research questions 1 and 2: '1. For 200 year sub-ensembles of the 600 year-long CTL and ATL experiments, how variable are the responses in SSW frequency for different months and the winter mean?' and '2. For 200 year sub-ensembles of the 600 year-long CTL and ATL experiments, to what extent does variability in the SSW frequency responses result in variability in the stratospheric and tropospheric AO responses?'. Addressing these questions will aid understanding of differences in the AO responses between ATL and ATL_{600}, where these results will be presented in the next section (Section 5.4.3).

5.4.2.1 December case

To understand internal variability in December SSWs in more detail, the left-hand side of Figure 5.2 shows the December SSW frequency for each ensemble member or year of CTL_{600}, ATL_{600}, and ATL_{600}-CTL_{600}. This shows that there is a clustering of SSWs into certain decadal time-periods: for example, there are no SSWs in CTL_{600} for most of the first 100 years, but then a period of many SSWs between around 350 years and 450 years. This clustering is likely entirely chaotically generated, since there is no autocorrelation in the December (or winter mean) SSW frequency for any yearly lag in either of the two 300 year-long segments that form the CTL_{600} experiment, or in ATL_{600}. Moreover, randomly generated 600 year-long datasets of December SSW frequency also produce a similar clustering of SSWs (see Figure 5.3 [left] for an example and a description of how these datasets are generated).

The effect of this clustering or internal variability in SSWs on the December SSW frequency responses for different 200 year sub-ensembles is visualised on the right-hand side of Figure 5.2, by applying a 200 year running mean to the left-hand plots of this figure. This shows that internal variability has a large influence on the responses for 200 year sub-ensembles, and can even lead to opposite signs of responses (between around -0.04/year and 0.08/year). The 200 year ATL ensemble appears to be an extreme case of a positive response (an increase of around 0.075/year centred on year 100), due to more clustering of SSWs in the first 200 years of ATL_{600} and a lack of SSW clustering in the first 200 years of CTL_{600}. However, the running mean method used in this figure does only give a small subset of possible 200 year sub-ensembles. When CTL_{600} and ATL_{600} are randomly resampled into 200 year sub-ensembles many thousands of times giving a bootstrap distribution as described in Section 5.3.2, there is an even larger range of responses found from between -0.06/year to 0.1/year (see left-hand side of Figure 5.4a below).

It is now examined whether variability in the December SSW frequency response is linked to variability in the December stratospheric and tropospheric AO responses. The left-hand side of Figure 5.4 shows the aforementioned bootstrap distribution of December SSW frequency responses for randomly resampled 200 year sub-ensembles of CTL_{600} and ATL_{600}, and corresponding bootstrap distributions of the December AO responses at 10 hPa and 500 hPa. This shows that in addition to the aforementioned large spread in SSW frequency responses, there is a large spread in both the stratospheric and tropospheric AO responses (between around -0.4 and 0.15). Since a difference

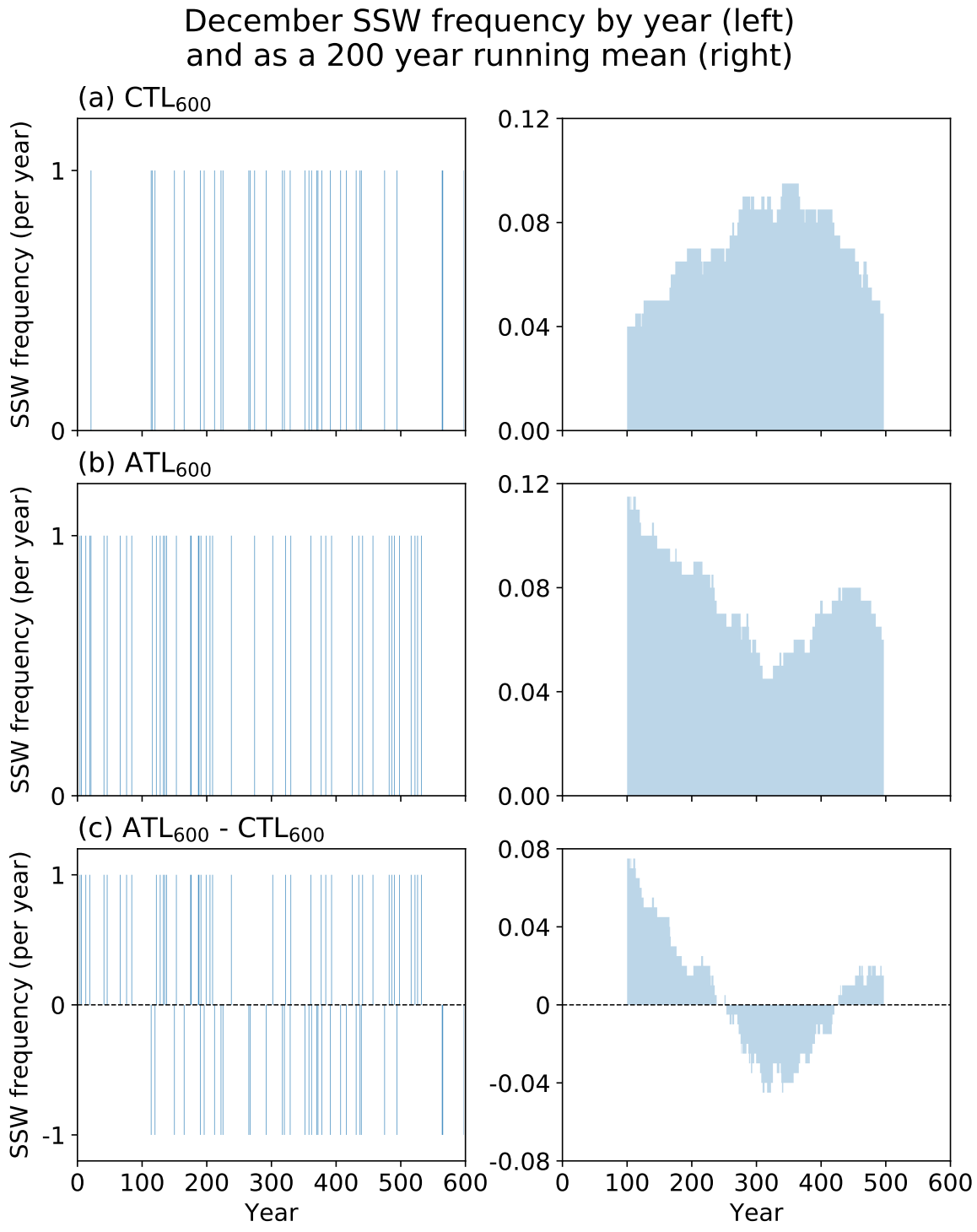

Fig. 5.2 December SSW frequency in each year [left] and as a 200 year running mean [right] for (a) CTL_{600}, (b) ATL_{600}, and (c) ATL_{600}-CTL_{600}. A comparison with Figure 5.3 suggests that the variability in SSW frequency present in these plots is chaotically generated.

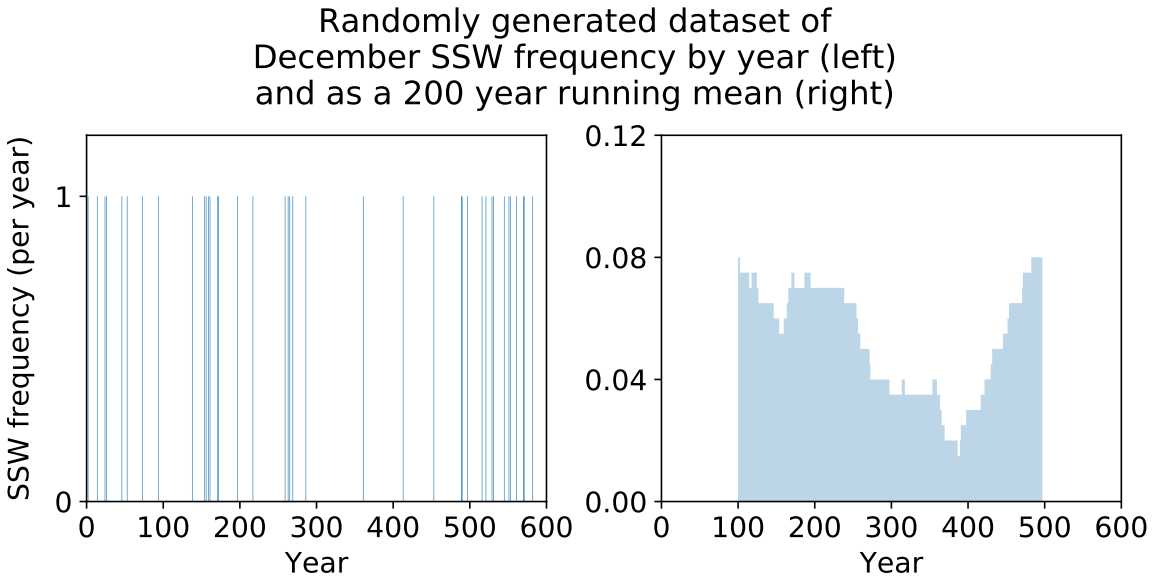

Fig. 5.3 Randomly generated 600 year-long dataset of December SSW frequency by year [left] and as a 200 year running mean [right]. This dataset is produced by randomly picking either 0 or 1 (an SSW not occurring or occuring) for each year, with these values assigned a probability of occurrence based on CTL_{600}.

in SSW frequency is expected to be anti-correlated with a difference in AO index, it might be expected that the mean and spread of these distributions are linked. Indeed, there is a mean positive difference in SSW frequency with a large spread from negative to positive differences, and a mean negative difference in the 10 hPa and 500 hPa AO with a large spread from positive to negative differences.

To examine whether the distributions are indeed linked, the right-hand side of Figure 5.4 shows the 200 year running mean of the same fields for ATL_{600}-CTL_{600}. This shows similarities between the shapes of the curves, since there is a trend towards more negative SSW frequency responses from around year 100 to 300 and towards more positive frequency responses thereafter, corresponding respectively with trends towards more positive then negative AO index responses. The 10 hPa AO responses are persistently negative – unlike the SSW frequency responses which switch sign – likely because of the additional influence of changes in SSW structure in ATL_{600} (where these changes are qualitatively the same as in ATL but weaker; see Figure 5.5). This influence will likely also involve SSWs in other months besides December. Similarly, the 500 hPa AO responses switch sign to a lesser extent than the SSW frequency responses, which may be associated with the downward influence of changes in SSW structure on the troposphere, and may also be because of the tropospheric pathway's

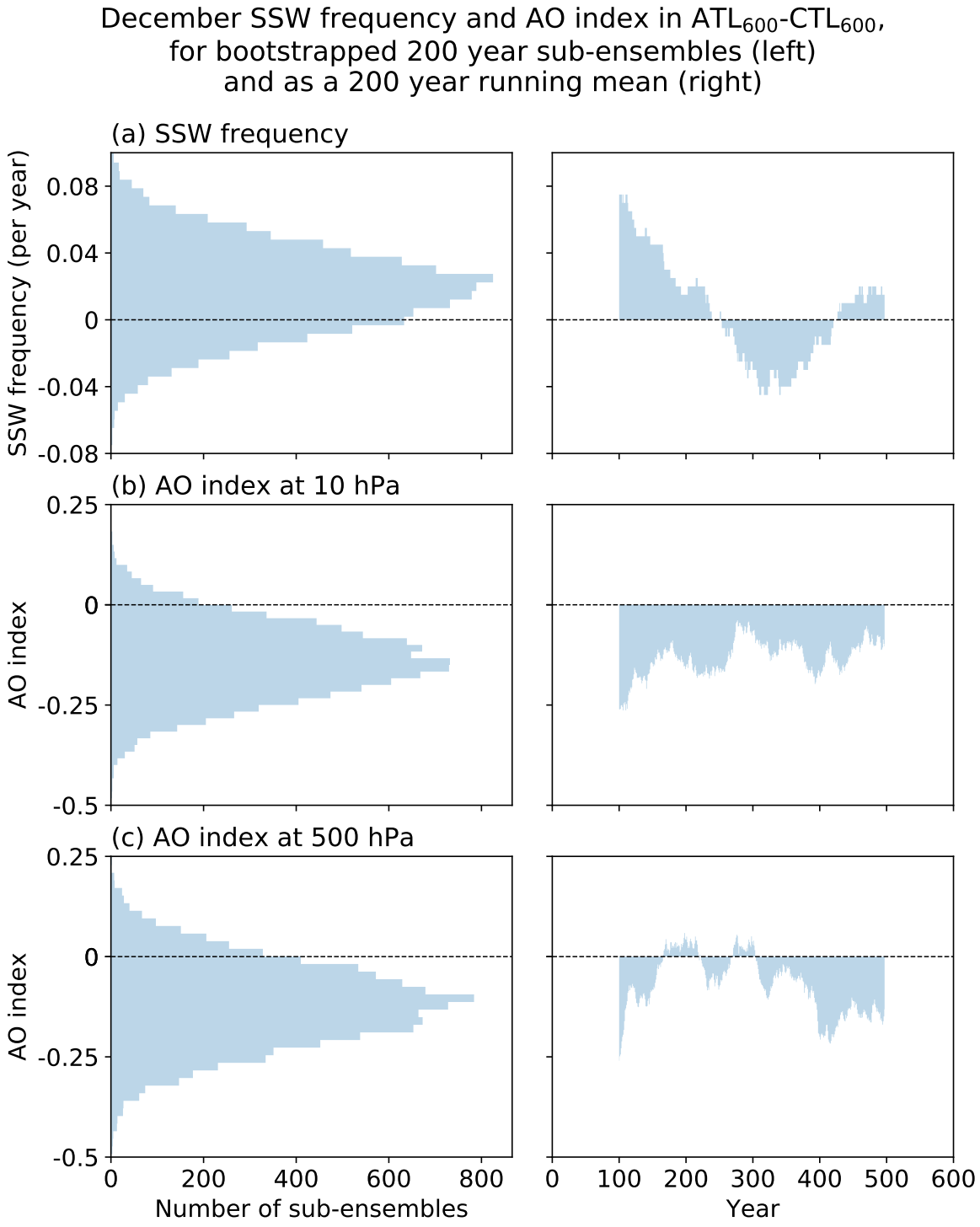

Fig. 5.4 December SSW frequency and December AO index in ATL_{600}-CTL_{600}, for 10000 randomly resampled 200 year sub-ensembles [left] and as a 200 year running mean [right]. (a) SSW frequency, (b) 10 hPa AO index, and (c) 500 hPa AO index.

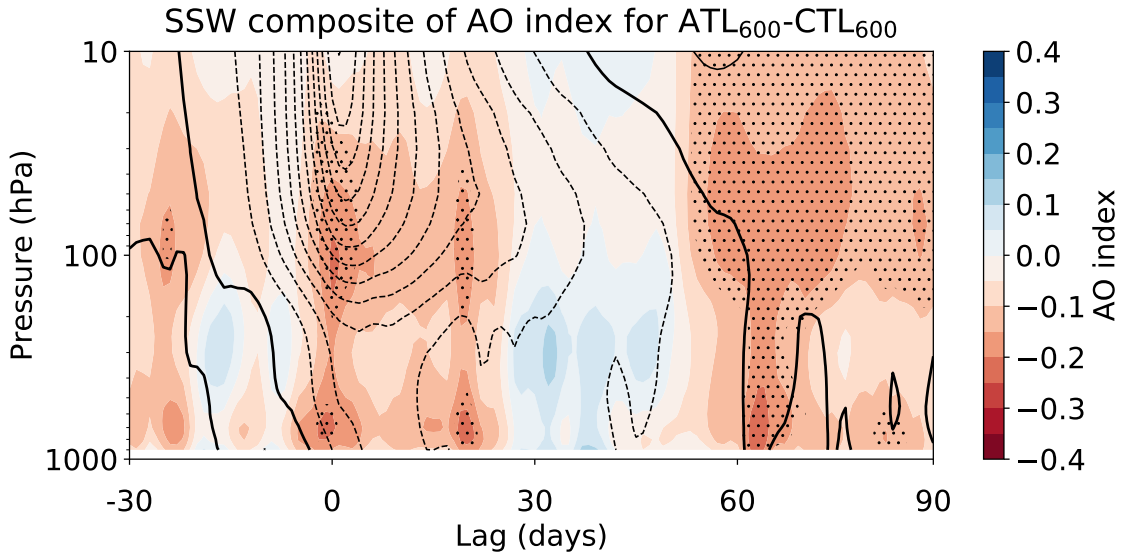

Fig. 5.5 Time-height evolution of the daily AO index for a composite SSW in CTL_{600} (contours; interval of 0.2), and for a composite SSW in ATL_{600} minus a composite SSW in CTL_{600} (shading). The composites are calculated as in Chapter 4, with N = 441 SSWs in CTL_{600} and N = 491 in ATL_{600}. Stippling indicates statistical significance at a 95% confidence level for the daily mean difference, calculated using a t-test.

contribution to a negative tropospheric AO response (as shown for ATL in Chapter 4). These additional effects on the stratospheric and tropospheric AO responses also likely explain why the AO bootstrap distributions are shifted away from zero more than the SSW frequency bootstrap distribution would imply.

A link between variability in the SSW frequency and AO responses can be examined more quantitatively using the CTL_{ndgSSW} experiment from Chapter 4. Recall Figure 4.9 in Section 4.3.4 of Chapter 4, which showed the evolution of the AO index at 10 hPa and 500 hPa for CTL_{ndgSSW}-CTL_{ndgCS}. The mean value of the AO response for the month following the SSW central date is 2.4 at 10 hPa and 0.94 at 500 hPa. These values can be used to give a rough estimate of the influence of variability in the December SSW frequency response on variability in the December AO response. For example, in the right-hand plots of Figure 5.4 the SSW frequency responses vary by approximately 0.12/year (from -0.04/year to 0.08/year), which when multiplied by 2.4 and 0.94 gives an associated variability in the AO responses of 0.29 at 10 hPa and 0.11 at 500 hPa. This accounts for all of the variability in the AO responses at 10 hPa (where the total range is 0.25) and around two-fifths at 500 hPa (where the total range is also 0.25).

However, while an effort was made to choose a specific reference SSW for CTL_{ndgSSW} (see Section 4.3.4 of Chapter 4 for details), it is still possible that the above estimate could be specific to this SSW. To give an idea of the likely range of estimates, the same calculation is performed using the SSW composite of the AO index for CTL_{600} in Figure 5.5. The value of the AO index for the month following the CTL_{600} SSW central date is 1.1 at 10 hPa and 0.4 at 500 hPa. Multiplying these values by the range in SSW frequency responses of approximately 0.12/year gives an explained range in AO responses of 0.13 at 10 hPa (around three-fifths of the total) and 0.05 at 500 hPa (around one-fifth of the total).

In summary, for 200 year sub-ensembles of CTL_{600} and ATL_{600}, variability in the December SSW frequency responses likely accounts for between one-fifth and two-fifths of the variability in the December tropospheric AO responses, and for between three-fifths and all of the variability in the December stratospheric AO responses. In other words, there is a measurable influence. The remaining variability in the December stratospheric AO responses to be explained could be due to other aspects of stratospheric variability such as that associated with minor SSWs, and also to the influence of SSW frequency variability in other months besides December. As for the remaining variability in the December tropospheric AO responses to be explained, this could be due in part to the downward influence of these additional sources of stratospheric variability on the troposphere, and a large part is also likely due to variability internally generated within the troposphere itself.

5.4.2.2 Other months and the winter mean

In winter months other than December, there is a similar clustering of SSWs into certain decadal time-periods. This is also found to be associated with chaotically generated internal variability in SSWs, which has a large influence on the SSW frequency responses for thousands of randomly resampled 200 year sub-ensembles of ATL_{600}-CTL_{600}. The magnitude of variability in these sub-ensemble responses for each month approximately follows the magnitude of the relevant climatological mean monthly SSW frequency and associated confidence intervals (see Figure 5.1), with the smallest variability in November, increasing to the largest in February, and slightly decreasing into March. For February, the range of responses is 0.25/year (between -0.1/year and 0.15/year). There is also large variability in the 10 hPa and 500 hPa AO randomly resampled 200 year sub-ensemble responses for all months, where the differences in variability between

months are similar to that for the SSW frequency responses. The largest range of AO responses, which also occurs in February, is around 0.75 (-0.5 to 0.25) for the 10 hPa AO and 0.7 (-0.5 to 0.2) for the 500 hPa AO.

As for December, in other winter months the bootstrap distributions of the SSW frequency responses appear to be anti-correlated with the bootstrap distributions of the 10 hPa and 500 hPa AO responses. However, while there is some evidence of an anti-correlation between the 200 year running means of SSW frequency responses and 10 hPa AO responses in every month, there is only some evidence of an anti-correlation between SSW frequency responses and 500 hPa AO responses in the early winter months (November to January) and not in the late winter months (January to March) – see Figure 5.6. It is suggested that this is because in late winter, there is the additional lagged influence of variability in SSWs in the months prior, which is opposite in influence here to the variability of SSWs in late winter (in other words, there are opposite signs of variability in early and late winter, which act to compensate each other). Therefore, while there appears to be an absence of correlation between the SSW frequency responses and 500 hPa AO responses in late winter, it is still possible that they are anti-correlated. Using the CTL_{600} SSW AO composite to more objectively estimate the contribution of variability in the SSW responses to variability in the AO responses, as done earlier for December, reveals similar sizeable contributions for each month. For example, in February it is found that variability in the SSW frequency responses can account for around one-quarter of the variability in the tropospheric AO responses.

The winter mean will now be discussed, which is – in this chapter – defined as November to March, since SSWs occur in these months. Figure 5.7a [left] shows that for the winter mean, there is also an apparently large range in SSW frequency responses of around 0.4/year (-0.1/year to 0.3/year) for thousands of randomly resampled 200 year sub-ensembles of ATL_{600}-CTL_{600}. This is a larger range than for any individual month, likely because the winter mean response is much larger (since it is the cumulative sum of the frequency responses for all winter months). However, the signal-to-noise ratio for the winter mean is actually around double of that for individual months (where the ratio is 0.2 (0.08/0.4) for the winter mean, and around 0.1 for both December (0.02/0.16) and February (0.02/0.25) for example; see Figure 5.1, Figures 5.4a and 5.7a, and the ranges of variability quoted above for the winter mean, December, and February). The bootstrap distributions in Figures 5.7b [left] and 5.7c [left] also show

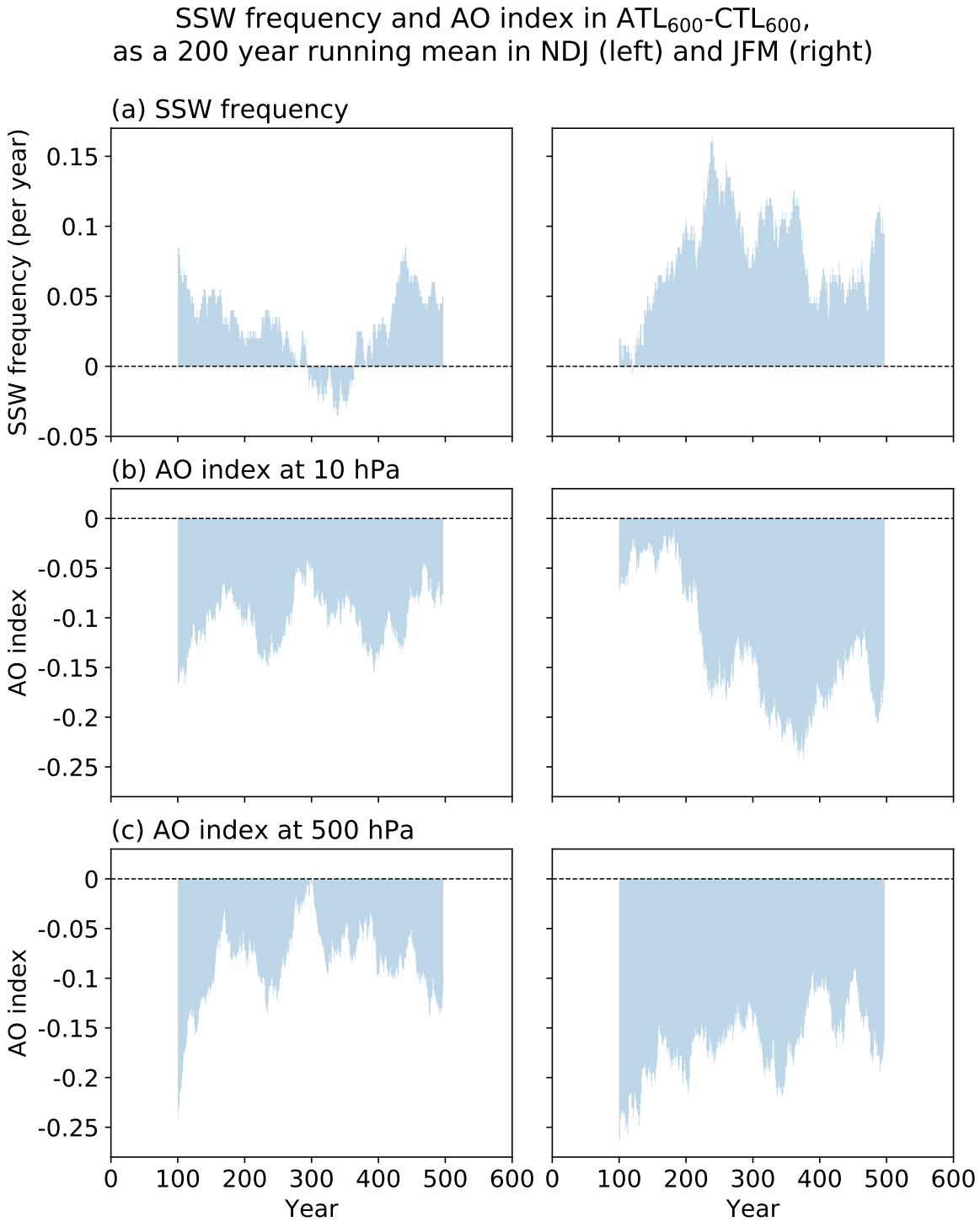

Fig. 5.6 SSW frequency and AO index in ATL_{600}-CTL_{600}, as a 200 year running mean in [left] November-January and [right] January-March. (a) SSW frequency, (b) 10 hPa AO index, and (c) 500 hPa AO index

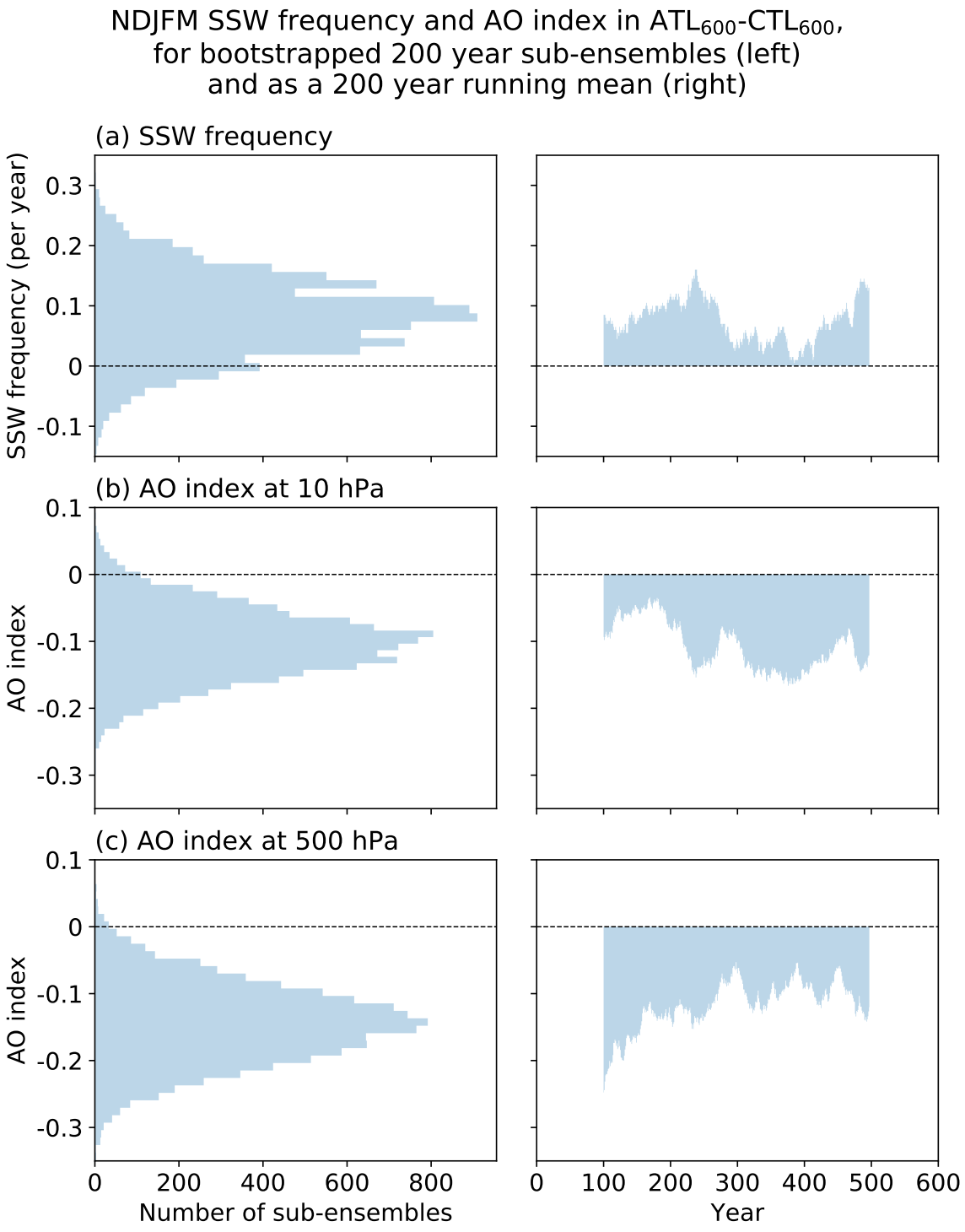

Fig. 5.7 November-March SSW frequency and November-March AO index in ATL_{600}-CTL_{600}, for 10000 randomly resampled 200 year sub-ensembles [left] and as a 200 year running mean [right]. (a) SSW frequency, (b) 10 hPa AO index, and (c) 500 hPa AO index.

apparently large variability in the 10 hPa AO responses – with a range of 0.4 (-0.3 to 0.1) – and in the 500 hPa AO responses – with a range of 0.35 (-0.3 to 0.05). This variability in the AO responses is however around half of that for individual months, as may be expected for the mean of a longer time-period.

As for individual winter months, there is an apparent anti-correlation between the bootstrap distribution of the winter mean SSW frequency responses, and the bootstrap distributions of the winter mean 10 hPa and 500 hPa AO responses. However, while there is – to some extent – evidence of an anticorrelation in the 200 year running means of the SSW frequency and 10 hPa AO responses, there is little evidence of any link between variability in the SSW frequency and 500 hPa AO responses (Figure 5.7 [right]). This may be due to the compensating effects between early and late winter described above, which could lead to an apparent absence of correlation when there is in fact an anti-correlation. However, it is quite likely that the relationship for the winter mean may actually be weaker, since while the influence of an SSW may be large for the month or two following the SSW, this does not determine how the AO behaves for the winter as a whole; this would be particularly true for SSWs occurring in late-winter, since they will only contribute to a small portion of the winter mean AO response. As suggested for individual winter months, it is likely that a large part of variability in the winter mean tropospheric AO responses is internally generated by the troposphere itself.

5.4.3 AO response for ATL versus ATL_{600}

The previous section showed that internal variability has a sizeable influence on responses in the SSW frequency, and the stratospheric and tropospheric AO, for thousands of randomly resampled 200 year sub-ensembles of ATL_{600}-CTL_{600}. Furthermore, for each winter month, variability in the monthly SSW frequency responses was found to contribute to variability in the monthly stratospheric and tropospheric AO responses.

Here, the extent to which internal variability in SSWs specifically explains differences in the AO responses between ATL and ATL_{600} is examined. In doing so, this section aims to address research question 2 specifically for the 200 year-long CTL and ATL experiments: 'For 200 year sub-ensembles of the 600 year-long CTL and ATL experiments, to what extent does variability in the SSW frequency responses result in variability in the stratospheric and tropospheric AO responses?'. As in previous

sections, a particular focus will be placed on the role played by internal variability in December SSWs given their importance found for the tropospheric AO response in ATL in Chapter 4.

Figure 5.8a shows the 10 hPa and 500 hPa AO index evolution for ATL_{600}-CTL_{600} compared to ATL-CTL, and the contribution of the relevant December SSW frequency response to each AO response (calculated by scaling CTL_{ndgSSW}-CTL_{ndgCS} by the frequency response, as in Chapter 4). Figure 5.8b shows the difference in the AO responses between ATL-CTL and ATL_{600}-CTL_{600}, and the difference in the contribution of December SSWs to these AO responses. The response in ATL_{600} gives a more accurate estimate of the model's forced changes due to ATL sea-ice loss, and any difference between it and the response in ATL is due to internal variability. Thus, the differences in Figure 5.8b show the contribution of internal variability to the response in ATL.

In the stratosphere, the AO response in ATL_{600} is the same for the winter mean as in ATL (around -0.1), but in terms of its evolution it is of a similar magnitude throughout winter unlike in ATL. These two aspects can largely be explained by the SSW responses in each experiment, since it is found that the stratospheric AO response in ATL_{600} can – as in ATL – be mostly interpreted in terms of changes in SSW frequency and structure, where each contributes to around half of the response (based on artificially constructed datasets as in Chapter 4; not shown). Indeed, the similar winter mean negative AO responses are consistent with the similar increases in winter mean SSW frequency for both experiments (around 0.085/year), and the differences in the evolution of the AO responses are consistent with the fact that there are similarly sized small increases in SSW frequency across the months of December to March in ATL_{600} but not in ATL. In December-January, the 10 hPa AO response is 100% more negative in ATL than in ATL_{600}, which can be largely explained by the difference in the December SSW frequency responses (and therefore by internal variability in December SSWs). It is also possible that the more positive AO in ATL in late-February and March reflects the difference in the February SSW frequency responses between ATL and ATL_{600} (a reduction in frequency compared to an increase).

In the troposphere, the AO response in ATL_{600} is similar in evolution to ATL but weaker in magnitude throughout winter, where the winter mean AO response in ATL is 67% stronger (-0.25 compared to -0.15). Since the winter mean stratospheric AO responses are of the same magnitude, this implies that the difference in the winter mean tropospheric AO responses is likely largely due to winter mean AO variability internally

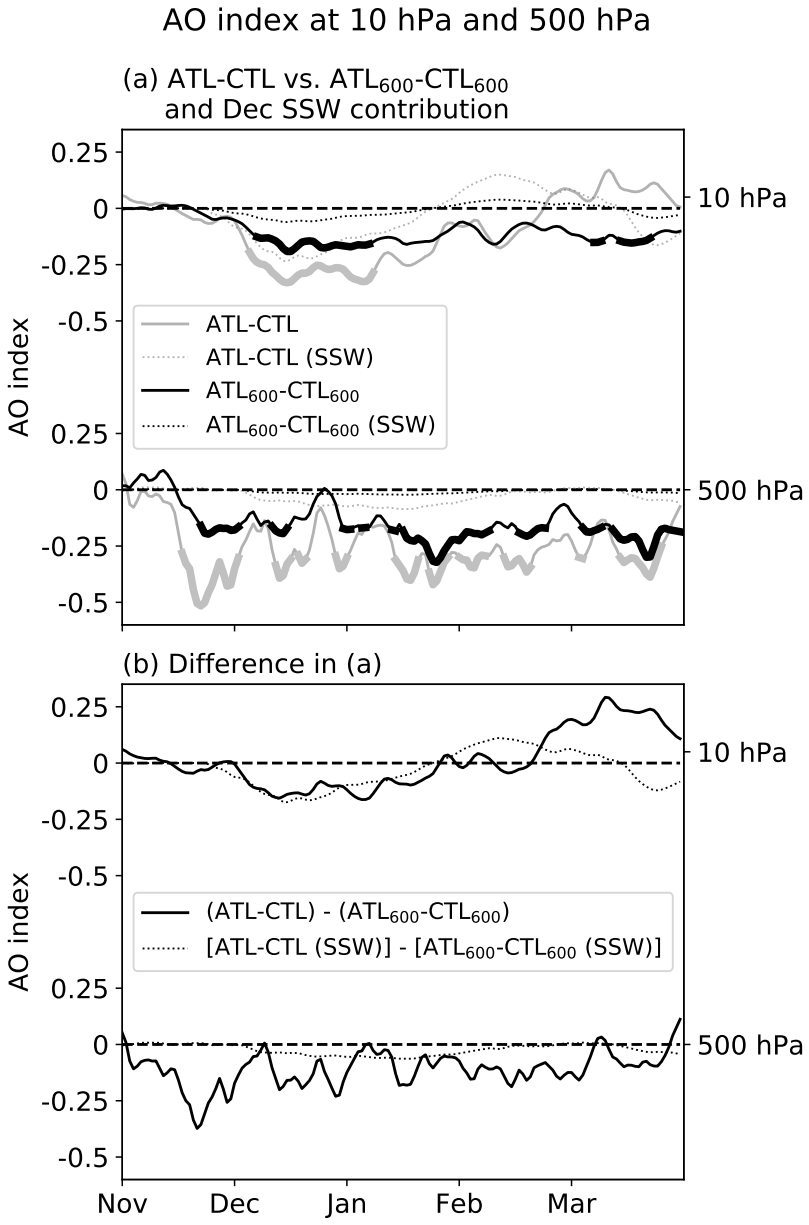

Fig. 5.8 Daily evolution of the AO index at 10 hPa and 500 hPa over winter for (a) ATL-CTL (solid grey) versus ATL_{600}-CTL_{600} (solid black), and the contributions of the relevant December SSW frequency response to each (dotted). The latter contributions are quantified by scaling CTL_{ndgSSW}-CTL_{ndgCS} by the December SSW frequency response for either ATL-CTL or ATL_{600}-CTL_{600} (as in Figure 4.19 of Chapter 4). (b) Difference in the AO responses between [ATL-CTL] and [ATL_{600}-CTL_{600}] (solid), and the contribution of differences in the December SSW frequency responses to this (dotted). Thick lines in (a) indicate statistical significance at a 95% confidence level for the daily mean response, calculated using a t-test.

generated by the troposphere (consistent with the previous section's results). For monthly as opposed to winter mean time-periods, however, internal variability of SSWs does have a large influence on the tropospheric AO response in ATL (also consistent with the previous section's results). Indeed, the difference in the December SSW frequency responses between ATL and ATL_{600} (due to internal variability) explains around 50% of the difference in the tropospheric AO responses between ATL and ATL_{600} in December-January. As such, internal variability of SSWs contributed to a mid-winter tropospheric AO response in ATL that overestimates the model's forced change due to ATL sea-ice loss.

On a side – but still important – note, other aspects of the response in ATL_{600} besides the AO response are qualitatively the same as in ATL. For example, there is still an increase in vertical EP-flux in early winter associated with constructive linear interference of anomalous and climatological Rossby waves, but the magnitude of this increase is around half of that in ATL. This is consistent with the weaker early-winter stratospheric AO response in ATL_{600} compared to ATL. In terms of the direct circulation response in ATL_{600} compared to ATL, this is identical in pattern and magnitude. This agrees with Deser et al. (2012) and Screen et al. (2014), who find that the local response to sea-ice loss is more robust and less affected by internal variability than the more remote indirect or AO response. This is likely because the local direct response is thermally driven by surface heat flux anomalies, while the indirect response is more dynamically driven and therefore more difficult to distinguish from the dynamically driven internal variability of the atmospheric circulation.

5.4.4 Quantification of the signal-to-noise ratio

The previous sections have shown that internal variability has a sizeable influence on the responses in SSW frequency, and the stratospheric and tropospheric AO, specifically for ATL-CTL and more broadly for randomly resampled 200 year sub-ensembles of ATL_{600}-CTL_{600}. In this section, the variability in the responses for different sizes of randomly resampled sub-ensembles will be compared, importantly leading to a quantification of the minimum ensemble sizes required to separate the signs of the model's forced tropospheric and stratospheric changes due to sea-ice loss from internal variability (which can be considered as a measure of the signal-to-noise ratio). This is with the aim of addressing research question 3: 'How does variability in the SSW frequency, stratospheric AO, and tropospheric AO responses compare for different

sub-ensemble sizes, and what is the minimum ensemble size required to obtain a statistically significant sign of response in each variable?'.

The focus is firstly placed on the winter mean. The left-hand side of Figure 5.9 shows bootstrap distributions of the November-March SSW frequency responses, and November-March 10 hPa and 500 hPa AO responses, for three sizes of randomly resampled sub-ensembles of CTL_{600} and ATL_{600} (N = 50, N = 200, and N $\sim$ 600 years/members). The grey shading on the right-hand side of this figure shows bootstrapped p-values calculated from the bootstrap distributions for a range of N from 10 years to $\sim$ 600 years. $p = 0.05$ is indicated to highlight the signal-to-noise ratio, which is defined here as the minimum sub-ensemble size for which $p \leq 0.05$.

As discussed in Section 5.3.2, this bootstrap method may underestimate the uncertainty in the response for larger resample sizes and, therefore, the minimum ensemble size. Hence, the black line on the right-hand side of Figure 5.9 shows an additional estimate of the variation in p-values with N, which is calculated using a method based on standard errors in the sample means. Using equation 5.1 in Section 5.3.2, the t-statistic is calculated for each N and the corresponding p-value is found for 2N-2 degrees of freedom; $\bar{x}$, $\bar{y}$, and s_p are calculated using all ensemble members in ATL_{600} and CTL_{600}. Note that this additional estimate is actually very similar to the bootstrapped estimate.

Regarding the SSW frequency, this figure shows that for smaller sub-ensemble sizes (N = 50 years and N = 200 years to a lesser extent), internal variability of SSWs has an influence on both the sign and magnitude of the response. Only for N $\sim$ 500 years does the response become statistically different from zero. This can be seen from the bootstrap distribution for N $\sim$ 600 years, where only a very small number of sub-ensemble responses are less than zero. However, while the sign of the response can be detected for this value of N, the magnitude of the response is still very variable.

Moving onto the 10 hPa AO, it can be seen that internal variability influences both the sign and magnitude of the response for a sub-ensemble size of N = 50 years, but that the sign of the response can be statistically detected when N $\sim$ 210 years. For N $\sim$ 600 years, the bootstrap distribution of responses becomes entirely shifted away from zero and, therefore, we can begin to identify the magnitude of the response. Similar statements can be made for the 500 hPa AO, but the sign of the response becomes statistically detectable even earlier (N $\sim$ 130 years) and the bootstrap distribution of responses is further shifted away from zero by N $\sim$ 600 years, suggesting that we

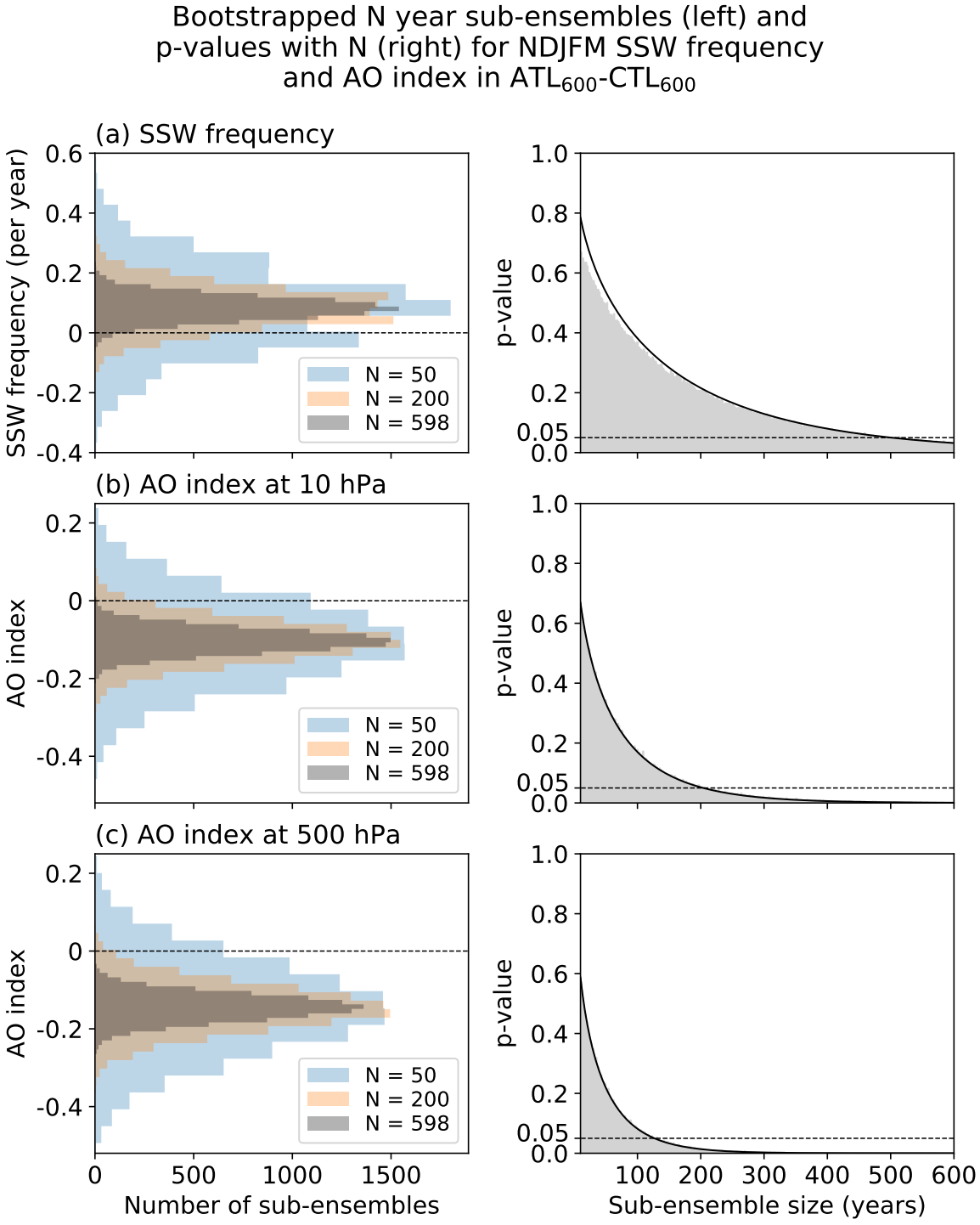

Fig. 5.9 [Left] November-March SSW frequency and November-March AO index for 10000 randomly resampled N year sub-ensembles of ATL_{600}-CTL_{600}. [Right] p-values calculated using the bootstrap distributions on the left (grey shading), and using standard errors in the means (black line), for different N from 10 years to $\sim$ 600 years. $p = 0.05$ is shown by the dashed line to indicate the minimum N required for a statistically significant sign of response. (a) SSW frequency, (b) 10 hPa AO index, and (c) 500 hPa AO index.

can also begin to identify the magnitude of the response earlier. These results agree well with the difference in winter mean tropospheric AO responses between ATL and ATL_{600}, in that these 200 and 600 year-long ensembles were both able to statistically detect the sign of the response, but suggested very different magnitudes of response.

Table 5.1 summarises the minimum number of ensemble members or years required to detect a statistically significant sign of response in each variable for all time-periods in winter, from monthly to two-monthly and so on. Estimates are given using both the bootstrapping method and standard error in the means method; however, note that the estimates are in fact very similar. The following results will use the upper estimate of the two, rounded to the nearest 10 years. The table shows that generally the minimum ensemble size becomes larger for shorter time-periods, which can be attributed to a smaller signal-to-noise ratio for shorter time-periods (see Section 5.4.2.2). For the 500 hPa AO, around 130 years are required for the winter mean, increasing to an average of 150 for four-monthly periods, 180 for three-monthly, 190 for two-monthly, and 330 for individual months (only including time-periods where the minimum number of ensemble members could be quantified). For the 10 hPa AO, around 210 years are required for the winter mean, 250 for four-monthly periods, 290 for three-monthly, 450 for two-monthly, and 440 for individual months. The sign of the SSW frequency response is only statistically significant for longer time-periods including the winter as a whole (around 500 years required) and December-March (450 years).

With regards to differences in the signal-to-noise ratios between different months, in November a statistically significant response cannot be detected in any variable even with $\sim$ 600 ensemble members/years, because there is little to no response (or signal) in the SSW frequency or stratospheric and tropospheric AO. In terms of other months, the signal-to-noise ratio for the SSW frequency tends to be the largest in December, decreasing to a minimum in February, and increasing into March to around the same level as in January (based on the p-values for N $\sim$ 600 years). Since the response in SSW frequency is similar in magnitude in each of these months, this must be due to the earlier discussed differences in SSW variability between these months (see Section 5.4.2.2). It would thus be expected that for ensemble sizes larger than 600 years, a response in SSW frequency in December (February) would be the first (last) to become statistically significant. For both the 10 hPa and 500 hPa AO, the signal-to-noise ratio largely follows a similar pattern across the winter months as for the SSW frequency, likely due to differences in AO variability between these months (again

Table 5.1 Minimum number of ensemble members or years required to detect a statistically significant sign of response in the SSW frequency, and 10 hPa and 500 hPa AO index, for different time-period lengths in ATL_{600}-CTL_{600}. Left-hand values are estimated using a bootstrapping method; this involves calculating the smallest sub-ensemble size for which $p \leq 0.05$ for the next five larger ensemble sizes (with an increment of 1 year), where the p-values for each ensemble size are calculated using a bootstrap distribution of 10000 randomly resampled sub-ensembles of ATL_{600}-CTL_{600}. Right-hand values are estimated based on standard errors in the means (equation 5.3). The red text shows variables for which $p > 0.05$ when all ensemble members in CTL_{600} and ATL_{600} are used, where the associated p-value is given in brackets.

Variable	Minimum number of ensemble members or years required for p ≤ 0.05				
	NDJFM				
SSW frequency	483 / 501				
10 hPa AO	207 / 204				
500 hPa AO	124 / 127				
	NDJF		DJFM		
SSW frequency	(p = 0.11 / 0.11)		448 / 454		
10 hPa AO	302 / 295		191 / 191		
500 hPa AO	177 / 176		125 / 121		
	NDJ		DJF		JFM
SSW frequency	(p = 0.12 / 0.14)		(p = 0.08 / 0.09)		(p = 0.07 / 0.07)
10 hPa AO	315 / 310		273 / 271		287 / 287
500 hPa AO	246 / 240		168 / 165		128 / 128
	ND	DJ		JF	FM
SSW frequency	(p = 0.31 / 0.31)	(p = 0.09 / 0.09)		(p = 0.23 / 0.23)	(p = 0.18 / 0.18)
10 hPa AO	547 / 538	266 / 263		492 / 492	482 / 473
500 hPa AO	(p = 0.06 / 0.07)	213 / 210		182 / 179	175 / 173
	N	D	J	F	M
SSW frequency	(p = 0.95 / 1.0)	(p = 0.19 / 0.21)	(p = 0.27 / 0.30)	(p = 0.53 / 0.57)	(p = 0.24 / 0.24)
10 hPa AO	(p = 0.82 / 0.80)	332 / 331	480 / 475	(p = 0.18 / 0.17)	497 / 492
500 hPa AO	(p = 0.43 / 0.42)	563 / 556	220 / 214	297 / 298	219 / 216

see Section 5.4.2.2). For the 500 hPa AO, however, this is only true for January-March; in December the signal-to-noise ratio is very low, likely because the response is much smaller in this month compared to January-March.

In terms of a link between the signal-to-noise ratios for the SSW frequency response, and 10 hPa and 500 hPa AO responses, it does seem that when N is larger for the SSW frequency it is also larger for the 10 hPa and 500 hPa AO. In particular, this is true when comparing the average N required for different lengths of time-period (from monthly up to the winter mean), and also when comparing N across different months. Since the previous results sections found little evidence of a connection between variability in the winter mean SSW frequency and variability in the winter mean AO, it is unclear whether the link is causal for longer time-periods such as the winter mean. For individual months, however, a link could partly be explained by the fact that variability in the monthly SSW frequency was found to explain a large portion of variability in the monthly 10 hPa AO and a sizeable portion of variability in the monthly 500 hPa AO (therefore implying that when the SSW frequency variability is larger, the AO variability is larger).

However, the signal-to-noise ratios for these three variables are clearly very different in size when comparing them for any same time-period (e.g. NDJFM or JF), where the ratios for the SSW frequency tend to be the smallest and the 500 hPa AO ratios tend to be the largest. The 10 hPa AO ratios are in-between likely because SSW frequency variability was found to be more directly related to 10 hPa AO variability than 500 hPa AO variability. To explain the larger signal-to-noise ratio for the 10 hPa AO than for the SSW frequency, recall that changes in SSW frequency were only found to contribute to half of the 10 hPa AO response in ATL_{600}, while changes in SSW structure account for the other half. As previously suggested in Section 5.4.2.1 of this chapter, these changes in SSW structure will shift the 10 hPa AO response to more negative values independent of changes in SSW frequency, which will increase the signal-to-noise ratio and, therefore, result in the 10 hPa AO response emerging before the SSW frequency response. As for the 500 hPa AO, the signal-to-noise ratio may be increased by the tropospheric pathway's contribution to a negative tropospheric AO response (as shown for ATL in Chapter 4), and also perhaps by the changes in SSW structure having a downward negative influence on the tropospheric AO.

These results suggest that an ensemble size as large as that required to obtain a robust sign in the SSW frequency response to sea-ice loss (around 450 years at least)

may only need to be considered if the magnitude of the tropospheric AO response needs to be accurately quantified, and/or if monthly details in the evolution of the tropospheric AO response over winter are important. This agrees with the difference in the AO responses between the 200 and 600 year-long ATL and ATL_{600} ensembles, which are entirely in terms of magnitude and evolution rather than sign.

5.5 Discussion and conclusions

Motivated by Chapter 4's finding that increases in December SSWs play an important role in the tropospheric AO response for Chapter 3's large-magnitude Atlantic sector sea-ice loss experiment (ATL), and the potentially large multi-decadal internal variability in the frequency of occurrence of SSWs, this chapter extended Chapter 3's control (CTL) and ATL experiments from 200 to 600 years in length. The aims of the extended experiments were to provide both a more accurate estimate of the model's forced changes due to sea-ice loss, and improved estimates of the influence of uncertainty due to atmospheric internal variability on the response for the shorter experiments.

The extended experiments were also used to more broadly explore the influence of atmospheric internal variability with regard to uncertainty in responses to sea-ice loss produced by model time-slice experiments of different lengths. This aided understanding within the above specific investigations, and also addressed important gaps in the literature by providing a quantification of the minimum ensemble size required to obtain a robust sign of stratospheric response to sea-ice loss.

The results from this chapter will now be summarised for each research question posed in the introduction:

1. For 200 year sub-ensembles of the 600 year-long CTL and ATL experiments, how variable are the responses in SSW frequency for different months and the winter mean?

   Specifically for the 200 year-long CTL and ATL experiments:

   - In ATL_{600} there are similarly sized small increases in SSW frequency for the months of December to March, but none of these increases are statistically significant. Internal variability in SSWs therefore must have contributed to the large increase in December SSW frequency in ATL (and indeed the

large decrease and increase in February and March frequencies respectively in ATL, although these were not statistically significant). There is, however, a statistically significant increase in the winter (November-March) mean frequency in ATL_{600} that is similar in magnitude to ATL.

More broadly:

- For each winter month, internal variability in the SSW frequency is found to have a large influence on the monthly SSW frequency responses for thousands of randomly resampled 200 year sub-ensembles of CTL_{600} and ATL_{600}. This is consistent with the sizeable influence of internal variability on the monthly SSW frequency responses in ATL. While internal variability appears to have little effect on the winter mean SSW frequency response in ATL, large variation in the winter mean SSW frequency responses is found for randomly resampled 200 year sub-ensembles of CTL_{600} and ATL_{600}.

2. For 200 year sub-ensembles of the 600 year-long CTL and ATL experiments, to what extent does variability in the SSW frequency responses result in variability in the stratospheric and tropospheric AO responses?

More broadly:

- Large variability is found in the 10 hPa and 500 hPa AO responses for thousands of randomly resampled 200 year sub-ensembles of CTL_{600} and ATL_{600}, both for individual winter months and for the winter mean. It is found that for individual months, variability in the SSW frequency responses accounts for around one- to two-fifths of variability in the 500 hPa AO responses, and for around three-fifths to all of the variability in the 10 hPa AO responses. For the winter mean, however, there is less clear evidence of a relationship between variability in the SSW frequency and 500 hPa AO responses. It is likely that a large portion of the variability in the tropospheric AO responses is internally generated by the troposphere itself (around three- to four- fifths based on the monthly results).

Specifically for the 200 year-long CTL and ATL experiments:

- The stratospheric and tropospheric AO responses in ATL_{600} are negative as in ATL, but there are some differences in evolution and magnitude.

- In the stratosphere, there are similarly sized winter mean AO responses in ATL and ATL_{600}, consistent with the similarly sized winter mean SSW frequency responses. However, the ATL_{600} response is of a similar magnitude throughout winter, while the ATL response is more strongly negative (by 100%) in mid-winter (December-January). This difference in the mid-winter negative stratospheric AO responses is found to be largely explained by internal variability in December SSWs.
- In the troposphere, the AO responses in ATL and ATL_{600} are similar in evolution, but the winter mean AO response is 67% stronger in ATL (-0.25 compared to -0.15). Internal variability in December SSWs is found to contribute to a sizeable part (50%) of the difference in the tropospheric AO responses in mid-winter (consistent with the broader results above regarding individual months). The remainder of the difference in the winter mean tropospheric AO responses is found to likely be largely due to variability internally generated by the troposphere (also consistent with the broader results above). The implications of these results for Chapter 4's results will be discussed shortly.

3. How does variability in the SSW frequency, stratospheric AO, and tropospheric AO responses compare for different sub-ensemble sizes, and what is the minimum ensemble size required to obtain a statistically significant sign of response in each variable?

   - Regarding the winter mean, thousands of randomly resampled N year or member sub-ensembles of ATL_{600}-CTL_{600} (where N = 50, N = 200, and N $\sim$ 600 years/members) suggest that the signal-to-noise ratio associated with the SSW frequency response is so low that the sign of this response can only be statistically detected using an ensemble size of 600 years. For the 10 hPa and 500 hPa AO responses, their signs can be detected using a sub-ensemble size of 200 years, and we can begin to identify their magnitudes using 600 years (particularly for the 500 hPa AO). More specifically, the minimum sub-ensemble size found to be required to obtain a statistically significant sign of response in each variable is around 500 years for the SSW frequency, around 210 years for the 10 hPa AO, and around 130 years for the 500 hPa AO. These results agree well with the difference in the winter mean tropospheric AO responses between ATL and ATL_{600}, in that these 200

and 600 year-long ensembles suggest the same sign of response but rather different magnitudes.

- Regarding individual winter months rather than the winter mean, larger sub-ensemble sizes are found to be required to detect a statistically significant sign of AO response (around 330 years and 440 years on average for the 500 hPa and 10 hPa AO respectively). A robust sign of response in SSW frequency could not be obtained for any month, or indeed for any time-period except for the winter mean and December-March. The largest sub-ensembles sizes were required in late winter, particularly February, when the variability is the largest in all three variables.
- The signal-to-noise ratio for the SSW frequency response appears to be partly related to the ratios for the 10 hPa and 500 hPa AO responses. For individual months this can be explained by the influence of variability in the SSW frequency on variability in the AO, but for longer time-periods such as the winter mean a causal link is less clear. The ratios are still very different in size for each variable, likely because other factors besides the SSW frequency response result in a response or signal in the 10 hPa and 500 hPa AO here (in particular, changes in SSW structure for both and the tropospheric pathway – see Chapter 4 – for the latter).

5.5.1 Wider relevance

The wider relevance, usefulness, and generality of the broader results regarding internal variability will now be discussed.

Firstly, of particular use is the quantification of the minimum ensemble sizes, or time-slice experiment lengths, required to obtain a robust sign of stratospheric response to sea-ice loss for different lengths of time-period (from sub-seasonal to the winter mean). This is because there is currently no guidance on this, and different modelling studies find stratospheric responses for different monthly-seasonal time-period lengths. Importantly, the results here suggest that none of the studies listed in the introduction use an ensemble size that is sufficiently large to obtain a robust stratospheric response: indeed, Sun et al. (2015) use the largest ensemble at 161 years/members, while the minimum requirement found here for any time-period length is around 450 years for the December-March mean SSW frequency response and around 210 years for the

winter (November-March) mean 10 hPa AO response. This may explain why some of these studies find contrasting stratospheric responses (e.g. Peings and Magnusdottir, 2014; Nakamura et al., 2016a). It may also have implications for the robustness of the tropospheric responses in these studies (at least in terms of magnitude), particularly for the many cases in which sub-seasonal stratospheric responses are found (e.g. Kim et al., 2014; Peings and Magnusdottir, 2014). It is recognised that the ensemble sizes recommended here may not be feasible – due to time and computational storage constraints, for example – and, therefore, it is simply suggested that caution should be taken when interpreting stratospheric and tropospheric responses to sea-ice loss for smaller ensemble sizes.

Recall the climate model experiments of Butchart et al. (2000) and others, where decadal variability of SSWs is similarly found to make it difficult to detect a robust trend in SSW frequency over multi-decadal time-periods in response to future transient GHG forcing. While the experiments here are different in that they are time-slice experiments, and the problem here is for sea-ice loss (implying a potentially different magnitude of signal), it is nevertheless interesting that internal variability in SSWs makes it difficult to detect a robust sign of response in SSW frequency even for several hundred years.

Butchart et al. (2000) do suggest, however, that the amplitude of internal variability in SSW frequency may be exaggerated (and therefore the signal-to-noise ratio underestimated) in climate models – such as IGCM4 – with no Quasi-Biennial Oscillation or QBO (this is an observed oscillation in equatorial stratospheric winds between easterlies and westerlies with an approximately two-year period). Indeed, there is evidence that including some representation of the QBO in climate models can introduce some regularity into the occurrence of SSWs, reducing the clustering behaviour that leads to larger SSW variability (Hamilton, 1998). However, Polvani et al. (2017) find a large decadal variability of SSWs in an atmosphere-only model with a realistic representation of the QBO, and Ayarzagüena et al. (2018) suggest that internal variability of SSWs may explain why they find no robust future changes in SSWs across 12 different climate models, 11 of which have some representation of the QBO. Furthermore, similar clustering is also seen in SSWs in the limited observations available, with 9 occurring in the 1980's, 2 in the 1990's, and 9 in the 2000's (Butler et al., 2017). Therefore, it is likely that this clustering behaviour is not just specific to models such as IGCM4 with no QBO.

The quantification of the minimum ensemble size required to obtain a robust sign of tropospheric AO response to sea-ice loss is also useful. Screen et al. (2014) quantify the ensemble size required to obtain a robust sign of the tropospheric response (in various variables) to observed sea-ice loss. However, the size required for the tropospheric AO response to sea-ice loss has not been quantified, even though many studies simulating the response to sea-ice loss find AO-like responses of a particular sign (see Chapter 1). The results here suggest that to obtain a robust sign of response in the AO – which is hemispheric in scale – more ensemble members are required than to obtain robust signs of responses in tropospheric circulation that are more limited in spatial extent. For example, Screen et al. (2014) find that around 70 years are required to obtain a statistically significant response in 500 hPa geopotential height in autumn and winter, where this is only calculated for grid-boxes with a statistically significant response (5% of the area north of 30°N). Here, however, the smallest ensemble size required to obtain a statistically significant response in the 500 hPa AO is around 130 years in November-March.

While the minimum ensemble sizes found here may be specific to the response in the ATL_{600} experiment, it is again highlighted that AO-like responses of a particular sign are typically found for sea-ice loss (see above). Furthermore, it was shown in Chapter 3 that for Atlantic sector, Pacific sector, and pan-Arctic (Atlantic and Pacific sector) sea-ice loss – the ATL, PAC, and ATL&PAC experiments – the responses are similar in terms of sign, magnitude, and pattern in the troposphere, as well as in the stratosphere for ATL and ATL&PAC. Therefore, the ensemble sizes calculated here for ATL may be applicable for other spatial patterns of loss. Also, since the ensemble sizes were calculated for ocean surface temperature anomalies representing an extreme case of sea-ice loss (RCP8.5 future loss), they may provide a useful lower bound on the ensemble size required for less extreme loss.

The result regarding ensemble sizes for which we can begin to identify the magnitude of the 500 hPa AO response is also insightful. For example, as discussed in Chapter 1, the circulation response to future GHG forcing includes the perhaps opposing effects of Arctic warming or sea-ice loss – which may shift the tropospheric jet stream equatorward – and tropical upper-tropospheric warming – which shifts the tropospheric jet poleward. The results here suggest that to more accurately quantify the contribution of sea-ice loss to this balance and, therefore, the overall balance itself, a large ensemble size on the order of several hundred members/years should be used.

The results of this chapter also suggest that our current view of non-linearity in the response to sea-ice loss may be significantly affected by statistical uncertainty, as suggested in Chapter 3 in relation to the moderate-magnitude sea-ice loss runs (0.5ATL and 0.5PAC). Previous studies have compared the responses to different loss magnitudes and have found the response to be non-linear, using simulation lengths of between 50 years and 150 years (Petoukhov and Semenov, 2010; Peings and Magnusdottir, 2014; Nakamura et al., 2016a). For example, Petoukhov and Semenov (2010) find that different magnitudes of sea-ice loss in the Barents-Kara Seas lead to different signs and magnitudes of AO-like or NAO-like tropospheric responses in winter in 100 year ensembles. However, here it is found that an ensemble size of 130 years is required as a minimum to obtain a robust sign of November-March tropospheric AO response. Furthermore, it is also found that such ensemble sizes are inadequate to accurately determine the magnitude of the response.

Further insight can also be provided with regards to non-linearity in the 200 year-long ATL&PAC combined sea-ice loss run from Chapter 3. In particular, the response in this run was apparently weaker than a linear addition of the responses for the separate ATL and PAC runs, suggesting non-linearity in the combined case response. It was suggested that this could entirely be due to sampling error, and the results here confirm this is likely the case. Sampling error may therefore also explain why other studies find similar apparently non-linear results. For example, Screen (2017b) find the response to pan-Arctic sea-ice loss to be weaker than suggested by a linear addition of the responses to 9 different regions of sea-ice loss, but use simulations of only 80 years in length.

Finally, while only a weak relationship is found between the signal-to-noise ratios for the SSW frequency, and the 10 hPa and 500 hPa AO, it is highlighted that this finding may be specific to the mechanisms at work in the experiments here. In particular, while it is found here that the 10 hPa and 500 hPa AO responses become statistically significant before the SSW frequency response – likely because their signal-to-noise ratios are increased by changes in SSW structure for both, and by the tropospheric pathway for the latter – this may not necessarily be the case in all studies. For instance, if a study found a stratospheric pathway involving changes in SSW frequency to play a dominant role in a model-produced response to sea-ice loss, then the minimum ensemble size required to detect a robust response in SSW frequency may be a more important consideration.

5.5.2 Revisiting the tropospheric and stratospheric pathways

This chapter's results will now be discussed in the context of Chapter 4's results specifically. In Chapter 4, the aim was to quantify the roles played by tropospheric and stratospheric mechanisms in the negative tropospheric AO responses for the large-magnitude Atlantic and Pacific sector sea-ice loss experiments (ATL and PAC) from Chapter 3.

A first point of relevance is that randomly resampled 200 year sub-ensembles of ATL_{600}-CTL_{600} were found in this chapter to only be large enough to statistically detect the sign of the tropospheric AO response, but not its magnitude, due to relatively large internal variability. Furthermore, the 200 year-long ATL experiment was specifically found to simulate a winter mean tropospheric AO response that is 67% larger in magnitude than in ATL_{600}. As such, the total tropospheric AO response that Chapter 4 aimed to decompose includes a sampling error of -0.1 (-0.25 in ATL compared to -0.15 in ATL_{600}), and the magnitude of the tropospheric pathway's contribution to this calculated from the 200 year-long ATL_{ndgCS} experiment (-0.06) may also include significant sampling error due to internal variability (although perhaps less than for ATL since the stratospheric nudging suppresses zonal mean stratospheric variability, and therefore the downward influence of this on tropospheric variability). Indeed, this could partly explain why the tropospheric and stratospheric pathways were not found to be linearly additive in Chapter 4. In terms of future work, it would be useful to use ATL_{600}, and to extend the ATL_{ndgCS} experiment to 600 years, to more accurately estimate the role played by a tropospheric pathway in forced tropospheric changes due to ATL sea-ice loss within the model. Since 200 years is found here to be a sufficient ensemble size to robustly determine whether there is a tropospheric AO response to sea-ice loss, it seems reasonable to conclude that the lack of response in the winter-mean stratospheric pathway experiment (CTL_{ndgAS}) is likely robust. While it is of course *possible* that it is non-robust, this is improbable.

While this issue of sampling error is not found or discussed by other modelling studies using a stratospheric nudging method to quantify the roles played by the tropospheric and stratospheric pathways in model-produced responses to sea-ice loss, this is likely because they took different approaches. Indeed, the stratospheric pathway is only implicitly calculated from the total response minus the tropospheric pathway in Nakamura et al. (2016b) and Zhang et al. (2018b), and therefore they were not able to address this issue. Wu and Smith (2016) do quantify both of the tropospheric

and stratospheric pathways explicity, but consider a more horizontally and vertically extensive Arctic warming. This likely increases the signal-to-noise ratio and, therefore, sampling error is perhaps less of an issue in their study.

With respect to a stratospheric pathway involving changes in SSWs, recall that both Chapter 4's results for ATL and this chapter's results for ATL_{600} find a stratospheric AO response to ATL sea-ice loss that can be largely explained by changes in SSWs, where changes in frequency and structure each contribute to around half of the response. Compared to Chapter 4, however, the results here for ATL_{600} show only a small increase in December SSWs, which is not statistically significant in terms of sign and only contributes to a small portion of the mid-winter tropospheric AO response (a 13% contribution compared to the 36% contribution in ATL; see Figure 5.8).

However, there are other aspects of the SSW response found here for ATL_{600} that imply a potentially broader role for SSWs in forced tropospheric changes due to ATL sea-ice loss than found for the December SSW frequency. Specifically, unlike the analysis of the 200 year-long ATL experiment in Chapter 4, here it is found within ATL_{600} that sea-ice loss causes a statistically significant increase in SSW frequency more broadly for the winter mean, due to small increases in frequency in every month from December to March. Furthermore, statistically significant changes in SSW structure are found – which are the same as found in Chapter 4 (including an increase in SSW duration, and a strengthening of anomalies in the mid to lower stratosphere during an SSW, which both have an apparent downward effect on the troposphere) – which could also be important. It would therefore be useful to conduct further nudging experiments to evaluate the importance of these changes in SSWs for forced tropospheric changes due to ATL sea-ice loss, as estimated by ATL_{600}. Possibilities for these experiments will be considered in Chapter 6.

To summarise, the extended 600 year-long experiments in this chapter still agree with the shorter 200 year-long experiments in Chapter 4, in that they suggest part of the negative tropospheric AO response to ATL sea-ice loss is likely to be caused by tropospheric mechanisms, and the other part likely involves changes in SSWs. However, this chapter has shown that the 200 year-long experiments used in Chapter 4 were too short to accurately quantify the magnitude of the total AO response, tropospheric pathway, and SSW stratospheric pathway, due to relatively large internal variability for time-slice means of 200 years. Since many studies use shorter experiments than 200 years to simulate the response to sea-ice loss, this result implies that disagreement

between these studies regarding the importance of tropospheric and stratospheric mechanisms (see Chapter 1) may be in part due to sampling error. Further longer nudging experiments will be required to better determine the relative importance of these pathways, which is key for understanding whether the time-mean response to sea-ice loss is sensitive to different model representations of SSWs for example.

While this chapter did not deal with the Pacific sea-ice loss case, the results here suggest that the magnitude of the tropospheric AO response in the PAC experiment may also include significant sampling error due to internal variability. This estimate may therefore also need re-examination and revision. As discussed for $\mathrm{CTL}_{\mathrm{ndgAS}}$ above, it is possible but improbable that the lack of responses in the 200 year-long tropospheric and winter-mean stratospheric pathway experiments ($\mathrm{PAC}_{\mathrm{ndgCS}}$ and $\mathrm{CTL}_{\mathrm{ndgPS}}$) are non-robust; it therefore seems reasonable to conclude that they are likely robust. The combined non-linear tropospheric and stratospheric pathway found to be important for this case is therefore likely still important. Established literature also exists in support of such a pathway, and a large amount of mechanistic evidence was presented in support of the pathway in Chapter 4.

Chapter 6

Conclusions

6.1 Overview

Over the past few decades, Arctic sea-ice extent has declined contributing to enhanced near-surface warming in the Arctic, while there has been an apparent increase in severe winter weather across some mid-latitude regions. This has led to much research into whether Arctic sea-ice loss and associated warming has an influence on mid-latitude weather and climate. Since all climate models project a continuation of Arctic sea-ice loss during the 21st century in response to anthropogenic radiative forcing, it is important that the potential influence of this on the highly populated mid-latitudes is better understood.

However, significant uncertainty still exists regarding the nature of the response to Arctic sea-ice loss and the mechanisms involved. This is because it is difficult to disentangle the complex web of potential processes involved, the modelled response to sea-ice loss is small relative to internal climate variability, and modelling studies find contrasting climatological mean responses to imposed sea-ice loss.

The overall aim of the research presented in this thesis was to improve understanding of the influence of Arctic sea-ice loss on mid-latitudes and the mechanisms involved. The issues of complexity and statistical robustness were partly addressed by conducting idealised several-century-long numerical modelling experiments using an intermediate complexity global circulation model, IGCM4. To understand contrasting model responses in past studies, a series of experiments was designed to systematically examine various aspects that may explain these contrasting results, including

different regions and magnitudes of ice loss as well as atmospheric internal variability. A better understanding of the mechanisms involved was obtained by implementing a stratospheric nudging method in IGCM4 to decompose the response into parts due to tropospheric and stratospheric mechanisms. These experiments addressed the following research questions:

1. What is the nature of the response to Arctic sea-ice loss within IGCM4, in terms of the impact on the large-scale atmospheric circulation and on mid-latitude surface temperatures? To what extent is the response sensitive to the region or magnitude of sea-ice loss? (Chapter 3)

2. What is the relative importance of tropospheric and stratospheric mechanisms in producing remote atmospheric responses to sea-ice loss? (Chapter 4)

3. How large is the influence of atmospheric internal variability with regard to uncertainty in responses to sea-ice loss produced by model time-slice experiments of different lengths? (Chapter 5)

While questions were not directly asked regarding the sensitivity of the response to the model's stratospheric representation, or to the background atmospheric state, the experiments designed in relation to question 2 provided a test of these aspects.

6.2 Answers to research questions

1. What is the nature of the response to Arctic sea-ice loss within IGCM4, in terms of the impact on the large-scale atmospheric circulation and on mid-latitude surface temperatures? To what extent is the response sensitive to the region or magnitude of sea-ice loss? (Chapter 3)

In Chapter 3, IGCM4 experiments were conducted with ocean surface temperature anomalies imposed in either the Atlantic or Pacific sectors of the Arctic (the Barents-Kara and Chukchi-Bering Seas) representing future sea-ice retreat. In both cases, either large-magnitude (late 21st century) or moderate-magnitude anomalies were imposed, where the relevant experiments were 200 and 300 years-long respectively. Chapter 5 found that 200 years is sufficient in the large-magnitude sea-ice loss case to

robustly detect the sign of the large-scale atmospheric circulation response, but not the magnitude of this response. Similar analysis was not conducted in Chapter 5 for the moderate-magnitude sea-ice loss case.

It was found that for different regions of sea-ice loss, there are different effects on the stratospheric polar vortex. In particular, Atlantic and Pacific sector sea-ice losses respectively result in a weakening and strengthening of the polar vortex due to differences in linear wave interference. Only the large-magnitude Atlantic case is found to have a statistically significant vortex response with respect to its climatological state, but a statistically significant difference in the vortex state is found between the Atlantic and Pacific cases for both magnitudes of sea-ice loss. Therefore, different spatial patterns of moderate- and large-magnitude sea-ice loss can explain the different (but not necessarily opposite) stratospheric responses in previous studies. These results provide insight that is additional to Sun et al. (2015)'s finding that different spatial patterns of (large-magnitude) sea-ice loss can explain the opposite stratospheric responses in previous studies.

Regarding the large-scale tropospheric circulation response, Atlantic and Pacific sector sea-ice losses of moderate-magnitude were found to lead respectively to statistically insignificant negative and positive tropospheric AO responses. For large-magnitude sea-ice loss, a statistically significant negative AO response is found in both cases. This implies that different spatial patterns of sea-ice loss cannot explain the contrasting tropospheric responses in previous studies. It also implies that for large-magnitude sea-ice loss, tropospheric mechanisms are relatively more important than stratospheric mechanisms. In Chapter 4 the response to large-magnitude sea-ice loss is decomposed into parts due to tropospheric and stratospheric mechanisms, allowing their roles to be better determined.

Finally, contrasting effects on mid-latitude surface temperatures were found for different regions of large-magnitude sea-ice loss, which are explained in this work using a method of decomposition into an 'indirect' part induced by the large-scale tropospheric AO response, and a residual 'direct' part that is found to be local to the region of loss. This decomposition of the temperature response into direct and indirect parts is a new approach, but is similar in concept to the 'thermodynamic' versus 'dynamic' decomposition described by Screen et al. (2015) and other studies in Chapter 1. Chapter 5 shows that for the 200 and 600 year-long versions of the

large-magnitude Atlantic sea-ice loss experiment, the direct response is robust in terms of pattern and magnitude.

In terms of their wider relevance, the large-magnitude sea-ice loss results can be used as an indication of the range of potential atmospheric responses for studies using state-of-the-art CMIP5 (Coupled Model Intercomparison Project Phase 5) climate models. This is because the spatial pattern of future Arctic surface warming – which is related to sea-ice loss – is uncertain across these models.

Regarding the moderate-magnitude sea-ice loss results, it was found that even a long simulation of length 300 years is insufficient to obtain a statistically robust response. As such, this makes it difficult to assess the linearity of the response to different magnitudes of sea-ice loss. Broader conclusions relating to the topic of linearity are discussed in the context of research question 3 (Chapter 5).

2. What is the relative importance of tropospheric and stratospheric mechanisms in producing remote atmospheric responses to sea-ice loss? (Chapter 4)

Chapter 4 aimed to determine the roles played by tropospheric and stratospheric mechanisms in the negative tropospheric AO responses to large-magnitude Atlantic and Pacific sector sea-ice losses. This was done by conducting 200 year-long experiments similar to those in Chapter 3, but in which the stratosphere is constrained to selected zonal mean states using a nudging method implemented in IGCM4. Furthermore, a combination of these nudging experiments, and a statistical analysis of Chapter 3's experiments, was used to determine the importance of a winter mean change in the stratospheric polar vortex versus a change in sudden stratospheric warming (SSW) events. While Chapter 5 subsequently showed that 200 year-long experiments are insufficiently long to accurately quantify the magnitude of the tropospheric and stratospheric pathways, they can at least robustly indicate qualitatively which pathways are likely to be important.

For both cases of sea-ice loss, nudging the stratosphere was found to have a large effect on the negative tropospheric AO responses, implying that the stratosphere plays an important role in these responses. Specifically, for Atlantic sector loss part of the response is likely caused by changes in SSWs, and the other part likely involves tropospheric mechanisms. While an increase in SSWs in December is found in Chapter 4 to contribute to a large part of the mid-winter (December-January) tropospheric

AO response, Chapter 5 suggests a broader role for SSWs (see research question 3 and Section 6.3.2). For Pacific sector loss the tropospheric AO response likely involves a non-linear interaction between tropospheric and stratospheric mechanisms. Specifically, the stratospheric state is found to alter vertical wave propagation in such a way that the direct stationary Rossby wave response projects onto a negative tropospheric AO. This effect is found to occur in strong vortex years arising as part of interannual variability. These results revise Chapter 3's suggestion that stratospheric mechanisms may not play an important role in the tropospheric responses for large-magnitude Atlantic and Pacific sector sea-ice losses.

There are important wider implications of these results. Firstly, they suggest that climate models with an inadequate representation of the stratosphere are likely missing an important requirement for fully capturing responses to sea-ice loss. The representation of the stratosphere varies widely across different climate models, which could therefore explain differences in the responses and dominant mechanisms found in past studies using different models. Other stratospheric nudging studies looking at the response to sea-ice loss also find the stratosphere to be important (Nakamura et al., 2016b; Wu and Smith, 2016; Zhang et al., 2018a,b), but here it is additionally found that model stratospheric representation is likely important regardless of the spatial pattern of future sea-ice loss, and that model representation of SSWs specifically may be important for simulating responses to Atlantic sector sea-ice loss.

The Pacific case results suggest that the characteristics of simulated tropospheric responses to Pacific sector sea-ice loss may be strongly sensitive to intermodel differences in the mean strength and interannual variability of the stratospheric polar vortex. This may help to explain why in their nudging experiments Zhang et al. (2018b) find tropospheric mechanisms alone to contribute to half of the negative tropospheric AO response for Pacific sector ice loss, whereas here tropospheric mechanisms alone are found to likely play little role. This may be because the model Zhang et al. (2018b) use has a stronger polar vortex than IGCM4.

Finally, the Pacific case results may also help explain the contradictory results of previous studies looking at the response to future pan-Arctic sea-ice loss. In particular, they may help us to understand why negative tropospheric AO-like responses have been found in many studies, where these studies report a wide range of stratospheric responses including a strengthening of the polar vortex (Peings and Magnusdottir, 2014; Sun et al., 2015; Nakamura et al., 2016a).

3. How large is the influence of atmospheric internal variability with regard to uncertainty in responses to sea-ice loss produced by model time-slice experiments of different lengths? (Chapter 5)

Motivated by the importance of SSWs in the large-magnitude Atlantic sector sea-ice loss experiment and the potentially large multi-decadal internal variability in their frequency of occurrence, Chapter 5 extended this experiment and the control experiment from 200 to 600 years in length. The aims of the extended experiments were to provide both a more accurate estimate of the model's forced changes due to sea-ice loss, and improved estimates of the influence of uncertainty due to atmospheric internal variability on the response for the shorter experiments.

The stratospheric and tropospheric AO responses are found to be of the same sign (negative) in the shorter and extended experiments, but with some differences in evolution and magnitude. Specifically, there are similarly sized winter (November-March) mean stratospheric AO responses, but in the shorter experiments the response is more strongly negative by around 100% in mid-winter (December-January). This difference in mid-winter can largely be explained by the difference in December SSW frequency responses between the shorter and extended experiments (and thus by internal variability in SSWs). Regarding the tropospheric AO responses, their evolution over winter is similar, but the winter mean response is more strongly negative in the shorter experiments by around 67%. In mid-winter, 50% of this difference can be explained by the difference in December SSW frequency responses (and thus again by internal variability in SSWs). Otherwise, the difference in the winter mean tropospheric AO responses is likely largely due to variability internally generated by the troposphere.

It is argued that while the extended experiments compared to the shorter experiments estimate a smaller contribution of increases in December SSWs to forced tropospheric changes due to Atlantic sector sea-ice loss, there are other aspects of changes in SSWs found in the extended experiments suggesting that a role for SSWs cannot be discounted. This, and other implications of Chapter 5's results for Chapter 4's results, will be discussed in more detail in the following section on further research.

The opportunity was also taken in Chapter 5 to use the extended experiments to more broadly examine the influence of atmospheric internal variability with regard to uncertainty in responses to sea-ice loss produced by model time-slice experiments of different lengths. First, it is found that the internal variability leading to uncertainty in the response for N year/member sub-ensembles of the extended experiments is

chaotically generated, since there is no autocorrelation for any yearly lag in the winter mean SSW frequency, or stratospheric and tropospheric AO. Randomly generated datasets of SSW frequency also contain similar levels of variability.

Furthermore, by calculating thousands of randomly resampled sub-ensemble differences for a sub-ensemble size of N years/members and repeating this for different N, the minimum ensemble sizes required to detect robust signs of tropospheric and stratospheric responses to sea-ice loss were quantified. This has not been quantified to date for the latter. The required ensemble size is found to be large for the tropospheric and stratospheric AO, and very large for the SSW frequency (respectively around 130, 190, and 450 years/members for the December-March mean, and even larger for shorter sub-seasonal time-periods). Importantly, this suggests that many studies use an ensemble size that is insufficient to obtain a robust stratospheric response to sea-ice loss (Cai et al., 2012; Kim et al., 2014; Peings and Magnusdottir, 2014; Sun et al., 2015; Nakamura et al., 2015, 2016a,b; Zhang et al., 2018a,b). This may explain the contrasting stratospheric responses in some of these studies (e.g. Peings and Magnusdottir, 2014; Nakamura et al., 2016a). It may also have implications for the robustness of the tropospheric responses in these studies (at least in terms of magnitude), particularly for the many cases in which sub-seasonal stratospheric responses are found (e.g. Kim et al., 2014; Peings and Magnusdottir, 2014).

The results of Chapter 5 also importantly suggest that our current view of non-linearity in the response to sea-ice loss may be significantly affected by statistical uncertainty. For example, previous studies have compared the responses to different loss magnitudes and have found the response to be non-linear in sign and magnitude, using ensemble sizes of between 50 years and 150 years (Petoukhov and Semenov, 2010; Peings and Magnusdottir, 2014; Nakamura et al., 2016a). However, here it is found that an ensemble size of 130 years is required as a minimum to obtain a robust sign of November-March tropospheric AO response, and that such ensemble sizes are inadequate to accurately determine the magnitude of the response. Furthermore, Chapter 5's results suggest that sampling error rather than non-linearity can help to explain Chapter 3's 200 year-long combined Atlantic and Pacific sector sea-ice loss experiment (ATL&PAC), and Screen (2017b)'s 80 year-long pan-Arctic sea-ice loss experiment. In particular, sampling error can entirely explain why the response to ATL&PAC or pan-Arctic sea-ice loss appears to be weaker than suggested by a linear addition of the responses to regional sea-ice losses.

The minimum ensemble sizes found to be required to simulate robust circulation responses to sea-ice loss may also have implications for detecting the 'real-world' observed response. In particular, the minimum ensemble size can be used to estimate the minimum number of years required to observe a robust response, assuming that IGCM4 can realistically simulate the forced response to sea-ice loss and atmospheric internal variability. Given that the smallest minimum ensemble size found is 130 years for any variable and time-period, we would not expect to observe a robust large-scale stratospheric or tropospheric circulation response to past sea-ice loss over the 40 year-long satellite era (1979 to present), or to future sea-ice loss over the 21st century. Screen et al. (2014) find similar conclusions for the observed tropospheric circulation response to past sea-ice loss, based on large ensembles using the full-complexity GCMs CAM3 and UM7.3. In reality, detection of an observed response to sea-ice loss will of course also depend on the magnitude of the sea-ice forced response compared to other forced responses (e.g. to tropical upper tropospheric warming), as well as compared to internal variability (Screen et al., 2014).

Climate models such as IGCM4 may, however, underestimate the signal-to-noise ratio of the 'real-world', as shown for predictions of the North Atlantic Oscillation or NAO (Eade et al., 2014; Scaife et al., 2014; Dunstone et al., 2016). In particular, ensemble-mean predictions of the NAO using climate models are generally more highly correlated with observations than with model ensemble members, suggesting that the signal-to-noise ratio in models is lower than in the 'real-world' (Scaife and Smith, 2018); this is the 'signal-to-noise paradox' discussed in Chapter 1. Since the total NAO variance in models is generally similar in magnitude to observations, this paradox has been attributed to a too weak forced signal in models rather than to too much noise (Scaife and Smith, 2018). Recently it has been suggested that this underestimation of the signal may be because a very high model resolution – far higher than that in state-of-the-art GCMs – is required to accurately simulate the magnitude of the eddy feedbacks involved in generating NAO responses (Scaife et al., 2019).

The too weak signal-to-noise ratio in model predictions of the NAO may also be applicable in the response to sea-ice loss, which is often NAO/AO-like. Indeed, there are various reasons that we might expect the response to sea-ice loss to be too weak in models, which could explain the weak responses to sea-ice loss that have been found in this thesis for IGCM4 and in past studies using state-of-the-art GCM's (e.g. Screen et al., 2014; McCusker et al., 2017; Mori et al., 2019). For example, insufficient

model resolution could be a factor as outlined above, and a lack of atmosphere-ocean coupling could also play a role for atmosphere-only models like IGCM4 (see Chapter 1). Another contributing factor could be that many climate models, even state-of-the-art ones, cannot produce a realistic internally generated QBO (Schenzinger et al., 2017). Indeed, IGCM4 has no QBO and it has been shown that an easterly QBO phase can enhance the Siberian High's response to sea-ice loss, enhancing Eurasian cold extremes (see Section 1.1.4.3 of Chapter 1). Furthermore, GCM simulations have shown that land-surface processes can amplify the response to sea-ice loss (Nakamura et al., 2019); in particular, sea-ice loss induced cooling over Eurasia can cause anomalies in the snow amount and soil temperature, which act to enhance the negative AO response. While this result is for one GCM and, therefore, does not necessarily represent the real-world, it is one possible mechanism by which a too weak response could occur in models with a less complex representation of land surface processes such as IGCM4.

In short, while the results presented in Chapter 5 for the 'atmospheric model-world' suggest that forced changes due to sea-ice loss over the 21st century will be dominated by the noise of internal variability, this assumes that the signal-to-noise ratio in IGCM4 is representative of the real-world. There is growing evidence that the forced response to sea-ice loss in the real-world may be larger than in models and, therefore, that it may emerge from this noise earlier and be detectable in our lifetimes. The observed response to sea-ice loss over the last few decades may therefore also have been larger than the model results here suggest. However, the signal-to-noise paradox is an ongoing topic of research. As such, coordinated experiments using a large number of different climate models will be required to determine whether models do in general have a signal-to-noise ratio that is systematically too low (Screen et al., 2018b), and to more fully understand the mechanisms that could contribute to this.

6.3 Further research

6.3.1 Role of tropospheric mechanisms

In Chapter 5 it was found that Chapter 3's 200 year-long large-magnitude Atlantic sector sea-ice loss experiment is long enough to statistically detect the sign of the winter mean tropospheric AO response, with significant uncertainty over its magnitude due to relatively large internal variability. It is also suggested that sampling error may

have significantly affected the magnitude of the tropospheric AO response in Chapter 4's 200 year-long nudging experiment designed to more precisely quantify the role of tropospheric mechanisms. In terms of future research, it would be useful to extend this nudging experiment to 600 years, and to use the extended 600 year-long Atlantic experiment from Chapter 5, to more precisely estimate the role played by tropospheric mechanisms in forced tropospheric changes due to Atlantic sector sea-ice loss within the model.

6.3.2 Role of sudden stratospheric warmings

For both the shorter and extended large-magnitude Atlantic sector sea-ice loss experiments considered in Chapters 4 and 5 respectively, it was found that the stratospheric AO response can largely be explained by changes in SSWs, where changes in frequency and structure each contribute to around half of the response. Compared to Chapter 4, however, Chapter 5 finds a smaller increase in December SSW frequency and, therefore, a smaller overall contribution of increases in December SSWs to the mid-winter tropospheric AO response (a 13% compared to 36% contribution).

However, there are other aspects of the SSW response found for the extended experiments in Chapter 5 that imply a potentially broader role for SSWs than found for the December SSW frequency. Specifically, unlike for the shorter experiments in Chapter 4, Chapter 5 finds that Atlantic sector sea-ice loss causes a statistically significant increase in SSW frequency more broadly for the winter mean, due to small increases in frequency in every month from December to March. Furthermore, statistically significant changes in SSW structure are found – which are the same as found in Chapter 4 (including an increase in SSW duration, and a strengthening of anomalies in the mid to lower stratosphere during an SSW, which both have an apparent downward effect on the troposphere) – which could also be important.

It would be useful to conduct further nudging experiments to evaluate the importance of these changes in SSWs for forced tropospheric changes due to Atlantic sector sea-ice loss, as estimated by Chapter 5's extended experiments. Determining this would be useful for confirming whether model representation of SSWs is important for simulating the time-mean response to sea-ice loss. Note that while the SSW frequency responses are not statistically significant in any individual winter month in the extended Atlantic experiment, the fact that the winter mean SSW frequency response is found

to be statistically significant suggests that the role of SSWs in the tropospheric AO response can at least be qualitatively evaluated for the winter mean.

For instance, new experiments could be designed in which the stratosphere is nudged toward some state chosen to represent the changes in SSWs found in Chapter 5's extended Atlantic experiment. This could be a series of four experiments, each of which could involve nudging toward a specific SSW from each of the four months between December to March. The AO response from each of these experiments could then be scaled by the SSW frequency response for the relevant month, and the results averaged together across the four experiments. The advantage of this method is that since the same SSW is nudged toward in every year, the problem would be more tractable and 600 year-long experiments may not be necessary.

Alternatively, two new experiments could be conducted with nudging toward the fully time-evolving stratospheric states of Chapter 5's extended control or Atlantic experiments (similar to Zhang et al. 2018a). These would have to be run for 600 years, but an advantage is that they would include the effects of changes in both SSW structure and frequency and, thus, could be used to fully quantify the contribution of SSWs to the tropospheric AO response.

6.3.3 Role of a combined non-linear pathway

It would also be interesting to further examine the 'combined non-linear pathway' that was found in Chapter 4 to play a role in the negative tropospheric AO response to large-magnitude Pacific sector sea-ice loss. Recall that this pathway involves a strengthened stratospheric polar vortex altering vertical wave propagation in such a way that the direct stationary Rossby wave response projects onto a negative tropospheric AO. This effect is found to occur in strong vortex years arising as part of interannual variability, and may also occur through sea-ice loss strengthening the stratospheric polar vortex; however, the latter effect is currently uncertain, since 200 years was found to be insufficient to determine the robustness of the stratospheric response in early winter.

In future work, it would be useful to firstly conduct a 600 year-long Pacific sector sea-ice loss experiment, in order to re-evaluate the magnitude of the tropospheric AO response and to determine whether the strengthened stratospheric polar vortex response is robust. Further nudging experiments could be then be conducted to more

quantitatively evaluate the influence of the stratospheric state on the tropospheric response to Pacific sector sea-ice loss. Specifically, various nudging experiments could be conducted in which Pacific sector sea-ice loss is imposed, and the stratosphere is nudged toward a choice of three different states: a control-like state including interannual variability, or the sea-ice loss induced strengthened polar vortex (if found to be robust), either without or with interannual variability included. These experiments would potentially allow for a quantification of the role played by a combined non-linear pathway in the negative tropospheric AO response, and the specific mechanisms involved, provided the experiments conducted were sufficiently long. Alternatively, a more idealised set of experiments could be conducted in which Pacific sector sea-ice loss is imposed, and the stratosphere is nudged toward various different idealised states containing different strengths of stratospheric polar vortex. This would allow for a more systematic examination of the dependence of the tropospheric AO response on the polar vortex strength and the mechanisms involved.

6.3.4 Sensitivity to the background SST state

Another interesting question to answer would be whether the response to sea-ice loss within IGCM4 is sensitive to the background sea surface temperature (SST) state. Recall from Chapter 1 that Smith et al. (2017) find opposite tropospheric NAO responses for the same sea-ice loss imposed in two atmospheric GCM experiments with two different background SST states. They find that this is because the different SST states are associated with different climatological eddy-driven jet strengths and latitudinal positions, which alters the nature of Rossby wave feedbacks on the mean flow and, therefore, the nature of the NAO response.

To the best of the author's knowledge, no studies have examined the generality of this relationship by testing it for further different SST states or eddy-driven jet strengths and latitudes. This would, however, be useful given its potential importance for understanding the contrasting climatological mean responses to sea-ice loss found in previous modelling studies.

In terms of future research, it is suggested here that the same large-magnitude Atlantic and Pacific sector sea-ice loss experiments could be run, but with zonal mean ocean surface temperature anomalies of magnitude 2 K or 3 K imposed in different latitudinal bands (e.g. of 10°) from the equator to the North Pole. By altering the

subtropical and mid-latitude SST gradients, such zonal mean anomalies have been found to alter the strength and latitude of the subtropical and eddy-driven jets in different models (Brayshaw et al., 2008; Graff and LaCasce, 2012), including IGCM-FASTOC (a chemistry-climate model version of IGCM; Winter and Bourqui, 2011). The advantage of imposing SST anomalies in this idealised manner is that it will likely make the problem more tractable. Imposing 3 K anomalies in 10° bands does, however, produce a range of subtropical and mid-latitude SST gradients that is representative of intermodel spread in these gradients across the CMIP5 models for 1979-2014 (based on historical runs appended with RCP8.5 runs after 2006; not shown).

As a first test, it may be useful to run experiments that are 200 years-long to determine whether the sign of the tropospheric AO response is systematically related to different jet strengths and/or latitudes. Longer experiments could then be run to more accurately identify the magnitudes of the AO responses, which would allow a determination of whether the relationship is linear for example.

6.4 Final comments

In summary, the research presented in this thesis has improved understanding of the influence of Arctic sea-ice loss on mid-latitude weather and climate, and the mechanisms involved. Various aspects were found to potentially explain why previous modelling studies have found contrasting results, in terms of both the nature of the response to sea-ice loss and the dominant mechanisms involved in this response. These aspects include differences in the region of sea-ice loss considered, intermodel differences in the model representation of the stratosphere, a sensitivity of the response to the stratospheric state, and spread in simulated responses due to atmospheric internal variability.

The results also showed – for the first time – that previous modelling studies simulating the response to sea-ice loss typically use experiment lengths that are not sufficient to robustly detect the signs of the SSW frequency or stratospheric AO responses, or the magnitude of the tropospheric AO response. Furthermore, they suggest that experiment lengths should be carefully considered when designing future experiments for the purposes of quantification. This includes, for example, experiments designed to quantify the roles played by tropospheric and stratospheric mechanisms in the response to sea-ice loss (a particular challenge encountered here), or to quantify

the influence of sea-ice loss on projections of future circulation change in response to radiative forcing by greenhouse gases.

References

Alexander, M. A., U. S. Bhatt, J. E. Walsh, M. S. Timlin, J. S. Miller, and J. D. Scott, 2004: The atmospheric response to realistic Arctic sea ice anomalies in an AGCM during winter. *J. Climate*, **17**, 890–905, doi:10.1175/1520-0442(2004)017<0890:TARTRA>2.0.CO;2.

Ambaum, M. H. P., B. J. Hoskins, and D. B. Stephenson, 2001: Arctic Oscillation or North Atlantic Oscillation? *J. Climate*, **14**, 3495–3507, doi:10.1175/1520-0442(2001)014<3495:AOONAO>2.0.CO;2.

Ayarzagüena, B., and J. A. Screen, 2016: Taking the chill off: Future Arctic sea-ice loss reduces severity of cold air outbreaks in midlatitudes. *Geophys. Res. Lett.*, **43**, 2801–2809, doi:10.1002/2016GL068092.

Ayarzagüena, B., and Coauthors, 2018: No robust evidence of future changes in major stratospheric sudden warmings: a multi-model assessment from CCMI. *Atmos. Chem. Phys.*, **18**, 11 277–11 287, doi:10.5194/acp-18-11277-2018.

Baldwin, M. P., and T. J. Dunkerton, 1999: Propagation of the Arctic Oscillation from the stratosphere to the troposphere. *J. Geophys. Res. Atmos.*, **104**, 30 937–30 946, doi:10.1029/1999JD900445.

Baldwin, M. P., and T. J. Dunkerton, 2001: Stratospheric harbingers of anomalous weather regimes. *Science*, **294**, 581–584, doi:10.1126/science.1063315.

Baldwin, M. P., H. J. Edmon, and J. R. Holton, 1985: A diagnostic study of eddy-mean flow interactions during FGGE SOP-1. *J. Atmos. Sci.*, **42**, 1838–1845, doi:10.1175/1520-0469(1985)042<1838:ADSOEM>2.0.CO;2.

Baldwin, M. P., D. B. Stephenson, D. W. J. Thompson, T. J. Dunkerton, A. J. Charlton, and A. O'Neill, 2003: Stratospheric memory and skill of extended-range weather forecasts. *Science*, **301**, 636–640, doi:10.1126/science.1087143.

Baldwin, M. P., and D. W. Thompson, 2009: A critical comparison of stratosphere–troposphere coupling indices. *Quart. J. Roy. Meteor. Soc.*, **135**, 1661–1672, doi:10.1002/qj.479.

Barnes, E. A., 2013: Revisiting the evidence linking Arctic amplification to extreme weather in midlatitudes. *Geophys. Res. Lett.*, **40**, 4734–4739, doi:10.1002/grl.50880.

Barnes, E. A., E. Dunn-Sigouin, G. Masato, and T. Woollings, 2014: Exploring recent trends in Northern Hemisphere blocking. *Geophys. Res. Lett.*, **41**, 638–644, doi:10.1002/2013GL058745.

Barnes, E. A., and D. L. Hartmann, 2011: Rossby wave scales, propagation, and the variability of eddy-driven jets. *J. Atmos. Sci.*, **68**, 2893–2908, doi:10.1175/JAS-D-11-039.1.

Barnes, E. A., and D. L. Hartmann, 2012: Detection of Rossby wave breaking and its response to shifts of the midlatitude jet with climate change. *J. Geophys. Res. Atmos.*, **117**, D09117, doi:10.1029/2012JD017469.

Barnes, E. A., D. L. Hartmann, D. M. W. Frierson, and J. Kidston, 2010: Effect of latitude on the persistence of eddy-driven jets. *Geophys. Res. Lett.*, **37**, L11804, doi:10.1029/2010GL043199.

Barnes, E. A., and L. M. Polvani, 2015: CMIP5 projections of Arctic amplification, of the North American/North Atlantic circulation, and of their relationship. *J. Climate*, **28**, 5254–5271, doi:10.1175/JCLI-D-14-00589.1.

Barnes, E. A., and J. A. Screen, 2015: The impact of Arctic warming on the midlatitude jet-stream: Can it? Has it? Will it? *WIREs: Climate Change*, **6**, 277–286, doi:10.1002/wcc.337.

Bindoff, N. L., and Coauthors, 2013: Detection and attribution of climate change: from global to regional. *Climate Change 2013: The Physical Science Basis. Contribution of Working Group I to the Fifth Assessment Report of the Intergovernmental Panel on Climate Change*, T. F. Stocker, D. Qin, G.-K. Plattner, M. Tignor, S. K. Allen, J. Boschung, A. Nauels, Y. Xia, V. Bex, and P. M. Midgley, Eds., Cambridge University Press, Cambridge, United Kingdom and New York, NY, USA, 867–952, doi:10.1017/CBO9781107415324.022.

Bintanja, R., E. C. van der Linden, and W. Hazeleger, 2012: Boundary layer stability and Arctic climate change: a feedback study using EC-Earth. *Climate Dyn.*, **39**, 2659–2673, doi:10.1007/s00382-011-1272-1.

Blackport, R., and P. J. Kushner, 2017: Isolating the atmospheric circulation response to Arctic sea ice loss in the coupled climate system. *J. Climate*, **30**, 2163–2185, doi:10.1175/JCLI-D-16-0257.1.

Blackport, R., and P. J. Kushner, 2018: The role of extratropical ocean warming in the coupled climate response to Arctic sea ice loss. *J. Climate*, **31**, 9193–9206, doi:10.1175/JCLI-D-18-0192.1.

Blackport, R., J. A. Screen, K. van der Wiel, and R. Bintanja, 2019: Minimal influence of reduced Arctic sea ice on coincident cold winters in mid-latitudes. *Nat. Climate Change*, **9**, 697–704, doi:10.1038/s41558-019-0551-4.

Boeke, R. C., and P. C. Taylor, 2016: Evaluation of the Arctic surface radiation budget in CMIP5 models. *J. Geophys. Res. Atmos.*, **121**, 8525–8548, doi:10.1002/2016JD025099.

Boeke, R. C., and P. C. Taylor, 2018: Seasonal energy exchange in sea ice retreat regions contributes to differences in projected Arctic warming. *Nat. Commun.*, **9**, doi:10.1038/s41467-018-07061-9.

Boland, E. J. D., T. J. Bracegirdle, and E. F. Shuckburgh, 2016: Assessment of sea ice-atmosphere links in CMIP5 models. *Climate Dyn.*, **37**, doi:10.1007/s00382-016-3367-1.

Bracegirdle, T. J., and D. B. Stephenson, 2012: Higher precision estimates of regional polar warming by ensemble regression of climate model projections. *Climate Dyn.*, **39**, 2805–2821, doi:10.1007/s00382-012-1330-3.

Brayshaw, D. J., B. Hoskins, and M. Blackburn, 2008: The storm-track response to idealized SST perturbations in an aquaplanet GCM. *J. Atmos. Sci.*, **65**, 2842–2860, doi:10.1175/2008JAS2657.1.

Butchart, N., J. Austin, J. R. Knight, A. A. Scaife, and M. L. Gallani, 2000: The response of the stratospheric climate to projected changes in the concentrations of well-mixed greenhouse gases from 1992 to 2051. *J. Climate*, **13**, 2142–2159, doi:10.1175/1520-0442(2000)013<2142:TROTSC>2.0.CO;2.

Butler, A. H., J. P. Sjoberg, D. J. Seidel, and K. H. Rosenlof, 2017: A sudden stratospheric warming compendium. *Earth Syst. Sci. Data*, **9**, 63–76, doi:10.5194/essd-9-63-2017.

Butler, A. H., D. W. J. Thompson, and R. Heikes, 2010: The steady-state atmospheric circulation response to climate change–like thermal forcings in a simple general circulation model. *J. Climate*, **23**, 3474–3496, doi:10.1175/2010JCLI3228.1.

Cai, D., M. Dameris, H. Garny, and T. Runde, 2012: Implications of all season Arctic sea-ice anomalies on the stratosphere. *Atmos. Chem. Phys.*, **12**, 11 819–11 831, doi:10.5194/acp-12-11819-2012.

Capua, G. D., and D. Coumou, 2016: Changes in meandering of the Northern Hemisphere circulation. *Environ. Res. Lett.*, **11**, 094 028, doi:10.1088/1748-9326/11/9/094028.

Castanheira, J. M., and H. F. Graf, 2003: North Pacific-North Atlantic relationships under stratospheric control? *J. Geophys. Res.*, **108**, doi:10.1029/2002JD002754.

Cattiaux, J., and C. Cassou, 2013: Opposite CMIP3/CMIP5 trends in the wintertime Northern Annular Mode explained by combined local sea ice and remote tropical influences. *Geophys. Res. Lett.*, **40**, 3682–3687, doi:10.1002/grl.50643.

Cavalieri, D. J., and C. L. Parkinson, 2012: Arctic sea ice variability and trends, 1979-2010. *The Cryosphere*, **6**, 881–889, doi:10.5194/tc-6-881-2012.

Charlton, A. J., A. O'Neill, W. A. Lahoz, and A. C. Massacand, 2004: Sensitivity of tropospheric forecasts to stratospheric initial conditions. *Quart. J. Roy. Meteor. Soc.*, **130**, 1771–1792, doi:10.1256/qj.03.167.

Charlton, A. J., and L. M. Polvani, 2007: A new look at stratospheric sudden warmings. Part I: climatology and modeling benchmarks. *J. Climate*, **20**, 449–469, doi:10.1175/JCLI3996.1.

Charlton-Perez, A. J., L. M. Polvani, J. Austin, and F. Li, 2008: The frequency and dynamics of stratospheric sudden warmings in the 21st century. *J. Geophys. Res.*, **113**, D16116, doi:10.1029/2007JD009571.

Charney, J. G., and P. G. Drazin, 1961: Propagation of planetary-scale disturbances from the lower into the upper atmosphere. *J. Geophys. Res.*, **66**, 83–109, doi:10.1029/JZ066i001p00083.

Chen, H. W., R. B. Alley, and F. Zhang, 2016: Interannual Arctic sea ice variability and associated winter weather patterns: a regional perspective for 1979-2014. *J. Geophys. Res. Atmos.*, **121**, 14 433–14 455, doi:10.1002/2016JD024769.

Chen, L., J. Francis, and E. Hanna, 2018: The "Warm-Arctic/Cold-continents" pattern during 1901–2010. *Int. J. Climatol.*, **38**, 5245–5254, doi:10.1002/joc.5725.

Climate Central, 2019: 2018-19 winter temps compared to historic average. Available at: https://www.climatecentral.org/gallery/maps/2018-19-winter-temps-compared-to-historic-average [accessed August 2019].

Close, S., M.-N. Houssais, and C. Herbaut, 2017: The Arctic winter sea ice quadrupole revisited. *J. Climate*, **30**, 3157–3167, doi:10.1175/JCLI-D-16-0506.1.

Cohen, J., 2016: An observational analysis: Tropical relative to Arctic influence on midlatitude weather in the era of Arctic amplification. *Geophys. Res. Lett.*, **43**, 5287–5294, doi:10.1002/2016GL069102.

Cohen, J., K. Pfeiffer, and J. A. Francis, 2018: Warm Arctic episodes linked with increased frequency of extreme winter weather in the United States. *Nat. Commun.*, **9**, 869, doi:10.1038/s41467-018-02992-9.

Cohen, J., and Coauthors, 2014: Recent Arctic amplification and extreme mid-latitude weather. *Nat. Geosci.*, **7**, 627–637, doi:10.1038/ngeo2234.

Collins, M., and Coauthors, 2013: Long-term climate change: Projections, commitments and irreversibility. *Climate Change 2013: The Physical Science Basis. Contribution of Working Group I to the Fifth Assessment Report of the Intergovernmental Panel on Climate Change*, T. F. Stocker, D. Qin, G.-K. Plattner, M. Tignor, S. K. Allen, J. Boschung, A. Nauels, Y. Xia, V. Bex, and P. M. Midgley, Eds., Cambridge University Press, Cambridge, United Kingdom and New York, NY, USA, 1029–1136, doi:10.1017/CBO9781107415324.024.

Comiso, J. C., and F. Nishio, 2008: Trends in the sea ice cover using enhanced and compatible AMSR-E, SSM/I, and SMMR data. *J. Geophys. Res.*, **113**, C02S07, doi:10.1029/2007JC004257.

Dai, A., D. Luo, M. Song, and J. Liu, 2019: Arctic amplification is caused by sea-ice loss under increasing CO2. *Nat. Commun.*, **10**, doi:10.1038/s41467-018-07954-9.

Dee, D. P., and Coauthors, 2011: The ERA-Interim reanalysis: configuration and performance of the data assimilation system. *Quart. J. Roy. Meteor. Soc.*, **137**, 553–597, doi:10.1002/qj.828.

Deser, C., G. Magnusdottir, R. Saravanan, and A. Phillips, 2004: The effects of North Atlantic SST and sea ice anomalies on the winter circulation in CCM3. Part II: Direct and indirect components of the response. *J. Climate*, **17**, 877–889, doi:10.1175/1520-0442(2004)017<0877:TEONAS>2.0.CO;2.

Deser, C., A. Phillips, V. Bourdette, and H. Teng, 2012: Uncertainty in climate change projections: the role of internal variability. *Climate Dyn.*, **38**, 527–546, doi:10.1007/s00382-010-0977-x.

Deser, C., L. Sun, R. A. Tomas, and J. Screen, 2016a: Does ocean coupling matter for the northern extratropical response to projected Arctic sea ice loss? *Geophys. Res. Lett.*, **43**, 2149–2157, doi:10.1002/2016GL067792.

Deser, C., L. Terray, and A. S. Phillips, 2016b: Forced and internal components of winter air temperature trends over North America during the past 50 years: mechanisms and implications. *J. Climate*, **29**, 2237–2258, doi:10.1175/JCLI-D-15-0304.1.

Deser, C., R. Tomas, M. Alexander, and D. Lawrence, 2010: The seasonal atmospheric response to projected Arctic sea ice loss in the late twenty-first century. *J. Climate*, **23**, 333–351, doi:10.1175/2009JCLI3053.1.

Deser, C., R. A. Tomas, and S. Peng, 2007: The transient atmospheric circulation response to North Atlantic SST and sea ice anomalies. *J. Climate*, **20**, 4751–4767, doi:10.1175/JCLI4278.1.

Deser, C., R. A. Tomas, and L. Sun, 2015: The role of ocean–atmosphere coupling in the zonal-mean atmospheric response to Arctic sea ice loss. *J. Climate*, **28**, 2168–2186, doi:10.1175/JCLI-D-14-00325.1.

Deser, C., J. E. Walsh, and M. S. Timlin, 2000: Arctic sea ice variability in the context of recent atmospheric circulation trends. *J. Climate*, **13**, 617–633, doi:10.1175/1520-0442(2000)013<0617:ASIVIT>2.0.CO;2.

Dessler, A. E., Z. Zhang, and P. Yang, 2008: Water-vapor climate feedback inferred from climate fluctuations, 2003–2008. *Geophys. Res. Lett.*, **35**, L20704, doi:10.1029/2008GL035333.

Ding, Q., J. M. Wallace, D. S. Battisti, E. J. Steig, A. J. E. Gallant, H.-J. Kim, and L. Geng, 2014: Tropical forcing of the recent rapid Arctic warming in northeastern Canada and Greenland. *Nature*, **509**, 209–212, doi:10.1038/nature13260.

Ding, Q., and Coauthors, 2019: Fingerprints of internal drivers of Arctic sea ice loss in observations and model simulations. *Nat. Geosci.*, **12**, 28–33, doi:10.1038/s41561-018-0256-8.

Duan, L., L. Cao, and K. Caldeira, 2019: Estimating contributions of sea ice and land snow to climate feedback. *J. Geophys. Res. Atmos.*, **124**, 199–208, doi:10.1029/2018JD029093.

Dunstone, N., D. Smith, A. Scaife, L. Hermanson, R. Eade, N. Robinson, M. Andrews, and J. Knight, 2016: Skilful predictions of the winter North Atlantic Oscillation one year ahead. *Nat. Geosci.*, **9**, 809–814, doi:10.1038/ngeo2824.

Eade, R., D. Smith, A. Scaife, E. Wallace, N. Dunstone, L. Hermanson, and N. Robinson, 2014: Do seasonal-to-decadal climate predictions underestimate the predictability of the real world? *Geophys. Res. Lett.*, **41**, 5620–5628, doi:10.1002/2014GL061146.

Eichelberger, S. J., and D. L. Hartmann, 2007: Zonal jet structure and the leading mode of variability. *J. Climate*, **20**, 5149–5163, doi:10.1175/JCLI4279.1.

England, M., A. Jahn, and L. Polvani, 2019: Nonuniform contribution of internal variability to recent Arctic sea ice loss. *J. Climate*, **32**, 4039–4053, doi:10.1175/JCLI-D-18-0864.1.

England, M., L. Polvani, and L. Sun, 2018: Contrasting the Antarctic and Arctic atmospheric responses to projected sea ice loss in the late twenty-first century. *J. Climate*, **31**, 6353–6370, doi:10.1175/JCLI-D-17-0666.1.

Faraway, J. J., 2016: *Linear Models with R.* Chapman and Hall/CRC, Boca Raton, FL.

Francis, J. A., 2017: Why are Arctic linkages to extreme weather still up in the air? *Bull. Amer. Meteor. Soc.*, **98**, 2551–2557, doi:10.1175/BAMS-D-17-0006.1.

Francis, J. A., and S. J. Vavrus, 2012: Evidence linking Arctic amplification to extreme weather in mid-latitudes. *Geophys. Res. Lett.*, **39**, L06801, doi:10.1029/2012GL051000.

Francis, J. A., and S. J. Vavrus, 2015: Evidence for a wavier jet stream in response to rapid Arctic warming. *Environ. Res. Lett.*, **10**, 014 005, doi:10.1088/1748-9326/10/1/014005.

García-Serrano, J., C. Frankignoul, G. Gastineau, and A. Cámara, 2015: On the predictability of the winter Euro-Atlantic climate: lagged influence of autumn Arctic sea ice. *J. Climate*, **28**, 5195–5216, doi:10.1175/JCLI-D-14-00472.1.

Garfinkel, C. I., D. L. Hartmann, and F. Sassi, 2010: Tropospheric precursors of anomalous Northern Hemisphere stratospheric polar vortices. *J. Climate*, **23**, 3282–3299, doi:10.1175/2010JCLI3010.1.

Garfinkel, C. I., D. W. Waugh, and E. P. Gerber, 2013: The effect of tropospheric jet latitude on coupling between the stratospheric polar vortex and the troposphere. *J. Climate*, **26**, 2077–2095, doi:10.1175/JCLI-D-12-00301.1.

Gerber, E. P., and G. K. Vallis, 2007: Eddy–zonal flow interactions and the persistence of the zonal index. *J. Atmos. Sci.*, **64**, 3296–3311, doi:10.1175/JAS4006.1.

Gerber, E. P., S. Voronin, and L. M. Polvani, 2008: Testing the annular mode autocorrelation time scale in simple atmospheric general circulation models. *Mon. Wea. Rev.*, **136**, 1523–1536, doi:10.1175/2007MWR2211.1.

Gong, T., S. Feldstein, and S. Lee, 2017: The role of downward infrared radiation in the recent Arctic winter warming trend. *J. Climate*, **30**, 4937–4949, doi:10.1175/JCLI-D-16-0180.1.

Goosse, H., and Coauthors, 2018: Quantifying climate feedbacks in polar regions. *Nat. Commun.*, **9**, doi:10.1038/s41467-018-04173-0.

Gordon, N. D., A. K. Jonko, P. M. Forster, and K. M. Shell, 2013: An observationally based constraint on the water-vapor feedback. *J. Geophys. Res. Atmos.*, **118**, 12 435–12 443, doi:10.1002/2013JD020184.

Graff, L. S., and J. H. LaCasce, 2012: Changes in the extratropical storm tracks in response to changes in SST in an AGCM. *J. Climate*, **25**, 1854–1870, doi:10.1175/JCLI-D-11-00174.1.

Graham, T., and M. Vellinga, 2013: Heat budget of the upper Arctic ocean under a warming climate. *Climate Dyn.*, **40**, 143–153, doi:10.1007/s00382-012-1454-5.

Graversen, R. G., and M. Wang, 2009: Polar amplification in a coupled climate model with locked albedo. *Climate Dyn.*, **33**, 629–643, doi:10.1007/s00382-009-0535-6.

Greening, K., and A. Hodgson, 2019: Atmospheric analysis of the cold late February and early March 2018 over the UK. *Weather*, **74**, 79–85, doi:10.1002/wea.3467.

Guirguis, K., A. Gershunov, R. Schwartz, and S. Bennett, 2011: Recent warm and cold daily winter temperature extremes in the Northern Hemisphere. *Geophys. Res. Lett.*, **38**, L17701, doi:10.1029/2011GL048762.

Hamilton, K., 1998: Effects of an imposed Quasi-Biennial Oscillation in a comprehensive troposphere–stratosphere–mesosphere general circulation model. *J. Atmos. Sci.*, **55**, 2393–2418, doi:10.1175/1520-0469(1998)055<2393:EOAIQB>2.0.CO;2.

Harvey, B. J., L. C. Shaffrey, and T. J. Woollings, 2014: Equator-to-pole temperature differences and the extra-tropical storm track responses of the CMIP5 climate models. *Climate Dyn*, **43**, 1171–1182, doi:10.1007/s00382-013-1883-9.

Harvey, B. J., L. C. Shaffrey, and T. J. Woollings, 2015: Deconstructing the climate change response of the Northern Hemisphere wintertime storm tracks. *Climate Dyn.*, **45**, 2847–2860, doi:10.1007/s00382-015-2510-8.

Haynes, P. H., M. E. McIntyre, T. G. Shepherd, C. J. Marks, and K. P. Shine, 1991: On the "Downward Control" of extratropical diabatic circulations by eddy-induced mean zonal forces. *J. Atmos. Sci.*, **48**, 651–678, doi:10.1175/1520-0469(1991)048<0651:OTCOED>2.0.CO;2.

Held, I. M., 1975: Momentum transport by quasi-geostrophic eddies. *J. Atmos. Sci.*, **32**, 1494–1497, doi:10.1175/1520-0469(1975)032<1494:MTBQGE>2.0.CO;2.

Held, I. M., and A. Y. Hou, 1980: Nonlinear axially symmetric circulations in a nearly inviscid atmosphere. *J. Atmos. Sci.*, **37**, 515–533, doi:10.1175/1520-0469(1980)037<0515:NASCIA>2.0.CO;2.

Held, I. M., M. Ting, and H. Wang, 2002: Northern winter stationary waves: theory and modeling. *J. Climate*, **15**, 2125–2144, doi:10.1175/1520-0442(2002)015<2125:NWSWTA>2.0.CO;2.

Hitchcock, P., and P. H. Haynes, 2016: Stratospheric control of planetary waves. *Geophys. Res. Lett.*, **43**, 11 884–11 892, doi:10.1002/2016GL071372.

Hitchcock, P., and I. R. Simpson, 2014: The downward influence of stratospheric sudden warmings. *J. Atmos. Sci.*, **71**, 3856–3876, doi:10.1175/JAS-D-14-0012.1.

Hitchcock, P., and I. R. Simpson, 2016: Quantifying eddy feedbacks and forcings in the tropospheric response to stratospheric sudden warmings. *J. Atmos. Sci.*, **73**, 3641–3657, doi:10.1175/JAS-D-16-0056.1.

Holland, M. M., and C. M. Bitz, 2003: Polar amplification of climate change in coupled models. *Climate Dyn.*, **21**, 221–232, doi:10.1007/s00382-003-0332-6.

Holton, J. R., and G. J. Hakim, 2013: *An Introduction to Dynamic Meteorology*. Academic Press, Waltham, MA.

Honda, M., J. Inoue, and S. Yamane, 2009: Influence of low Arctic sea-ice minima on anomalously cold Eurasian winters. *Geophys. Res. Lett.*, **36**, L08707, doi:10.1029/2008GL037079.

Hoshi, K., J. Ukita, M. Honda, T. Nakamura, K. Yamazaki, Y. Miyoshi, and R. Jaiser, 2019: Weak stratospheric polar vortex events modulated by the Arctic sea-ice loss. *J. Geophys. Res. Atmos.*, **124**, 858–869, doi:10.1029/2018JD029222.

Hoskins, B. J., and I. N. James, 2014: *Fluid Dynamics of the Midlatitude Atmosphere*. Wiley Blackwell, 363–365 pp.

Hoskins, B. J., and D. J. Karoly, 1981: The steady linear response of a spherical atmosphere to thermal and orographic forcing. *J. Atmos. Sci.*, **38**, 1179–1196, doi:10.1175/1520-0469(1981)038<1179:TSLROA>2.0.CO;2.

Hoskins, B. J., and A. J. Simmons, 1975: A multilayer spectral model and the semi-implicit method. *Quart. J. Roy. Meteor. Soc.*, **101**, 637–655, doi:10.1002/qj.49710142918.

Inoue, J., M. E. Hori, and K. Takaya, 2012: The role of Barents Sea ice in the wintertime cyclone track and emergence of a Warm-Arctic Cold-Siberian anomaly. *J. Climate*, **25**, 2561–2568, doi:10.1175/JCLI-D-11-00449.1.

Jaiser, R., K. Dethloff, and D. Handorf, 2013: Stratospheric response to Arctic sea ice retreat and associated planetary wave propagation changes. *Tellus A*, **65**, doi:10.3402/tellusa.v65i0.19375.

Jaiser, R., K. Dethloff, D. Handorf, A. Rinke, and J. Cohen, 2012: Impact of sea ice cover changes on the Northern Hemisphere atmospheric winter circulation. *Tellus A*, **64**, doi:10.3402/tellusa.v64i0.11595.

Jaiser, R., T. Nakamura, D. Handorf, K. Dethloff, J. Ukita, and K. Yamazaki, 2016: Atmospheric winter response to Arctic sea ice changes in reanalysis data and model simulations. *J. Geophys. Res. Atmos.*, **121**, 7564–7577, doi:10.1002/2015JD024679.

Joshi, M., M. Stringer, K. Wiel, A. O'Callaghan, and S. Fueglistaler, 2015: IGCM4: a fast, parallel and flexible intermediate climate model. *Geosci. Model Dev.*, **8**, 1157–1167, doi:10.5194/gmd-8-1157-2015.

Kay, J. E., T. L'Ecuyer, H. Chepfer, N. Loeb, A. Morrison, and G. Cesana, 2016: Recent advances in Arctic cloud and climate research. *Curr. Clim. Change Rep.*, **2**, 159–169, doi:10.1007/s40641-016-0051-9.

Kim, B.-M., S.-W. Son, S.-K. Min, J.-H. Jeong, S.-J. Kim, X. Zhang, T. Shim, and J.-H. Yoon, 2014: Weakening of the stratospheric polar vortex by Arctic sea-ice loss. *Nat. Commun.*, **5**, 4646, doi:10.1038/ncomms5646.

King, M. P., M. Hell, and N. Keenlyside, 2016: Investigation of the atmospheric mechanisms related to the autumn sea ice and winter circulation link in the Northern Hemisphere. *Climate Dyn.*, **46**, 1185–1195, doi:10.1007/s00382-015-2639-5.

Koenigk, T., M. Caian, G. Nikulin, and S. Schimanke, 2016: Regional Arctic sea ice variations as predictor for winter climate conditions. *Climate Dyn.*, **46**, 317–337, doi:10.1007/s00382-015-2586-1.

Kretschmer, M., D. Coumou, L. Agel, M. Barlow, E. Tziperman, and J. Cohen, 2018: More-persistent weak stratospheric polar vortex states linked to cold extremes. *Bull. Amer. Meteor. Soc.*, **99**, 49–60, doi:10.1175/BAMS-D-16-0259.1.

Kretschmer, M., D. Coumou, J. F. Donges, and J. Runge, 2016: Using Causal Effect Networks to analyze different Arctic drivers of midlatitude winter circulation. *J. Climate*, **29**, 4069–4081, doi:10.1175/JCLI-D-15-0654.1.

Kubo, R., 1966: The fluctuation-dissipation theorem. *Reports on Progress in Physics*, **29**, 255–284, doi:10.1088/0034-4885/29/1/306.

Kug, J.-S., J.-H. Jeong, Y.-S. Jang, B.-M. Kim, C. K. Folland, S.-K. Min, and S.-W. Son, 2015: Two distinct influences of Arctic warming on cold winters over North America and East Asia. *Nat. Geosci.*, **8**, 759–762, doi:10.1038/ngeo2517.

Kutzbach, J. E., 1970: Large-scale features of monthly mean Northern Hemisphere anomaly maps of sea-level pressure. *Mon. Wea. Rev.*, **98**, 708–716, doi:10.1175/1520-0493(1970)098<0708:LSFOMM>2.3.CO;2.

Labe, Z., Y. Peings, and G. Magnusdottir, 2019: The effect of QBO phase on the atmospheric response to projected Arctic sea ice loss in early winter. *Geophys. Res. Lett.*, **46**, 7663–7671, doi:10.1029/2019GL083095.

Lee, S., T. Gong, N. Johnson, S. B. Feldstein, and D. Pollard, 2011: On the possible link between tropical convection and the Northern Hemisphere Arctic surface air temperature change between 1958 and 2001. *J. Climate*, **24**, 4350–4367, doi:10.1175/2011JCLI4003.1.

Lee, S., and H.-k. Kim, 2003: The dynamical relationship between subtropical and eddy-driven jets. *J. Atmos. Sci.*, **60**, 1490–1503, doi:10.1175/1520-0469(2003)060<1490:TDRBSA>2.0.CO;2.

Leith, C. E., 1975: Climate response and fluctuation dissipation. *J. Atmos. Sci.*, **32**, 2022–2026, doi:10.1175/1520-0469(1975)032<2022:CRAFD>2.0.CO;2.

Li, C., and J. J. Wettstein, 2012: Thermally driven and eddy-driven jet variability in reanalysis. *J. Climate*, **25**, 1587–1596, doi:10.1175/JCLI-D-11-00145.1.

Li, J., F. Zheng, C. Sun, J. Feng, and J. Wang, 2019: Pathways of influence of the Northern Hemisphere mid-high latitudes on East Asian climate: a review. *Adv. Atmos. Sci.*, **36**, 902–921, doi:10.1007/s00376-019-8236-5.

Limpasuvan, V., and D. L. Hartmann, 2000: Wave-maintained annular modes of climate variability. *J. Climate*, **13**, 4414–4429, doi:10.1175/1520-0442(2000)013<4414:WMAMOC>2.0.CO;2.

Lindzen, R. S., and A. V. Hou, 1988: Hadley circulations for zonally averaged heating centered off the equator. *J. Atmos. Sci.*, **45**, 2416–2427, doi:10.1175/1520-0469(1988)045<2416:HCFZAH>2.0.CO;2.

Liu, Y., J. R. Key, A. Schweiger, and J. Francis, 2006: Characteristics of satellite-derived clear-sky atmospheric temperature inversion strength in the Arctic, 1980–96. *J. Climate*, **19**, 4902–4913, doi:10.1175/JCLI3915.1.

Lorenz, E. N., 1951: Seasonal and irregular variations of the Northern Hemisphere sea-level pressure profile. *J. Meteor.*, **8**, 52–59, doi:10.1175/1520-0469(1951)008<0052:SAIVOT>2.0.CO;2.

Luo, D., Y. Xiao, Y. Yao, A. Dai, I. Simmonds, and C. L. E. Franzke, 2016: Impact of Ural blocking on winter Warm Arctic–Cold Eurasian anomalies. Part I: blocking-induced amplification. *J. Climate*, **29**, 3925–3947, doi:10.1175/JCLI-D-15-0611.1.

Magnusdottir, G., C. Deser, and R. Saravanan, 2004: The effects of North Atlantic SST and sea ice anomalies on the winter circulation in CCM3. Part I: main features and storm track characteristics of the response. *J. Climate*, **17**, 857–876, doi:10.1175/1520-0442(2004)017<0857:TEONAS>2.0.CO;2.

Manabe, S., and R. Wetherald, 1975: The effects of doubling the CO2 concentration on the climate of a general circulation model. *J. Atmos. Sci.*, **32**, 3–15, doi:10.1175/1520-0469(1975)032<0003:TEODTC>2.0.CO;2.

Matsuno, T., 1970: Vertical propagation of stationary planetary waves in the winter Northern Hemisphere. *J. Atmos. Sci.*, **27**, 871–883, doi:10.1175/1520-0469(1970)027<0871:VPOSPW>2.0.CO;2.

Matsuno, T., 1971: A dynamical model of the stratospheric sudden warming. *J. Atmos. Sci.*, **28**, 1479–1494, doi:10.1175/1520-0469(1971)028<1479:ADMOTS>2.0.CO;2.

May, W., and L. Bengtsson, 1998: The signature of ENSO in the Northern Hemisphere midlatitude seasonal mean flow and high-frequency intraseasonal variability. *Meteorology and Atmospheric Physics*, **69**, 81–100, doi:10.1007/BF01025185.

McCusker, K. E., J. C. Fyfe, and M. Sigmond, 2016: Twenty-five winters of unexpected Eurasian cooling unlikely due to Arctic sea-ice loss. *Nat. Geosci.*, **9**, 838–842, doi:10.1038/ngeo2820.

McCusker, K. E., P. J. Kushner, J. C. Fyfe, M. Sigmond, V. V. Kharin, and C. M. Bitz, 2017: Remarkable separability of circulation response to Arctic sea ice loss and greenhouse gas forcing. *Geophys. Res. Lett.*, **44**, 7955–7964, doi:10.1002/2017GL074327.

McGraw, M. C., and E. A. Barnes, 2016: Seasonal sensitivity of the eddy-driven jet to tropospheric heating in an idealized AGCM. *J. Climate*, **29**, 5223–5240, doi:10.1175/JCLI-D-15-0723.1.

McIntyre, M. E., and T. N. Palmer, 1983: Breaking planetary waves in the stratosphere. *Nature*, **305**, 593–600, doi:10.1038/305593a0.

McIntyre, M. E., and T. N. Palmer, 1984: The 'surf zone' in the stratosphere. *J. Atmos. Terr. Phys.*, **46**, 825–849, doi:10.1016/0021-9169(84)90063-1.

McIntyre, M. E., and T. N. Palmer, 1985: A note on the general concept of wave breaking for Rossby and gravity waves. *Pure Appl. Geophys.*, **123**, 964–975, doi:10.1007/BF00876984.

McKenna, C. M., T. J. Bracegirdle, E. F. Shuckburgh, P. H. Haynes, and M. M. Joshi, 2018: Arctic sea ice loss in different regions leads to contrasting Northern Hemisphere impacts. *Geophys. Res. Lett.*, **45**, 945–954, doi:10.1002/2017GL076433.

McLandress, C., and T. G. Shepherd, 2009: Impact of climate change on stratospheric sudden warmings as simulated by the Canadian Middle Atmosphere Model. *J. Climate*, **22**, 5449–5463, doi:10.1175/2009JCLI3069.1.

Met Office, 2018: March statistics may challenge your perception. Available at: https://www.metoffice.gov.uk/about-us/press-office/news/weather-and-climate/2018/march-statistics [accessed August 2019].

Mitchell, D. M., S. M. Osprey, L. J. Gray, N. Butchart, S. C. Hardiman, A. J. Charlton-Perez, and P. Watson, 2012: The effect of climate change on the variability of the Northern Hemisphere stratospheric polar vortex. *J. Atmos. Sci.*, **69**, 2608–2618, doi:10.1175/JAS-D-12-021.1.

Mitchell, J. F. B., C. A. Senior, and W. J. Ingram, 1989: CO2 and climate: a missing feedback? *Nature*, **341**, 132–134, doi:10.1038/341132a0.

Mori, M., Y. Kosaka, M. Watanabe, H. Nakamura, and M. Kimoto, 2019: A reconciled estimate of the influence of Arctic sea-ice loss on recent Eurasian cooling. *Nat. Climate Change*, **9**, 123–129, doi:10.1038/s41558-018-0379-3.

Mori, M., M. Watanabe, H. Shiogama, J. Inoue, and M. Kimoto, 2014: Robust Arctic sea-ice influence on the frequent Eurasian cold winters in past decades. *Nat. Geosci.*, **7**, 869–873, doi:10.1038/ngeo2277.

Nakamura, T., K. Yamazaki, M. Honda, J. Ukita, R. Jaiser, D. Handorf, and K. Dethloff, 2016a: On the atmospheric response experiment to a Blue Arctic Ocean. *Geophys. Res. Lett.*, **43**, 10 394–10 402, doi:10.1002/2016GL070526.

Nakamura, T., K. Yamazaki, K. Iwamoto, M. Honda, Y. Miyoshi, Y. Ogawa, Y. Tomikawa, and J. Ukita, 2016b: The stratospheric pathway for Arctic impacts on midlatitude climate. *Geophys. Res. Lett.*, **43**, 3494–3501, doi:10.1002/2016GL068330.

Nakamura, T., K. Yamazaki, K. Iwamoto, M. Honda, Y. Miyoshi, Y. Ogawa, and J. Ukita, 2015: A negative phase shift of the winter AO/NAO due to the recent Arctic sea-ice reduction in late autumn. *J. Geophys. Res. Atmos.*, **120**, 3209–3227, doi:10.1002/2014JD022848.

Nakamura, T., K. Yamazaki, T. Sato, and J. Ukita, 2019: Memory effects of Eurasian land processes cause enhanced cooling in response to sea ice loss. *Nat. Commun.*, **10**, doi:10.1038/s41467-019-13124-2.

Nishii, K., H. Nakamura, and T. Miyasaka, 2009: Modulations in the planetary wave field induced by upward-propagating Rossby wave packets prior to stratospheric sudden warming events: a case-study. *Quart. J. Roy. Meteor. Soc.*, **135**, 36–51, doi:10.1002/qj.359.

Notz, D., and J. Stroeve, 2016: Observed Arctic sea-ice loss directly follows anthropogenic CO2 emission. *Science*, **354**, 747–750, doi:10.1126/science.aag2345.

NSIDC, 2016a: Arctic sea ice news and analysis: yearly archives: 2016. Available at: http://nsidc.org/arcticseaicenews/2016/ [accessed December 2017].

NSIDC, 2016b: Rapid ice growth follows the seasonal minimum, rapid drop in Antarctic extent. Available at: http://nsidc.org/arcticseaicenews/2016/10/rapid-ice-growth-follows-the-seasonal-minimum-rapid-drop-in-antarctic-extent/ [accessed December 2017].

NSIDC, 2018a: 2018 winter Arctic sea ice: Bering down. Available at: http://nsidc.org/arcticseaicenews/2018/04/2018-winter-arctic-sea-ice-bering-down/ [accessed August 2019].

NSIDC, 2018b: A warm approach to the equinox. Available at: http://nsidc.org/arcticseaicenews/2018/03/a-warm-approach-to-the-equinox/ [accessed August 2019].

NSIDC, 2018c: Sea ice tracking low in both hemispheres. Available at: http://nsidc.org/arcticseaicenews/2018/02/sea-ice-tracking-low-in-both-hemispheres/ [accessed August 2019].

NSIDC, 2019: Chartic interactive sea ice graph. Available at: https://nsidc.org/arcticseaicenews/charctic-interactive-sea-ice-graph/ [accessed July 2019].

O'Callaghan, A., M. Joshi, D. Stevens, and D. Mitchell, 2014: The effects of different sudden stratospheric warming type on the ocean. *Geophys. Res. Lett.*, **41**, 7739–7745, doi:10.1002/2014GL062179.

Ogawa, F., and Coauthors, 2018: Evaluating impacts of recent Arctic sea ice loss on the Northern Hemisphere winter climate change. *Geophys. Res. Lett.*, **45**, 3255–3263, doi:10.1002/2017GL076502.

Onarheim, I. H., T. Eldevik, L. H. Smedsrud, and J. C. Stroeve, 2018: Seasonal and regional manifestation of Arctic sea ice loss. *J. Climate*, **31**, 4917–4932, doi:10.1175/JCLI-D-17-0427.1.

Orsolini, Y. J., R. Senan, R. E. Benestad, and A. Melsom, 2012: Autumn atmospheric response to the 2007 low Arctic sea ice extent in coupled ocean–atmosphere hindcasts. *Climate Dyn.*, **38**, 2437–2448, doi:10.1007/s00382-011-1169-z.

Osborn, T. J., 2011: Winter 2009/2010 temperatures and a recordbreaking North Atlantic Oscillation index. *Weather*, **66**, 19–21, doi:10.1002/wea.660.

Osborn, T. J., K. R. Briffa, S. F. B. Tett, P. D. Jones, and R. M. Trigo, 1999: Evaluation of the North Atlantic Oscillation as simulated by a coupled climate model. *Climate Dyn.*, **15**, 685–702, doi:10.1007/s003820050310.

Osborne, J. M., J. A. Screen, and M. Collins, 2017: Ocean–atmosphere state dependence of the atmospheric response to Arctic sea ice loss. *J. Climate*, **30**, 1537–1552, doi:10.1175/JCLI-D-16-0531.1.

Oudar, T., E. Sanchez-Gomez, F. Chauvin, J. Cattiaux, L. Terray, and C. Cassou, 2017: Respective roles of direct GHG radiative forcing and induced Arctic sea ice loss on the Northern Hemisphere atmospheric circulation. *Climate Dyn.*, **49**, 3693–3713, doi:10.1007/s00382-017-3541-0.

Overland, J. E., K. R. Wood, and M. Wang, 2011: Warm Arctic–cold continents: climate impacts of the newly open Arctic sea. *Polar Res.*, **30**, 15 787, doi:10.3402/polar.v30i0.15787.

Overland, J. E., and Coauthors, 2016: Nonlinear response of mid-latitude weather to the changing Arctic. *Nat. Climate Change*, **6**, 992–999, doi:10.1038/nclimate3121.

Palmer, T. N., 1981: Diagnostic study of a wavenumber-2 stratospheric sudden warming in a transformed Eulerian-mean formalism. *J. Atmos. Sci.*, **38**, 844–855, doi:10.1175/1520-0469(1981)038<0844:DSOAWS>2.0.CO;2.

Panetta, R. L., 1993: Zonal jets in wide baroclinically unstable regions: persistence and scale selection. *J. Atmos. Sci.*, **50**, 2073–2106, doi:10.1175/1520-0469(1993)050<2073:ZJIWBU>2.0.CO;2.

Pedersen, R. A., I. Cvijanovic, P. L. Langen, and B. M. Vinther, 2016: The impact of regional Arctic sea ice loss on atmospheric circulation and the NAO. *J. Climate*, **29**, 889–902, doi:10.1175/JCLI-D-15-0315.1.

Peings, Y., and G. Magnusdottir, 2014: Response of the wintertime Northern Hemisphere atmospheric circulation to current and projected Arctic sea-ice decline: a numerical study with CAM5. *J. Climate*, **27**, 244–264, doi:10.1175/JCLI-D-13-00272.1.

Perlwitz, J., and H. F. Graf, 2001: Troposphere-stratosphere dynamic coupling under strong and weak polar vortex conditions. *Geophys. Res. Lett.*, **28**, 271–274, doi:10.1029/2000GL012405.

Petoukhov, V., and V. A. Semenov, 2010: A link between reduced Barents-Kara sea ice and cold winter extremes over northern continents. *J. Geophys. Res.*, **115**, D21111, doi:10.1029/2009JD013568.

Pithan, F., and T. Mauritsen, 2014: Arctic amplification dominated by temperature feedbacks in contemporary climate models. *Nat. Geosci.*, **7**, 181–184, doi:10.1038/ngeo2071.

Plumb, R. A., 1985: On the three-dimensional propagation of stationary waves. *J. Atmos. Sci.*, **42**, 217–229, doi:10.1175/1520-0469(1985)042,0217:OTTDPO.2.0.CO;2.

Polvani, L. M., L. Sun, A. H. Butler, J. H. Richter, and C. Deser, 2017: Distinguishing stratospheric sudden warmings from ENSO as key drivers of wintertime climate variability over the North Atlantic and Eurasia. *J. Climate*, **30**, 1959–1969, doi:10.1175/JCLI-D-16-0277.1.

Räisänen, J., 2007: How reliable are climate models? *Tellus A*, **59**, 2–29, doi:10.1111/j.1600-0870.2006.00211.x.

Rhines, P. B., 1975: Waves and turbulence on a β-plane. *J. Fluid Mech.*, **69**, 417–443, doi:10.1017/S0022112075001504.

Ronalds, B., E. Barnes, and P. Hassanzadeh, 2018: A barotropic mechanism for the response of jet stream variability to Arctic amplification and sea ice loss. *J. Climate*, **31**, 7069–7085, doi:10.1175/JCLI-D-17-0778.1.

Ruggieri, P., R. Buizza, and G. Visconti, 2016: On the link between Barents-Kara sea ice variability and European blocking. *J. Geophys. Res. Atmos.*, **121**, 5664–5679, doi:10.1002/2015JD024021.

Ruggieri, P., F. Kucharski, and L. Novak, 2019: The response of the midlatitude jet to regional polar heating in a simple storm-track model. *J. Climate*, **32**, 2869–2885, doi:10.1175/JCLI-D-18-0257.1.

Scaife, A. A., and D. Smith, 2018: A signal-to-noise paradox in climate science. *npj Clim. Atmos. Sci.*, **1**, doi:10.1038/s41612-018-0038-4.

Scaife, A. A., and Coauthors, 2014: Skillful long-range prediction of European and North American winters. *Geophys. Res. Lett.*, **41**, 2514–2519, doi:10.1002/2014GL059637.

Scaife, A. A., and Coauthors, 2019: Does increased atmospheric resolution improve seasonal climate predictions? *Atmos. Sci. Lett.*, **20**, doi:10.1002/asl.922.

Schenzinger, V., S. Osprey, L. Gray, and N. Butchart, 2017: Defining metrics of the Quasi-Biennial Oscillation in global climate models. *Geosci. Model Dev.*, **10**, 2157–2168, doi:10.5194/gmd-10-2157-2017.

Scinocca, J. F., M. C. Reader, D. A. Plummer, M. Sigmond, P. J. Kushner, T. G. Shepherd, and R. Ravishankara, 2009: Impact of sudden Arctic sea-ice loss on stratospheric polar ozone recovery. *Geophys. Res. Lett.*, **36**, L24701, doi:10.1029/2009GL041239.

Screen, J. A., 2014: Arctic amplification decreases temperature variance in northern mid- to high-latitudes. *Nat. Climate Change*, **4**, 577–582, doi:10.1038/nclimate2268.

Screen, J. A., 2017a: The missing Northern European winter cooling response to Arctic sea ice loss. *Nat. Commun.*, **8**, 14603, doi:10.1038/ncomms14603.

Screen, J. A., 2017b: Simulated atmospheric response to regional and pan-Arctic sea-ice loss. *J. Climate*, **30**, 3945–3962, doi:10.1175/JCLI-D-16-0197.1.

Screen, J. A., and R. Blackport, 2019: Is sea-ice-driven Eurasian cooling too weak in models? *Nat. Climate Change*, **9**, 934–936, doi:10.1038/s41558-019-0635-1.

Screen, J. A., T. J. Bracegirdle, and I. Simmonds, 2018a: Polar climate change as manifest in atmospheric circulation. *Curr. Clim. Change Rep.*, **4**, 383–395, doi:10.1007/s40641-018-0111-4.

Screen, J. A., C. Deser, and I. Simmonds, 2012: Local and remote controls on observed Arctic warming. *Geophys. Res. Lett.*, **39**, L10709, doi:10.1029/2012GL051598.

Screen, J. A., C. Deser, I. Simmonds, and R. Tomas, 2014: Atmospheric impacts of Arctic sea-ice loss, 1979–2009: separating forced change from atmospheric internal variability. *Climate Dyn.*, **43**, 333–344, doi:10.1007/s00382-013-1830-9.

Screen, J. A., C. Deser, and L. Sun, 2015: Reduced risk of North American cold extremes due to continued Arctic sea ice loss. *Bull. Amer. Meteor. Soc.*, **96**, 1489–1503, doi:10.1175/BAMS-D-14-00185.1.

Screen, J. A., and I. Simmonds, 2010: The central role of diminishing sea ice in recent Arctic temperature amplification. *Nature*, **464**, 1334–1337, doi:10.1038/nature09051.

Screen, J. A., and I. Simmonds, 2013: Exploring links between Arctic amplification and mid-latitude weather. *Geophys. Res. Lett.*, **40**, L09501, doi:10.1002/grl.50174.

Screen, J. A., and I. Simmonds, 2014: Amplified mid-latitude planetary waves favour particular regional weather extremes. *Nat. Climate Change*, **4**, 704–709, doi:10.1038/nclimate2271.

Screen, J. A., I. Simmonds, C. Deser, and R. Tomas, 2013: The atmospheric response to three decades of observed Arctic sea ice loss. *J. Climate*, **26**, 1230–1248, doi:10.1175/JCLI-D-12-00063.1.

Screen, J. A., and Coauthors, 2018b: Consistency and discrepancy in the atmospheric response to Arctic sea-ice loss across climate models. *Nat. Geosci.*, **11**, 155–163, doi:10.1038/s41561-018-0059-y.

Seierstad, I. A., and J. Bader, 2009: Impact of a projected future Arctic sea sce reduction on extratropical storminess and the NAO. *Climate Dyn.*, **33**, 937–943, doi:10.1007/s00382-008-0463-x.

Sellevold, R., S. Sobolowski, and C. Li, 2016: Investigating possible Arctic–midlatitude teleconnections in a linear framework. *J. Climate*, **29**, 7329–7343, doi:10.1175/JCLI-D-15-0902.1.

Serreze, M. C., A. P. Barrett, J. C. Stroeve, D. N. Kindig, and M. M. Holland, 2009: The emergence of surface-based Arctic amplification. *Cryosphere*, **3**, 11–19, doi:10.5194/tc-3-11-2009.

Serreze, M. C., and R. G. Barry, 2011: Processes and impacts of Arctic amplification: a research synthesis. *Glob. Planet. Change*, **77**, 85–96, doi:10.1016/j.gloplacha.2011.03.004.

Serreze, M. C., J. D. Kahl, and R. C. Schnell, 1992: Low-level temperature inversions of the Eurasian Arctic and comparisons with Soviet drifting station data. *J. Climate*, **5**, 615–629, doi:10.1175/1520-0442(1992)005<0615:LLTIOT>2.0.CO;2.

Seviour, W. J. M., 2017: Weakening and shift of the Arctic stratospheric polar vortex: internal variability or forced response? *Geophys. Res. Lett.*, **44**, 3365–3373, doi:10.1002/2017GL073071.

Shaw, T. A., and Coauthors, 2016: Storm track processes and the opposing influences of climate change. *Nat. Geosci.*, **9**, 656–664, doi:10.1038/ngeo2783.

Shepherd, T. G., 2014: Atmospheric circulation as a source of uncertainty in climate change projections. *Nat. Geosci.*, **7**, 703–708, doi:10.1038/ngeo2253.

Shepherd, T. G., 2016: Effects of a warming Arctic. *Science*, **353**, 989–990, doi:10.1126/science.aag2349.

Simpson, I., P. Hitchcock, T. G. Shepherd, and J. F. Scinocca, 2011: Stratospheric variability and tropospheric annular-mode timescales. *Geophys. Res. Lett.*, **38**, L20806, doi:10.1029/2011GL049304.

Simpson, I. R., M. Blackburn, J. D. Haigh, and S. N. Sparrow, 2010: The impact of the state of the troposphere on the response to stratospheric heating in a simplified GCM. *J. Climate*, **23**, 6166–6185, doi:10.1175/2010JCLI3792.1.

Simpson, I. R., and L. M. Polvani, 2016: Revisiting the relationship between jet position, forced response, and annular mode variability in the southern midlatitudes. *Geophys. Res. Lett.*, **43**, 2896–2903, doi:10.1002/2016GL067989.

Singarayer, J. S., J. L. Bamber, and P. J. Valdes, 2006: Twenty-First-Century climate impacts from a declining Arctic sea ice cover. *J. Climate*, **19**, 1109–1125, doi:10.1175/JCLI3649.1.

Smith, D. M., N. J. Dunstone, A. A. Scaife, E. K. Fiedler, D. Copsey, and S. C. Hardiman, 2017: Atmospheric response to Arctic and Antarctic sea ice: the importance of ocean-atmosphere coupling and the background state. *J. Climate*, **30**, 4547–4565, doi:10.1175/JCLI-D-16-0564.1.

Smith, D. M., and Coauthors, 2019: The Polar Amplification Model Intercomparison Project (PAMIP) contribution to CMIP6: investigating the causes and consequences of polar amplification. *Geosci. Model Dev*, **12**, 1139–1164, doi:10.5194/gmd-12-1139-2019.

Smith, K. L., C. G. Fletcher, and P. J. Kushner, 2010: The role of linear interference in the annular mode response to extratropical surface forcing. *J. Climate*, **23**, 6036–6050, doi:10.1175/2010JCLI3606.1.

Song, Y., and W. A. Robinson, 2004: Dynamical mechanisms for stratospheric influences on the troposphere. *J. Atmos. Sci.*, **61**, 1711–1725, doi:10.1175/1520-0469(2004)061<1711:DMFSIO>2.0.CO;2.

Spielhagen, R. F., and Coauthors, 2011: Enhanced modern heat transfer to the Arctic by warm Atlantic Water. *Science*, **331**, 450–453, doi:10.1126/science.1197397.

Stroeve, J., and D. Notz, 2018: Changing state of Arctic sea ice across all seasons. *Environ. Res. Lett.*, **13**, 103001, doi:10.1088/1748-9326/aade56.

Stroeve, J. C., V. Kattsov, A. Barrett, M. Serreze, T. Pavlova, M. Holland, and W. N. Meier, 2012: Trends in Arctic sea ice extent from CMIP5, CMIP3 and observations. *Geophys. Res. Lett.*, **39**, L16502, doi:10.1029/2012GL052676.

Sun, J., and B. Tan, 2013: Mechanism of the wintertime Aleutian Low-Icelandic Low seesaw. *Geophys. Res. Lett.*, **40**, 4103–4108, doi:10.1002/grl.50770.

Sun, L., C. Deser, L. M. Polvani, and R. Tomas, 2014: Influence of projected Arctic sea ice loss on polar stratospheric ozone and circulation in spring. *Environ. Res. Lett.*, **9**, 084016, doi:10.1088/1748-9326/9/8/084016.

Sun, L., C. Deser, and R. A. Tomas, 2015: Mechanisms of stratospheric and tropospheric circulation response to projected Arctic sea ice loss. *J. Climate*, **28**, 7824–7845, doi:10.1175/JCLI-D-15-0169.1.

Sun, L., J. Perlwitz, and M. Hoerling, 2016: What caused the recent "Warm Arctic, Cold Continents" trend pattern in winter temperatures? *Geophys. Res. Lett.*, **43**, 5345–5352, doi:10.1002/2016GL069024.

Taylor, K. E., R. J. Stouffer, and G. A. Meehl, 2012: An overview of CMIP5 and the experiment design. *Bull. Amer. Meteor. Soc.*, **93**, 485–498, doi:10.1175/bams-d-11-00094.1.

Taylor, P. C., M. Cai, A. Hu, J. Meehl, W. Washington, and G. J. Zhang, 2013: A decomposition of feedback contributions to polar warming amplification. *J. Climate*, **26**, 7023–7043, doi:10.1175/JCLI-D-12-00696.1.

Thompson, D. W. J., and T. Birner, 2012: On the linkages between the tropospheric isentropic slope and eddy fluxes of heat during Northern Hemisphere winter. *J. Atmos. Sci.*, **69**, 1811–1823, doi:10.1175/JAS-D-11-0187.1.

Thompson, D. W. J., and J. M. Wallace, 1998: The Arctic Oscillation signature in the wintertime geopotential height and temperature fields. *Geophys. Res. Lett.*, **25**, 1297–1300, doi:10.1029/98GL00950.

Thompson, D. W. J., and J. M. Wallace, 2000: Annular modes in the extratropical circulation. Part I: month-to-month variability. *J. Climate*, **13**, 1000–1016, doi:10.1175/1520-0442(2000)013<1000:AMITEC>2.0.CO;2.

Thorncroft, C. D., B. J. Hoskins, and M. E. McIntyre, 1993: Two paradigms of baroclinic-wave life-cycle behaviour. *Quart. J. Roy. Meteor. Soc.*, **119**, 17–55, doi:10.1002/qj.49711950903.

Ukita, J., M. Honda, H. Nakamura, Y. Tachibana, D. J. Cavalieri, C. L. Parkinson, H. Koide, and K. Yamamoto, 2007: Northern Hemisphere sea ice variability: lag structure and its implications. *Tellus A*, **59**, 261–272, doi:10.1111/j.1600-0870.2006.00223.x.

Uppala, S. M., and Coauthors, 2005: The ERA-40 re-analysis. *Quart. J. Roy. Meteor. Soc.*, **131**, 2961–3012, doi:10.1256/qj.04.176.

Van Oldenborgh, G. J., R. Haarsma, H. De Vries, and M. R. Allen, 2015: Cold extremes in North America vs. mild weather in Europe: the winter of 2013-14 in the context of a warming world. *Bull. Amer. Meteor. Soc.*, **96**, 707–714, doi:10.1175/BAMS-D-14-00036.1.

Vaughan, D. G., and Coauthors, 2013: Observations: Cryosphere. *Climate Change 2013: The Physical Science Basis. Contribution of Working Group I to the Fifth Assessment Report of the Intergovernmental Panel on Climate Change*, T. F. Stocker, D. Qin, G.-K. Plattner, M. Tignor, S. K. Allen, J. Boschung, A. Nauels, Y. Xia, V. Bex, and P. M. Midgley, Eds., Cambridge University Press, Cambridge, United Kingdom and New York, NY, USA, 317–382, doi:10.1017/CBO9781107415324.012.

Vavrus, S., 2004: The impact of cloud feedbacks on Arctic climate under greenhouse forcing. *J. Climate*, **17**, 603–615, doi:10.1175/1520-0442(2004)017<0603:TIOCFO>2.0.CO;2.

von Storch, H., and F. W. Zwiers, 1999: *Statistical Analysis in Climate Research*. Cambridge University Press, Cambridge UK.

Wallace, J. M., and D. S. Gutzler, 1981: Teleconnections in the geopotential height field during the Northern Hemisphere winter. *Mon. Wea. Rev.*, **109**, 784–812, doi:10.1175/1520-0493(1981)109<0784:TITGHF>2.0.CO;2.

Winter, B., and M. S. Bourqui, 2011: Sensitivity of the stratospheric circulation to the latitude of thermal surface forcing. *J. Climate*, **24**, 5397–5415, doi:10.1175/2011JCLI4006.1.

Wu, Y., and K. L. Smith, 2016: Response of Northern Hemisphere midlatitude circulation to Arctic amplification in a simple atmospheric general circulation model. *J. Climate*, **29**, 2041–2058, doi:10.1175/JCLI-D-15-0602.1.

Yang, X. Y., X. Yuan, and M. Ting, 2016: Dynamical link between the Barents-Kara sea ice and the Arctic Oscillation. *J. Climate*, **29**, 5103–5122, doi:10.1175/JCLI-D-15-0669.1.

Yao, Y., D. Luo, A. Dai, and I. Simmonds, 2017: Increased quasi stationarity and persistence of winter Ural blocking and Eurasian extreme cold events in response to Arctic warming. Part I: insights from observational analyses. *J. Climate*, **30**, 3549–3568, doi:10.1175/JCLI-D-16-0261.1.

Yim, B. Y., H. S. Min, and J.-S. Kug, 2016: Inter-model diversity in jet stream changes and its relation to Arctic climate in CMIP5. *Climate Dyn.*, **47**, 235–248, doi:10.1007/s00382-015-2833-5.

Zappa, G., F. Pithan, and T. G. Shepherd, 2018: Multimodel evidence for an atmospheric circulation response to Arctic sea ice loss in the CMIP5 future projections. *Geophys. Res. Lett.*, **45**, 1011–1019, doi:10.1002/2017GL076096.

Zelinka, M. D., S. A. Klein, and D. L. Hartmann, 2012: Computing and partitioning cloud feedbacks using cloud property histograms. Part II: attribution to changes in cloud amount, altitude, and optical depth. *J. Climate*, **25**, 3736–3754, doi:10.1175/JCLI-D-11-00249.1.

Zhang, J., W. Tian, M. P. Chipperfield, F. Xie, and J. Huang, 2016: Persistent shift of the Arctic polar vortex towards Eurasian continent in recent decades. *Nat. Climate Change*, **6**, 1094–1099, doi:10.1038/nclimate3136.

Zhang, P., Y. Wu, I. R. Simpson, K. L. Smith, X. Zhang, B. De, and P. Callaghan, 2018a: A stratospheric pathway linking a colder Siberia to Barents-Kara Sea sea ice loss. *Science Advances*, **4**, doi:10.1126/sciadv.aat6025.

Zhang, P., Y. Wu, and K. L. Smith, 2018b: Prolonged effect of the stratospheric pathway in linking Barents-Kara Sea sea ice variability to the midlatitude circulation in a simplified model. *Climate Dyn.*, **50**, 527–539, doi:10.1007/s00382-017-3624-y.

Zhang, Y., D. J. Seidel, J. C. Golaz, C. Deser, and R. A. Tomas, 2011: Climatological characteristics of Arctic and Antarctic surface-based inversions. *J. Climate*, **24**, 5167–5186, doi:10.1175/2011JCLI4004.1.

Appendix A

Datasets

A.1 CMIP5 dataset

The projected surface temperature changes shown in Figure 1.1 are based on the World Climate Research Programme's Coupled Model Intercomparison Project Phase 5 (CMIP5) dataset (Taylor et al., 2012). For each model (see Table A.1 for a list of these) the future projections shown are from the Representative Concentration Pathway 8.5 (RCP8.5) future scenario (time-slice mean 2070-2099) and late twenty-first century change was quantified relative to the model's historical forcing simulation (time-slice mean 1970-1999). All models were used for which monthly mean surface temperature data (variable name 'ts') in both the historical and RCP8.5 scenarios were successfully downloaded.

Table A.1 Models used in CMIP5, their associated modeling centre (or group), and institute ID

Modeling Centre (or Group)	Institute ID	Model Name
Commonwealth Scientific and Industrial Research Organization (CSIRO) and Bureau of Meteorology (BOM), Australia	CSIRO-BOM	ACCESS1.0 ACCESS1.3
Beijing Climate Center, China Meteorological Administration	BCC	BCC-CSM1.1 BCC-CSM1.1(m)

Continued on next page

Table A.1 – *continued from previous page*

Modeling Centre (or Group)	Institute ID	Model Name
College of Global Change and Earth System Science, Beijing Normal University	GCESS	BNU-ESM
Canadian Centre for Climate Modelling and Analysis	CCCMA	CanESM2
National Center for Atmospheric Research	NCAR	CCSM4
Community Earth System Model Contributors	NSF-DOE-NCAR	CESM1(BGC) CESM1(CAM5) CESM1(WACCM)
Centro Euro-Mediterraneo per I Cambiamenti Climatici	CMCC	CMCC-CESM CMCC-CM CMCC-CMS
Centre National de Recherches Météorologiques / Centre Européen de Recherche et Formation Avancée en Calcul Scientifique	CNRM-CERFACS	CNRM-CM5
Commonwealth Scientific and Industrial Research Organization in collaboration with Queensland Climate Change Centre of Excellence	CSIRO-QCCCE	CSIRO-Mk3.6.0
EC-EARTH consortium	EC-EARTH	EC-EARTH
LASG, Institute of Atmospheric Physics, Chinese Academy of Sciences and CESS, Tsinghua University	LASG-CESS	FGOALS-g2
The First Institute of Oceanography, SOA, China	FIO	FIO-ESM

Continued on next page

Table A.1 – *continued from previous page*

Modeling Centre (or Group)	Institute ID	Model Name
NOAA Geophysical Fluid Dynamics Laboratory	NOAA GFDL	GFDL-CM3 GFDL-ESM2G GFDL-ESM2M
NASA Goddard Institute for Space Studies	NASA GISS	GISS-E2-H GISS-E2-H-CC GISS-E2-R GISS-E2-R-CC
National Institute of Meteorological Research / Korea Meteorological Administration	NIMR/KMA	HadGEM2-AO
Met Office Hadley Centre (additional HadGEM2-ES realizations contributed by Instituto Nacional de Pesquisas Espaciais)	MOHC (additional realizations by INPE)	HadGEM2-CC HadGEM2-ES
Institute for Numerical Mathematics	INM	INM-CM4
Institut Pierre-Simon Laplace	IPSL	IPSL-CM5A-LR IPSL-CM5A-MR IPSL-CM5B-LR
Japan Agency for Marine-Earth Science and Technology, Atmosphere and Ocean Research Institute (The University of Tokyo), and National Institute for Environmental Studies	MIROC	MIROC-ESM MIROC-ESM-CHEM
Atmosphere and Ocean Research Institute (The University of Tokyo), National Institute for Environmental Studies, and Japan Agency for Marine-Earth Science	MIROC	MIROC5

Continued on next page

Table A.1 – *continued from previous page*

Modeling Centre (or Group)	Institute ID	Model Name
and Technology		
Max-Planck-Institut für Meteorologie (Max Planck Institute for Meteorology)	MPI-M	MPI-ESM-LR MPI-ESM-MR
Meteorological Research Institute	MRI	MRI-CGCM3 MRI-ESM1
Norwegian Climate Centre	NCC	NorESM1-M NorESM1-ME

Appendix B

Numerical model code edits

B.1 Stratospheric nudging code

This section details the code edits made to the IGCM4 Fortran 77 program to implement the stratospheric nudging method in Chapter 4.

In practical terms, the code edits were made using the NUPDATE utility, which allows you to edit specified lines of specified model subroutines or common blocks (named decks in NUPDATE), or add new decks, without ever permanently changing the official model program code. Instead, a temporary copy of the program is made with the edits you send to NUPDATE. For reference, note that the main NUPDATE commands used are '*/' (comment), '*I DECKNAME.LINENUMBER' (insert the lines written below this command into the deck specified at the line number specified), '*D DECKNAME.LINENUMBER' (delete the line number specified within the deck specified and insert the lines written below this command instead), and '*DECK DECKNAME' (insert a new deck containing the lines written below this command).

The edits that were sent here to NUPDATE are shown below. In brief, the edits consist first of adding various parameters required for the nudging to the IGCM4 common blocks or parameter decks. The most important parameters added are in the INNUDG namelist, including LNUDG which is set to '.TRUE.' to turn on the nudged version of IGCM4. The ININDG deck is then added, which initialises the nudging reference state for the day of the year on which the model run is started. READNDG is added after that, which reads in subsequent records of the nudging reference state for each day of the year. It also calculates factors used for cubic spline interpolation of

the reference state for each model time-step between each new model day. The edits to the DIFUSE deck, which is called close to the end of the model time-step, then apply the nudging.

```
*/ ======================================
*/ NUDGING EDITS
*/ ======================================
*/
*/ ------------------------------------------------
*/     Add required parameters for nudging
*/ ------------------------------------------------
*I PARAM2.16
      INTEGER, PARAMETER :: IDN=IDM*NL
      INTEGER, PARAMETER :: IGM=IDM*NHEM
      INTEGER, PARAMETER :: IGN=IDN*NHEM
*D RESTOR.5
      COMMON/RESTOR/ZRES,DRES,TRES,SPRES,DAMP,ZNDGI,DNDGI,TNDGI,
     +             SPNDGI,ZNDGJ,DNDGJ,TNDGJ,SPNDGJ,LNUDG,LNDCYC,
     +             DNUDG,SPNUDG,NDGI,NDGJ,NDGI3,NDGJ3,KINN,KINND,
     +             DNDMAX,LNUDGGP,KNUDG,KMX,KMN,TAUND
*I RESTOR.10
      REAL :: DNUDG(NL)
      REAL :: SPNUDG
      REAL :: NDGI
      REAL :: NDGJ
      REAL :: NDGI3
      REAL :: NDGJ3
      REAL :: DNDMAX
      REAL :: KNUDG(NL)
      REAL :: KMX
      REAL :: KMN
      REAL :: TAUND
      INTEGER :: KINN
      INTEGER :: KINND
      COMPLEX :: ZNDGI(2,NNTx,NHEM,NL)
```

```
      COMPLEX :: DNDGI(2,NNTx,NHEM,NL)
      COMPLEX :: TNDGI(2,NNTx,NHEM,NL)
      COMPLEX :: SPNDGI(2,NNTx,NHEM)
      COMPLEX :: ZNDGJ(2,NNTx,NHEM,NL)
      COMPLEX :: DNDGJ(2,NNTx,NHEM,NL)
      COMPLEX :: TNDGJ(2,NNTx,NHEM,NL)
      COMPLEX :: SPNDGJ(2,NNTx,NHEM)
      LOGICAL :: LNUDG
      LOGICAL :: LNDCYC
      LOGICAL :: LNUDGGP
*D MPIDECK.63
     &     II1,JJ1,KK1,MMT1,NNT1,NNT10,
*I MPIDECK.94
! For m=0, NNT10(Px,1) has the starting position for
! (even or odd) n of each column of PEs and NNT10(Px,2)
! has the end position
      INTEGER :: NNT10(Px,2)
*/
*/ ----------------------------------------------------------
*/     Now call ININDG in initialisation subroutine
*/     INITAL and add ININDG subroutine code.
*/     ININDG initialises the nudging reference state.
*/ ----------------------------------------------------------
*I INITAL.62
      CALL ININDG
*DECK ININDG
!=======================================================
! Initialises nudging reference state
!=======================================================
      SUBROUTINE ININDG
      IMPLICIT NONE
!
*CALL PARAM1
*CALL PARAM2
*CALL PARAM3
```

```
*CALL SPECTR
*CALL BLANK
*CALL MPIDECK
*CALL BATS
*CALL RESTOR
*CALL OUTCON
!-------------------------------------------------------
! Local variables
!-------------------------------------------------------
! Loop variable
      INTEGER :: iCol2,L,IHEM,J
      INTEGER :: countLHEM,countHEM,countJ
! MPI variables
      INTEGER, PARAMETER :: TagRef=100000
      INTEGER, PARAMETER :: TagRefJ=100001
      INTEGER(KIND=Type) :: iTagJ
! Nudging variables
      REAL :: RDAY
      REAL :: KTND
      REAL :: RNT1,RNT2
      COMPLEX :: ZNDGItmp(2,IGN)
      COMPLEX :: DNDGItmp(2,IGN)
      COMPLEX :: TNDGItmp(2,IGN)
      COMPLEX :: SPNDGItmp(2,IGM)
      COMPLEX :: ZNDGJtmp(2,IGN)
      COMPLEX :: DNDGJtmp(2,IGN)
      COMPLEX :: TNDGJtmp(2,IGN)
      COMPLEX :: SPNDGJtmp(2,IGM)
      COMPLEX :: HoldVar(2,NNTx,NHEM,3*NL+1)
      COMPLEX :: HoldVarJ(2,NNTx,NHEM,3*NL+1)
!-----------------------------------------------------------------------
  800 FORMAT(/' ***ABORT*** Nudging reference state file (nudg.bin)',
     + ' not in correct format. Sentinels (',2F12.3,') should equal',
     + ' RNTAPE (',2F12.3,').')
  801 FORMAT(94G13.4)
```

```
  202 FORMAT(/' SPECTRAL NUDGING TIMESCALE PROFILE (GLOBAL MEAN),',
     + days')
  203 FORMAT(15F12.2)
!
      NAMELIST/INNUDG/  LNUDG,LNDCYC,LNUDGGP,KINND,DNUDG,SPNUDG,DNDMAX
     +                 ,KNUDG,KMX,KMN,TAUND
      !-------------------------------------------------------------
      ! Variables are set on PE 0 and then passed to the other PEs
      !-------------------------------------------------------------
      IF (MYPE.EQ.0) THEN
         !---------------------------------------------------------
         ! Set default values and override as desired through
         ! INNUDG NAMELIST input
         !---------------------------------------------------------
         LNUDG=.FALSE.
         LNDCYC=.FALSE.
         LNUDGGP=.FALSE.
         KINND=-1
         SPNUDG=0.
         DNDMAX=-1.
         KMX=0.
         KMN=0.
         TAUND=0.
         DO 31 L=1,NL
            DNUDG(L) = 0.
            KNUDG(L) = 0.
  31     CONTINUE
         !---------------------------------------------------------
         ! Read NAMELIST, overwrite defaults, and write them out
         !---------------------------------------------------------
         READ(7,INNUDG)
         WRITE(2,INNUDG)
         !---------------------------------------------------------
         ! Calculate the height-dependent prefactor K (here DNUDG)
         !---------------------------------------------------------
```

```
         IF (LNUDG) THEN
            RDAY = WW/PI2
            KTND = (24./TAUND)*RDAY
            KNUDG = (SIGMA - KMX)/(KMN - KMX)
            DO 23 L=1,NL
               IF (KNUDG(L).LT.0.0) THEN
                  KNUDG(L) = 0.0
               ELSE IF (KNUDG(L).GT.1.0) THEN
                  KNUDG(L) = 1.0
               ENDIF
  23        CONTINUE
            DO 22 L=1,NL
               IF (KNUDG(L).GT.0.0) THEN
                  DNUDG(L) = KTND*KNUDG(L)/WW
               ELSE
                  DNUDG(L) = 0.0
               ENDIF
  22        CONTINUE
!
            WRITE(2,202)
            WRITE(2,203) DNUDG
         ENDIF
      ENDIF
      !-------------------------------------------------
      ! Pass information from PE 0 to other PEs
      !-------------------------------------------------
      IF (NPE.GT.1) THEN
         iSend=0
         nBuffSize=1
         CALL MPI_BARRIER(MPI_COMM_WORLD,ierr)
         CALL MPI_BCAST(LNUDG,nBuffSize,ParaLog,iSend,
     &        MPI_COMM_WORLD,ierr)
         CALL MPI_BCAST(LNDCYC,nBuffSize,ParaLog,iSend,
     &        MPI_COMM_WORLD,ierr)
         CALL MPI_BCAST(LNUDGGP,nBuffSize,ParaLog,iSend,
```

```
     &        MPI_COMM_WORLD,ierr)
         CALL MPI_BCAST(KINND,nBuffSize,ParaInt,iSend,
     &        MPI_COMM_WORLD,ierr)
         CALL MPI_BCAST(SPNUDG,nBuffSize,ParaReal,iSend,
     &        MPI_COMM_WORLD,ierr)
         CALL MPI_BCAST(DNDMAX,nBuffSize,ParaReal,iSend,
     &        MPI_COMM_WORLD,ierr)
         nBuffSize=NL
         CALL MPI_BCAST(DNUDG,nBuffSize,ParaReal,iSend,
     &        MPI_COMM_WORLD,ierr)
         CALL MPI_BARRIER(MPI_COMM_WORLD,ierr)
      ENDIF
      !-----------------------------------------------------
      ! If a nudging run read in zonal mean state
      ! (reference climatology) to nudge towards
      !-----------------------------------------------------
      IF (LNUDG) THEN
         ! Set J loop ranges for each PE
         DO iCol2=1,Px-1
            NNT10(iCol2,1) = NNT1(iCol2)+1
            NNT10(iCol2,2) = NNT1(iCol2+1)
         ENDDO
         NNT10(Px,1) = NNT1(Px)+1
         NNT10(Px,2) = IDM
!
         IF (KINND.EQ.0) THEN
         !-----------------------------------------------
         ! Time-independent zonal mean state
         !-----------------------------------------------
         [Code omitted since only used a time-varying
          reference climatology for the nudging
          experiments in this thesis]
         ELSE
         !-------------------------------------------------------------
         ! Time-varying zonal mean state; read in first two records
```

```
      ! to set up cubic spline interpolation
      !-------------------------------------------------------------
         IF (iRow.EQ.1) THEN
         !-------------------------------------------------
         ! Zonal wavenumber 0 is stored on row 1 of PEs
         !-------------------------------------------------
            IF (MYPE.EQ.0) THEN
            !-----------------------
            ! Read in on PE 0
            !-----------------------
               OPEN(17,FILE='nudg.bin',STATUS='OLD',
     &              FORM='UNFORMATTED')
               READ(17) RNT1,ZNDGJtmp,DNDGJtmp,TNDGJtmp,
     &                  SPNDGJtmp,RNT2
               IF (RNT1.NE.RNT2 .OR. RNT1.NE.RNTAPE) THEN
                  WRITE (2,800) RNT1,RNT2,RNTAPE
                  CALL ABORT
               ENDIF
               READ(17) RNT1,ZNDGItmp,DNDGItmp,TNDGItmp,
     &                  SPNDGItmp,RNT2
               IF (RNT1.NE.RNT2 .OR. RNT1.NE.RNTAPE) THEN
                  WRITE (2,800) RNT1,RNT2,RNTAPE
                  CALL ABORT
               ENDIF
               WRITE(2,204)
               WRITE(2,201) (REAL(TNDGJtmp(1,1::IGM)) + T0)*CT
  204          FORMAT(/' TIME VARYING NUDGING PROFILE',/
     &                ' SPECIFIED. INITAL PROFILE',/
     &                ' (GLOBAL MEAN), K = ')
               !-------------------------------------------------
               ! Pass relevant data to other PEs on row 1
               !-------------------------------------------------
               DO iCol2=Px,1,-1
                  HoldVar(:,:,:,:) = 0.0
                  HoldVarJ(:,:,:,:) = 0.0
```

```
                countLHEM = 0
                DO L=1,NL
                   DO IHEM=1,NHEM
                      countJ = 0
                      DO J=NNT10(iCol2,1),NNT10(iCol2,2)
                         countJ = countJ + 1
                         HoldVar(:,countJ,IHEM,L) =
&                                   ZNDGItmp(:,J+countLHEM*IDM)
                         HoldVar(:,countJ,IHEM,L+NL) =
&                                   DNDGItmp(:,J+countLHEM*IDM)
                         HoldVar(:,countJ,IHEM,L+2*NL) =
&                                   TNDGItmp(:,J+countLHEM*IDM)
                         HoldVarJ(:,countJ,IHEM,L) =
&                                   ZNDGJtmp(:,J+countLHEM*IDM)
                         HoldVarJ(:,countJ,IHEM,L+NL) =
&                                   DNDGJtmp(:,J+countLHEM*IDM)
                         HoldVarJ(:,countJ,IHEM,L+2*NL) =
&                                   TNDGJtmp(:,J+countLHEM*IDM)
                      ENDDO
                      countLHEM = countLHEM + 1
                   ENDDO
                ENDDO
                countHEM = 0
                DO IHEM=1,NHEM
                   countJ = 0
                   DO J=NNT10(iCol2,1),NNT10(iCol2,2)
                      countJ = countJ + 1
                      HoldVar(:,countJ,IHEM,3*NL+1) =
&                                 SPNDGItmp(:,J+countHEM*IDM)
                      HoldVarJ(:,countJ,IHEM,3*NL+1) =
&                                 SPNDGJtmp(:,J+countHEM*IDM)
                   ENDDO
                   countHEM = countHEM + 1
                ENDDO
                !---------------------------------------
```

```
                  ! Send data needed by other PEs
                  !---------------------------------------
                  ! for PEs 1-(Px-1) (Px=no. PE's in x/lon dir)
                  IF (iCol2.GT.1) THEN
                     iRecv=PeGrid(iCol2,1)
                     nBuffSize=2*NNTx*NHEM*(3*NL+1)
                     iTag=TagRef+iRecv
                     iTagJ=TagRefJ+iRecv
                     CALL MPI_BSEND(HoldVar,nBuffSize,ParaCom,
&                         iRecv,iTag,MPI_COMM_WORLD,ierr)
                     CALL MPI_BSEND(HoldVarJ,nBuffSize,ParaCom,
&                         iRecv,iTagJ,MPI_COMM_WORLD,ierr)
                  ENDIF
               ENDDO
            ENDIF
         ENDIF
         CALL MPI_BARRIER(MPI_COMM_WORLD,IERR)
         IF (iRow.EQ.1) THEN
            IF (MYPE.GT.0) THEN
               !---------------------------------------
               ! Receive the data on PEs 1-(Px-1)
               !---------------------------------------
               iSend=0
               nBuffSize=2*NNTx*NHEM*(3*NL+1)
               iTag=TagRef+MyPe
               iTagJ=TagRefJ+MyPe
               CALL MPI_RECV(HoldVar,nBuffSize,ParaCom,iSend,
&                   iTag,MPI_COMM_WORLD,istat,ierr)
               CALL MPI_RECV(HoldVarJ,nBuffSize,ParaCom,iSend,
&                   iTagJ,MPI_COMM_WORLD,istat,ierr)
            ENDIF
            !-----------------------------------------------------
            ! Write all the data in ZNDGI etc. on PEs 0-(Px-1)
            !-----------------------------------------------------
            DO L=1,NL
```

```
                  DO IHEM=1,NHEM
                     DO J=mTwin1(1,1)+1,mTwin1(2,1)
                        ZNDGI(:,J,IHEM,L)=HoldVar(:,J,IHEM,L)
                        DNDGI(:,J,IHEM,L)=HoldVar(:,J,IHEM,L+NL)
                        TNDGI(:,J,IHEM,L)=HoldVar(:,J,IHEM,L+2*NL)
                        ZNDGJ(:,J,IHEM,L)=HoldVarJ(:,J,IHEM,L)
                        DNDGJ(:,J,IHEM,L)=HoldVarJ(:,J,IHEM,L+NL)
                        TNDGJ(:,J,IHEM,L)=HoldVarJ(:,J,IHEM,L+2*NL)
                     ENDDO
                  ENDDO
               ENDDO
               DO IHEM=1,NHEM
                  DO J=mTwin1(1,1)+1,mTwin1(2,1)
                     SPNDGI(:,J,IHEM)=HoldVar(:,J,IHEM,3*NL+1)
                     SPNDGJ(:,J,IHEM)=HoldVarJ(:,J,IHEM,3*NL+1)
                  ENDDO
               ENDDO
            ENDIF
         ENDIF
         IF (NPE.GT.1) CALL MPI_BARRIER(MPI_COMM_WORLD, ierr)
      ENDIF
      END
*/
*/ ------------------------------------------------------------
*/      Now call READNDG in main program
*/      MLTRI and add READNDG subroutine code.
*/      READNDG reads in subsequent records for
*/      time-dependent nudging reference states
*/ ------------------------------------------------------------
*/ -----  First determine if it is time to update the nudging ------
*/ -----  reference state. KINND is the number of time-steps --------
*/ -----  between updates and KINN keeps a count of what the -------
*/ -----  current time-step is. When KINN is equal to KINND, an ----
*/ -----  update to the reference state will be made. For e.g., ----
*/ -----  if KINND = 96 (the no. of time-steps per day), then ------
```

```
*/ -----  there will be daily updates. ----------------------------
*/
*I INISTR.124
            KINN=0
*I INISTR.130
            KINN=1-KITS
*I INISTR.190
               KINN=0
*I INISTR.196
               KINN=1-KITS
*I INISTR.311
            IF (KINND.GT.0) THEN
               KINN=KTEMP-KINND*(KTEMP/KINND)
            ELSE
               KINN=0
            ENDIF
*I MLTRI.549
            !-------------------------------------------------------
            ! Update nudging reference climatology and cubic spline
            ! interpolating factors (for time-dependent nudging
            ! reference states)
            !-------------------------------------------------------
            IF (KINND.GT.0.AND.KINN.EQ.KINND) THEN
               CALL READNDG
               KINN=0
            ENDIF
            IF (KINND.GT.0) THEN
               NDGI=REAL(KINN)/REAL(KINND)
               NDGI3=(NDGI**3 - NDGI)/6.
               NDGJ=1.-NDGI
               NDGJ3=(NDGJ**3 - NDGJ)/6.
            ENDIF
*I MLTRI.558
               KINN=KINN+1
*DECK READNDG
```

```
!=====================================================
! Read subsequent record for nudging reference state
!=====================================================
      SUBROUTINE READNDG
      IMPLICIT NONE
!
*CALL PARAM1
*CALL PARAM2
*CALL PARAM3
*CALL BLANK
*CALL MPIDECK
*CALL BATS
*CALL RESTOR
*CALL OUTCON
!-----------------------------------------------
! Local variables
!-----------------------------------------------
! End of nudg.bin file error variable
      INTEGER :: IOS
! Loop variable
      INTEGER :: I,II,iCol2,L,IHEM,J
      INTEGER :: countLHEM,countHEM,countJ
! MPI variables
      INTEGER, PARAMETER :: TagRef=10000
! Nudging variables
      REAL :: RNT1,RNT2
      DIMENSION :: UU(2)
      COMPLEX :: UU
      COMPLEX :: ZNDGJtmp(2,IGN)
      COMPLEX :: DNDGJtmp(2,IGN)
      COMPLEX :: TNDGJtmp(2,IGN)
      COMPLEX :: SPNDGJtmp(2,IGM)
      COMPLEX :: HoldVar(2,NNTx,NHEM,3*NL+1)
!---------------------------------------------------------------------
  800 FORMAT(/' ***ABORT*** Nudging file (nudg.bin) not in correct',
```

```
     +      ' format. Sentinels (',2F12.3,') should equal RNTAPE. (R)')
  801 FORMAT(94G13.4)
  802 FORMAT(/' No more records in nudging file (nudg.bin),',
     +       'restarting from beginning of file.')
      !-----------------------------------------------------------------
      ! If a nudging run read in next record and update linear
      ! interpolation parameter
      !-----------------------------------------------------------------
      IF (LNUDG) THEN
         IF (iRow.EQ.1) THEN
         !-------------------------------------------------
         ! Zonal wavenumber 0 is stored on row 1 of PEs
         !-------------------------------------------------
            IF (MYPE.EQ.0) THEN
            !---------------------------
            ! Read in on PE 0
            !---------------------------
               READ(17,IOSTAT=IOS) RNT1,ZNDGJtmp,DNDGJtmp,TNDGJtmp,
     &                             SPNDGJtmp,RNT2
               IF (IOS.LT.0) THEN
               !-----------------------------------------
               ! If we have come to the end of the file
               ! go back to the beginning
               !-----------------------------------------
                  WRITE (2,802)
                  REWIND 17
                  READ(17) RNT1,ZNDGJtmp,DNDGJtmp,TNDGJtmp,
     &                     SPNDGJtmp,RNT2
               ENDIF
!
               IF (RNT1.NE.RNT2 .OR. RNT1.NE.RNTAPE) THEN
                  WRITE (2,800) RNT1,RNT2
                  CALL ABORT
               END IF
               !-----------------------------------------
```

```
            ! Pass relevant data to other PEs on row 1
            !-------------------------------------------
            DO iCol2=Px,1,-1
               HoldVar(:,:,:,:) = 0.0
               countLHEM = 0
               DO L=1,NL
                  DO IHEM=1,NHEM
                     countJ = 0
                     DO J=NNT10(iCol2,1),NNT10(iCol2,2)
                        countJ = countJ + 1
                        HoldVar(:,countJ,IHEM,L) =
     &                                 ZNDGJtmp(:,J+countLHEM*IDM)
                        HoldVar(:,countJ,IHEM,L+NL) =
     &                                 DNDGJtmp(:,J+countLHEM*IDM)
                        HoldVar(:,countJ,IHEM,L+2*NL) =
     &                                 TNDGJtmp(:,J+countLHEM*IDM)
                     ENDDO
                     countLHEM = countLHEM + 1
                  ENDDO
               ENDDO
               countHEM = 0
               DO IHEM=1,NHEM
                  countJ = 0
                  DO J=NNT10(iCol2,1),NNT10(iCol2,2)
                     countJ = countJ + 1
                     HoldVar(:,countJ,IHEM,3*NL+1) =
     &                             SPNDGJtmp(:,J+countHEM*IDM)
                  ENDDO
                  countHEM = countHEM + 1
               ENDDO
               !---------------------------------------
               ! Send data needed by other PEs
               !---------------------------------------
               IF (iCol2.GT.1) THEN
                  iRecv=PeGrid(iCol2,1)
```

```
                  nBuffSize=2*NNTx*NHEM*(3*NL+1)
                  iTag=TagRef+iRecv
                  CALL MPI_BSEND(HoldVar,nBuffSize,ParaCom,
&                      iRecv,iTag,MPI_COMM_WORLD,ierr)
               ENDIF
            ENDDO
         ENDIF
      ENDIF
      CALL MPI_BARRIER(MPI_COMM_WORLD,IERR)
      IF (iRow.EQ.1) THEN
         IF (MYPE.GT.0) THEN
            !-----------------------------------------
            ! Receive the data on PEs 1-(Px-1)
            !-----------------------------------------
            iSend=0
            nBuffSize=2*NNTx*NHEM*(3*NL+1)
            iTag=TagRef+MyPe
            CALL MPI_RECV(HoldVar,nBuffSize,ParaCom,iSend,
&                iTag,MPI_COMM_WORLD,istat,ierr)
         ENDIF
         !-------------------------------------------------------
         ! Write all the data in ZNDGJ etc. on PEs 0-(Px-1)
         !-------------------------------------------------------
         DO L=1,NL
            DO IHEM=1,NHEM
               DO J=mTwin1(1,1)+1,mTwin1(2,1)
                  ZNDGJ(:,J,IHEM,L)=HoldVar(:,J,IHEM,L)
                  DNDGJ(:,J,IHEM,L)=HoldVar(:,J,IHEM,L+NL)
                  TNDGJ(:,J,IHEM,L)=HoldVar(:,J,IHEM,L+2*NL)
               ENDDO
            ENDDO
         ENDDO
         DO IHEM=1,NHEM
            DO J=mTwin1(1,1)+1,mTwin1(2,1)
               SPNDGJ(:,J,IHEM)=HoldVar(:,J,IHEM,3*NL+1)
```

```
            ENDDO
         ENDDO
         !-----------------------------------------------------
         ! Need to swap ZNDGI etc and ZNDGJ etc arrays
         ! around so the I's contain the most recent
         ! record and J's contain the previous record
         !-----------------------------------------------------
         DO L=1,NL
            DO IHEM=1,NHEM
               DO J=mTwin1(1,1)+1,mTwin1(2,1)
                  UU=ZNDGI(:,J,IHEM,L)
                  ZNDGI(:,J,IHEM,L)=ZNDGJ(:,J,IHEM,L)
                  ZNDGJ(:,J,IHEM,L)=UU
                  UU=DNDGI(:,J,IHEM,L)
                  DNDGI(:,J,IHEM,L)=DNDGJ(:,J,IHEM,L)
                  DNDGJ(:,J,IHEM,L)=UU
                  UU=TNDGI(:,J,IHEM,L)
                  TNDGI(:,J,IHEM,L)=TNDGJ(:,J,IHEM,L)
                  TNDGJ(:,J,IHEM,L)=UU
               ENDDO
            ENDDO
         ENDDO
         DO IHEM=1,NHEM
            DO J=mTwin1(1,1)+1,mTwin1(2,1)
               UU=SPNDGI(:,J,IHEM)
               SPNDGI(:,J,IHEM)=SPNDGJ(:,J,IHEM)
               SPNDGJ(:,J,IHEM)=UU
            ENDDO
         ENDDO
      ENDIF
      IF (NPE.GT.1) CALL MPI_BARRIER(MPI_COMM_WORLD, ierr)
   ENDIF
!
   END
*/
```

```
*/ ------------------------------------------------
*/           Edit DIFUSE to include nudging
*/           Applies nudging in spectral space
*/ ------------------------------------------------
*/ --- Add required nudging parameters ---
*/
*I DIFUSE.16
*CALL OUTCON
*I DIFUSE.29
! Nudging variables
      REAL :: NDFAC
      COMPLEX :: REF,REF0
*I DIFUSE.83
      !--------------------------------------------
      ! Apply nudging to zonal mean state
      !--------------------------------------------
      IF (LNUDG) THEN
         !-------------------------------------------------
         ! Nudging applies for zonal wavenumber 0
         !-------------------------------------------------
         IF (iRow.EQ.1) THEN
            IF (DAY.GT.DNDMAX.OR.DNDMAX.LE.0.) THEN
               NDFAC = 1.
            ELSE IF (DAY.GT.0) THEN
               NDFAC = SIN(PI*DAY/(2*DNDMAX))**2
            ELSE
               NDFAC = 0.
            END IF
            !-------------------------------------------------------
            ! Remove planetary vorticity to avoid damping it
            !-------------------------------------------------------
            IF (MYPE.EQ.0) THEN
               DO L=1,NL
                  Z(1,1,1,L)=Z(1,1,1,L)-EZ
               ENDDO
```

```
        ENDIF
        DO L=1,NL
           DO IHEM=1,NHEM
              DO J=1,mTwin1(2,1)
                 REF=NDGI*ZNDGI(1,J,IHEM,L) +
&                    NDGI3*ZNDGI(2,J,IHEM,L) +
&                    NDGJ*ZNDGJ(1,J,IHEM,L) +
&                    NDGJ3*ZNDGJ(2,J,IHEM,L)
                 ZT(J,1,IHEM,L)=ZT(J,1,IHEM,L)-NDFAC*
&                    DNUDG(L)*(Z(J,1,IHEM,L)-REF)
                 REF=NDGI*DNDGI(1,J,IHEM,L) +
&                    NDGI3*DNDGI(2,J,IHEM,L) +
&                    NDGJ*DNDGJ(1,J,IHEM,L) +
&                    NDGJ3*DNDGJ(2,J,IHEM,L)
                 DT(J,1,IHEM,L)=DT(J,1,IHEM,L)-NDFAC*
&                    DNUDG(L)*(D(J,1,IHEM,L)-REF)
                 REF=NDGI*TNDGI(1,J,IHEM,L) +
&                    NDGI3*TNDGI(2,J,IHEM,L) +
&                    NDGJ*TNDGJ(1,J,IHEM,L) +
&                    NDGJ3*TNDGJ(2,J,IHEM,L)
                 TT(J,1,IHEM,L)=TT(J,1,IHEM,L)-NDFAC*
&                    DNUDG(L)*(T(J,1,IHEM,L)-REF)
              ENDDO
           ENDDO
        ENDDO
        DO IHEM=1,NHEM
           DO J=1,mTwin1(2,1)
              REF=NDGI*SPNDGI(1,J,IHEM) +
&                  NDGI3*SPNDGI(2,J,IHEM) +
&                  NDGJ*SPNDGJ(1,J,IHEM) +
&                  NDGJ3*SPNDGJ(2,J,IHEM)
              VP(J,1,IHEM)=VP(J,1,IHEM)-NDFAC*
&                  SPNUDG*(SP(J,1,IHEM)-REF)
           ENDDO
        ENDDO
```

```
            REF0=NDGI*TNDGI(1,1,1,1) +
     &           NDGI3*TNDGI(2,1,1,1) +
     &           NDGJ*TNDGJ(1,1,1,1) +
     &           NDGJ3*TNDGJ(2,1,1,1)
          IF (MYPE.EQ.0) THEN
              WRITE(2,500)
              WRITE(2,501) NDGI,NDGJ,REF0
  500         FORMAT(/' NDGI, NDGJ, REF0 (T NUDGING PROFILE',/
     &                ' FOR L=1, IHEM=1, J=1, in K) = ')
  501         FORMAT(3F12.6)
              !---------------------------------
              ! Restore planetary vorticity
              !---------------------------------
              DO L=1,NL
                 Z(1,1,1,L)=Z(1,1,1,L)+EZ
              ENDDO
            ENDIF
        ENDIF
        IF (NPE.GT.1) CALL MPI_BARRIER(MPI_COMM_WORLD, ierr)
      ENDIF
```

B.2 Code to increase hyper-diffusion in uppermost model levels

This section shows the code edits made to the IGCM4 Fortran 77 program to increase the hyper-diffusion in the uppermost model levels. This prevents high frequency waves from blowing-up in the uppermost model levels when the stratospheric nudging method is implemented within IGCM4 in Chapter 4.

```
*/ ====================================
*/ HYPER-DIFFUSION EDITS
*/ ====================================
*/
```

```
*/ ------------------------------------------------
*/ Edit hyperdiffusion in DIFUSE
*/ Increase the hyperdiffusion in the uppermost
*/ levels to prevent high frequency waves from
*/ becoming unstable in nudging runs
*/ ------------------------------------------------
*I DIFUSE.21
      REAL :: facnudge
*I DIFUSE.88
            facnudge=1.0
            IF (L.EQ.1) facnudge=7.0
            IF (L.EQ.2) facnudge=5.0
            IF (L.EQ.3) facnudge=3.0
            IF (L.EQ.4) facnudge=2.0
            IF (L.EQ.5) facnudge=1.5
            IF (L.EQ.6) facnudge=1.25
*D DIFUSE.93,94
C                     AKZ = AK(NVAL+3-IHEM)
C                     AKDT = AK(NVAL+IHEM)
                     AKZ = AK(NVAL+3-IHEM)*facnudge
                     AKDT = AK(NVAL+IHEM)*facnudge
*D DIFUSE.108
C                        AKDT = AK(NVAL+IHEM)
                        AKDT = AK(NVAL+IHEM)*facnudge
*D DIFUSE.122
C               ZT(1,1,1,L) = ZT(1,1,1,L)+AK(2)*EZ
               ZT(1,1,1,L) = ZT(1,1,1,L)+AK(2)*EZ*facnudge
```